IDENTIFYING GROWTH CRITERIA AND SEDIMENT MOVEMENT MECHANISMS OF NEEDLE ICE USING HIGH-FREQUENCY ENVIRONMENTAL AND VISUAL MONITORING

by

Carl-Johan Borg

Submitted in fulfilment of the requirements for the degree

Doctor of Philosophy (Geography)

Department of Geography, Rhodes University

Grahamstown

January 2017

Abstract:

Environmental growth conditions and mechanisms involved in sediment transport by needle ice have historically been difficult to assess and are poorly documented. The spatial and temporal dynamics that relate to the environment, growth and decay of needle ice are not fully understood. This study monitored needle ice growth, melt and visually identified sediment displacement mechanisms by needle ice, with the aim of revealing environmental growth criteria, timing of growth/melt, ground-surface-air energy balance and sediment displacement mechanisms. Furthermore, the impact of needle ice displacement on vegetation and patterned ground formation was analysed.

High-frequency visual monitoring, using three cameras, supplemented by high-frequency measurements of air temperature, soil moisture and wind speed was used to investigate needle ice growth and decay dynamics. Results from visual and environmental monitoring of needle ice growth, showed that the needle ice growing environment was more dynamic, especially in terms of surface temperature, than previously argued. Needle ice growth was observed to occur during surface temperatures from -2.0°C to 2.2°C, soil moisture levels from 0.4% to 37.4% and in winds speeds of 0 m/s to 12.6 m/s. Needle ice initiation was documented a few minutes to hours before or after the onset of surface temperature dropping to below 0°C. Imagery displayed that the depth of ice nucleation was variable within the soil column, possibly relating to the energy balance of radiative cooling, convective heat loss, ground conductivity and latent heat release at the air-surface-ground boundary. Heaving and resettling, toppling and rolling were identified as slope displacement mechanisms when needle ice decayed. Animal trampling and hail were additionally documented as substantial surface altering processes. Furthermore, no impact of needle ice reducing vegetation stability was identified, although a tendency to hinder vegetation expansion was noted. Also, no creation of patterned ground was observed as a result of needle ice decay.

List of Figures:

List of Tables

Glossary

- Biogeomorphology
  - The term is a loosely defined term used in describing the causality of organisms impact on landscape development (Naylor, 2005).
- Gelifluction
  - "The slow saturated flowage of near-surface soil that occurs during thaw consolidation of ice-rich sediments" (French and Harbour, 2013, p.1).
- Image logger discrepancy (ILD)
  - Image logger discrepancy show the difference in timing of visual identification of needle ice growth and measured below 0°C temperature. Positive ILD indicate that visual identification of needle ice growth occurred after below 0°C temperatures. ILDs are positive (below 0°C after) or negative (below 0°C before) in reference of visual identification.
- Needle ice sediment displacement (NISD)
  - Movement of material through growing, melting, blowing, toppling, sliding or other physical/environmental displacement mechanisms/processes associated with needle ice
- Pahoehoe
  - A type of slow-moving, but abundant, lava (Self et al., 1998).
- Periglacial
  - An area dominated by cold-dominated geomorphic processes often relating to snow, running water and wind (French and Harbor, 2013).
- Solifluction
  - A mass-wasting process that occurs in cold nonglacial (periglacial) environments (French and Harbour, 2013, p.1).
- Terracette
  - "Normal terracettes display wide treads with a low angle but very wide risers with an angle similar to that of the slope. Their long, unbroken lengths are parallel to each other and approximately normal to the slope" (Anderson, 1972, p.19).
- Zoogeomorphology
  - Similar term to biogeomorphology but with the emphasis on animal impact by burrowing, trampling and building etc.

Table of Contents

Acknowledgements

It is my pleasure to acknowledge individuals that were instrumental in me initiating and completing my PhD research.

Firstly, I would like to thank my supervisors. I would like to express my deepest gratitude towards Professor Ian Meiklejohn for allowing me to embark on this journey and for supplying knowledge and guidance, being a master of the English language and opening doors for my future research possibilities. I would also like to recognise the significance of Professor Jan Boelhouwers, for motivating me as a scientist, pushing me to do better, setting me down the path of Physical Geography and for inspiringly telling me I'm wrong… a lot. I would also like to direct my gratitude toward Professor Werner Nel, for sharing some of the toughest and most astounding outdoor moments of my life, always being positive and for gooi-ing it.

These acknowledgements would not be complete without mentioning of colleagues, field assistants and further personnel aiding me during the data collection phase. I am forever grateful for the help that Christel Hansen, Jessica Rosenfels and Elizabeth Rudolph have provided. Amongst plentiful laughs, sandwiches, gherkins, Steri-stumpies and songs, we managed to complete a lot of work, thank you.

A special thank you to Professor David Hedding for providing equipment that was essential for completing this thesis, and for being a fantastic hiking buddy on Marion. I would also like to thank Daniël Kotzé and Abuyiselwe Nguna for providing assistance with logger downloads and equipment on Marion Island and Maarten den Heyer and the staff of Tiffindell Ski Resort for providing very comfortable accommodation and safe housing for my cameras and sensors. I would also like to thank the crew of SA Agulhas II and Marion base, for housing and transporting me during data collection.

My deepest appreciation belongs to my family for their endless support, encouragement and understanding. Thank you! None of this would ever have been possible without your unwavering care.

This work would not have been possible without the financial support of the South African National Research Foundation (NRF). I am truly thankful for your support.

Lastly, I would like to thank Hasan Ibn al-Haytham, Sir Isaac Newton, Michael Faraday, Albert Einstein, Neil deGrasse-Tyson and Brian Cox for pioneering, expanding, maintaining, inspiring and teaching science, in addition to helping us all understand the universe we live in.

Chapter 1 – Introduction

1.1 Background

Needle ice (also known as mush frost, ice filaments, rouste, shimo bashira, pipkrake) is a type of segregation ice active on a diurnal cycle, described in literature by Elliott (1824), Hesselman (1907), Troll (1958) and Washburn (1979) as the following:

- "... a remarkable protrusion of crystalline fibres of ice from the stems of the *Conyza bifron" – Elliot (1824, p322)*
- "... 6-8 cm tall, 1-2 cm wide, often bent pillars of ice" (translated by the author) – Hesselman (1907, p3)
- "... ground ice which takes the form of fine needle-like ice crystals in compact clusters beneath the ground surface, with the ice needles standing upright perpendicular to the cooling surface." – Troll (1944, p24)
- "... accumulation of slender, bristle-like ice crystals (needles) practically at, or immediately beneath, the surface of the ground." – Washburn (1979, p92)

Needle ice is commonly observed in wet loamy soils just before sunrise, after nights displaying sub-zero temperatures (Troll, 1944; Outcalt, 1971a; Lawler, 1988). Ice growth creates fine ice crystals emerge from soil or plants, often heaving soil and/or plant debris (Figure 1.1). Needle ice growth is active on a diurnal scale in periglacial areas, reworking the topmost soil layer (Branson *et al.*, 1996). Rates of needle ice induced geomorphic change have been recorded to depend on the frequency of diurnal freeze-thaw cycles (Lawler, 1988). The phenomenon is most active in periglacial settings like the sub-Antarctic and sub-Arctic as well as low-latitude, high-altitude locations (Lawler, 1988). Needle ice is less active in locations that experience seasonal freezing, rather than diurnal, for example southern Scandinavia and parts of Canada (Lawler, 1988; Rempel 2007).

Active periglacial areas may experience a large number of freeze-thaw or frost cycles, for example records for sub-Antarctic islands showed 170, 70 and 200 cycles annually by Löffer (1983), Boelhouwers *et al.* (2003) and Haussmann (2009a) respectively. Locations that experience seasonal periglacial conditions, commonly experience fewer frost cycles annually, usually in spring or autumn (Outcalt, 1969; Lawler, 1993). The frequency of freeze-thaw events are affected by altitude, as tropical and sub-tropical environments can experience periglacial conditions at high elevations (Troll, 1958; Schubert, 1973; Hastenrath, 1977; Pérez, 1987a). Pérez (1987) showed that in the Piedras Blancas of Venezuela at 4300m, ca 350 freeze-thaw cycles are experienced annually and he suggests needle ice being one of the most dynamic geomorphic agents.

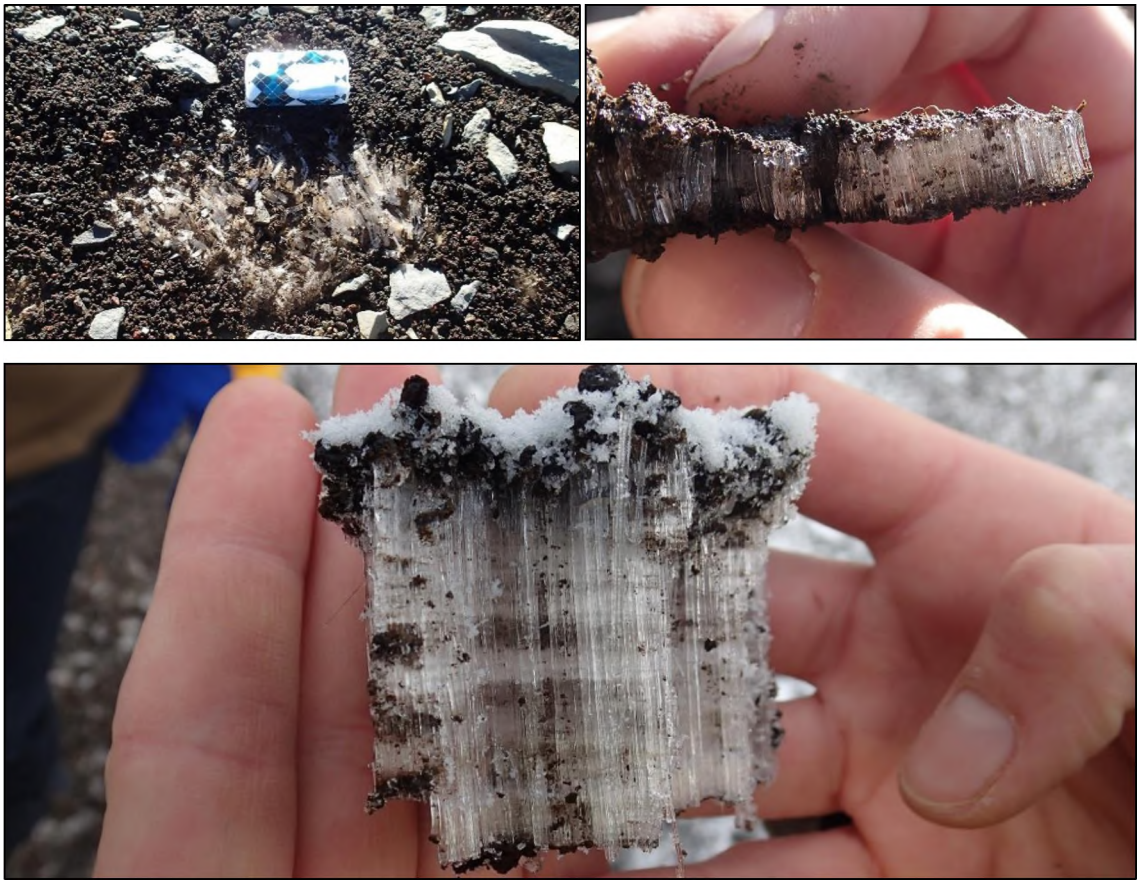

Figure 1.1. Needle ice seen at Marion Island, sub-Antarctic (top left [April 9 2014[, bottom [April 27 2014]) and at Tiffindell, South Africa (top right [May 29 2014])

Troll (1944), Pérez (1987) and Lawler (1988) recorded needle ice to have the greatest influence at locations with a high frequency of freeze-thaw cycles, often coinciding with areas portraying periglacial conditions. Historically, periglacial areas were described being relict glacial environments and, thus, are in close proximity to ice sheets. However, this interpretation was subsequently discarded (Loziński 1912; French, 2000). Currently, periglacial environments are described as areas where the effect of seasonal and diurnal freezing, permafrost, snow accumulation, running water and ice processes are active in changing the landscape, which do not necessarily require extreme cold (French and Harbor, 2013). Perennially periglacial locations where needle ice growth is common, include snow-free parts of Alaska and Scandinavia, the Yukon, Siberia and the Tibetan plateau in the Northern Hemisphere and Marion Island, Macquarie Island, Signy Island in the Southern Hemisphere, amongst many other locations (French and Harbor, 2013; Lawler, 1988).

1.2 Theoretical context

Needle ice is suggested to be an important agent in moving and reworking soil, in addition to altering surface vegetation (Hesselman, 1907; Troll, 1944; Higashi and Corte, 1971; Matsuoka, 2005). Early literature relating to needle ice has mostly focused on the environmental parameters controlling its

growth and less on movement modalities attained by its destruction (Argyll, 1880; Schwalbe, 1884; Davison, 1889; Fukuda, 1936; Fujita *et al.*, 1937). It is during melt, destruction or collapsing of needle ice that sediment transport distinguishes itself from transport by frost creep, soliflucton or gelifluction (Troll 1958; Higashi and Corte 1971; Outcalt 1971; Mackay and Mathews 1974b, Matsuoka, 2000). Physical mechanisms like toppling and rolling take place after melt, due to ice needles falling, produce additional movement apart from the resettling after lift by gravity. Quantifying and modelling the effect of sediment transport by needle ice has been undertaken by several authors for almost 60 years (Gradwell, 1957; Higashi and Corte, 1971; Mackay and Mathews, 1974a; Matsuoka, 1996; 2005; 2014), although, currently not all mechanisms involved in movement are known, let alone incorporated into models.

For needle ice to grow, sufficiently cold temperatures are required for ice nucleation to commence. However, temperatures for ice nucleation could possibly vary significantly depending on environmental conditions. Outcalt (1971) proposed a soil surface ice nucleation temperature of approx. -2°C. This value was derived from environmental equations based on empirically gathered data from wet soils on clear and windless nights in Virginia, US. He proposed that the top soil must be undercooled to balance the energy budget at the surface for freezing to initiate. In a recent study by Nel and Boelhouwers (2014), they empirically measure needle ice initiation temperatures that were close to -0.2°C from sub-Antarctic Marion Island. Environmental conditions at the two above study sites were however distinctly different, with Marion seldom experiencing calm and clear nights (Hall, 1979; Haussmann *et al.,* 2009; Nel and Boelhouwers, 2014). Given the above variability, needle ice research requires longer term studies of numerous needle ice events to record initiation temperature, to identify ice nucleation conditions and processes.

Geomorphological changes to the landscape from needle ice activity are not limited to the direct processes of particle displacement (Hesselman, 1907; Pérez, 1991; Pérez, 1993; Haussmann *et al.,* 2009). Needle ice has been observed to affect vegetation stability by actively destroying vegetation or by disrupting roots and preventing seedlings from creating stabile colonies (Hesselman, 1907; Pérez, 1993; Grab, 2002; Haussmann *et al.,* 2009). Studies have shown that the growth of ice needles require a fine soil texture, sufficient moisture, and temperatures below freezing (Troll, 1944; Outcalt, 1971; Lawler, 1988). Effectively, this excludes needle ice from growing in most vegetated areas (Pérez, 1993; Grab, 2002; Butler *et al.,* 2004). However, in areas where the initial growth of needle ice has already commenced, constant reworking allows for continued needle ice impact on vegetation (Hesselman, 1907). Intricate knowledge on small scale active deformation by needle ice vegetation destruction is mostly unknown, apart from observations and work on rates undertaken by Pérez (1993), Grab (2002), Butler *et al.* (2004) and Haussmann (2009).

Certain patterned ground features in periglacial environments are suggested to be strongly influenced by needle ice sediment movement and sorting (Gradwell, 1957; Lundqvist, 1962; Noguchi et al., 1987; Ballantyne, 1996; Grab, 2002b). Interaction between environmental effects and needle ice-produced patterned ground is discussed in Troll (1944), Mackay and Mathews (1974a), Hall (1979) and Holness (2001).

The following section will outline previous research methodologies used for determining sediment movement and initiation temperatures of needle ice, while emphasising areas were previous study methodologies require improvement.

1.3 Theoretical framework and research methodologies

Investigating needle ice influence in the context of global periglacial geomorphology, requires a firm theoretical understanding of both processes involved in sediment movement by needle ice and its interaction with the immediate surroundings. Complex interactions are observed (Troll, 1958; Lawler, 1988; Pérez, 1991; Haussmann et al., 2009b) between biotic/abiotic and needle ice induced processes, making separation of specific surface altering processes difficult, especially in terms of quantifying their impact. Apparent gaps in current needle ice knowledge and the approaches to investigating sediment movement and initiation of growth, and how the observed limitations can be addressed are highlighted below.

The intricate details and mechanisms of physical clast movement by needle ice are poorly understood, and to achieve advances in this field new study methodologies are needed (Lawler, 1993; Matsuoka, 2014; 1996). Much of the difficulty experienced in attempting to model needle ice sediment movement originates from the uncertainty of which specific mechanisms are involved in needle ice sediment displacement (Higashi and Corte 1971; Mackay and Mathews 1974a; Matsuoka, 1996). The well understood effect of gravity resettling is considered to be the primary movement mechanism, complemented by less understood mechanisms of toppling, rolling, tumbling or sliding contributing to final clast displacement (Deckert, 1913; Gradwell, 1957; Troll, 1958; Higashi and Corte, 1971; Mackay and Mathews, 1974b; Matsuoka, 1996). Studies of sediment movement by needle ice have been problematic, as the mechanisms involved have been difficult to assess, in both qualitative and quantitative ways (Troll 1944; Higashi & Corte 1971; Mackay & Mathews 1974a; Matsuoka 1996; Matsuoka 2005). Also, complexity is added by environmental parameters (climate, lithology, vegetation, slope angle, animal influence) that influence final displacement both actively by physical movement and passively by modifying needle ice growth surroundings (Troll, 1944; Outcalt, 1971; Pérez, 1987; Lawler, 1988). Environmental parameters also change in a seasonal context.

Over the last 60 years there has been little work, apart from Matsuoka (2005; 2014) and Ueno *et. al.* (2015), on the evolution of methodologies examining needle ice sediment displacement mechanisms. Publications by Rempel (2010) and Ballantyne (2013) have contributed to the evolution of periglacial geomorphology by studying the physics of ice lens formation and solifluction. Haussmann (2009a;2009b) and Eriksson (2011) added the relatively new field of biogeomorphology examining faunal impact on flora and their relation to physical processes on Marion Island. The most recent published work has been on needle ice's initiation temperature, Nel and Boelhouwers (2014), and on needle ice growth and deforestation (Ueno et al., 2015).

Needle ice growth has an inherent consequence of erosion and sediment displacement, which was modelled by Higashi and Corte (1971), Mackay and Mathews (1974a) and Matsuoka (1996; 2005), although with less than satisfactory results when compared with empirically measured results. The focus of all authors' models was on identifying mechanisms and controls involved in downslope movement and on modelling sediment displacement distance by needle ice heave and melting. Parameters considered to affect displacement distance include: slope angle, grain size, freeze-thaw cycle abundance and total heave. The aforementioned authors, in line with several others (e.g. Fukuda, 1936; Gradwell, 1957; Troll, 1958; Soons, 1967; Pérez, 1987a) agree that additional factors may be important in sediment displacement by needle ice, but that these are difficult to identify and quantify. Matsuoka (2005) improved the accuracy of his model by including surface texture as a parameter, but with little success.

There is a need to develop a method that identifies downslope movement by needle ice that is based not only on initial and final displacement over an extended period of time with numerous freeze-thaw cycles, but that can also observe clast movement during each individual frost cycle. Identifying the single/multiple movement mechanisms involved in one event, through the use of high-frequency visual monitoring in conjunction with high-frequency environmental monitoring and observation, is possible.

The research undertaken for this thesis intends to increase knowledge on initiation temperature, sediment movement mechanisms, surface energy balance, biological interactions, patterned ground formation in relation to environmental conditions (temperature, soil moisture, wind speeds), as well as identifying additional areas for further research. A methodology using high-frequency repeat photography has been used to observe geomorphological processes at both short (e.g. daily environmental influence, catastrophic failures, surface energy dynamics) and long (e.g. solifluction, rock glaciers, patterned ground formation) time-intervals.

1.4 Aim and objectives

The primary aims of this thesis are, first, to investigate small scale high-frequency variability in environmental parameters, identifying possible threshold limits and criteria relevant to needle ice initiation, growth and melt. Second, gained knowledge is coupled with sediment transport, adding new empirically observable evidence of needle ice growth, its destruction and displacement of material. Third, observations develop and apply a new methodology that visually documented needle ice growth/melt fusing high-frequency stationary photography. Fourth, the results of the research were then used to identify and show *in situ* mechanisms involved in slope transport by needle ice and comparing these to those suggested by previous authors (Fukuda, 1936; Gradwell, 1957; Troll, 1958; Higashi & Corte, 1971; Outcalt, 1971; Mackay & Mathews, 1974a; Pérez, 1987; Matsuoka, 1996).

To achieve above aims, the following objectives were formulated:

1. To determine detailed growth criteria for needle ice, which included:
    1.1. Identifying needle ice nucleation temperature;
    1.2. Identifying needle ice growth location;
    1.3. Identifying contribution of soil moisture to needle ice growth;
    1.4. Identifying soil textural controls on needle ice growth; and
    1.5. Identifying conditions that are not suitable for the growth of needle ice.
2. To determine the temporal regime of needle ice growth and melt, by:
    2.1. Recording needle ice growth/melt timing;
    2.2. Recording needle ice growth/melt timing in relation to sunrise/sunset;
    2.3. Recording needle ice event duration;
    2.4. Recording environmental conditions that alter the timing of needle ice growth and melting.
3. To examine latent heat release and zero-curtain effects during needle ice growth events.
4. To visually identify mechanisms of sediment displacement by needle ice from repeat photography by:
    4.1. Recording needle ice growth events;
    4.2. Recording needle ice displacement mechanisms;
    4.3. Recording timing of needle ice growth and melt;
    4.4. Recording mechanisms of Needle Ice Sediment Displacement (NISD);
    4.5. Recording needle ice growth dynamics from three different settings;
    4.6. Measuring slope angles influence on sediment displacement distance;
    4.7. Identifying, explaining and measuring inter-site heave variability;
    4.8. Measuring sediment displacement distance by needle ice decay;

4.9. Identifying and measuring sediment displacement distance by mechanism other than needle ice.

5. To identify and record the influence of needle ice growth on vegetation degradation and patterned ground formation.

1.5 Structure of the thesis

This thesis comprises four parts, an introduction, results, discussion and appendix. The introduction includes Chapters 1 and 2, which aim to familiarize the reader with past and current understanding of needle ice development, and to place this thesis in a contemporary research context. Following the introduction, Chapter 3 and 4 discuss how and where the results were gathered, which are presented in Chapter 5 and 6. The discussion and conclusions are presented in Chapter 7 and 8. Appendix A comprises tables with datasets too large to be presented in the text, and Appendix B consists of integrated videos of needle ice events. The following chapter presents a literature review of needle ice knowledge accumulated from the early 19th century to date.

Chapter 2 - Literature review

The focus of this chapter will be on the initiation temperature of needle ice, mechanisms of needle ice sediment displacement and needle ice as a geomorphic agent. The literature reviewed is relevant to the aims stated in Chapter 1, and the objectives to achieve these aims will be identified at the end of each subsequent section.

The first published observations of needle ice are found in articles by Elliot (1824) and Herschel (1833), which describe an "unusual ice formation" emerging from the stems of plants. Following Elliot's (1824) and Herschel's (1833) papers, LeConte (1850) observed ice filaments protruding from stems of plants and in fine soils along road sides in Georgia, USA. Observations by LeConte (1850) describe the phenomenon present in dense soils, and observed that needle ice loosens compacted surface material. The phenomenon was observed during the first hours after dawn on clear mornings in early autumn after rainy conditions (LeConte, 1850). LeConte (1850) observed needle ice reoccurring at the same locations under similar environmental conditions, producing soil aggregates on the soil surface. He additionally noted that the ice needles seemingly emerge from within the soil or plants and suggested that soil moisture is crucial to needle ice growth.

After LeConte (1850), a number of authors (e.g Argyll, 1880; Fisher, 1880; Meldola, 1880; Rae, 1880; Paul, 1885; Wetterhan, 1880; Schwalbe, 1884; Woodd Smith, 1884; Pollock and Collier, 1885) studied needle ice growth environments, using the term "peculiar ice forms", providing descriptions of the phenomenon at various locations around England and Switzerland. King (1880) described observations of capillary suction from needle ice growth in chalk from the Southern Downs in south western England. Following the work of King (1880), Schwalbe (1884) grew needle ice experimentally in laboratories showing the effect of capillary suction induced at the surface (Schwalbe, 1884). However, literature detailing the morphology and environmental effects of needle ice growth was lacking until the early 1900's when a Swedish forestry scientist, Henrik Hesselman (1907), published an article describing the destruction of vegetation in swamps.

Hesselman (1907) observed that swamps in northern Sweden often displayed surface disturbance in the form of soil aggregates and limited vegetation. Upon further examination, he noted an uplifted layer by ice needles below the disturbed surface. He sketched ice needle morphology, noting its ability to heave soil and organic material, and described the capillary suction caused by the needle ice creation and was the first to observe the damage of vegetation caused by needle ice. The core attributes of needle ice growth, soil heaving and surface disturbance were further detailed in work by Deckert (1913), Högbom (1914), Beskow (1935), Krumme (1935), Fukuda (1936) and Fujita *et al. (1937)*.

Following the basic establishment of needle ice growth parameters, Gradwell (1957) quantified earlier observations that needle ice displaces soil (LeConte, 1850; Hesselman, 1907; Deckert, 1913; Krumme, 1935). His paper used a new methodology for measuring surface displacement; his results displayed the first assessment of sediment movement rates caused by needle ice. Gradwell's (1957) methodology involved positioning painted stones in a line between two fixed markers and measured individual clast movement at regular time-intervals as they were displaced by needle ice. The method, described as "painted marker movement" (Gradwell, 1957, p801) subsequently became a standard methodology for measuring surface sediment displacement by needle ice and solifluction, and was used in publications by Rapp (1960), Mackay & Mathews (1974a) and Matsuoka (2005).

Independent of Gradwell's (1957) findings, Troll (1944) published a summary of global periglacial conditions, which also described and evaluated sediment transport by needle ice. Although the monograph's main focus was on general periglacial geomorphology, a chapter of Troll's (1944) publication focused on growth, geomorphic effects and spatial distribution of needle ice. He presented results on sediment transport from the Drakensberg of South Africa as well as from Mount Kenya, stressing the importance of understanding sediment transport rates by needle ice and needle ice as a geomorphic agent. Troll (1944) and Gradwell (1957) both proposed needle ice to be significant in the creation of patterned ground features like sorted stripes, polygons and stone filled nets.

An understanding of the basic growth conditions and effects of needle ice was in place by the late 1950s, and subsequent work focused on detailing environmental parameters (temperature, soil moisture, wind speeds) for growth and mechanisms (heave, toppling, rolling, sliding) involved in needle ice induced landscape changes.

2.1 Environmental parameters for needle ice growth

The formation of needle ice is arguably controlled by environmental factors such as moisture availability, temperature and soil surface texture (Troll, 1958). Needle ice can ideally be found in soils with a large component of the fine fraction (less than 0.063mm in diameter), such as silt or loess, in wet environments that experience freezing at night, while not being subjected to snow cover (Gradwell, 1957; Outcalt, 1969; Soons and Greenland, 1970). Locations ideal for needle ice growth are maritime mid- to high-latitude or low-latitude high-altitude areas. Needle ice also influences other parts of the globe on a seasonal basis (Lawler, 1988). Ice needles can grow over a single night to heights of 1-3cm, but have been recorded to grow in excess of 6-8cm during several night-time growths under favourable environmental conditions (Hesselman, 1907; Fujita *et al.*, 1937; Soons and Greenland, 1970; Outcalt, 1971). During freeze days, ice needles will not melt, or only partially melt, during the day, and growth will continue when conditions for growth are again met. Such events have been

recorded to create ice needles in excess of 20cm (Troll, 1944). Establishing growth conditions for needle ice is crucial for understanding its global geomorphic influence (Hesselman, 1907; Fukuda, 1936; Lawler, 1988).

2.1.1 Temperature dynamics for needle ice growth

Needle ice nucleation occurs close to the ground surface when temperatures cross the freezing point (Hesselman, 1907; Troll, 1958; Branson *et al*., 1996). Beskow (1935) showed that for freezing to take place, the freezing rate, overburden pressure and the soil properties are important variables while pressure, geochemistry and cooling rate affect the timing of freezing. Outcalt (1971a) proposed that the surface energy balance was facilitated by an energy exchange between the ground surface and air, the rates of which are controlled by environmental conditions. The rate of heat transport by convective flow, soil conductivity and latent heat release control the possibility of needle ice growth in the near ground surface boundary layer. The surface energy balance for needle ice initiation requires radiative and/or evaporative heat loss at the surface, against soil heat conduction and latent heat release in the soil. Outcalt (1971a) constructed a flow chart for the initiation of needle ice, as well as for continued needle ice growth (Figure 2 in Outcalt, 1971a). His chart showed that for needle ice to grow, the heat loss rate at the surface needed to be greater than the soil heat conductivity and latent heat release to the ground surface, combined. However, the surface-air heat flux cannot be too strong as ice conversion is balanced by the rate of soil moisture supply. If the soil moisture supply was lowered, the energy balance would no longer be counteracted by latent heat release, and the soil freezes instead of the soil water. Hence, needle ice growth is dependent on the relationship between air-surface and soil-surface heat fluxes and moisture connectivity (Outcalt, 1971a).

Wind has been suggested to influence the occurrence and growth of needle ice, as it alters the surface to air and latent heat release fluxes (Outcalt, 1971; Hall, 1979; Holness, 2001; Boelhouwers et al., 2003). Changing the convective heat flow dynamics for the ground surface to air boundary is suggested to alter needle ice initiation temperature, timing of needle ice initiation and ice needle height (Outcalt, 1971a). Historically, needle ice was suggested to grow during calm clear nights where there was an abundance of available moisture (Troll, 1958; Outcalt, 1971). While this still holds true, recent studies (Holness, 2001; Nel and Boelhouwers, 2014) show that needle ice growth may also take place during windy conditions.

2.1.2 Moisture dynamics for needle ice growth

Available soil moisture is crucial to needle ice growth (Branson et al., 1996). Freezing initiates the conversion of liquid moisture to ice at the freezing front, creating a moisture gradient between the sub-surface and the surface (Rempel, 2007). The gradient results in moisture transport by capillary

suction from depth to the freezing front (Schwalbe, 1884; Arakawa, 1966; Outcalt, 1969; Sharp, 1976). For continued growth, moisture needs to be available, and to avoid *in situ* freezing, the supply of moisture has to be sufficiently fast to match the heat loss from radiative cooling with latent heat release from phase transition (Outcalt, 1971a). The dynamics between soil moisture availability and soil textural properties are integral in allowing sufficient moisture transfer, while not losing suction potential across the moisture gradient produced at the freezing front (Fukuda, 1936; Gradwell, 1957; Troll, 1958; Rempel, 2007). Soil moisture availability is argued to be the greatest limiting factor to needle ice growth when basic temperature conditions are met (LeConte, 1850; Hesselman, 1907; Beskow, 1935; Troll, 1958; Higashi and Corte, 1971; Meentemeyer and Zippin, 1981; Branson *et al.*, 1996).

From laboratory work by Branson *et al.* (1996), fluctuations in moisture supply were suggested to explain the process of sediment inclusion in needle ice growth observed by Hesselman (1907), Fukuda (1936), Troll (1944) and Pérez (1993). Typically, clear ice needles grow just below the surface and lift the overlying material normal to the slope. Micro-scale changes in the growing environment that reduced moisture supply can alter growth parameters below threshold values for stable ice needle creation (Branson *et al.,* 1996). Such changes allow the freezing front to descend into the soil column and produce *in situ* freezing. Increases in moisture supply would reinitiate needle ice growth creating a new tier of ice needles growing beneath the new equilibrium plane, uplifting the previous frozen soil column (Branson *et al.,* 1996). The needle ice cluster now incorporates a discrete band of frozen soil into its structure, producing a multi-tiered needle ice column with sediment inclusion (Soons, 1967; Soons and Greenland, 1970; Branson *et al.*, 1996; Grab, 2002a). Sediment inclusion in the needle ice structure was initially observed by Fukuda (1936) and Fujita *et al.* (1937) and later detailed by Outcalt (1969) and Branson *et al.* (1996). Similar inclusions were observed to coincide with fluctuations in heat loss at the surface-air boundary (Outcalt, 1971a; Branson *et al.* 1996). Apart from the heaving of surface material, sediment inclusion allows for additional sediment transport by needle ice.

2.1.3 Textural controls on needle ice growth and needle ice morphology

Beskow (1935) reported on the textural controls of segregation ice growth. He observed that in fine soils the potential for capillary suction was greater than in coarser soils. Additionally, Beskow (1935) saw no suction potential in cobble and block sized material. A significant suction potential entails that fine soils can transport deeper moisture to supply the near surface freezing front, but at a limited throughput. The opposite is true for coarser material. Beskow (1935) produced a fundamental understanding of the dynamics of frost susceptible soil and noted that fine silty soils were perceivably the most frost susceptible, which has been confirmed by various authors since (Lundqvist, 1962; Troll, 1958; Meentemeyer and Zippin, 1981; Pérez, 1987a; Ballantyne, 1996; Matsuoka, 1996).

Empirical work on soil textural controls and needle ice growth was explored by Boelhouwers (1997, 1995), who examined diurnal frost influences at two environmentally similar, but texturally different mountainous sites in southern Africa over a period of five years. Results showed a distinct diurnal frost impact primarily by needle ice at one site, while no surface reworking by frost occurred at the other. Boelhouwers (1997) concluded that surface cover on the site lacking surface disturbance was not frost susceptible and would not produce needle ice, despite climatic conditions being suitable. Limitations resulting from surface texture constraints is also discussed by Troll (1944), Burt (1981), Meentemeyer and Zippin (1981) and Lawler (1988).

2.1.4 Latent heat release and zero-curtain effects

Latent heat release is the expulsion of stored heat in water as a phase-change from liquid to solid occurs (Arakawa, 1966; Outcalt, 1971; Outcalt *et al.*, 1990; Rempel, 2007). The specific latent heat fusion of ice is 334J, meaning that to melt 1 gram of ice into water that much energy needs to be input into the system. Consequently, that amount of energy is released when the water phase shifts into ice as the release of latent heat (Paterson, 1994). In the case of needle ice, as moisture migrates to the freezing front and freezes, a constant supply of released latent heat hinders the freezing front from descending further into the soil column. The energy balance between surface radiative cooling and energy input from latent heat release determines the occurrence/rate of needle ice growth and ground freezing. A strong radiative heat flux at the surface, with an ample supply of soil moisture, produces fast growing needle ice, as the latent heat release flux is proportional to the amount of ice generated (Outcalt, 1971; Rempel, 2007). Release of latent heat during needle ice growth is integrally connected to the "zero curtain" effect (Outcalt, 1990).

The term "zero curtain" is an ambiguous term relating to a state of constant temperature during the release of latent heat (Outcalt, 1990). Definitions of the term differ between authors. Descriptions include describing a zone or region, a soil layer, a freezing boundary or a time lag (Sumgin *et al.*, 1940; Muller, 1947; Washburn, 1973; Harlan and Nixon, 1978; Johnston, 1981; French and Harbor, 2013). The term has mostly been applied to large scale seasonal melting of permafrost (French and Harbor, 2013). However, in this thesis, a "zero curtain effect" is used to describe the diurnal effect relating to night-time stagnation of soil temperatures within the soil column during needle ice growth.

Walton (1982) observed isothermal temperatures or a "zero curtain" in temperature measurements during melting of ground ice from sub-Antarctic Signy Island while Outcalt *et al.* (1990) recorded non-fluctuating surface temperatures at the freezing boundary at the onset of freeze in an Alaskan study. Resulting from the release of latent heat during phase transition, Outcalt *et al.* (1990) observed a time lag between the initial freezing and sub-surface freezing on both a diurnal and

seasonal scale. The effect results in surface temperatures being able to decrease well below 0°C, without the freezing front penetrating to depth. Outcalt *et al.* (1990) only observed the effect while a continuous supply of moisture to the freezing front was available. "Zero-curtain effects" are proposed to be dependent on moisture supply and freezing rate, but currently few detailed studies on the phenomenon have been published (Walton, 1982; Outcalt *et al.*, 1990; Hinkel *et al.*, 2001; Boelhouwers, 2003).

2.1.5 Summary

Current research lacks more extensive field observations of temperature, soil moisture, wind speed and their relation to needle ice initiation, melt, duration and heave. Surface heat fluxes and moisture migration have been experimentally and theoretically investigated; however, very few empirical studies have measured and observed these variables in natural environments. This thesis aims to contribute to the understanding of needle ice growth environments by studying and determining the initiation temperature and timing of the phenomenon. In addition, temperature and moisture fluxes and their relation to textural and wind influence will be studied. Results on environmental monitoring aim to assess Objectives 1, 2 and 3 stated in Chapter 1.

2.2 Needle ice as a geomorphic agent

Geomorphological effects induced by needle ice are presented in work by Hesselman (1907), Schubert (1973), Mackay and Mathews (1974a), Pérez (1992), Grab (2002) Boelhouwers *et al. (2003),* Butler *et al.* (2004), Holness (2004), Haussmann (2009) and Hedding *et al.* (2015). Both biological and physical changes, and a combination of the two, are exerted by needle ice on its surroundings. Also, strong feedback mechanisms are linked to the expansion of needle ice influenced ground. The following sections will present work on landscape changes induced by needle ice and related processes.

2.2.1 Vegetation destruction by needle ice

Hesselman (1907) investigated the influence of diurnal frost on vegetation, vegetation growth and vegetation stability. He worked on swamps and mires in northern Sweden where he observed non-vegetated open areas in otherwise forested environments. The aim of Hesselman's (1907) study was to evaluate the conversion of mires to woodlands for commercial use, and it was commissioned by Swedish commercial forestry companies. Results showed that sown or planted seedlings were being heaved out of the soil. He concluded that reworking by needle ice was the most likely reason why areas were not able to produce fully grown trees. Hesselman (1907) provided the first observational evidence of vegetation change induced by needle ice, which Goulet (1995) later qualitatively and quantitatively showed by investigating needle ice and frost heaving on seedling mortality in Scandinavia.

In areas where vegetative cover is stable, physical factors can alter vegetation stability to enable needle ice growth. Such surface altering processes include turf-exfoliation, erosion and trampling by animals (zoogeomorphology). The term turf-exfoliation was minted in Troll (1973) from Iceland and is discussed in Pérez (1992), Pérez (1993), Grab (2002), Boelhouwers *et al.* (2003) and Butler (2004). The impact of animals has been noted to be synergistic with needle ice in altering the landscape in several publications, including Pérez (1993), Holness (2001), Boelhouwers *et al.* (2003), Le Roux *et al.* (2005), Haussmann *et al.* (2009), Eriksson (2011) and Borg (2012).

Turf-exfoliation is the processes of vegetation destruction by the soil removing and reworking processes of predominately needle ice (Pérez, 1992). The process is active in periglacial areas that experience frequent freeze-thaw cycles and has been studied in the Venezuelan Andes by Pérez (1992, 1993), in the Drakensberg of South Africa by Grab (2002), on Marion Island by Boelhouwers *et al.* (2003) and in Glacier National Park in the USA by Butler (2004). Material is excavated from the margins of ground depressions or terraces by needle ice growth, and is subsequently displaced by aeolian deflation or by surface wash (Troll, 1944; Grab, 2002a; Boelhouwers *et al.*, 2003). Pérez (1992) quantified the volume of material eroded by turf-exfoliation over a 10-year period from the Piedras Blancas in Venezuela. His results showed that relatively small amounts of material were removed from the system by turf-exfoliation, although a change in vegetation cover did occur. Vegetation destruction by turf-exfoliation was further detailed in publications by Troll (1944), Gradwell (1955), Hastenrath (1977), Pérez (1987), Grab (2002) and Boelhouwers *et al.* (2003).

Pérez (1993) studied cattle trampling in the Venezuelan highlands as an enabling process for needle ice to affect previously vegetated ground. He showed that herds of cattle disrupt the vegetation carpet and allowed turf-exfoliation by physical ground frost processes to rework and enlarge areas of exposed soil. Pérez (1993) concluded that cattle trampling will most likely not lead to total destruction of the vegetation carpet in the Piedras Blancas, but that the impact on soil erosion rates and soil degradation was significant.

On Marion Island in the southern Indian Ocean, Eriksson (2011) studied the geomorphological impact of invasive house mouse populations on Sub-Antarctic vegetation. He observed that grazing and trampling on the islands biota by mice allowed frost processes to commence and alter the micro-topography around the cushion plant *Azorella Selago*. Eriksson's (2011) results showed that mice are an added contributor to the degradation of *A. Selago* cushions previously documented by Haussmann (2009a; 2009b). Degradation of *A. Selago* impacts vegetation banked terraces, which are forms created when cushions obstructed material moved downslope by solifluction and/or needle ice displacement (Holness, 2001; Boelhouwers et al., 2003; Le Roux et al., 2005; Haussmann et al., 2009b). Destruction

of these vegetation banked terraces by needle ice has been documented by Haussmann (2009b), and may alter bank stability and local geomorphology.

Borg (2012) studied the influence of diurnal frost on ground vegetation cover in the Drakensberg of southern Africa and in the Abisko mountains of northern Sweden. Results from the analysis showed that along a 650m transect in the Drakensberg, the majority of slope surfaces were influenced by needle ice growth (64% of the South facing and 52% of the North facing). Areas affected by heavy grazing and trampling by livestock were increasingly influenced by needle ice, and displayed the lowest vegetation density. Borg (2012) argued that diurnal frost processes hinder vegetation growth in the trampled and over-grazed areas by further reworking of the soil where needle ice initiation was possible. Borg (2012) as well as Pérez (1992; 1993), Haussmann (2009) and Eriksson (2011) noted a dependency relationship between animal influence and needle ice growth. Observations showed that where animal burrowing and trampling created surfaces conductive to needle ice growth, increased surface erosion rates and soil/vegetation degradation was seen.

2.2.2 Summary

Needle ice as an active geomorphic agent was seen to destroy vegetation and alter surfaces for secondary geomorphic change by the process of wind deflation and surface runoff. In combination with the influence of animals, vegetation stability was seen to be affected. The current understanding of needle ice influence of vegetation is, however, based on indirect observations of change over a relatively short period of time (Haussmann et al., 2009b; Eriksson, 2011). No long term visual study of the breakdown of vegetation by needle ice is available. This thesis aims to provide visual evidence of the physical influence on vegetation by needle ice in addition to zoogeomorphological influence. Results aim to assess Objective 5 from Chapter 1.

2.3 Pattered ground formation

Patterned ground formations are often seen in areas influenced by needle ice (Gradwell, 1957; Lundqvist, 1962; Grab, 1997; Boelhouwers, 1991; Hinkel *et al.*, 2001). In periglacial areas somewhat symmetrical forms of circles, polygons, nets, steps and stripes are created by a combination of processes relating to frost action (French and Harbor, 2013). These patterns emerge on ground surfaces that experience frequent freeze-thaw cycles and, depending on the process active (needle ice, frost wedging, thermal contraction cracking) and local environmental parameters, create a range of patterned ground features. Processes of patterned ground formation occur on time-scales that range from seasonal to catastrophic (French and Harbor, 2013). This thesis, however, focuses on formations occurring in a diurnal frost environment.

Sorting of surface material is evident both in deep and surficial freezing and can involve distinctly different processes (Krantz, 1990; Grab, 1997; Van Vliet-Lanoë, 1998; French and Harbor, 2013). The process of expulsion of larger clasts from deep freezing by free convection was proposed in Krantz (1990). He determined water density differences during freezing and thawing to produce convection cells that expelled large clasts from the soil matrix through frost-pull mechanisms. However, similar forms are created by surficial sorting by needle ice (Mackay and Mathews, 1974a; Hallet and Prestrud, 1986; Boelhouwers, 1995), suggesting that observably similar features can have different modes of genesis (Grab, 2002).

Patterned ground is a common occurrence in periglacial areas and is documented in Canada (Mackay and Mathews, 1974b), Sweden (Lundqvist, 1962), Scotland (Ballantyne, 1996), Tibet (Wang and French, 1994), South Africa (Boelhouwers and Meiklejohn, 2002; Sumner, 2004), Sub-Antarctic Islands (Frenot et al., 1995; Holness, 2001; Selkirk-Bell and Selkirk, 2013), Venezuela (Pérez, 1992a), and several other locations across the world (Soons, 1967; Outcalt, 1969; Beaty, 1974; Meentemeyer and Zippin, 1980; Noguchi *et al*., 1987; Boelhouwers, 1997; Matsuoka, 2005). The origin of different patterned ground forms is said to be controlled by the interaction between environmental properties (temperature, wind speeds, soil moisture availability) and specific active processes (e.g. sorting by needle ice displacement, deflation, frost pull) noted by Gradwell (1957), and further detailed in Lundqvist (1962), Hall (1971) and Noguchi *et al.* (1987).

Patterned ground can be used as diagnostic tools for understanding soil frost processes active in a specific region. Additionally, relict or inactive forms can be used to diagnose a change in past climatic conditions and may reveal periods of inactivity (Washburn, 1970; French and Harbor, 2013). Recent advances in technology have allowed for computer modelling to increase the understanding of patterned ground features and their formation *(Kessler et al., 2001; Plug and Werner, 2002; Walker et al.*, 2008).

2.3.1 Needle ice induced patterned ground formations

Needle ice is an active process and was observed early by Troll (1934) to be a mechanisms for the creation of striated ground features. Subsequently, needle ice has been observed by several authors to be important in the creation of pattered ground formations, such as sorted stripes (Gradwell, 1957; Lundqvist, 1962; Pérez, 1992a; Ballantyne, 1996; Grab, 2002b; Sumner, 2004). Gradwell (1944) proposed that needle ice displacement fills the margins of polygonal shrinkage crack features with small stones in the periglacially active New Zealand Alps. Similarly, Ballantyne (1996) observes the same shallow freezing, surface displacement and concentration of larger clasts by preferential frost heave to the margins of upheaved domes near sea-level in Scotland. He also notes that the formation

of patterned features by needle ice are generated quickly, in the order of a few frost cycles, which was also noted by Hastenrath (1976) and Pérez (1984).

On sub-Antarctic Marion Island, Holness (2001) found needle ice activity to be responsible for the formation of sorted stripes. His results showed strong vertical and lateral sorting of the slope material which are indicative of active frost processes. Holness (2001) proposes that needle ice activity at his study sites was the dominant slope process in moving sediment and creating landforms. In addition, Holness (2001) showed that clast size impacts sediment displacement distance. He measured displacement within clasts size categories of 16-32mm, 32-64mm, 40-60mm and 50-80mm, showing from over 2300 clasts monitored that surface sediment movement was faster in the finer material.

2.3.2 Wind in relation to patterned ground formation

Troll (1944) describes what he called "wind-striped frost-heaved soil" from the Drakensberg of South Africa and from Mount Kenya. He defined the origin of these stripes to be distinctly different from striped ground orientated along slope gradient. Wind-striped frost-heaved soil patterns were noted as being oriented along the prevailing wind direction and were seen to cut diagonally across sloping mountain sides. Hall (1979) described similar features from Marion and Kerguelen Island, with horizontal surfaces on both islands displaying clear striping along the prevailing wind direction.

Contrary to Troll's (1944) and Hall's (1979) proposed processes for stripe origin, Mackay and Mathews (1974b) describe another process for the creation of sorted stripes from British Columbia and New Zealand. They observed stripes in the New Zealand Alps with a preferential orientation related to the position of the sun, arguing that shadows cast by the sun in the early hours induce differential thaw, which aligned the collapse of ice needles, and their included sediment, with the suns position. From observations on orientation of sorted stripes on Marion Island and Kerguelen Island, Hall (1979) deemed it unlikely that the main influence on studied stripe alignment on Sub-Antarctic islands was due to angle of incoming radiation. Sub-Antarctic islands receive a limited amount of daily incoming radiation due to their almost constant cloud cover, which doubtfully would be able to produce clear striping in the manner described by Mackay and Mathews (1974b).

Wind as a controlling factor on oriented sorted stripes formation was also examined by Holness (2001) from Marion Island. He did not provide a mechanism for stripe creation but observed a preferential downslope alignment of stripes alongside a tendency to be more pronounced on windward slopes. Similarly, Kiernan and McConnell (2008) described terraces and sorted ground being aligned to the dominant wind direction on Heard Island in the Southern Indian Ocean, however, no in depth analysis was done.

Unlike previous authors Walton and Heilbronn (1984), Pérez (1992), Grab (1996) and Boelhouwers (1995; 1998) found no correlation between wind direction and stripe orientation at their respective study sites, but found stripes to be aligned down the maximum slope gradient.

2.3.3 Summary

Patterned ground formation in active needle ice environments is suggested to be a self-organizing system where water density differences drive frost-pull, expelling larger rocks and producing internal sorting of material (Krantz, 1990). However, surficial sorting by needle ice acting by different processes on clasts sizes or a combination of the two are as well suggested to account for surface sorting (Mackay and Mathews 1974a; Pérez, 1991). In addition, wind and slope angle are suggested to influence the formation of patterned ground features in a needle ice active area (Troll, 1944). This thesis aims to display needle ice movement based on particle sizes and analyse the occurrence of patterned ground features of the study sites see Objective 5 from Chapter 1.

2.4 Needle ice sediment displacement

Patterned ground formations are produced by needle ice's ability to heave material. The following sections will present work on needle ice heave and related sediment displacement.

Heaving of material by needle ice, together with the incorporation of soil into its structure, has initiated questions regarding sediment transport rates by the needle ice (Fukuda, 1936; Troll, 1958; Soons and Rainer, 1968). Ice needles can lift pebble sized surface material several centimetres creating a thin layer of uplifted debris, while incorporating finer material into its base structure forming a sharp boundary between the reworked material and the usually more densely packed substrate (Outcalt 1971; Lawler 1993; Branson *et al.* 1996).

2.4.1 Initial observations on needle ice sediment displacement

The ability of needle ice to rework and displace sediment was documented early by Von Richthofen (1901), who observed heaving of soil clasts, which were subsequently redistributed during melt. Von Richthofen (1901) noted enhanced soil displacement on sloping surfaces. The mechanisms of heaving and subsequent resettling of clasts were reported by Davison (1889), Hesselman (1907), Deckert (1914) and Fukuda (1935), and are considered core processes in sediment transport by needle ice. Clasts are heaved normal to the freezing plane, which is usually aligned with the slope of the surface (Lawler, 1993). Subsequent melting of ice needles resettles clasts along the gravitational gradient, which may induce downslope displacement (Outcalt 1971; Mackay and Mathews 1974a; b). Apart from displacement by gravitational resettling, several authors propose other mechanisms, including toppling, rolling, tumbling, bouncing, and sliding to produce additional movement of clasts uplifted by

needle ice (Von Richthofen, 1901; Deckert, 1913; Gradwell, 1957; Troll, 1958; Soons and Greenland, 1970; Mackay and Mathews, 1974b; Washburn, 1979; Meentemeyer and Zippin, 1980; Pérez, 1987b; Lawler, 1989; Embleton, 1992; Lawler, 1993; Matsuoka, 1996; 1998; 2005). Authors similarly suggest that downslope movement of these additional mechanisms is enhanced on steeper sloping surfaces (e.g. Mackay and Mathews, 1974b; Pérez, 1987b; Matsuoka, 1998; 2005). Rolling of clasts down slope during melt of needle ice was observed in the Appalachian Mountains (Deckert, 1913) and the Japanese Alps (Matsuoka, 1998). Matsuoka (1998) recorded an increase in displacement by diurnal frost processes by an order of magnitude when comparing a 14° to a 30° slope. He proposes that bending of ice needles produces a rotational component during melt, causing additional downslope movement by rolling of clasts. Pérez (1987) describes failure of chunks of needle ice at steep sections of slope during ablation from the Piedras Blancas in Venezuela, observing that particles supported by single ice needles bounce and roll during melt alongside clusters of needle ice supporting larger amounts of sediment sliding over denser substrate.

2.4.2 Displacement mechanisms

Core mechanisms of sediment transport by needle ice were described by Hesselman (1907), Troll (1958) and Outcalt (1971) and further detailed by Lawler (1993) from the Ilston river valley in the UK. Lawler (1993) described river bank erosion by the effects of needle ice and measured micro-topography, rates and amounts of sediment moved during a two-year study. His paper proposed four mechanisms for sediment movement, two previously undocumented, by the effects of needle ice:

- *Direct particle fall* – Movement of clasts heaved normally to the sloping surface and resettled along the gravitational gradient;
- *Sediment-laden rivulets* – Melting of ice needles incorporating flow of sediment from the top or bottom of the needle ice cluster;
- *Needle ice sliding failure* – Cluster or chunk of combined ice needles sliding down slope by basal lubrication;
- *Needle ice toppling failure* – Weakening of ice needle structure during melt causing sediment movement by toppling;

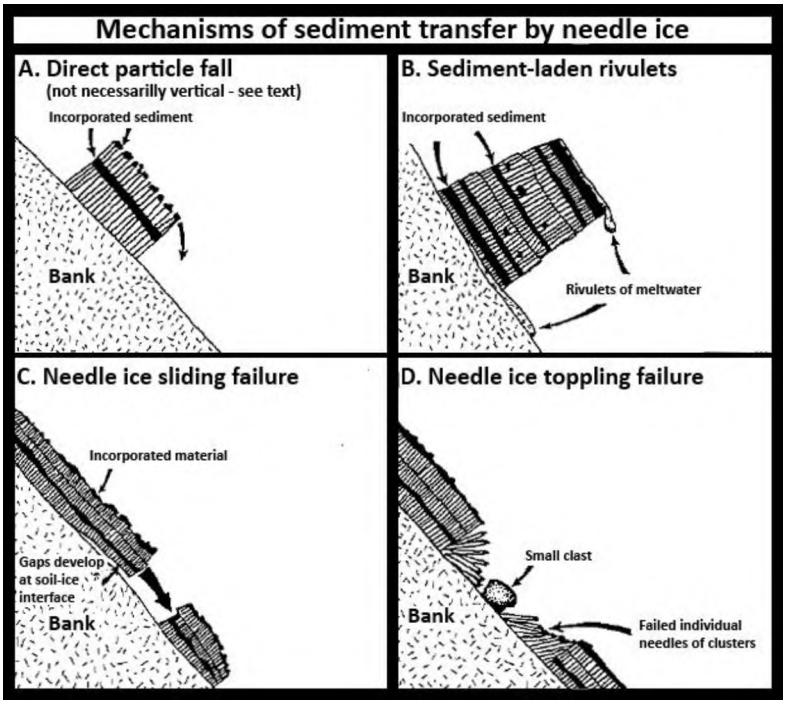

Figure 2.1. Mechanisms involved in sediment transport by needle ice on steep slopes (after Lawler, 1993). Reprinted with permission from John Wiley and sons License (Feb 2, 2016)

Lawler (1993) displayed unique data on the geomorphological effects of needle ice and qualitatively and semi-quantitatively (Lawler, 1993, p109) showed the influence of needle ice in erosion and sediment transport. He did not propose any quantitative ways of measuring the contribution of each of the displacement mechanisms, or provide a model for predicting sediment transport. Lawler (1993) acknowledged the fact that quantification of needle ice displacement was of importance and stresses the significance of further research in this area.

Since Lawler (1993), no substantial work has been undertaken to produce a better understanding of mechanisms responsible for slope movement by needle ice, although a noteworthy number of authors in the field have observed toppling, rolling, sliding and tumbling of clasts (e.g. Von Richthofen, 1901; Deckert, 1913; Gradwell, 1957; Troll, 1958; Soons and Greenland, 1970; Mackay and Mathews, 1974b; Washburn, 1979; Meentemeyer and Zippin, 1980; Pérez, 1987b; Lawler, 1989; Embleton, 1992; Lawler, 1993; Matsuoka, 1996; 1998; 2005).

2.4.3 Modelling transport rates by needle ice

Following Gradwell's (1957) measurements of sediment movement by needle ice, Higashi and Corte (1971) conducted laboratory work with the aim of distinguishing the effects of frost creep and gelifluction from that of needle ice induced movement. Their experiment took place in an insulated box where soil moisture, slope angle and temperature could be carefully controlled. Air temperatures were lowered at a rate of 2-5°C per day and heaving height and the depth of the 0°C isotherms were

measured. The effect of soil movement by frost creep, gelifluction and needle ice creep were recorded and the experiment repeated on different slope angles. Results of Higashi and Corte's (1971) experiment presented needle ice as a fast-moving surface sediment movement process and suggested, like Gradwell (1957), that slope angle has a profound impact on the distance sediment is displaced. The above authors initially hypothesized that the distance travelled by sediment affected by needle ice creep, would be proportional to the tangent of the slope. Melting, and thus weakening of the ice needles showed that the crystals tend to bend producing movement (D) more closely described by the height of segregated ice times the tangent of the slope angle (α) squared (Equation 1) (Higashi and Cortes, 1971). Higashi and Corte (1971) are however vague in producing a model for calculating displacement.

$$D = H \tan^2 \alpha \qquad (1)$$

In line with earlier observations of Fukuda (1936) and Troll (1944), Higashi and Corte (1971) concluded that there are additional mechanisms involved in needle ice affected soil movement (rolling, bouncing and basal slipping), which have profound influences on final soil displacement. Higashi and Corte (1971) argued that these mechanisms could not be included in the model as they were not sufficiently studied and hard to quantify.

The effects of periglacial processes inducing movement within sorted stripes on a cinder cone in British Columbia were examined by Mackay and Mathews (1974a). They proposed that a majority of the measured soil movement produced on the cinder cone was by the effects of needle ice. Results showed frequent uplift and settling of material generating downslope movement at rates much quicker than that of gelifluction or solifluction alone. Mackay and Mathews (1974a) proposed a model of needle ice induced movement (D) that describe the movement due to gravity settling as proportional to the height of the needle ice crystal (H) times the tangent of the slope angle (α) (Equation 2).

$$D = H \tan \alpha \qquad (2)$$

Mackay and Mathews (1974a) note, that they were not able to include additional physical mechanisms apart from resettling by gravity for similar reasons as Higashi and Corte (1971), even suggesting that resettling by gravity and slope angle might not even be the most significant process in producing downslope movement. They proposed that the actual average movement of particles could possibly more resemble Equation 3, below, than Equation 2 on some slopes.

$$D = H \qquad (3)$$

D describes displacement and H heave, suggesting that the most prominent process of sediment movement is produced by toppling of ice needles.

Following Equation 1), 2) and 3), Matsuoka (1998) aimed to develop a more reliable sediment movement model by analysing three years of soil movement data from alpine slopes in the Japanese Alps. His work incorporated both manual (painted stones) an automatic (strain probe) measurements of downslope movement with the goal of predicting movement based on measured heave. Matsuoka (1998) used the model developed by Mackay and Mathews (1974a) as a foundation, but further developed it by the incorporation of summarized annual heave (cumulative frost heave [∑H]) multiplied by the tangent of the slope angle (α) and produces annual potential frost creep (PFC) (Equation 4).

$$PFC = \sum H \tan \alpha \qquad (4)$$

Compared with empirical data, Matsuoka (1998) suggested that Equation 4 considerably underestimated sediment movement on steep slopes (30°) while somewhat overestimated sediment movement on gentler (14°) slopes.

Further developing his periglacial modelling work, Matsuoka (2005) interpreted and described long term ground climate monitoring over ten years at two sites within seasonally periglacial/alpine environments in the Swiss and Japanese Alps. Both manual and automatic measurements of heave, temperature, strain and moisture were used to identify trends and internal dynamics of the mountain slope system. Calculating PFC using Equation 4 showed that at three out of four sites the PFC model overestimated the amount of sediment transported while at one site it was underestimated. Matsuoka (2005) noted that results from using the PFC model only indicated whether needle ice was a major contributor in producing downslope movement. He outlined the shortcomings of the model and attempted to increase its accuracy by breaking down H (heave) into more basic components of N (number of frost heave cycles), T (total thickness of frost susceptible soil within the top 15cm of soil) and SC (frost susceptibility by silt and clay content) (Matsuoka, 1998). Displacement (D) was calculated by inserting the new sub-components into Equation 4 while aligning the model using empirically measured local data, creating Equation 5:

$$D = 1.14\ N\ D\ SC \tan^2 \alpha \qquad (5)$$

Incorporation of surface texture as a component in sediment movement by needle ice is an important step to improve sediment movement modelling, but Matsuoka (2005) realized the inherent problems of making the model too site specific by using empirically measured data, as local environmental factors may vary significantly between locations.

2.4.4 Summary

The understanding of needle ice sediment displacement is severely hindered by a lack of knowledge on sediment movement mechanisms active in displacing clasts by needle ice. Although, Higashi and Corte (1971), Mackay and Mathews (1974a), Lawler (1993), Matsuoka (1998), Matsuoka (2005) and Matsuoka (2014) all propose mechanisms of sediment movement, there is still a great uncertainty on which mechanisms are active, how they are augmented by slope angle and how they displace sediment. This thesis aims to visually observe movement of sediment in addition to mechanisms involved in sediment displacement by needle ice, answering Objectives 2 and 4 from Chapter 1.

2.5 Current methodologies for needle ice sediment displacement

In reviewing past literature, notable shortcomings in the methodologies previously used become apparent. Current literature, apart from Matsuoka (2014) and Ueno *et al*. (2015), exclusively use non-direct observation methods to measure displacement by needle ice. To clarify, these methods do not actively and perceivably measure movement. Instead, movement is inferred as the total displacement of recognizable surface clasts over a set time period, often months. Identifying whether the total displacement was achieved during a single "catastrophic" event or gradually over longer time periods, is often not possible using these methodologies. The impact of surface disturbance by weather and animal influence, and their contribution to measured displacement also remains unknown (Eriksson, 2011; Hall et al., 1999; Haussmann Boelhouwers, et al., 2009; Pérez, 1987; Pérez, 1993). Surface movement by the effects of trampling, but also digging and burrowing by animals are often not considered in the context of needle ice sediment movement.

The following sections will detail and evaluate currently used methods of measuring needle ice displacement and processes involved in related movement, while outlining uses and limitations of these methodologies.

2.5.1 Painted marker movement

The most commonly used method for analysing sediment movement by needle ice, and other periglacial processes, is the measurement of movement by painted markers. Initially used by Gradwell (1957), the concept of its use is simple. Position clearly marked clasts in a pre-determined pattern along a baseline and measure deformation of the set pattern. This will in addition to total displacement, display variability along the baseline. The markers for the baseline need to be firmly anchored in the substrate to not be affected by the process they intend to measure. The use of painted markers is appropriate at time scales from a few months (Ballantyne, 1996) to years (Matsuoka, 2005). Clast size of painted markers should be similar to the moved material by the process studied. Extensive use of painted markers is seen in literature (e.g. Soons, 1967; Soons and Rainer, 1968; Mackay &

Mathews, 1974a; Pérez, 1987; Pérez, 1988; Pérez, 1992a; Matsuoka, 1998; 2005; Ballantyne 2013; Matsuoka 2014).

Figure 2.2. Painted stone lines as reference for deformation.

2.5.1.1 Advantages/drawbacks of painted marker use

The advantages of using painted markers to measure sediment transport are that they are easy to use, affordable and an effective solution in a periglacial setting (Gradwell, 1957; Pérez 1992a). Environmental impacts are minimal and if parent material is used as the marker no alien materials, foreign shapes/sizes alter the slope characteristics impacting movement. Spray-painted lines are often used to fully remove reworking of parent material and, hence, do not introduce an initial disturbance changing the setting for movement (Matsuoka, 2014).

Limitations discussed in published literature on the use of painted markers are often related to non-recovery. This is highlighted in work by Pérez (1987; 1988) where he lost almost 30% of deposited markers. Pérez (1987) argued that the loss of markers could result from the burying of clasts by snow creep, deflation, small debris flows and animal influence. However, conclusions on which processes are most influential are mostly speculative. His work indicated the main issue with the use of painted markers was the inherit uncertainty of movement. Many processes influence clast displacement and single events, like cattle trampling, or a sudden mud flow, can produce displacement distances orders of magnitude greater than needle ice. Pérez (1987), as well as Mackay and Mathews (1974a), show considerable variability in displacement between individual clasts ranging between two orders of magnitude. Identifying the reason for such a discrepancy is not possible with the use of painted markers.

2.5.2 Erosion pin measurements

Erosion pins can be used for measuring the retreat of banks of rivers, turf-exfoliation hollows/terraces and similar surfaces which are regularly exposed and affected by diurnal frost (Pérez, 1992b; Lawler, 1993; Selkirk-Bell and Selkirk, 2013). Insertion of pins can be done either vertically or horizontally. However, in terms of needle ice erosion horizontal insertion may be preferable as measuring bank

retreat rates is of most interest. Unlike painted markers, erosion pin monitoring focuses on amounts of material displaced and less on displacement distance. Studies using erosion pins to specifically measure needle ice displacement were undertaken by Pérez (1992b), Lawler (1993) and Grab (2002b).

2.5.2.1 Advantages/drawbacks of using erosion pins

Similar to the use of painted markers the use of erosion pins is an easy, affordable way of attaining estimations of sediment movement amounts from areas experiencing diurnal freezing and needle ice (Lawler, 1993). Systematic positioning of pins can also reveal local variations of sediment removal rates from the studied terrace or bank, identifying intensity differences of the process.

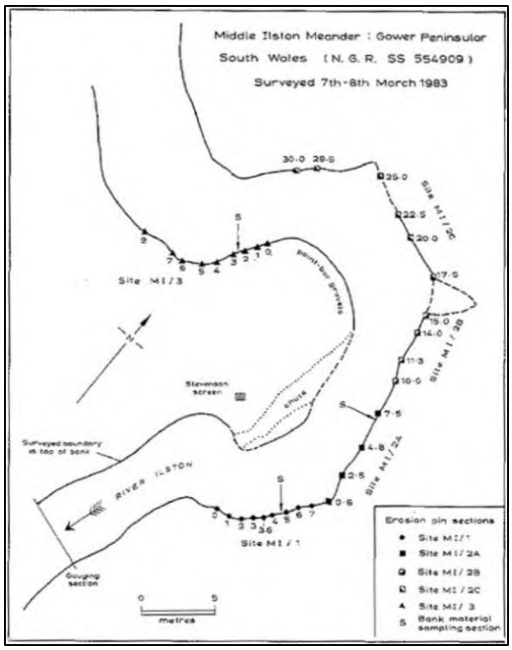

Figure 2.3. Lawler's (1993) erosion pin setup at the river Ilston. Used with permission from John Wiley and sons License (Feb 2, 2016)

Figure 2.4. Erosion pin installed in a river bank (Alamakee County, 2015)

Limiting the use of erosion pins is the accuracy achieved (Grab, 2002). The measurements undertaken provide no conclusions on the processes active in producing seen retreat. Hence, measuring the volume of soil material removed may indicate the general erosional regime, but it does not specifically quantify erosion by needle ice. The influence of rain, wind and animal burrowing on bank erosion is, similar to painted marker loss, hard to reliably quantify (Pérez, 1992). Additionally, alterations to bank stability and susceptibility to environmental factors are induced while inserting the, often metal, rods into the studied bank (Lawler, 1993).

2.5.3 Strain gauges

Strain on the soil column exerted by frost action is connected to the long-term movement of solifluction or gelifluction and not to surficial needle ice movement (Matsuoka, 2005). It was suggested by Ballantyne (2013) in a long-term study (35 years), that needle ice movement induces rates orders

of magnitude faster than those of solifluction and gelifluction. Strain gauges measure the deformation of the soil by mentioned slow processes but do not accurately measure shallow displacement by needle ice, and will thereby not be considered in this thesis (Matsuoka, 2005).

2.5.4 Time-lapse photography

Using imagery as a way to capturing displacement and deformation is a non-invasive method only adopted recently (Matsuoka, 2014; Ueno *et al.*, 2015). Using visual evidence as a way of determining processes, mechanisms and digital measuring of surface movement instead of relying on inferred evidence and the use of tape measures, is a new concept. Coupled with environmental data, pictures can be used to solidify thresholds and limitations previously only suggested. Imagery can be applied at various temporal scales focusing on small scale events or long term deformation. Images do not alter the study area and has no perceivable impact on surface movement.

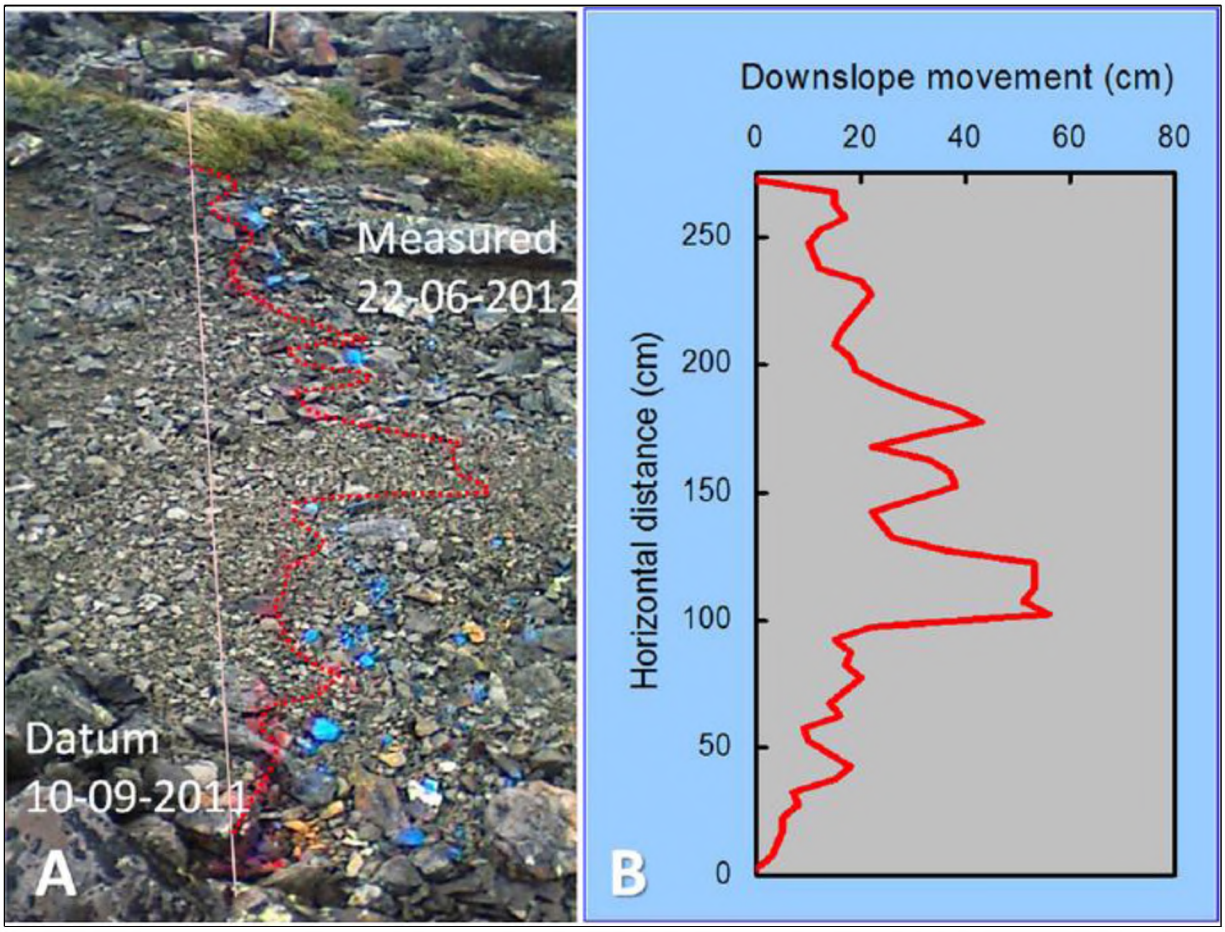

Figure 2.5. Painted line deformation seen by 7 months of frost activity (Matsuoka 2014). Used with permission from John Wiley and sons License (Dec 5, 2016)

The use of photography to measure needle ice movement was applied by Matsuoka (2014). He visually documented the movement of a painted line in a periglacially active mountainous area, using imagery to monitor its deformation of over a study period of 5 years. Preferential deformation and

"catastrophic" events of sediment displacement were noted (Matsuoka, 2014). The camera setup used by Matsuoka (2014) took three images daily at 08.00, 12.00 and 16.00 during the study period creating a time-lapse of deformation taken place.

2.5.4.1 Advantages/drawbacks of using Time lapse photography

The most notable advantage of using photography is reliability of the image. Methods not involving direct measurements tend to draw conclusions based on assumptions between process and end result. While, depending on interval of imagery, the uncertainty can be greatly reduced using repeat photography. As seen in Matsuoka (2014) the use of repeat photography can be used on a time scale sufficient to monitor seasonal deformation. A substantial increase in photograph frequency would allow for monitoring of other aspects of needle ice growth/decay including mechanisms involved in movement and needle ice growth initiation setting.

Repeat photography can be used as a complement to all other methodologies of study while drawbacks to its use are few. However, the use of cameras is relatively expensive and require regular maintenance and support. Weather conditions can reduce the clarity and resolution of the imagery and night-time illumination can be difficult to implement.

2.5.5 Summary

Analysis of small scale variability in needle ice growth and melting is still limited by data collected using current methodologies. A majority of authors working with sediment displacement by needle ice repeatedly suggest that additional mechanisms (toppling, rolling, bouncing and sliding) apart from slope gradient and heave height play an important role in creating displacement (Von Richthofen, 1901; Deckert, 1913; Gradwell, 1957; Troll, 1958; Soons and Greenland, 1970; Mackay and Mathews, 1974a; Washburn, 1979; Meentemeyer and Zippin, 1980; Pérez, 1987; Lawler, 1989; Embleton, 1992; Lawler, 1993; Matsuoka, 1996; 1998; 2005). However, the impact of these mechanisms has not been quantified and visual observation of these mechanisms moving material is lacking. This thesis aims to use time lapse photography to visually analyse growth and melt dynamics, in addition to mechanisms of sediment movement by needle ice, assessing Objectives 1-5.

2.6 Academic problem

One problem in current needle ice research is that the temperature and soil moisture dynamics of needle ice growth have not been sufficiently studied in the field. In addition, sediment movement modelling by needle ice is currently limited by an uncertainty of which mechanisms are involved in movement, how they move sediment and which environmental parameters (slope angle, surface texture, soil moisture, wind) impact sediment displacement. This thesis aims to use environmental

monitoring and time-lapse photography to analyse initiation temperature of needle ice as well as active sediment movement mechanisms during needle ice ablation. For accurate measuring of sediment displacement, a combination of methodologies seen in section 2.5.1 and 2.5.5 will be incorporated. Chapter 1 displays objectives for answering said aims using visual and environmental monitoring, while the following chapter (Chapter 3) will present the study setting in which needle ice growth was monitored.

Chapter 3 – Environmental setting

To assess aims and objectives from Chapter 1, the literature review in Chapter 2 outlines the need for study locations to be influenced by frequent needle ice activity. Hence, the following chapter will present the two study locations favourable for needle ice growth used in this study.

Outside of the Antarctic regions in the Southern Hemisphere, periglacial activity is generally only seasonal, and potential study areas are often inaccessible. Preferred sites include, either high-latitude maritime, or high-altitude sub-tropical/tropical locations, where diurnal freeze-thaw cycles are in abundance (Lawler, 1988). At high latitudes (over 70°N in the Northern Hemisphere and over 40°S in the Southern Hemisphere), annual average temperature is generally low (Lawler, 1988), and especially in continental locations (e.g. Siberia) (Shulgina *et al*., 2009), snow and long term freezing inhibit needle ice growth, making them unsuitable for study. However, in maritime conditions, a buffering effect induced by a surrounding ocean, produce only night-time freezing that is ideal for needle ice growth when ambient temperatures are within a few degrees of 0°C. Locations experiencing temperature buffering allows for frequent freeze-thaw cycles, include the maritime sub-Arctic and sub-Antarctic (Arnalds *et al*., 1987; Lawler, 1988; Holness, 2001; Ólafsdóttir and Guòmundsson, 2002; Boelhouwers *et al*., 2003).

Additional needle ice prone areas include high-altitude, low latitude locations. Elevated low-latitude locations experience the opposite of temperature buffering seen at maritime locations. Instead of a buffering effect from a large body of water, such areas show large temperature ranges, nocturnal freezing and daytime temperatures well above freezing, particularly well-suited for needle ice growth (Lawler, 1988).

Based on aforementioned prerequisites and limitations, two locations were identified as being the most suitable for erecting needle ice monitoring stations. The first comprising of two separate sites, at high altitude (3000 m.a.s.l) in the Drakensberg Mountains, at Tiffindell, in continental southern Africa and the second on maritime sub-Antarctic Marion Island (Figure 3.1, 3.2). The following sections will detail study site properties.

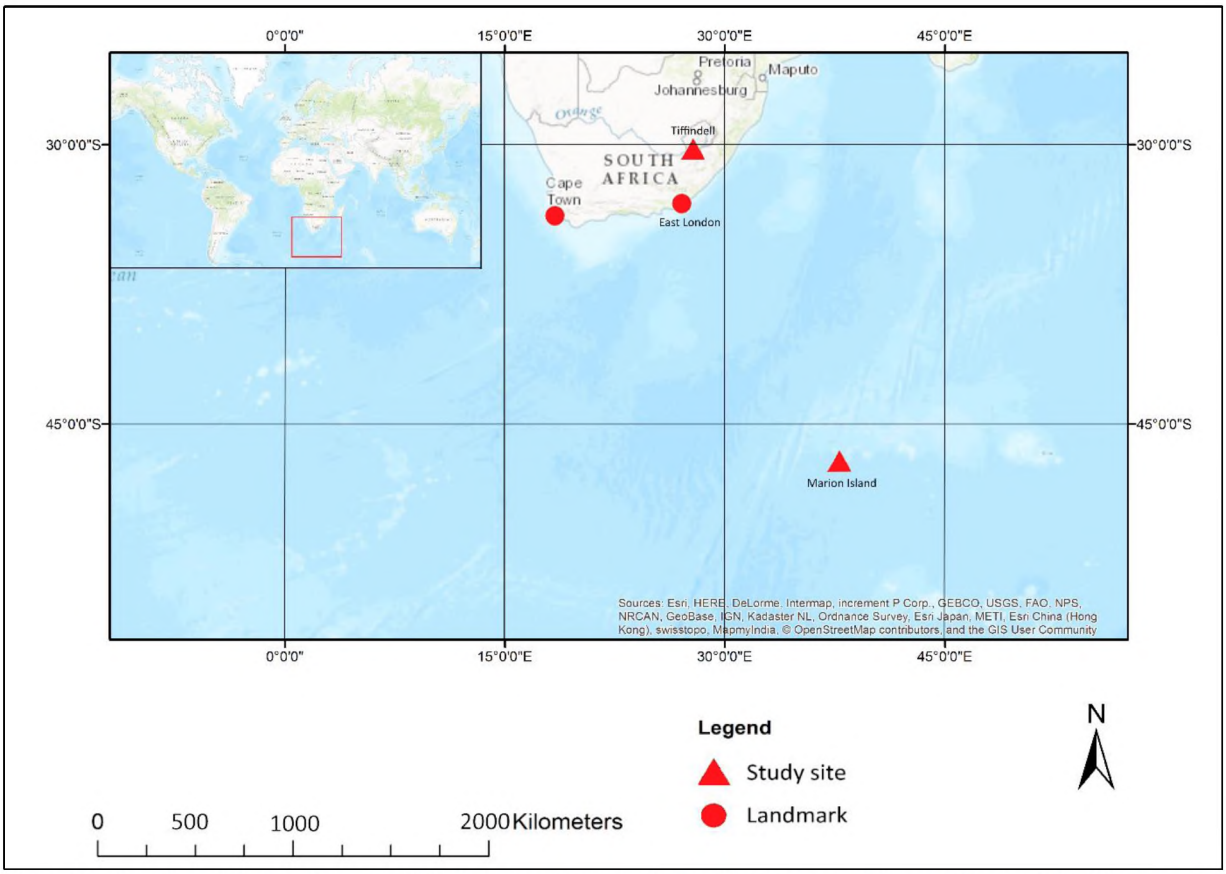

Figure 3.1. Location of the study areas. Tiffindell on the boarder to Lesotho in South Africa and Marion Island in the sub-Antarctic Indian Ocean.

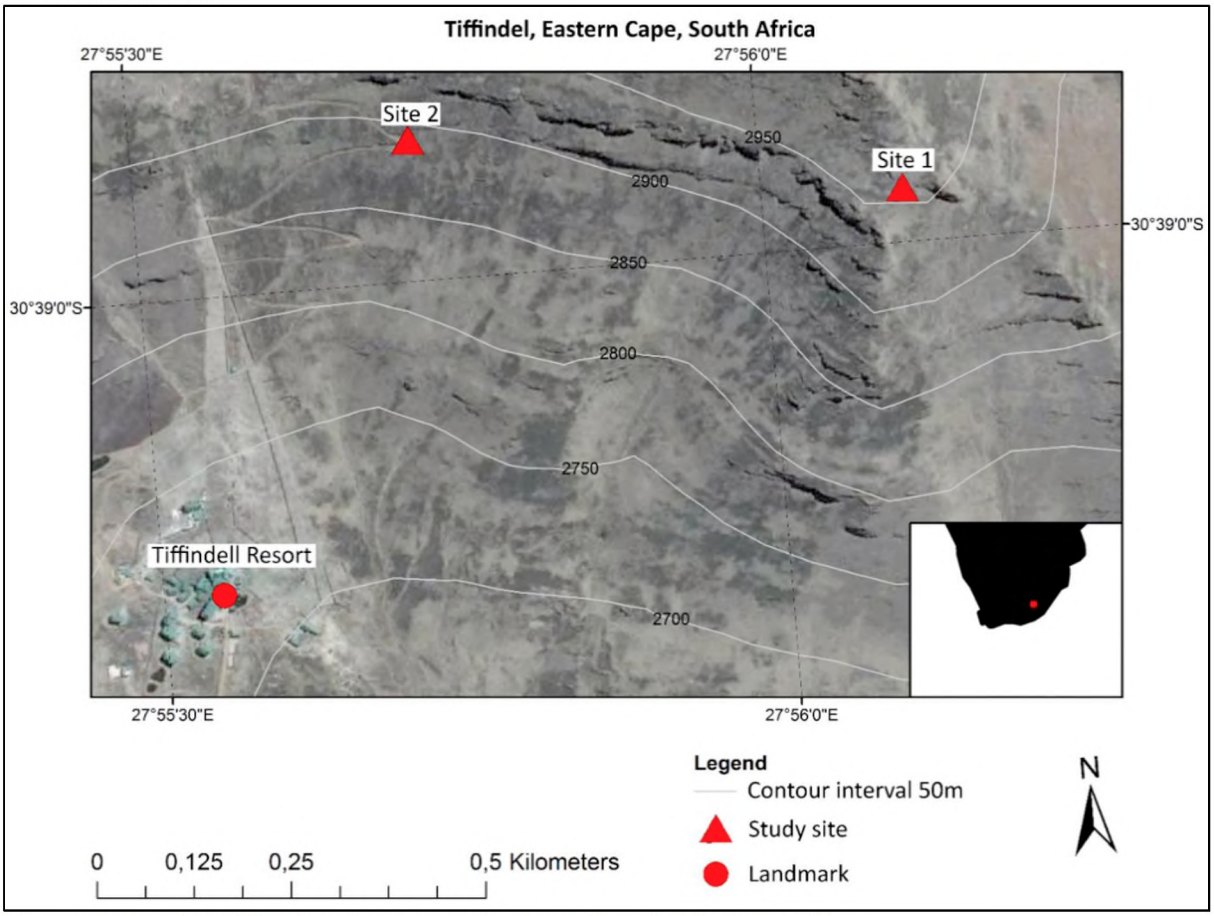

Figure 3.2. Map of the Tiffindell study area including the position of study site 1 and 2.

3.1 Tiffindell

Tiffindell Ski resort is one of few alpine locations in southern Africa where recreational skiing is possible. The resort has a capacity of approximately 150 beds, which is open throughout the year, and offers skiing from June to October. It is a popular hiking, mountain biking and motor biking destination during the summer months.

3.1.1 Geography

Located at 30° 39' 12" S 27° 55' 38" E (Figure 3.1), Tiffindell is part of the Eastern Cape Drakensberg of South Africa. The resort is located on a south-facing aspect of Ben Macdhui, whose peak reaches 3001 m.a.s.l. and which borders Lesotho to the North. The mountain is steep, with 20-30° slopes, and has numerous terracettes superimposed on larger vegetation and stone banked terraces (Kück and Lewis, 2002). These terracettes are on average 70cm wide with a surface inclination of 4-7° (Kück and Lewis, 2002). Excavation of several terracettes displayed a sediment depth of ca 20-70cm with no large stones, and are suggested to be created from sediment movement by surface frost creep (personal observations). Tiffindell is 22km north of the small village of Rhodes and 50km north west of the closest town, Barkley East. Land use in the area is predominantly commercial agriculture with large numbers of sheep and goats that influence surface cover by grazing and trampling.

3.1.2 Climate

Described as seasonally alpine, Tiffindell experiences dry cold winters and warm wet summers (Tyson *et al.,* 1976*;* Killick*,* 1978a). Climatological data from Tiffindell is scarce, with only one year of environmental measurements found in the literature (Kück and Lewis, 2002). However, the relative proximity and topographic similarity between Tiffindell and Sani Pass (ca 175km distance) supports comparison. Kück and Lewis (2002) measured a MAAT for 1995-1996 of 7.5°C with summer and winter averages of 16.3°C and 3.1°C, based on only one year of data. Measurements from Sani Pass and surrounding areas produced average MAAT of 3-7°C above 2800 m.a.s.l from similar locations (Boelhouwers, 1994; Grab, 1997; 2002b). Grab (1999) showed January and June MAAT of 11°C and 0°C respectively from Sani Pass.

Measurements interpolated from three weather stations within 375km of Tiffindell, displaying 10-year air temperatures, precipitation and wind speeds from 2000-2009 are shown in Table 3.1 (Meteotest, 2012).

Table 3.1. Air temperature estimations for Tiffindell interpolated between 2000-2009 (Meteotest, 2012)

Month	Average	Min	Max	Precipitation	Wind speed
	°C			mm	m/s
Jan	16.2	5.5	28.7	88	3.7
Feb	15.8	6.0	26.1	75	3.3
Mar	14.0	2.7	26.3	72	3.1
Apr	10.8	0.0	24.4	39	2.7
May	7.0	-5.1	21.4	29	2.6
Jun	4.1	-7.2	16.6	14	2.5
Jul	3.7	-8.6	19.1	5	2.7
Aug	6.3	-6.6	22.0	20	3.2
Sep	9.5	-4.1	24.2	22	3.6
Oct	12.7	-0.2	26.1	65	3.9
Nov	13.9	1.0	26.7	91	4.0
Dec	15.6	5.3	27.2	77	4.0
Average	10,8	-0,9	4,2	50	4,8

Precipitation in the Drakensberg is quoted to be in a range of ca 600mm to over 2000mm annually (Tyson et al., 1976; Schulze, 1979; Grab, 2002b; Carbutt and Edwards, 2003; Sumner, 2004). However, more recent studies suggest that the highest values of ca 2000mm are exaggerated (Nel and Sumner, 2008). Measurements of 750 mm per annum were recorded at Sani Pass in a four year study (Nel and Sumner, 2008). Rain, on a synoptic scale, at Tiffindell is associated with cut-off low pressures (westerly waves), orographic precipitation and mid-latitude cyclones. Such conditions reduce the chances of needle ice occurrence, while cold clear conditions associated with high-pressure systems and easterly wind flows, are prone to needle ice growth (Mulder, 2009). During winter, the dominance of high-pressure systems produces clear and cloud free days and nights in the Drakensberg (Tyson *et al.*, 1976). Clear days allow for high insolation inputs producing warm days, while clear nights allow substantial loss of long-wave radiation, often resulting in sub-zero temperatures (Grab, 2001). With sufficient soil moisture, such weather conditions are ideal for needle ice growth.

The frost environment at Tiffindell was shown by Kück and Lewis (2002) to consist of 62 and 65 freeze-thaw days from May and September for1995 and 1996 respectively. However, interpolated air temperature data (Meteotest, 2012) suggests that freezing may be possible from April to October, which has, indeed, been confirmed by personal observations.

3.1.3 Landforms

Kück and Lewis (2002) record abundant terraces and terracettes on the slopes of Tiffindell. They suggest that the larger terraces are moved by gelifluction flow, while the smaller terracettes are being controlled by needle ice movement. However, given that the environment does not support permafrost, nor, based on research by Sumner (2003), is it likely to have had permafrost during the Last Glacial, and hence solifluction, rather than gelifluction, is most likely to result in the observed landforms. Personal observations suggest that solifluction and needle ice movement occur simultaneously, with terracettes being superimposed on terraces by the more intense and frequent influence of needle ice.

3.1.4 Vegetation

The local vegetation surrounding Tiffindell is part of the Alpine Grassland Biome, supporting grasses (*poaceae*) and flowering plant (*asteraceae)* species (Mucina and Rutherford, 2006). In the study area the most abundant species include tussocks grasses and *Helichrysum* herbs (Carbutt and Edwards, 2003). Vegetation is mostly closed, with short grasses in addition to shrublands. However, in proximity to the study site, the vegetation is discontinuous with numerable patches of unvegetated soil related to the surface of observed terracettes (Mucina and Rutherford, 2006). Terraces are predominantly vegetation-banked with non-vegetated treads, suggesting that vegetation dams or restricts downslope movement of surface material, while being strongly influenced by diurnal frost (Kück and Lewis, 2002). High organic contents of ca 20% were measured by Herbst and Roberts (1974) in slope soils from the Drakensberg, from abundant decaying grass and slow decomposition; which produced soils with a high water-retention capacity.

3.1.5 Geology

Tiffindell is positioned in the uniform basaltic orogeny of the Drakensberg group from 160-180 Ma, underlain by sandstones from the Elliot and the Clarens formation (Burley *et al.*, 1982). Weathering of the basaltic rocks and decaying of vegetation produced frost susceptible soil textures, as seen in the abundance of frost reworked ground in the high Drakensberg (Boelhouwers, 1991; Grab, 2001). Soils derived from the basalt display an even distribution of particle sizes comprising coarse sand, fine sand, silt, and organic matter (Mucina and Rutherford, 2006).

3.1.6 Summary

Tiffindell was considered ideal for needle ice measurements as plentiful frost cycles are suggested by literature and needle ice growth was documented from the area (Kück and Lewis, 2002). Personal experience and communication with authors familiar to the region helped (Boelhouwers, 1991; Boelhouwers and Meiklejohn, 2002; Borg, 2012). Furthermore, the measuring stations could be

erected in a relatively safe location with little worry about theft and interference from outside factors. Tiffindell was easily accessed by motor vehicle and could be visited routinely every three months.

3.2 Marion Island

Marion Island is a sub-Antarctic island discovered in the 1600s by Dutch seafarers, however only disembarked upon in the following century by Captain Marion du Fresne in 1772. Marion was used for sealing during the 1800 and early 1900s, but annexation of the island by South Africa in 1948 repurposed the islands use as a meteorological station (SANAP, 2015). In 2003, Marion Island was declared a Special Nature Reserve by the South African government and is today used strictly for research purposes (SANAP, 2015). A team of ca 20 researchers overwinter on the island from April to May, the following year, while during team switching, a take-over period of less than a month (April-May), a total of 90 researchers and support staff inhabit the island.

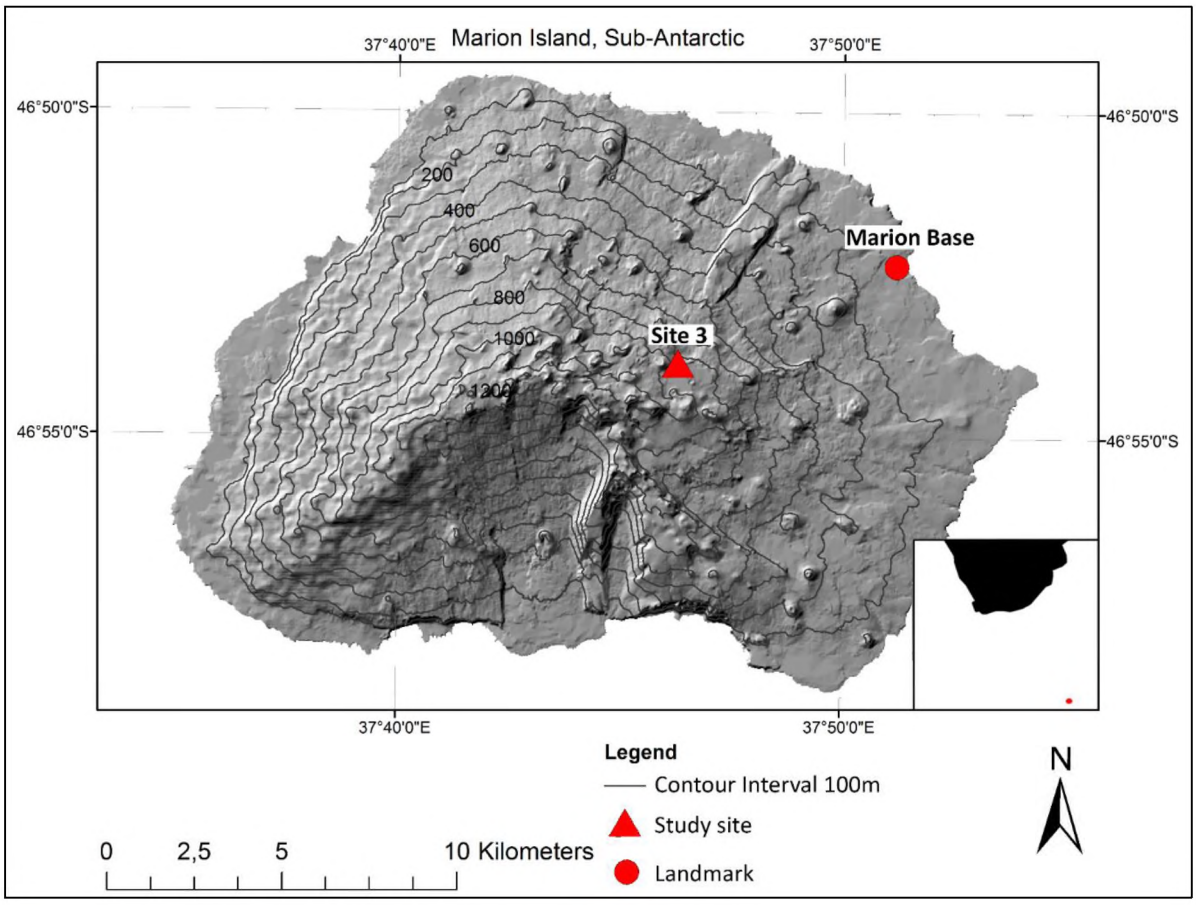

Figure 3.3. Map of Marion Island including the position of study site 3.

3.2.1 Geography

Located at 46°55′ S 37°15′ E (Figure 3.3) Marion is a volcanic island in the sub-Antarctic Indian Ocean. Marion and Prince Edward Islands together form the Prince Edward Island group, situated ca 1700km South East off the closest main land city, East London in South Africa (Figure 3.1). The islands are two

of the most remote land masses on the planet. Marion, the bigger of the two islands, extends over an area of 290km^2 (longest axis is ca 25km) with the highest peak, Mascarin Peak, reaching 1242 m.a.s.l. in the Island's interior. Owing to intense wave action on the basaltic lava flows, the islands coastline exhibits generally high cliffs with few coves. The island interior exhibits undulating terrain between roughly 500 to 1000 m.a.s.l with a small permanent ice cap close to the highest peaks *(McDougall et al.*, 2001; Sumner *et al.*, 2004).

3.2.2 Climate

Located in the longitudinal belt nicknamed the roaring forties, Marion Island frequently experiences strong winds, ample rains and snow (Vowinckel, 1954; Le Roux and McGeoch, 2008; Nel, 2012). Lowland conditions are perennially wet, with few freeze-thaw cycles, transitioning into frost active mid-altitudes, while elevated inland locations experience seasonal snow cover and possibly permafrost (Schulze, 1971; Hall, 1979b; Boelhouwers *et al.*, 2003). Classified as a sub-Antarctic hyper-maritime environment, Marion Island displays low air temperatures (ca 5°C), in addition to a low average annual temperature range (ca 5°C) (Smith and Steenkamp, 1990; Holness, 2004; Le Roux and McGeoch, 2008). The base on the island generally experiences north-westerly winds with few windless and cloud free days (Schulze, 1971). Owing to the low temperatures (that decrease with increasing elevation), small temperature ranges and high mountains, numerous annual freeze-thaw cycles have been reported from Marion by authors including Vowinckel, (1954), Schulze, (1971), Hall (1979a; b, 1979b; a), Holness (2001, 2004), Boelhouwers (2002; 2003), Haussmann (2009a; 2009b), Nel (2012; 2014) and (Le Roux and McGeoch, 2008). Freeze-thaw frequency is strongly influenced by elevation (Holness, 2004) with the highest number of cycles suggested to be in a altitudinal range of 600-800 m.a.s.l. (Holness, 2004; personal communications). Sporadic needle ice growth has been noted at less than 100m elevation to over 800m (personal observations).

Marion Island experiences rain on an average on 25 days a month and a total annual precipitation of ca 2500mm, evenly distributed throughout the year (Schulze, 1971). However, recent studies (Smith, 2002; Le Roux and McGeoch, 2008) show a general warming trend on the island since 1948, while precipitation has declined, showing fewer and less intense rainfall events (Smith, 2002).

The island's synoptic weather is influenced by mid-latitude depressions (cyclones), frontal systems, and anti-cyclones, producing a range of climatological influences (Vowinckel, 1954; Le Roux and McGeoch, 2008). These influences include approaching (pre-frontal) cyclones associated with mild temperatures, strengthening of the north-westerly winds and increased cloud cover, while post frontal conditions are often clear and cold (Smith and Steenkamp, 1990; Nel, 2012). Post frontal conditions are generally well-suited for needle ice growth. It, therefore, stands to reason that the frost

environment at certain elevations on Marion Island are conductive for needle ice growth throughout the year (Smith and Steenkamp, 1990; Holness, 2004; Le Roux and McGeoch, 2008)

3.2.3 Landforms

Owing to the influence of frost action, periglacial landforms are well developed on Marion Island. Landforms seen across the island include sorted stripes, vegetation and stone banked terraces, solifluction forms, hummocks, patterned ground forms and turf-exfoliation (Hall, 1979a; Holness, 2001; Boelhouwers *et al.*, 2003; Sumner *et al.*, 2004). These landforms are most prominent in areas where frost action is intense and the formation of sorted stripes, turf-exfoliation and other patterned ground formations are strongly connected to the growth of needle ice, similar to the needle ice influences reported from other locations by Gradwell (1957), Lundqvist (1962), Lawler (1988), Gradwell, 1957; Lundqvist, 1962; Lawler, 1988; Pérez, 1992b; Ballantyne, 1996;;;;). Longer term frost processes linked to solifluction have been observed throughout the Island, except at the highest inland altitudes, and are associated with the formation of vegetation and stoned banked lobes (Hall, 1979a; Holness and Boelhouwers, 1998; Holness, 2001).

3.2.4 Vegetation

Marion Island exhibits a mesic fellfield vegetation, where the dominant species is the cushion plant *Azorella Selago*, along with sub-dominant grass species, *Agrostis magellanica,* and several mosses (Smith et al., 2001). Lowland vegetation is thick and supports deep mires and boggy terrain (Smith and Steenkamp, 1992; Mucina and Rutherford, 2006), while vegetation cover gradually thins with increasing elevation. Continuous vegetation cover transitions into discontinuous patches at approximately 200-300 m.a.s.l, while very little vegetation, apart from small moss colonies, is seen above 700 m.a.s.l. *Azorella Selago* cushions are observed to develop into large discontinuous colonies at elevations between 400-500 m.a.s.l producing *A. Selago* hummocks in flat areas while in sloping terrain the species creates vegetation banked terraces (Haussmann *et al.*, 2009; personal observations). *A. Selago* terraces, vegetation banked lobes, hinder downslope movement of material by frost action and are seen as important biogeomorphic controllers on landscape development (Smith and Steenkamp, 1990; Smith *et al.*, 2001; Haussmann *et al.*, 2009a; b). Interaction between biotic and abiotic processes are seen in degradation of *A. Selago* colonies due to erosion by diurnal frost processes (Haussmann *et al.*, 2009b).

3.2.5 Geology

Marion and Prince Edward Island are the exposed tip of an oval shaped, mostly submerged shield volcano of ca 450ka age (McDougall *et al.*, 2001). Geologically, Marion Island displays three types of surface lithology distinctly discernible in the field, including the red scoria cones and two types of

basaltic lavas. The lavas are distinctly different, with mostly non-glaciated black lavas and older glacially reworked grey lavas (Hall, 1979; McDougall *et al.*, 2001). Grey lavas are generally flat and smoothed by glacial reworking, easily navigated on foot, while black lavas are found as either coastal basalt floods, comprising Pahoehoe (nicknamed "toffee") lavas, or as demanding, sharp, steep and brittle Aa lavas that form undulating ridges roughly 5-30m from crest to bottom (McDougall *et al.*, 2001). Scoria cones exhibit a deep red colour (sometimes with a minor portion of black scoria) with a generally steep, 20-30° inclination, and are composed of a solid core covered in loose sediment.

Surface textures produced by physical and chemical weathering of scoria and grey lava are seen to be frost susceptible and thus suitable for needle ice growth. The same is not true for black lavas, which generally are not influenced by needle ice due to a prevailing sandy surface texture (personal observations). The island group is still considered volcanically active with a documented eruption in 1980 (Verwoerd *et al.*, 1981) and other more recent reports of volcanism was noted in 2004 (Meiklejohn *et al.*, 2005)

3.2.6 Summary

Marion Island is ideal for diurnal frost activity, as environmental conditions include frequent freeze-thaw cycles and ample moisture availability, and thus, suited for needle ice growth. The Island's ample research legacy provides numerous publications in addition to long term temperature and wind measurements relating to past climate. Furthermore, the minimal impact of humans, reduces the chance of study site disruption or contamination, especially as research personal based there are educated to not interfere with ongoing research.

3.3 Study sites

To achieve objectives formulated in Chapter 1, and based on the literature review in Chapter 2, three study sites were deemed to be suitable. Monitoring stations in the discussions that follow are identified as Site 1, Site2 and Site 3. Site 1 and 2 were located at Tiffindell and Site 3 on Marion Island. Descriptions of each site together with environmental and physical aspects are presented below and in. Site 1 was studied from May 31 of 2014 to June 9 2015, Site 2 from March 5 2015 to June 9 2015 and Site 3 from 24 April 2014 to 3 May 2015.

Table 3.2. Study sites geographic details

Site	Slope angle (°)	Latitude	Longitude	Elevation(m)
Site 1	~5	30°38'55.44"S	27°56'08.43"E	2987
Site 2	~25	30°38'53.42"S	27°55'45.49"E	2905
Site 3	~5	46°53'56.30"S	37°46'18.27"E	766

3.3.1 Site 1

Site 1 was located on a wind-exposed vegetation banked terracette, measuring roughly 100 x 50 cm, situated near an exposed cliff edge. The site was positioned ca 15m vertically below the mountain summit, facing 160° (south, south-east). Rocks and low grass are seen at the surface of Site 1, while the main study area is surrounded by herbaceous plants and low shrubs (Figure 3.4). The surrounding environment has similar features to those seen around Site 1, however varying in extent and aspect. A 25cm long PVC scale bar was positioned at Site 1 for scale reference, and after March 2015 a painted marker line was positioned at Site 1. The area is utilized for sheep grazing, but no manuring or trampling was seen in close proximity to the site during setup.

Figure 3.4.Overview of Site 1 at 2987m.a.s.l. from Tiffindell.

Figure 3.5. Close-up of Site 1 with visible painted marker stone line in the centre of the study site.

Figure 3.6. Digital 3D surface model of Site 1.

3.3.1 Site 2

Site 2 was located ca 600m west of Site 1, at an elevation of 2905m.a.s.l. covering ca 150 x 50 cm. Positioned in a different setting from Site 1, Site 2 was more sheltered and had a much steeper inclination (ca 25°). Site 2 was positioned in a road cutting, where overhanging slope material had collapsed forming a mound. The site was chosen because a large surface area was exposed and needle ice was visually evident at the surface during inspection.

Banked by rocks to the west and by a vegetated bank on the east (Figure 3.7, Figure 3.8), the study site faced 165°. Evidence of animal influence was noted close to the study site, in the form of manure and trampling sheep. As the site was located on a road cutting, it risked disturbance by vehicles and human trampling. However, the land owner ensured that no road works or other alteration was done during the study period. Two 30-centimeter-long painted marker stone lines were positioned at the surface of the study area.

Figure 3.7. Overview of Site 2 at 2905 m.a.s.l. Location of Site 1 can be seen in the background

Figure 3.8. Pictures of study site 2 from Tiffindell, pictures facing north north-west. Two lines of painted markers are visible on the study site surface.

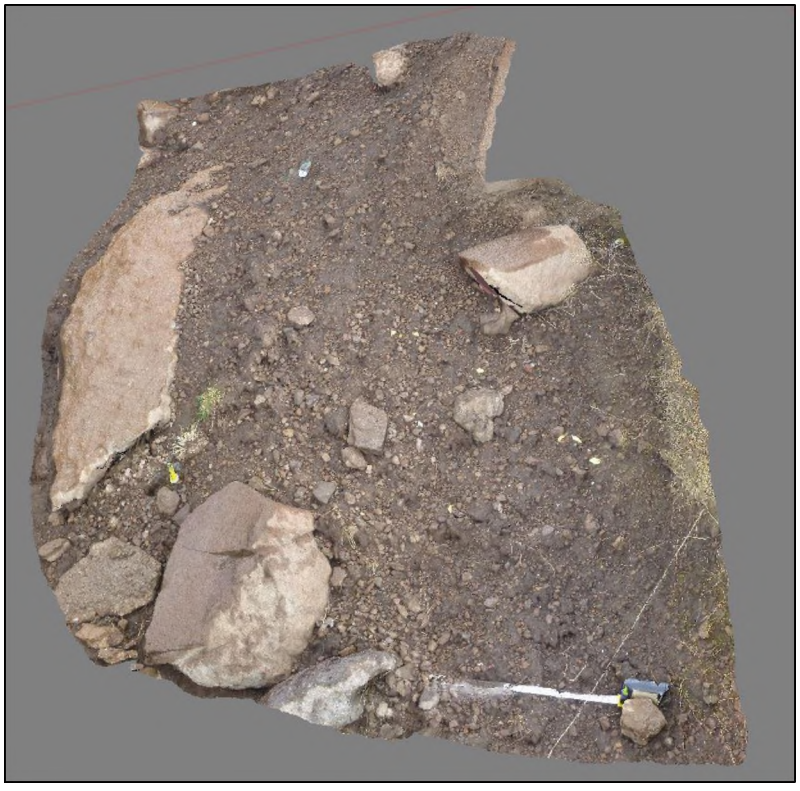

Figure 3.9. Digital 3D surface model of Site 1.

3.3.3 Site 3

Site 3 was located on Marion Island in a distinctly different environment to the other two sites. At an elevation of 766m.a.s.l., Site 3 was less than one third of the altitude of Site 1 and 2. The site faced 90° (east) and was not aligned with the general incoming wind direction of 271° (west) (Figure 5.13 from Chapter 5). Unlike Site 1 and 2, the orientation of Site 3 caused the wind to blow from "behind" Site 3, directly into the face of the camera lenses. Site 3 was situated on a gentle slope of ca 5° at the edge of a depression between two rock outcrops and was five meters vertically from the bottom of the depression. The site tilts in two directions of equal inclination (ca 5°), visible in Figure 3.10 as to the left and inward in the picture.

Wind was channelled between two rock outcrops, thus, exposing the site to strong winds. The surface morphology of Site 3 was dominated by wind-generated ripples (Figure 3.10) (Zimbelman *et al.*, 2012; Hedding *et al.*, 2015). The surface had no vegetative cover, apart from some small moss colonies. The surface of Site 3 consisted of permeable, loosely packed volcanic scoria with a large portion of coarse sand and small pebble sized material, underlain by a much less permeable layer of silt and clay at ca 5-15 centimetres depth (Figure 5.16 in Chapter 5, Figure 3.12). A 25cm long PVC pipe was placed at Site 3 for reference scale.

Figure 3.10. Picture of Site 3 from Marion, picture facing east.

Figure 3.11. Pictures of Site 3 at 766m.a.s.l. on Marion Island.

Figure 3.12. Stratified surface close to Site 3 with ice needles emerging from a less permeable layer of fine material below the surface.

The following chapter details a new methodology for examining needle ice growth, consisting of three monitoring site positioned at Site 1, 2 and 3.

Chapter 4 – Methodology

A new methodology for monitoring needle ice was developed in this thesis. Descriptions on how the new method was conceived as well as early problems and experiences gained during initial trials will be presented. First, a section describing terminology will define the use of needle ice related vocabulary.

4.1 Terminology

Growing, melting and sediment movement by needle ice are the main foci of this thesis, thus terminology used in describing needle ice needs to be defined. The process of growing of ice needles and its ability to heave sediment requires little explanation, as the process shows little variability. However, the process of destruction of needle ice is more complex. Ice needles have been observed to melt, topple, roll, slide and bounce during melting, hence a single term is currently not in use which describes a general view of needle ice destruction. The term needle ice *decay* will subsequently be used as to describe destruction of ice needles by aforementioned processes/mechanisms.

In addition, terminology used to describe movement created by the processes involved in needle ice decay include “needle ice creep”, “needle ice displacement, “needle ice induced particle transport”, “needle ice movement” and “needle ice transport”, however these terms are loosely defined (Mackay and Mathews, 1974b; Pérez, 1987a; 1988; Branson *et al.*, 1996). Uncertainties in definition create doubts in how terms are applied and misuse or misunderstanding follows.

“Needle ice creep” is a term currently used to describe an ambiguous process coined during early years of needle ice research (Davison, 1889; Troll, 1944; Mackay and Mathews, 1974b; Lawler, 1993; Matsuoka, 2005; French and Harbor, 2013). The term evolved in several directions and nowadays portrays a general description of diurnal frost movement. Heaving and resettling are considered the core mechanisms of movement from “needle ice creep”, although the incorporation of additional processes is not clearly defined. Incorporation of additional movement mechanisms that can be classified as ”needle ice creep” in literature are dependent on which author describes the process (Outcalt, 1971; Mackay and Mathews, 1974b; Lawler, 1993; Boelhouwers, 1997; Matsuoka, 2005).

The methodologies used in this thesis were designed to measure movement from all mechanisms produced by needle ice decay. Hence, a general term for such movement is needed. None of currently used terminology for sediment movement by needle ice was sufficient to explain all sediment displacement produced by needle ice. To combine processes and mechanisms involved in creating movement from the effects of needle ice, including melting an associated sediment movement, was developed, the term *needle ice sediment displacement* (NISD) is used throughout the document.

Needle ice sediment displacement, is defined as;

"Movement of material through growing, melting, blowing, toppling, sliding or other physical/environmental displacement mechanisms/processes associated with needle ice",

The term is used to describe sediment movement attributed to needle ice decay. Displacement achieved by heaving during growth, melt, toppling of needles as a result of wind or bouncing from gravitational acceleration during ablation are all considered to be a part of NISD. The proposed term significantly shortens mechanism/process description of achieved movement, which currently requires extensive explanation. Movement by additional frost related surface processes including solifluction and gelifluction was not within the scope of this thesis, thus no measurements of their impact on surface movement was considered. However, the possible addition of movement by these processes is noted.

Chapter 6 will focus on intricate details of sediment movement mechanisms related to needle ice, which will deem the term NISD too broad in context. Hence, displacement will be broken down into individual components.

The following section will summarize previously used methodologies presented in Chapter 2 and how adaptations of these were incorporated into the new methodology.

4.2 Adaptations of previous methodologies

Limitations of past methodologies documented in Chapter 2, which were used for studying displacement by needle ice, provide a point of departure for developing new methods to improve the accuracy of results in the field. Combining methods and using appropriate technology for the processes and mechanisms examined is suggested to increase the precision of measurements. It is clear that one of the most significant drawbacks of past methodologies was the uncertainty in determining the timing of needle ice growth and the specific mechanisms that are active in displacing sediment, in addition to possible interactions between modes of movement.

Chapter 2 outlined the use of environmental monitoring as well as currently used methodologies for measuring surface movement by needle ice. As the methodology used in this study was applied in the field prior to the publication of Matsuoka (2014) and Ueno *et al.* (2015), benefits from their findings could not be incorporated into the construction of the monitoring stations. However, as the use of high-frequency visual monitoring of diurnal frost movement was applied in both Matsuoka (2014) and Ueno *et al.* (2015), their work is briefly discussed in this thesis.

The deployed monitoring stations combined the use of painted markers with repeat photography to allow the identification of short- and longer-term deformation at each study site. In addition,

imagery was used to create 3D surface models for Sites 1 and 2, which aided in measuring surface movement with precision.

The next sections will describe the evolution and details of the methodologies applied, discussing particulars concerning equipment, setup, terminology, measurement methods and problems encountered during development/deployment.

4.3 Needle ice monitoring methodology

Limitations in past research by Gradwell (1957), Outcalt (1971), Pérez (1987) and Matsuoka (2005) show that methods for both environmental and visual monitoring of needle ice could be improved. Published literature draws conclusions on initiation temperature and movement mechanisms based on qualified assumptions of movement (e.g. Outcalt, 1971; Mackay and Mathews, 1974b; Pérez, 1988; Matsuoka, 1998), more than the identification of specific movement mechanisms. Hence, the need exists for refining and applying a more rigorous observational technique.

To alleviate the aforementioned limitations, a station using cameras for visual monitoring was conceptualised and implemented. Environmental and visual monitoring required loggers, sensors and cameras (detailed in Section 4.3.4) capable of recording high-frequency measurements for an extended period. A monitoring station incorporating six temperature sensors, two soil moisture sensors, an anemometer and three cameras was used. The setup was deemed sufficient for environmental and visual monitoring of needle ice growth, alleviating limitations seen in publications by Gradwell (1957), Outcalt (1971a), Lawler (1993), Holness (2001) and Matsuoka (2005). Matsuoka (1996), Grab (2001) and Holness (2001) presented methods for placing environmental sensors to measuring needle ice growth. However, the concurrent placement and setup for the visual monitoring was novel.

The following sections will show incorporation of amended methodology and technology aimed to increase accuracy of needle ice related measurements.

4.3.1 Study site monitoring systems

Accurate, high frequency environmental monitoring is fundamental to investigate needle ice growth, especially to establish the location of ice needle nucleation and the environmental conditions during growth. As shown in Chapter 2, much previous work has concerned growth parameters for needle ice and the surrounding environmental preferences (Outcalt, 1971; Lawler, 1988; Grab, 2001; Holness, 2001). The study required long-term (months to a year) measurements of temperature, soil moisture, wind speeds, wind directions, all which have been proposed to affect growing of needle ice (Troll, 1958; Outcalt, 1971; Lawler, 1988).

4.3.1.1 Temperature monitoring

Understanding temperature changes in the air and ground is essential in the context of working with energy balances impacting the creation and melting of ice needles. Identifying how changes in temperature through the movement of air masses, ground heat flux or by radiative heat loss affect the top soil, is crucial in linking ice nucleation timing/location to environmental conditions (Outcalt, 1971a). In addition, it is critical to establish the link between processes of energy redistribution and the release of latent heat at phase transition, which is also pertinent to so-called "zero-curtain" effects.

The monitoring station in this study used a total of six temperature thermistors to measure soil, surface and air temperature at specific intervals. Temperature was measured from a depth of -10cm to ambient air temperature at a maximum height of +30cm. Sensors were positioned at +30 and +10 cm above the ground to measure air temperature, while ground sensors recorded temperatures at +0 (surface), -2.5, -5, -7.5 and -10 cm. Initially, air temperature measurements were meant to include logging at +50 and +100cm, however, due to a limit to the number of channels available for sensors and the need to have a long logger battery life, this was not feasible.

The monitoring stations recorded ambient air temperature, near-ground air temperature and surface temperature along with a systematic view on temperature regime, energy movement from ground to air or *vice versa*. Consideration was given to placing ground temperature probes deeper, however, none of the study sites were in permafrost areas, and cooling/freezing was not expected below 10cm (Boelhouwers *et.al*, 2003). A temperature measurement interval of five minutes was deemed frequent enough to monitor small scale temperature variance and to locate freeze initiation with an error margin small enough to be considered accurate. Additionally, a higher frequency than five minutes would limit the recording time and battery life of the data loggers.

4.3.1.2 Soil moisture monitoring

Schwalbe (1884), Hesselman (1907), Beskow (1935) and Meentemeyer and Zippin (1981) acknowledge the significance of soil moisture on controlling needle ice growth. Branson *et al.* (1996) argued that volumetric soil moisture levels of between 15% and 75% were required for needle ice growth in their study. They do, however, stress that the amount of available soil moisture for sustainable growth of needle ice is also dependant on freezing intensity and soil textural properties.

The above studies showed that the initiation of needle ice growth and subsequent lengthening of ice needles is controlled by the subsurface movement of water. Hence, the use of multiple soil moisture probes allowed for measurements of soil moisture movement within the soil column. Needle ice is suggested to grow within the top few centimetres of soil (LeConte, 1850; Washburn, 1979; Hesselman, 1907) and, therefore, soil moisture sensors were positioned at -2.5 and -5 cm depths.

These specific depths allowed for the -2.5 cm sensor to closely resemble the soil moisture conditions at the suggested depth of needle ice initiation (Higashi and Corte, 1971; Branson *et al.*, 1996; Nel and Boelhouwers, 2014), while the deeper sensor would reflect ambient soil moisture (Matsuoka 2005).

4.3.1.3 Wind monitoring

Troll (1944), Outcalt, (1971a), Mackay and Mathews (1974b), Hall (1979), Lawler (1993), Grab (2001) and (Hedding *et al.*, 2015) discuss wind related influence on needle ice growth. Highlighted are the effects of change to the surface to air energy fluxes by augmented convective flow during stronger winds. In addition, latent heat flux is suggested to be impacted by wind speeds as evaporation rates change (Outcalt, 1971a).

To assess the impact of wind speed and wind direction on needle ice growth, an anemometer was incorporated in the monitoring station, measuring average wind speeds, peak wind speeds and wind direction. The wind cups and wind vane were positioned at a height of +150 cm above the ground.

4.3.1.4 Sunrise, sunset and daylight hours

Seasonal changes induce a shift in the amount of daylight hours during the year. Summer in the Southern Hemisphere (December to – February) produces the most daylight hours, while winter (June to August), the opposite. Similarly, sunrise and sunset timings change. In summer, sunrise occur early and in winter the opposite. Chapter 5 investigates timing and duration of needle ice events over a year, hence, the change in sunrise, sunset and duration is relevant.

No radiation sensors were incorporated into the monitoring station, hence, sunrise, sunset and daylight hours were collected externally from Timenaddate.com (Timeanddate.com, 2016). Sunrise and sunset was available for Marion Island while proximate sunrise and sunset for Tiffindell was collected from the closest city, the capital of Lesotho Maseru; located ca 150km north north-west of Tiffindell. Table 9.1 in Appendix A shows average and specific sunrise, sunset and daylight hours for each needle ice events during the study.

4.3.2 Visual monitoring

Based on the literature review in Chapter 2 and considering the research aims and objectives formulated in Chapter 1, the keywords for the monitoring stations are “high-frequency time-lapse photography”. To identify movement mechanisms acting at a small scale (centimetres) at a high temporal resolution (5min), visual observations at the same scale were required. It is the author’s belief that the most reliable and accurate method of monitoring needle ice growth, and to assess objectives stated in Chapter 1, was to use repeat photography. Designing and implementing such a monitoring station required certain prerequisites to be met.

4.3.2.1 Camera equipment and trials

The camera and logger equipment used for this study needed to be able to withstand harsh conditions and functioning over an extended period of time. Additionally, considerations in choosing appropriate equipment included;

- Sufficient battery life for continued photography for to four to five months;
- Allowing for night-time photography;
- Sufficient storage capacity for four to five months of images (ca 15 000 pictures at 15min interval);
- Time-lapse photograph in 5-15min intervals; and
- Mounting of cameras for oblique photography.

The Bushnell Trophy Cam® system provided all characteristics needed for visual monitoring. The Bushnell Trophy Cam® series are tough, high-resolution outdoor cameras built to automatically capture wildlife with the use of time-lapse photography or triggered motion sensor. They are weather resistant and include an infrared camera designed for night-time photography. Additionally, with the use of 8 AA batteries, the manufacturers suggest a battery life of up to one year. Three Bushnell Trophy Cam® cameras were acquired, and an additional six were borrowed from Professor. D. Hedding of the University of South Africa (UNISA), for use in the monitoring stations.

High-frequency monitoring at small temporal scales require accurate camera-clock and logger-clock synchronization. Synchronization occurred automatically in the loggers as they adapted the internal clock of the computer used during programming, while cameras had to be synchronized manually. In all cases, the same computer was used for base time. Measurements during the study recorded a maximum desynchronization of logger and camera clocks of 10 minutes, however, rarely exceeding five minutes. This is based on comparison between the final timing between loggers and cameras during de-assembling, downloading and during the final removal of the measuring station.

4.3.2.2 Camera programming, placement and trials

The initial trial setup using the Bushnell systems had the three cameras taking pictures of a single study site every 15min. As a central part of the study focuses on high-frequency monitoring, the idea of staggering camera pictures for each of the three cameras by 5min would effectively triple the temporal resolution of the study.

To be able to create a time-lapse video showing needle ice growth, sequential pictures were essential. Initially unknown, the Bushnell system has an active optical trigger which takes a picture

when disturbed. This sensor could not be turned off and hence had to be taped shut to not interrupt the image-sequence for time-lapse photography.

Night-time photography used an IR-flash integrated into the camera. Purpose-built for night-time wildlife imagery, and taking pictures of large areas, the IR-flash illumination was too strong for small scale photography and hence over-exposed imagery. Two thirds of the flash diodes were therefore, covered with duct tape allowing for moderate night-time illumination. Cameras were kept in padlocked heavy duty iron cases protecting them from the harsh environment as well as from theft.

Each study site had a 25-cmlong PVC pipe to act as scale, placed within the visually monitored plot. The PVC pipe was firmly anchored into the substrate to prevent movement by heaving.

Figure 4.1. Image showing the 25-cm long PVC scale bar used for in scale measurement of clast movement at Site 3

Images produced (e.g. Figure 4.1), displayed a tilted view of the study sites. Hence, for visual heaving and displacement measurements to be accurate, a reference grid showing surface slope in imagery was needed. The following sections will describe how a reference grid was created for each site.

4.3.3 Measurements and scale in imagery

Chapter 6, and to a lesser degree Chapter 5, focus on measuring within the camera imagery. As stated above, a reference grid displaying scale in imagery was required for accurate in scale measurements.

The setup of the cameras created an oblique view of the study sites. This produces the effect of objects closer to the camera lens appearing larger than objects further away from the camera. Hence, for accurate image measurements, a 3D reference grid was created for each site that allowed correction for distortion cause by the lens angles and positions.

Inputs used in creation of the reference grid included measurements of the plots, the angle of the surface, the angle of the camera, the in-picture scale bar and a 3D surface model of the study site. The 3D surface model was created using AgriSoft PhotoScan®. PhotoScan® uses a number of overlapping images taken 360° around an object to create a high-detail 3D surface map from the images. Using 33 and 35 images respectively, 3D plots were created for Site 1 and 2 (Figure 3.6 and 3.9 in Chapter 3). However, Site 3 lacked 360° images, hence no 3D surface model could be created.

The completed grids were either 25x25 or 25x50 squares, where each square represented 1x1 cm in the image. Since lens to ground distance of each camera setup was not exactly the same, grid squares are not of equal size or position in the imagery between study sites. Similarly, removal, download and subsequent refitting of the cameras slightly altered the cameras perspective, thus, the reference grid needed to be re-aligned for every change in camera position.

Figure 4.2. Reference grid showing 25x25cm aligned with the surface of the study site

To align the grids, the plot surface was compared to the angle of the camera and the angle of the study site. With the use of these angles, and the distance from the camera, the size of the scale bar and measurements of distance within the plots, alignment of the grid with the surface was possible. In addition, the digitally created surface model from AgriSoft PhotoScan®, increased accuracy of the grid by comparing the digital 3D surface model, grid and camera imagery.

Although the camera imagery was of a relatively high-resolution and the interval of imagery was frequent, the estimated accuracy of measurements using imagery is considered to be ca 0,5cm. The reason for this accuracy is that the camera position was not fully stable. Even small changes in the cameras position, alter in-picture measurements between two images. The reference grids do not move when comparing two images, but the camera position can, so the images used for measuring heave may not have had an identical coverage, and, therefore, resulted in a degree of uncertainty for all measurements. In addition, the variability in heave over the study site was substantial at times, increasing uncertainty, even when using in-picture reference points, like large unmoving rocks. Although, accuracy is suggested to be higher during events of shorter needle ice, determining accuracy for each individual event was difficult. Hence, an average accuracy of ca 0.5cm was considered to be suitable.

As mentioned above, heave variability within the study site was substantial at times. Therefore, the average heave from each needle ice event was calculated. Average heave was determined by measuring height of 3-5 ice needles in each of the needle ice events. The number of ice needles seen in the monitored events ranged from a few, to the whole study area being heaved. These 3-5 ice needles were subjectively chosen as representative for the average heave over the study site, and the average of these 3-5 ice needles was considered close to the study site average. Measuring of the average needle ice height was considered to be of the same accuracy as explained above.

4.3.3.1 Portraying intra-site heave variability

Measuring heave and displacement within the camera imagery was done using the aforementioned reference grid as well as the in-picture scale bar. However, the observed intra-site variability meant that the average heave was compared to the measured minimum and maximum heave. Many needle ice events showed patches of heaving and non-heaving. Hence, to understand inter-site heave variability, a map was created. Several events (used for further study in Chapter 5 and 6) were analysed in detail regarding intra-site heave variability. Measurements of heave height over the study site produced an estimation of surface heave from the individual events. The events were subsequently translucently superimposed (50% transparency) on top of each other using Adobe Photoshop®,

creating a map of needle ice heave height over the area from several needle ice events (Figure 4.3 and Figure 6.1, 6.2 and 6.3 in Chapter 6).

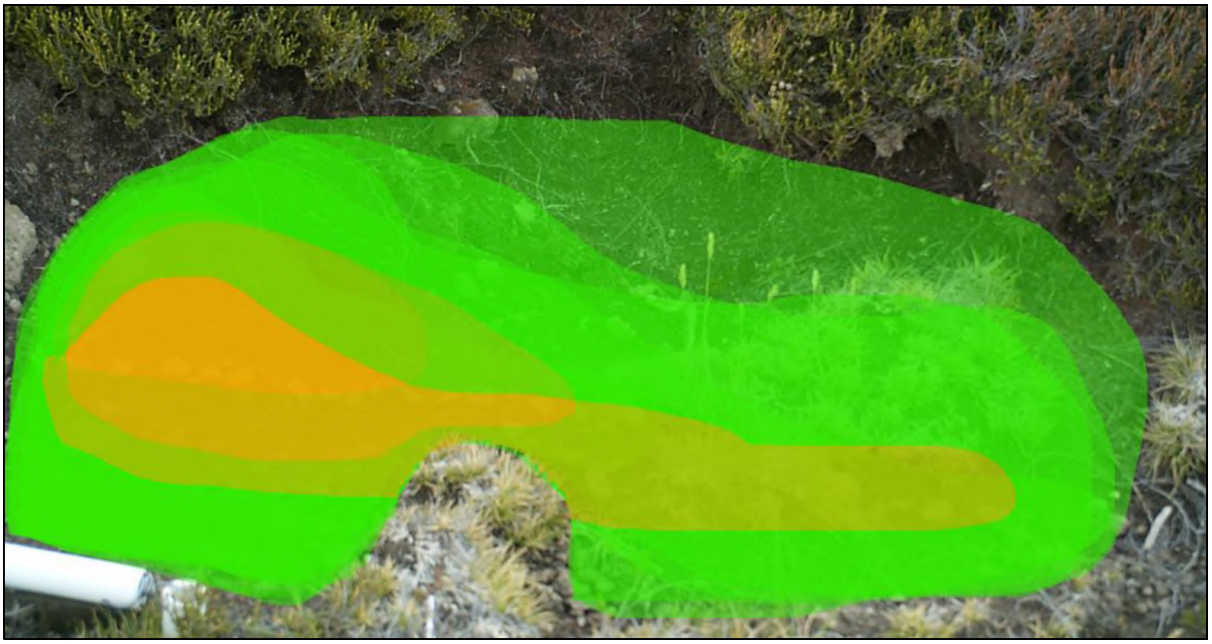

Figure 4.3. Needle ice heave height of five needle ice events superimposed on each other. Green layers show heave of 0.5-1.5cm and orange layers show heave over 1.5cm.

Superimposing the layers on top of each other show areas of colour intensification as less translucent. Such areas coincide with areas frequently displaying needle ice height of that colour class. Figure 4.3 shows three classes, where no colour displays an area not influenced by needle ice, green shows needle ice of 0.5-1.5cm and orange ice needle over 1.5cm tall. Inter-site heave variability maps are produced to display intra-site heave differences. The transition between high heave and low heave classes seen in Figure 4.3 are considered approximate.

The use of inter-site heave variability surface maps is used in displaying heave variability from needle ice videos in Chapter 6.

4.3.3.2 Displacement measurements

Holness (2001) showed that surface displacement by diurnal frost processes was affected by clast size. The methods used in this thesis are able to distinguish movement of certain particle sizes, as well as to identify mechanisms that produce observed displacement. Videos are attached in digital form in Appendix B of this thesis. The videos focus on sediment displacement by needle ice, in addition to how surface movement is dependent on particle size. Using vector arrows elongated based on particle transport distance, needle ice sediment movement is displayed. Arrows are sub-grouped into particle sizes, with green arrows portraying movement of the soil matrix (<2mm), blue arrows small clasts (2-20mm) and yellow arrows display movement of larger stones (>20mm). Particle sizes are sub-grouped

in accordance with classes subsequently defined in Section 4.5. Figure 4.4 shows particles moved with aforementioned vector arrows. Some particles move very small distances requiring small arrows for accurate in scale movement in imagery. However, arrows are hard to display visually for distances smaller than 0.5cm. Hence, arrows for very short movement distances are over-sized.

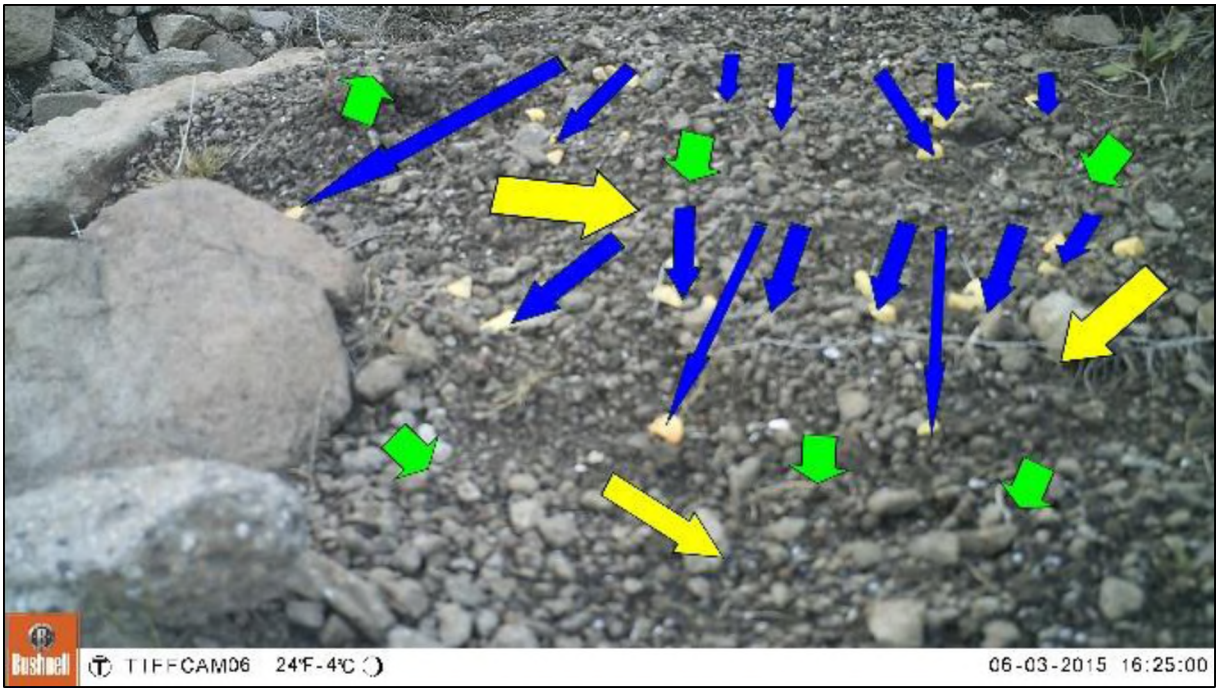

Figure 4.4. Movement distance and direction of different particle sizes at Site 2. Yellow arrows show movement of large stones (>20mm), blue arrows small stones (2-20mm) and green arrows the soil matrix (<2mm).

Chapter 6 focuses on measuring the total displacement of surface material from each site by comparing initial and final imagery. Twelve months of imagery were recorded at Site 1 and 3, while at Site 2 imagery was collected for three months (Section 4.4.1.1). Site 1 only had painted markers installed for the last three months of study, hence, clasts movement was split into two groups. Before and after painted marked installation. The majority of Site 1 and all of long term measurements for Site 3 measured displacement by observing changes in significant features, like distinct rocks, clearly identifiable in both initial and final imagery. While long term displacement at Site 2 and the last three months of Site 1 were measured using the movement of painted markers.

4.3.3.3 Measuring Image-Logger-Discrepancy

Chapter 5 presents measurements of the timing of onset of freeze from loggers and in imagery. However, comparing the timing of visually identifiable growth (T_{vis}) and the timing of the soil surface temperatures falling below 0°C (T_0), the two did frequently not align. A time-lag was seen between visual growth and the onset of below zero temperatures, named *Image-logger Discrepancy*, where ILD = $T_0 - T_{vis}$. This means ILD has a *positive* value when T_{vis} occurs *before* the soil surface temperature falls below 0°C, and vice versa. This discrepancy in time was subsequently termed ILD and is expressed in

hours and minutes from visual identification of needle ice growth to the +0cm temperature sensor recording temperatures below 0°C.

A central part of Chapter 5 focuses on initiation timing of needle ice growth and decay. Imagery presented in Chapter 5 was scrutinized to observe surface disturbance as a marker for needle ice growth, and initial breakdown of ice structures as an indicator for needle ice decay. Freezing of the study site surfaces was identified prior to initiation of heave, but was not regarded as ice initiation. For each of the 82 significant needle ice events, the timing of initiation of growth, onset of freeze, start of decay and end of decay of needle ice was noted with 15min accuracy (Table 9.3, 9.4 and 9.5 in Appendix A). To identify final melt, and subsequent calculation of melt duration, only visual inspection of imagery was used. The timing of end of melt was deemed at a point where two subsequent camera images showed no further resettling of surface material.

ILD will be used as a base for dynamics in needle ice growth and decay timing, as well as to display variability in needle ice initiation depth in the soil column.

4.3.4. Equipment details

The equipment used for the monitoring stations needed to withstand high, at times extremely high wind speeds (winds of 55 m/s were measured by Hall [1979] on Marion Island), snowfall and cold temperatures. Hence, all equipment used was certified for use in cold climates and had adequate protection.

The following list will detail all logging equipment used in the monitoring station setup along with relevant properties:

- Pace XR5-SE-M Data Logger
    - 8 multifunction inputs
    - 12 channels
    - Memory 520kb (ca 260 000 readings)
    - Logging time span of 10 months (using proposed setup)
- Pace PT960 Temperature Probe
    - Measuring range -40°C to +75°C
    - Measuring resolution 0.02°C
    - Measuring accuracy ±0.15°C at 0 to 40°C

- Decagon EC-5 Soil Moisture Sensor
    - Measuring range 0 to 100% volumetric water content
    - Measuring accuracy ±3%
- Pace WSD-100 Wind Speed and Direction Sensor
    - Measuring wind speed range 0 to 78m/s
    - Measuring wind speed accuracy ±5%
    - Measuring wind direction accuracy ±7°
- Bushnell Trophy Cam HD®
    - Resolution 5 mega pixels (2560x1920)
    - Storage 32gb SD-card
    - Picture interval 15min
    - Battery life up to 1 year (longest measured battery life 4 months)

Figure 4.5. Pace logging equipment

Figure 4.6. Bushnell Trophy Cam HD

Figure 4.7. A.W.R. Smith Process Instrumentation Weatherproof case for the XR5 Data Loggers

Figure 4.8. Bushnell Bear Safe® security case

The EC-5 soil moisture sensor uses the dielectric constant of the media to determine volumetric soil moisture content. The sensors were calibrated in a laboratory setting using deionized water, resulting measurements from the sensor held in air and submerged in the water sample were approximately -13.5% and 60% respectively, matching Pace Scientifics guideline for calibration. Negative soil moisture readings obtained indicate the sensor being disconnected from the medium i.e. measuring in air.

To store images, 32 gigabyte SD-cards provided ample storage. Initial testing produced image size of ca 1 megabyte per image at 5 megapixels (2592x1944) and ca 1.5mb at 8 megapixels (3264x2448), securing that the 32 gigabyte SD-card would suffice for each download (ca 32 000 and 21 000 images at respective resolution). Each of the three cameras used identical eight AA rechargeable batteries at a minimum of 2100 mAh, which would produce a battery life of ca 1 year based on manufacturer specifications. Apart from logging equipment containers and mounts were used to secure and position the setup. To keep loggers dry and secure, cameras were housed in Bushnell Bear Safe® security cases, while loggers were placed in waterproof and robust A.W.R. Smith Process Instrumentation cases (Figure 4.7 and Figure 4.8).

The following section will describe installation procedures from top to bottom of the measuring station.

4.3.5 Deploying the monitoring stations

An anemometer arm was fastened securely to a metal pole at a height of +150cm with the use of heavy duty cable ties, wire and bolts. Approximately half-way down the pole, pre-drilling at predetermined heights allowed for the installation of the three Bushnell Security Cases at heights of +50, +30 and +10cm, using several bolts and washers for a stable fitting. Insertion of the pre-programmed, activated and silicone sealed Bushnell cameras into the protective cases was done with care to minimize chance of failure. Once inserted into the casing, the cameras were unable to move in any direction, providing stable images.

To avoid exposure of the air temperature probes to direct sunlight and thereby skew the readings, two Mierij Metro Systems MA 33 radiation shields were positioned on the pole at +30 and +10 cm, housing air temperature probes. The radiation shield was likewise firmly secured to the pole using tough cable ties and wire.

The anchoring pole was installed downslope of the study area to minimize casting of shadows from the pole over the study area. Avoiding shadow effects is especially important during the first hours of light, as most of sediment displacement was observed to occur then. Using a mallet, the pole was firmly inserted into the ground at an angle of ca 10-20° giving images an oblique view of the study area (Figure

4.11). Additionally, rocks were used to stabilize the bottom of the pole hindering movement by wind, as wind speeds of over 30 m/s were expected in the study areas (wind speeds of 31.7 m/s were measured).

Measurements of ground temperature at different depths was made easy by strapping sensors upside down on a 40cm long PVC pipe using "cable-ties" ("wire-tidies") (Figure 4.9). Probes were attached to the pipe in a manner that when the pipe was pushed into the soil, each probe was positioned at the correct depth. Additionally, probes were positioned in a rotated way to allow for cables to run to the surface along the pipe and not interfere with temperature readings. The full length of the PVC pipe was pushed firmly into the substrate to act as an anchor, preventing heaving of the temperature probes through frost action. The PVC pipe supporting temperature probes was inserted into the ground approximately 30-40cm from the study areas.

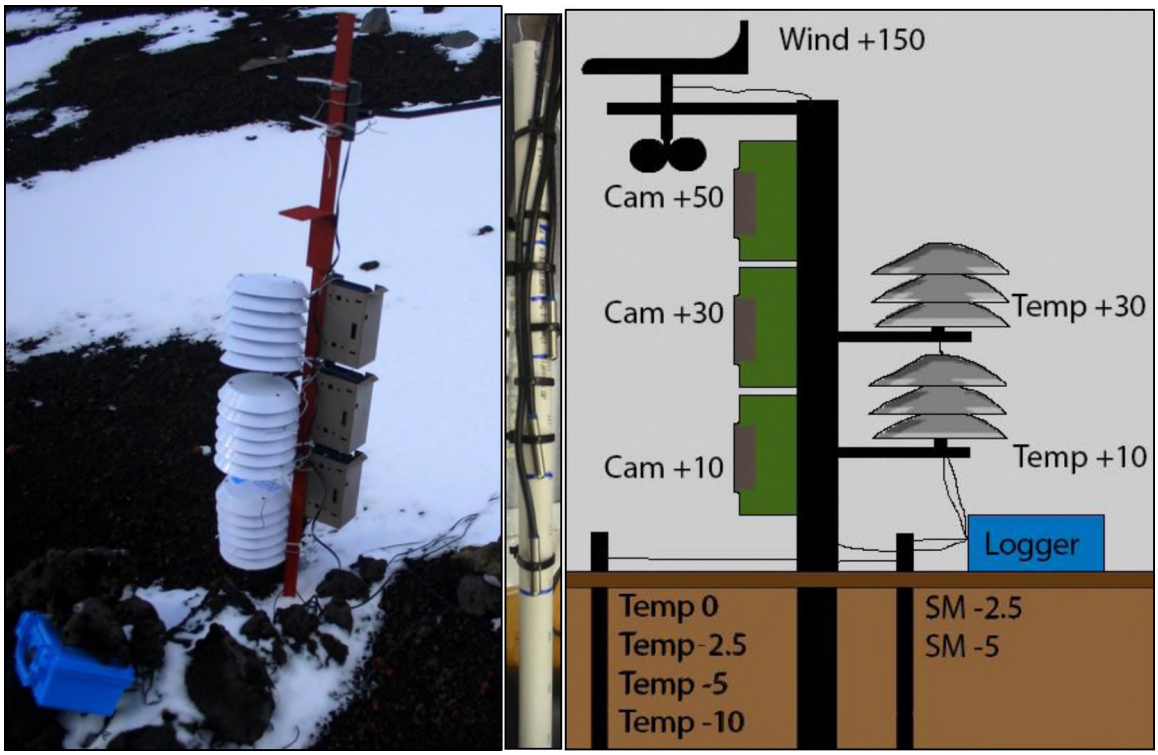

Figure 4.9. Picture of deployed setup at Marion Island alongside ground temperature PVC pipe (Photo: J. Rosenfels)

Figure 4.10. A schematic of the setup of one of the study sites

A 5cm deep trench was carefully excavated ca 20-40cm away from the study areas. Care was taken to ensure minimal site disturbance. In the side wall of the excavation, soil moisture sensors were inserted at -2.5 and -5cm. Sensors were inserted horizontally, along the surface. Pace® suggest that the EC-5 Soil Moisture Sensor should be installed vertically, to not experience pooling next to, or heaving of the sensor. This suggestion was, however, not headed, as positioning the sensor along the vertical axis would provide a mean soil moisture over the ca 5cm long prong of the sensor, defeating

the intended purpose of specific soil depth moisture measurements. The EC-5 soil moisture sensors were calibrated in water according to the manufacturers guide.

Three XR-5 loggers were needed per setup and could be housed in a single Pace EC55 case (Figure 4.12). The back of the case allows for insertion of sensor cables through a waterproof opening, while also securing the cables, preventing accidental dislodgement of sensors from the logger during transport or rough weather. XR-5 loggers have a detachable bracket (Figure 4.12), where sensor cables are attached, providing easy and safe downloading of data without unnecessary unscrewing of the connectors, likewise especially useful in harsh weather conditions.

Figure 4.11. Deploying the metal pole

Figure 4.12. Weatherproof case with XR-5 loggers (Photo: J. Rosenfels)

Moisture could easily destroy the loggers, hence the EC55 case was placed in a stabilizing rock pile, cable tied to the adjacent metal pole. This positioning additionally prevents pooling in and around the case minimizing chance of moisture entering the housing. A schematic view of the setup can be seen in Figure 4.10 and the finished deploying of the monitoring station in Figure 4.11.

4.4 Data management

Analysis of camera imagery from April 2014 to June 2015 revealed a total of 178 needle ice events from the three monitoring stations (Table 4.1 and Table 9.2 in Appendix A). To organize and to categorize findings, needle ice events were initially sub-grouped into significant and non-significant events based on 24h data availability, visually distinguishable growth and duplicates from several cameras measuring the same event. Not all events were comparable, ranging from events covering the whole study site with several centimetres of ice needles to events partially heaving the study site and/or heaving not visually distinguishable. Only significant needle ice events were scrutinized with further study, as visual confirmation and analysis of minor events proved difficult.

Deployed stations measured environmental conditions on twelve sensors every 5 minutes 10 seconds (Site 1), 5 minutes (Site 2) or ten minutes (Site 3). Each of the three cameras per study site captured images every 15 minutes. Three such study sites generated a vast amount of data, providing more than 2.2 million measuring points and over 93 000 images during the study. The following sections will provide information of data availability and consistency.

4.4.1 Availability and inconsistency of measured data

Recording consistency was important to allow comparisons to be made between stations. However, due to technical difficulties (Section 4.6) consistency proved difficult. In case of the cameras, the tri-camera (Camera 1, 2 and 3 for each site) setup offered some redundancy in the case of camera failure. The failed camera could be substituted for a working camera, as the three cameras observed roughly the same site area. The only observable difference would be that the substituted camera would either show images 5 or 10 minutes before or after compared to the malfunctioning camera, due to image staggering. Similar flexibility was however not available for the environmental sensors/loggers. Camera and sensor recording period is presented in Figure 4.13, 4.14, 4.15 and 4.16.

Measurements from Site 1 showed the least consistency (Figure 4.13), as no sensor had a full 12-month data set. Although Site 1 displayed the most identified needle ice events, attributed to its relatively long recording period (Figure 4.13). Site 1 had a non-functional +0cm temperature sensor, impacting analysis of needle ice initiation temperature from needle ice events prior to October 2014.

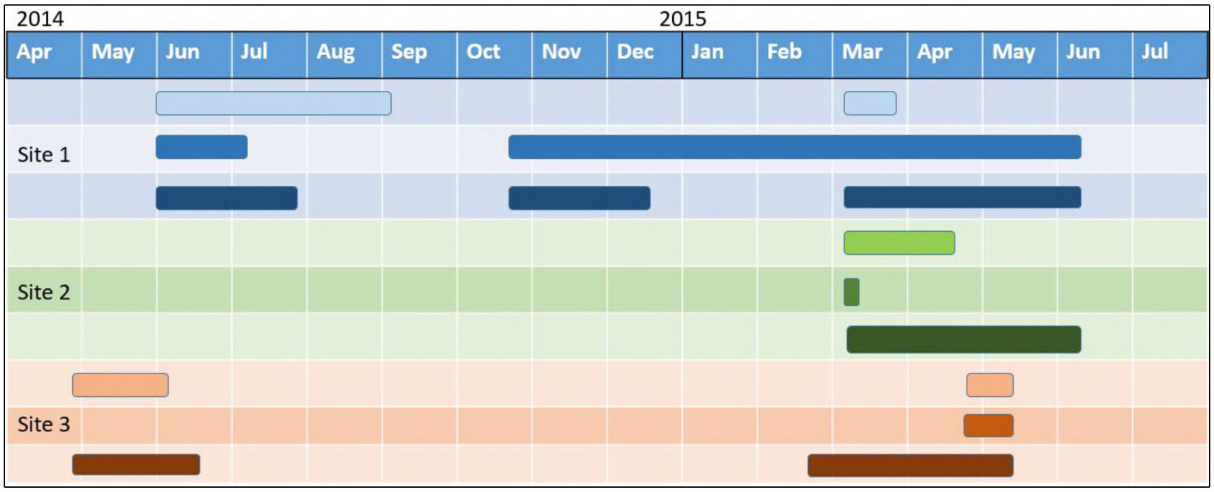

Figure 4.13. Camera recording period 2014-2015. Each sites camera (camera 1, 2 and 3) are represented in descending order

Site 2 provided consistent environmental data from all sensors except for ground temperature from April 18 to June 9 2015 (Figure 4.15). Site 2 provides full image covering of the three-month study period from Camera 3 (Figure 4.16).

Sensor data was continuous for Site 3, with the only gap in shallow soil moisture and wind related logging in the final two months of data collection (Figure 4.16). Similarly, camera functionality was consistent from late April 29 to June 9 2014 and from February 20 to May 5 2015. Between the two periods, thick, over 150cm, snow covered the study area and battery replacement for cameras was not possible.

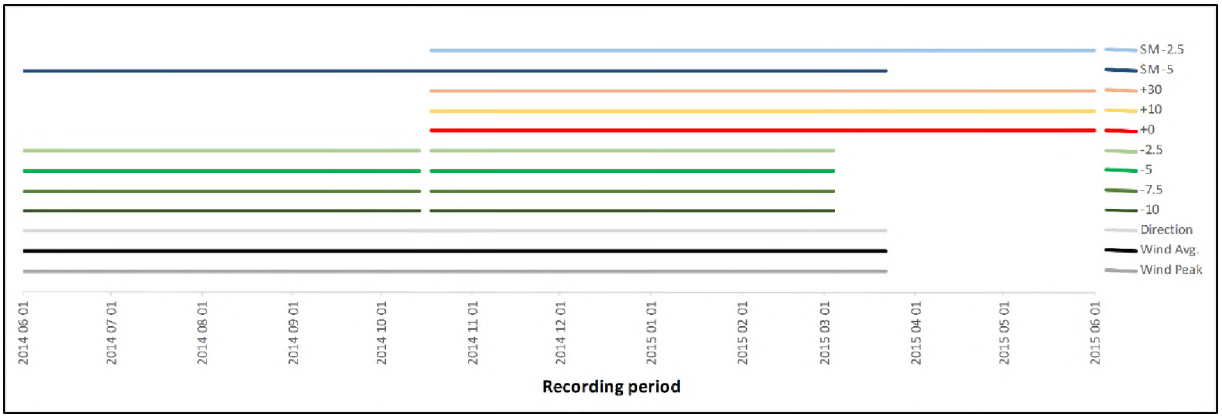

Figure 4.14. Site 1's individual sensors recording period from June 2014 to June 2015

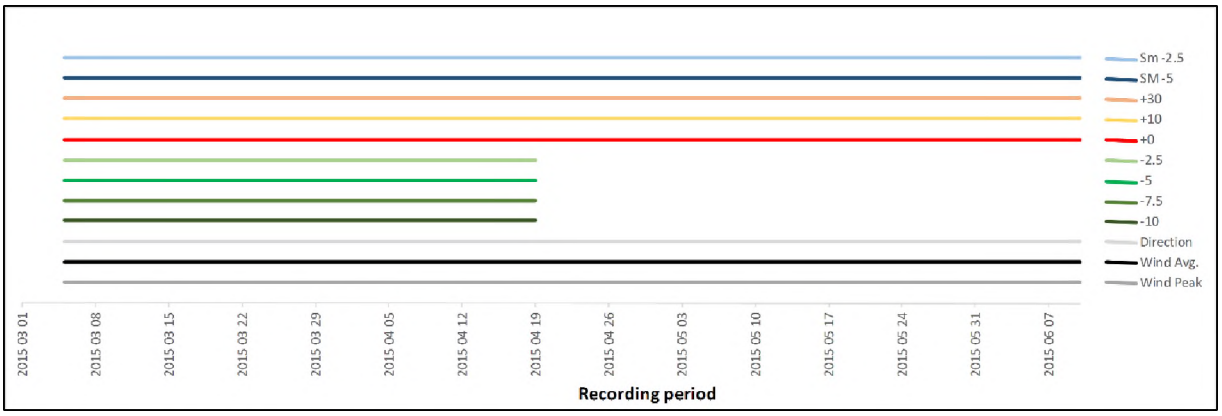

Figure 4.15. Site 2's individual sensors recording period March 2015 to June 2015.

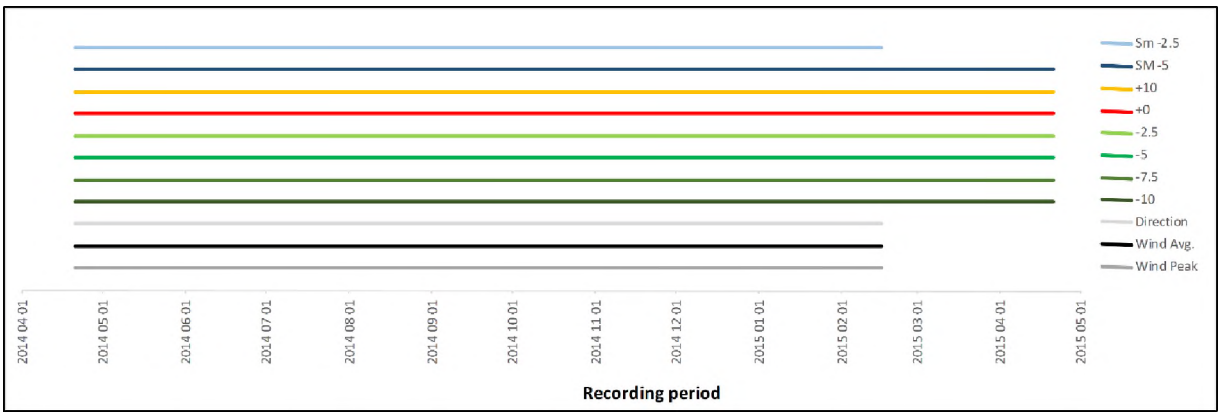

Figure 4.16. Site 3's individual sensors recording period from April 2014 to June 2015

Missing data or faulty readings are seen during maintenance of the logger stations. Battery changes and downloading occurred between October 14-18 2014 and March 4-6 2015 for Site 1, hence data measures indoor environments over that time-span. Site 2 only ran for one consolidated period and, hence, needed no maintenance. Site 3's maintenance was undertaken in the field, and took in less than an hour to complete, and did therefore not affect the analysis.

4.4.2 Data extraction, data merger and data analysis

The majority of data recorded did not directly relate to needle ice growth; the same is true for camera imagery. Removal of redundant data provided significant shortening of analysis times. Initial screening of camera imagery was undertaken by importing sequential images from each camera into Adobe Premiere®, creating a continuous video clip. Identification of 178 needle ice events resulted from repeat screening of created videos. Following identification of dates displaying needle ice growth, needle ice events were classified as significant, non-significant or non-events.

Each monitoring station produced duplicate images of needle ice sightings, resulting from the multi camera setup. Cameras captured 178 needle ice events; however, some individual events were captured by more than one camera. Duplicate sightings were removed from the 178 events, revealing 106 unique needle ice events. Additional classification based on event significance relating to visibility and continuity resulted in 82 events appropriate for further study. For an event to be classified as significant, visually clear initiation of growth and decay, no obstruction by freezing on camera lens as well as a full 24h of environmental monitoring were prerequisites. The 178 events were sub-grouped into study sites, classes and significance (Table 4.1).

Needle ice event distribution in all three locations focused on the winter months, with almost 75% of events occurring between April and July. However, this data is skewed as Site 2 did only measure from March to June 2015 and Site 3 was mostly non-functional between August 2014 and February 2015 (Figure 4.13).

Table 4.1. Distribution of needle ice events between sites and classification of event prominence.

Site	Significant	Non-significant	Unique events	Total
Site 1	44	78	68	122
Site 2	22	6	25	28
Site 3	16	12	23	28
Total	**82**	**96**	**106**	**178**

4.4.3 Grouping of environmental data

For each needle ice growth to decay event studied, environmental data ranging from 12h prior to, to 12h after midnight of the event was collected. To clarify, if needle ice initiation is seen at 18:00 on the 5thof a particular month, and decay initiation at 07:00 on the 6th, monitoring of environmental conditions were extracted from 12:00 on the 5th to 12:00 on the 6th, and the event was classified as taking place on the 6th.

For managing environmental measurements during these events, data extraction equations were created. Specific date and time supplied equation input, extracting sensor data from 12h prior to 12h after the specific input date. Similar equations extracted values for average, minimum and maximum sensor reading form the consolidated Excel-file during the specific event. Consolidated Excel-data from the loggers consisted of rows representing each sensor. Row letter in the equation indicated corresponding sensor while $Date_{prior}$ and $Date_{after}$ represent the row 12h prior and after midnight of the night of the needle ice event, which varied as the logging time was not consistent between the three loggers. Input values for date was semi-manually input into each equation using Excel (Extraction 1, 2 and 3).

Extraction 1 = AVERAGE(INDIRECT("Row" &$ $Date_{prior}$):INDIRECT("Row" &$ $Date_{after}$))

Extraction 2 = MIN(INDIRECT("Row" &$ $Date_{prior}$):INDIRECT("Row" &$ $Date_{after}$))

Extraction 3 = MAX(INDIRECT("Row" &$ $Date_{prior}$):INDIRECT("Row" &$ $Date_{after}$))

Outputs from Extraction 1, 2 and 3 could be varied depending on input time-span.

4.5 Physical soil properties

Soil analysis of particle size distribution and organic content was carried out for each study site. A 7.9 x 5.9 x 5 cm (233cm^3) soil sample was collected from the surface to 5cm depth for analysis using a bulk density square. Soil profiles from both Site 1 and 2 in Tiffindell and from Site 3 on Marion Island show an above surface layer comprised of rocks and pebbles while the subsurface soil is homogenous (Figure 4.17). After drying at 105°C for 24h, grain size distribution and carbon loss on ignition was performed. Textural analysis was undertaken using 8000, 4000, 2000, 1000, 500, 250, 125, 63 and less than 63 µm sieves, while loss on ignition technique exposed the dried soil samples to 450°C in a muffle oven for 4 hours. The weight loss of combusted carbon proxies organic content in the sample (Cambardella et al., 2001). Porosity was additionally calculated from density and volume using methods described in (Brady et al., 1996). Results on particle size distribution, loss on ignition and porosity are displayed in Table 5.10 and Figure 5.20, 5.21 and 5.22 in Chapter 5. Imagery from study sites, showed surface movement of particles from fines (<0.064mm) to large stones (>20mm). Holness (2001) showed a

relation between particle size and movement distance from Marion Island. Particles in this dissertation will be classified into three groups depending on size. The three classes are soil matrix, small stones and large stones. Incorporated into the matrix are particles smaller than 2mm, while small stones are defined as ranging from 2-20mm. Stones larger than 20mm are classified as being large rocks. A single boulder with a calculated weight of ca 25kg was observed to be displaced by needle ice action; this observation will be discussed separately in Section 6.2.1.

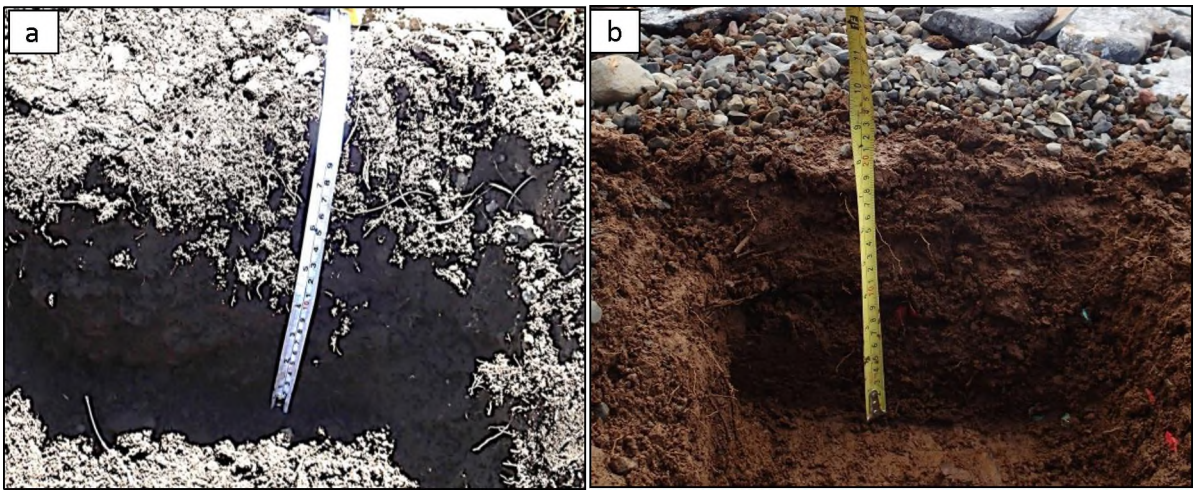

Figure 4.17. Typical soil profiles for Site 1 and 2 at Tiffindell (a) and Site 3 on Marion Island (b).

4.6 Limitations

Three identical setups were deployed in the field over a time period of 14 months. Problems encountered with each setup were recorded and used to subsequently improve following deployments. However, certain technical problems were hard to predict and even when precautions are taken, they still occurred.

The intention of the methods applied was to deploy identical setups. However, due to limitations in equipment and errors during measurements, perfect mirrors were not established. The most significant difference was encountered with logging intervals. All loggers had an intended logging interval of 5 minutes, however due to a mistake during programming one of the loggers from Site 1 was setup to log at an interval of 5 minutes and 10 seconds. Alleviation of this error was done by removing every 31st logged measurement from the other loggers from Site 1, re-aligning the measurements with the other loggers every five minutes. This ensued a constant increase in discrepancy of 10 seconds for 30 measurements before the removal of the 31st logging, thereby synchronizing the two correctly programmed loggers with the faulty logger. The increase in discrepancy creates a maximum shift of 4 minutes and 50 seconds before synchronization occurs. Additionally, due to logger inaccessibility and limited battery life, the environmental measurement interval at Site 3 was changed from five to ten minutes.

The discussion that follows identifies specific problems encountered during field measurements.

4.6.1 Problems encountered with field setup

Technical and environmental problems prevented a full time-series of pictures from each camera and logger during the study. Some malfunctions had critical impact on data gathered while others could be circumvented.

4.6.1.1 Battery life

The most unpredictable and variable problem encountered with the Bushnell cameras was the vast difference in battery life between camera setups. Cameras, batteries and software setups were identical, yet battery life ranged from a minimum of 2500 pictures takes to a maximum of over 11 000 in a single charge. There was no apparent consistency in battery capacity between cameras, despite the same batteries and cameras being used.

To ensure maximum battery capacity, overnight charging of each set of eight batteries with brand specific chargers preceded each installation. Additionally, great care was taken to not allow moisture into the camera battery housing by the use of a silicone seal of each camera. The Pace® EC55 cases were additionally sealed with silicone.

4.6.1.2 Battery dislodgement

Bushnell cameras do not have a power light, making external identification of camera power supply difficult. Hence, unplanned dislodgement of camera batteries took place while transporting cameras to the study site, as well as during rough weather conditions. The cameras will instantly lose its time and date setting if power connection is broken for just a second and then reconnected. Upon disconnection, the camera reverts time and date back to factory settings. Resetting of camera time-stamps was not detrimental to the study, as cameras would not loose data. Noting previous sequential images time and date, time stamps can be adjusted to correct dates using third party software (Adobe Lightroom®). However, in the situations where batteries were dislodged and did not reconnect, significant data was lost. Similar dislodgement occurred with one of the loggers during a single event causing the loss of four months of near surface temperatures, surface temperatures and -5 cm soil moisture at Site 1.

Following the battery mishaps, to minimize the chance of battery dislodgement, duct tape was applied over the battery row inside the housing of each camera. This problem has subsequently been resolved in later models of the Bushnell Camera system, as the battery housing in recent models have lips, preventing such dislodgement.

4.6.1.3 Damaged/obstructed equipment

The harsh weather conditions (described in Chapter 3) encountered at the study sites made installation of equipment difficult, and impacted results. Most notably is the anemometer fitting from Site 3 snapping during strong winds. Fortunately, the arm did not damage surrounding equipment e.g. the cameras, however wind related measurements were lost for the last two months of monitoring.

Rime ice growth on the camera lenses obstructed many of the images (Figure 4.19). This was unavoidable, and no action was possible to reduce the impact of such failure. From analysis of partial images, this blocked visual inspection of several needle ice events.

4.6.1.4 Swaying of the pole

Wind speeds were at times strong enough that, despite stabilization of the metal pole supports with rocks, the camera still swayed, resulting in blurry or shifted imagery. With the use of third party software (Adobe Premiere®) this could however be visually corrected to great success by using image filters and stabilizing effects.

4.6.1.5 Deep snow

Site 3 was located in an environment with seasonal snow cover, despite previous records to the contrary (see Holness 2001). The entire monitoring station was submerged by snow for six months of the 14-month study. Snow was deep enough to stop the anemometer from moving, providing a possible indication of snow depth in excess of 150cm (Figure 4.18).

4.6.2 Summary

The most severe impacts resulting from malfunctioning equipment or environmental properties arose from a logger failure and the unfortunately snow-covered measuring site (Section 3.3.3), both resulting in loss of data. The logger that failed due to battery dislodgement, was unfortunately the logger measuring temperature at +30, +10, +0 cm and soil moisture -5 cm.

Temperature measurements at +0 cm are most crucial to the study, as the logger provides temperature measurements for needle ice initiation. As the +0 cm was not logging, the -2.5cm sensor was used as a proxy for subsurface temperatures for portions of Site 1 temperature data analysis. Using temperatures 2.5 cm deeper than the surface had major impact of the analysis of needle ice growth, as very shallow freezing events would not register at -2.5 cm depth, and thereby initiation of growth

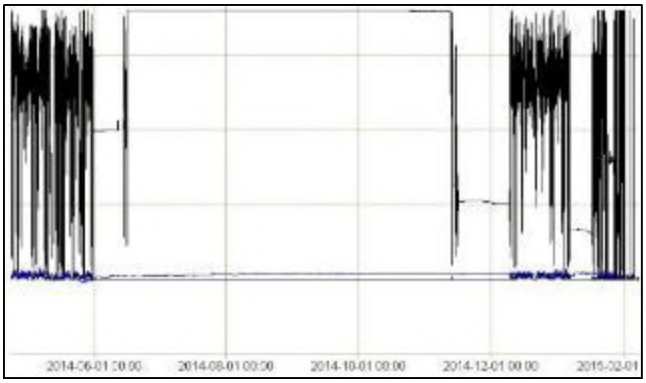

Figure 4.18. Anemometer results showing the effect of snow cover

Figure 4.19. Icing up of camera lens by wind and snow

could not be accurately observed. The second major circumstance impacting results was the six months of snow cover at Site 3. Placing the logging station at that specific location was intended to supply the study with 14 months of diurnal needle ice imagery; however, this was severely reduced to less than six months because of equipment being buried in snow, cutting the data set in half.

Aforementioned methodologies describe setup of the used monitoring stations and methodologies for data acquisition. The subsequent chapter will present results focusing on needle ice environmental and temporal dynamics.

Chapter 5 – Results: Needle ice growth and decay

The growth and melting of needle ice, as discussed in Chapter 2, has been studied and measured for close on 200 years. There are still uncertainties regarding the dynamics of needle ice initiation temperature, surface energy movement, growth depth and temporal growth and decay, as relatively few needle ice events have been studied in great detail.

The following chapter aims to present high-frequency data identifying the environmental signatures for needle ice growth, in conjunction with imagery from needle ice events captured from three monitoring stations between April 2014 and June 2015. Observations focus on environmental parameters during initiation of growth and melt as well as circumstances that do not produce ice needles. In addition, the duration of needle ice events, needle ice initiation depth, latent heat release and zero-curtain effects will be analysed. Supporting imagery will be presented alongside time-series analysis of camera and environmental data recorded.

Results gathered from the three measuring stations, two located at Tiffindell and one on Marion Island, will be differentiated between two main groups: sensors readings and images. Sensor readings were gathered from the six temperature and two soil moisture sensors and a single anemometer mounted at each site, while images were produced from the three cameras similarly equipped at each measuring station.

To answer the research questions, numeric results, such as temperature, soil moisture and wind speeds, were analysed mainly through the use of descriptive statistics. However, a similarly large portion of data was in the form of imagery. The imagery was analysed by visual inspection, measuring displacement distances and active movement mechanisms by observing changes in sequential images as well as combining images into videos, making changes in surface material more distinguishable during image analysis. Measured distances and identified active mechanisms where thereafter statically analysed.

As the dataset is big and incorporated several ways of visualizing results, the following sections aim to familiarise the reader with the data obtained during the study.

5.1 Data overview

Environmental data gathered from a variety of sensors connected to data loggers was downloaded as comma separated text files and imported into excel. However, the more than 2.2 million measurement points were difficult to oversee. Working with environmental data on a diurnal basis with a fractured data set, as explained in Section 4.6, makes comparison and statistical analysis difficult. Therefore, this study refrains from using yearly or seasonal averages and instead focuses on diurnal conditions where

a full 24-hour measuring record was available for sensors and cameras, Figure 5.1, 5.3 and 5.5 present an overview of the gathered environmental data from Site 1, 2 and 3 respectively. Due to the fractured data and considering Site 2 only had three months of measurements, the extremes and intra-site variability (Figure 5.1, 5.3 and 5.5) is of more relevance than a direct comparison between the three study sites. Figure 5.2, 5.4 and 5.6 show all sensor data for Site 1, 2 and 3 over the complete study period. Each sensor type and position retains the same colour scheme in all subsequent figures, i.e. blue for soil moisture, yellow-red-brown for air and surface temperature, greens for soil temperatures and grey-black for wind speed. Similarly, all soil moisture measurements are displayed in percent (%), temperature reading in degrees Celsius (°C) and wind speeds in meter per second (m/s).

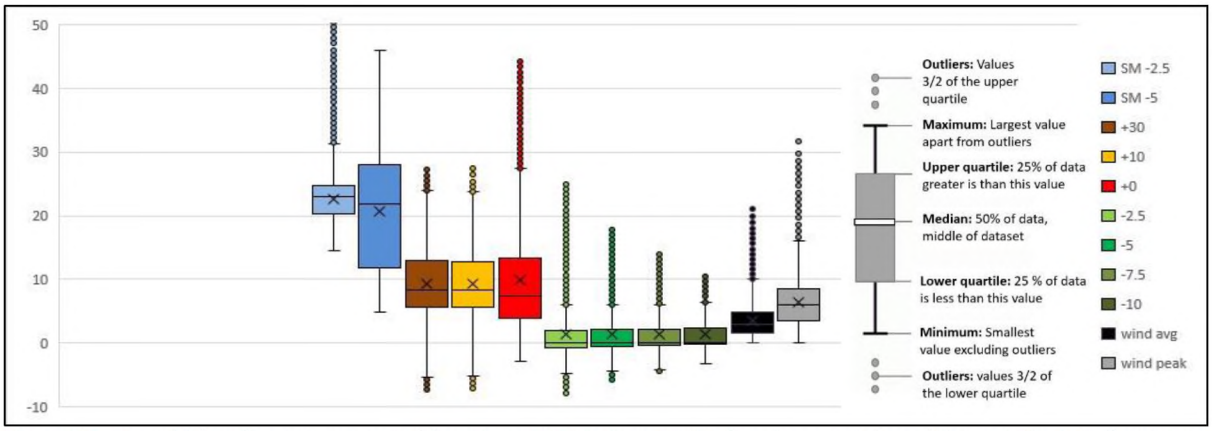

Figure 5.1. Box-whisker diagram generated from June 2014 to June 2015 of environmental conditions at Site 1. Soil moisture, temperature and wind speeds are measured in percent, degrees Celsius and meters per second respectively.

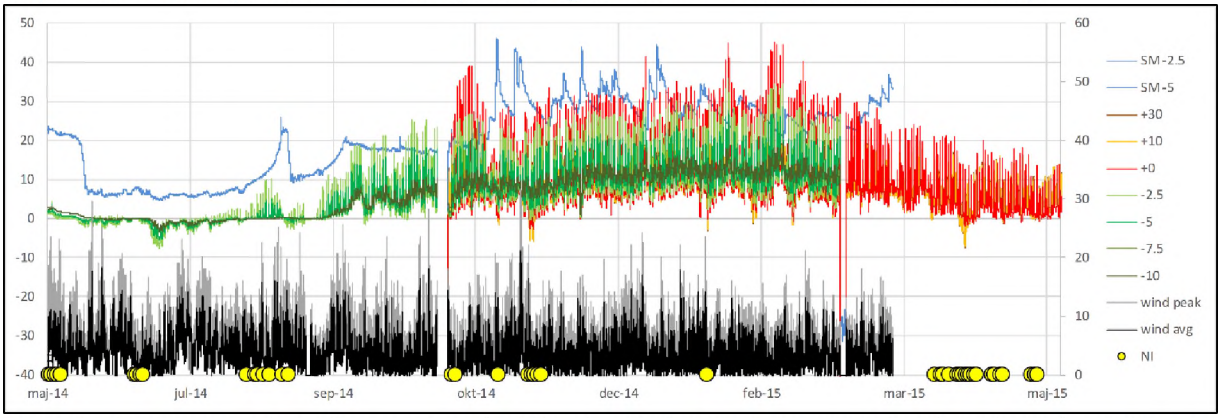

Figure 5.2. Measurements from all sensors over the full study period at Site 1. Average and peak wind speeds are shown on the secondary axis. Soil moisture, temperature and wind speeds are measured in percent, degrees Celsius and meters per second respectively. The yellow dots (NI) show needle ice events.

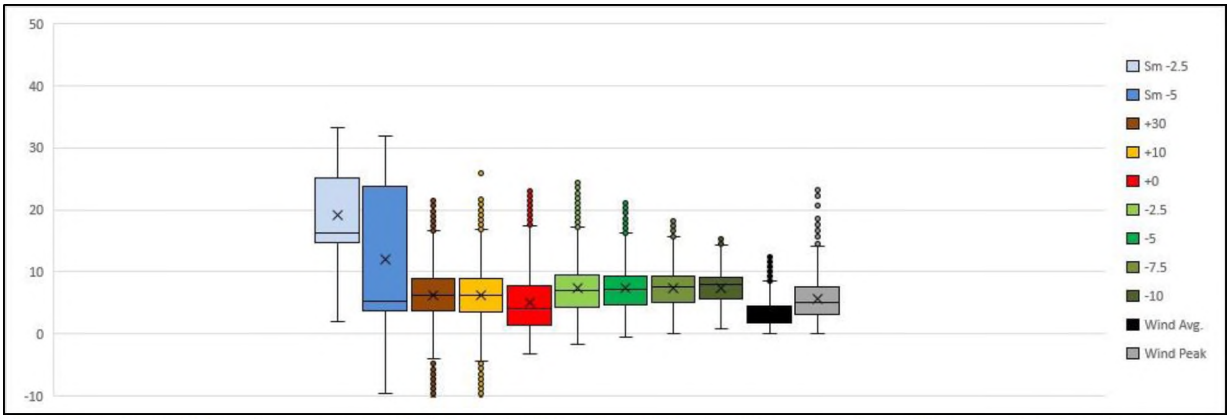

Figure 5.3. Box-whisker diagram generated from April to May 2015 of environmental conditions at Site 2. Soil moisture, temperature and wind speeds are measured in percent, degrees Celsius and meters per second respectively.

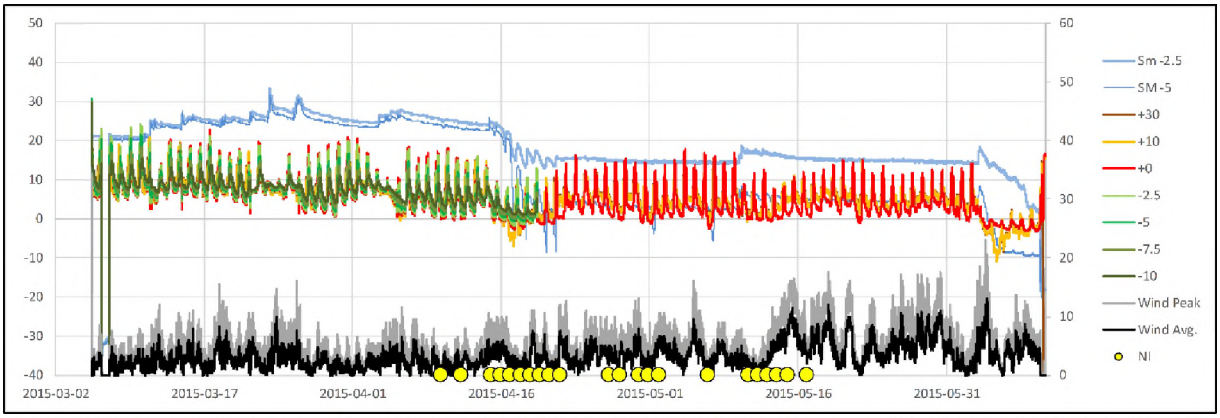

Figure 5.4. Measurements from all sensors over the full study period at Site 2. Average and peak wind speeds are shown on the secondary axis. Soil moisture, temperature and wind speeds are measured in percent, degrees Celsius and meters per second respectively. The yellow dots (NI) show needle ice events.

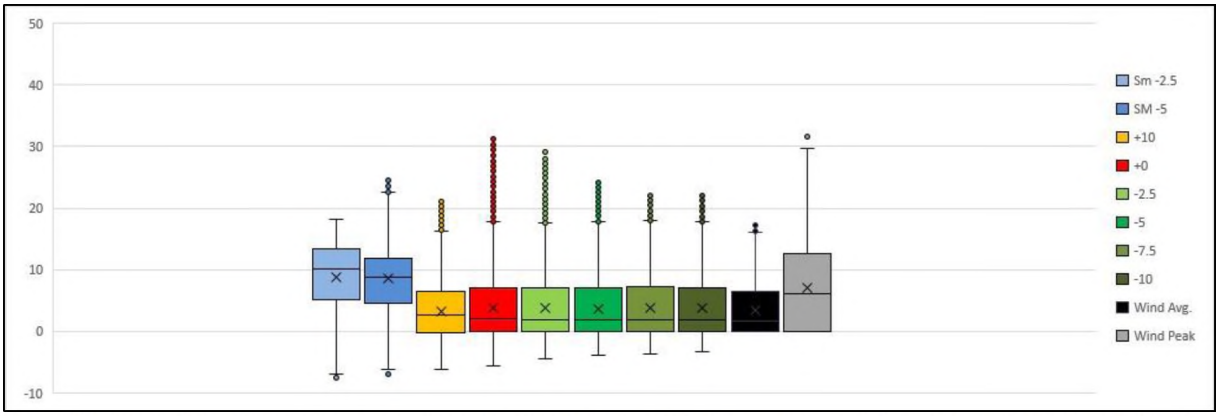

Figure 5.5. Box-whisker diagram generated from April 2014 to April 2015 of environmental conditions at Site 3 excluding the six month of snow cover from July 2014 to Jan 2015. Soil moisture, temperature and wind speeds are measured in percent, degrees Celsius and

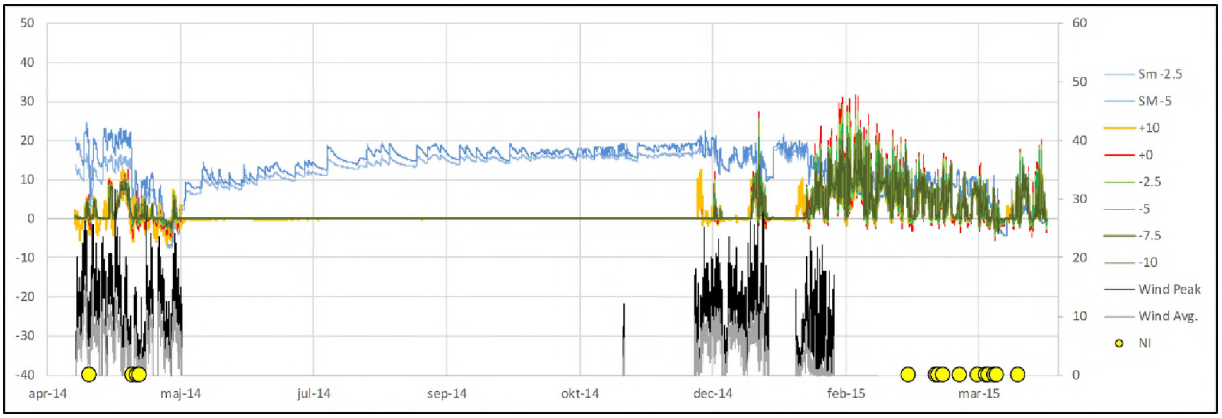

Figure 5.6. Measurements from all sensors over the full study period at Site 3 including the six months of snow cover. Average and peak wind speeds are shown on the secondary axis. The yellow dots (NI) show needle ice events.

In addition to the environmental sensor data, a very large data set of images was acquired during the study. Imagery from the nine cameras at the three study sites over the 14-month study resulted in 93 952 images. Even when combining the images into a video-file, the video was more than 60-minutes long, hence difficult to display in a thesis. Imagery and videos in the following chapters (5 and 6) focus on illustrating events that highlight processes essential to answering the questions set in Chapter 1. The videos display active surface material displacement in addition to *needle ice sediment displacement* (NISD) distance, while images show specific initiation timing and pre and post states of the processes.

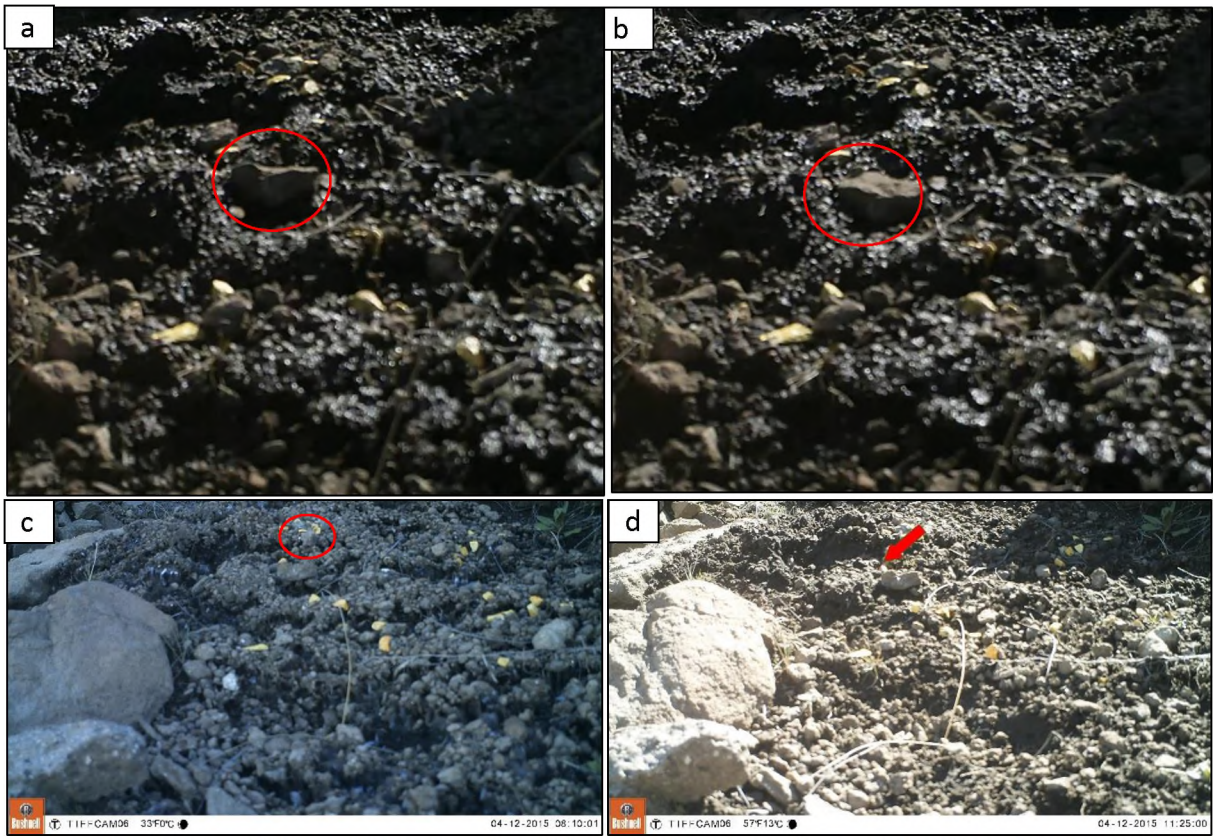

Figure 5.7. Frames a) and b) show displacement of a cobble sized rock by the mechanisms of toppling, while frames c) and d) display displacement by rolling. Events occurred on the 12th and 16th of April 2015 at Site 2.

As an example, Frames 5.7a and 5.7b in Figure 5.7 show the displacement of a cobble sized rock during a single night. In Video 10 the rock can be seen to be lifted by needle ice, resettling downslope several centimetres from its original position. Furthermore, Frames 5.7c and 5.7d in the same figure show the displacement (red arrow) of a small stone, which can be seen rolling in Video 11.

5.2 Needle ice events

The following section will present analysed needle ice events captured from each study site and their date of observation, overlain by sensor and camera recording period. Analysis of imagery from Site 1, 2 and 3 show a total of 178 needle ice events. After removal of duplicates and events without a full dataset, 82 out of the 178 were used for further analysis. Sites 1, 2 and 3 had 44, 22 and 16 needle ice events respectively, as summarized in Table 4.1. Needle ice events were observed from May 31 2014 to May 12 2015 at Site 1, from April 10 to May 17 2015 at Site 2 and from April 27 2014 to April 11 2015 at Site 3. Figure 5.8, 5.9 and 5.10 show dates in which needle ice growth was observed (yellow circles), overlain by sensor (line with corresponding sensor colour) and camera recording periods (coloured bar) for each study site. Several needle ice events show overlapping sensor and camera recordings of the same event, while other periods do not display sensor or camera coverage.

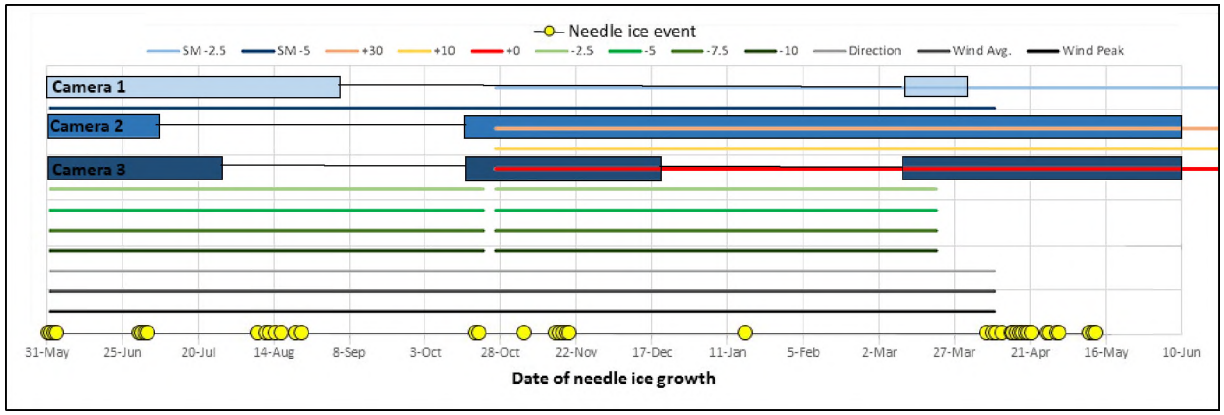

Figure 5.8. Needle ice events (yellow circles) recorded by the three cameras (blue bars) from Site 1 between May 2014 and May 2015 and sensor data availability (coloured lines)

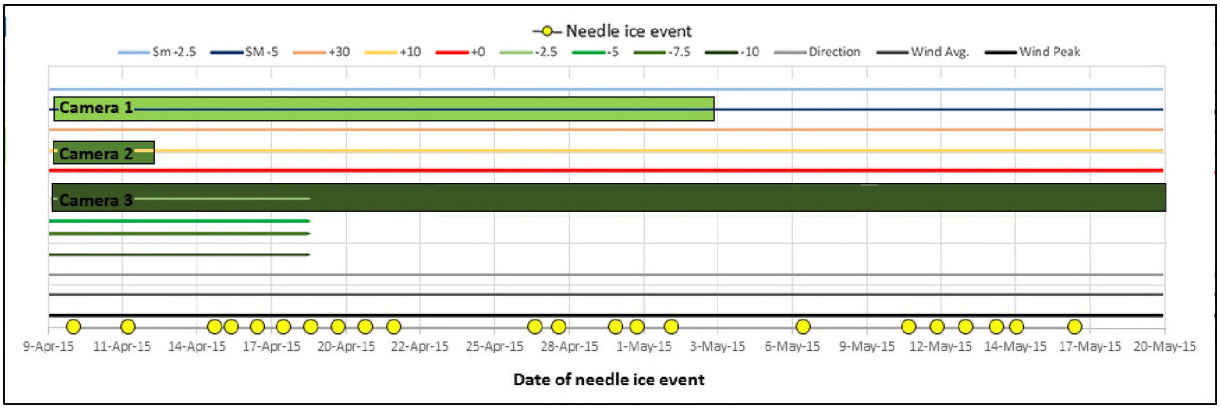

Figure 5.9. Needle ice events (yellow circles) recorded by the three cameras (green bars) from Site 2 between April 10 and May 17 2015 and sensor data availability (coloured lines)

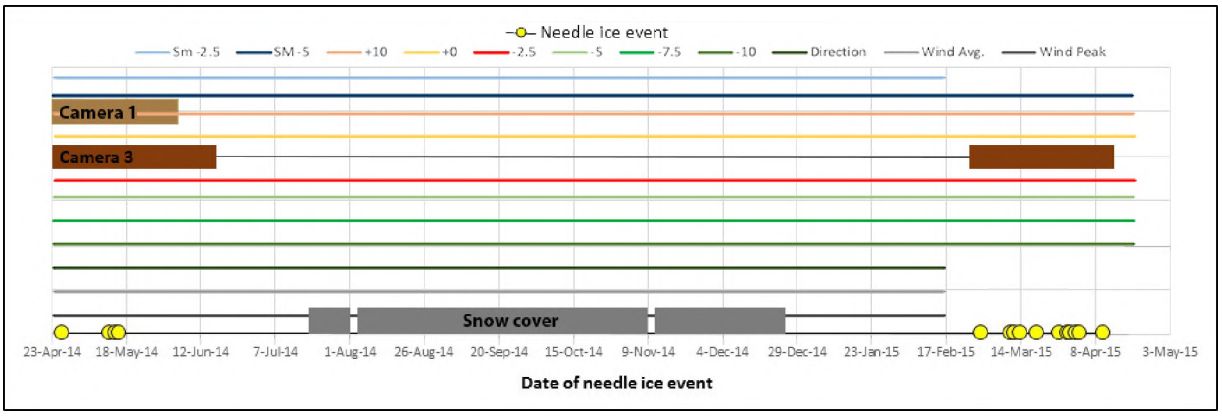

Figure 5.10. Needle ice events (yellow circles) recorded by three cameras (brown bars) from Site 3 between April 27 2014 and April 11 2015 and sensor data availability (coloured lines).

The record period at Site 1 covered the majority of a calendar year, while Site 2 and 3's imagery only covered parts of the year. Although Site 2 showed the most continuous monitoring, the station was only established in March 2015 and only covered a study period of three months. Observations at Site 3, as shown in Section 4.6, were influenced by snow cover over a major of the period, drastically reducing the period of useful sensor and image coverage.

5.3 Environmental conditions of needle ice growth and decay

A lack of documented direct field observations of needle ice growth events was noted from the literature review in Chapter 2. This section will present environmental conditions for visually observed needle ice growth events as well as the environmental signature for needle ice initiation and decay. Focus will be on showing under which environmental conditions needle ice grows and does not grow, verified with camera imagery.

5.3.1 Site 1

The station at Site 1 captured a total of 44 needle ice events during the 12-month measurement period. Table 5.1 summarises the environmental conditions associated with all 44 events at the moment of

visually observable needle ice growth initiation. Needle ice initiation occurred under a range of environmental conditions; soil surface temperatures at the moment of initiation spanned 2.3°C (between -0.1 and +2.2°C), soil moisture ranged 8.5% (between 17.4% and 25.9°C) and 30.4% (between 7.1% and 31.5%) at -2.5cm and -5cm respectively. Furthermore, wind speeds varied between 0m/s and 12.6m/s at growth initiation.

Table 5.1. Environmental measurements from Site 1 at the point of visual needle ice growth initiation. Blank cells indicate sensor failure.

Site 1												
	Soil moisture		Temperature							Wind speed/Direction		
	%		°C							°	m/s	
	May 2014 - May 2015											
	-2.5	-5,0	+30	+10	+0	-2.5	-5	-7.5	-10	Direction	Avg Wind	Peak Wind
2014-05-31 19:30		23,0				1,5	2,0	2,3	2,6	301,6	6,8	12,6
2014-06-01 18:30		23,0				2,1	2,8	3,1	3,1	300,9	2,3	7,0
2014-06-02 18:00		22,6				0,7	1,4	1,9	2,3	360,0	4,1	9,6
2014-06-03 15:30		21,9				0,4	0,9	1,4	1,9	327,7	4,1	10,1
2014-06-04 20:15		21,9				0,4	0,7	1,2	1,6	292,1	3,1	9,1
2014-06-30 21:45		8,0				-0,1	-0,1	-0,1	-0,1	319,4	0,6	2,0
2014-07-01 18:00		8,2				0,0	-0,1	-0,1	-0,1	235,9	1,2	3,5
2014-07-02 18:30		7,8				-0,1	-0,1	-0,1	-0,1	298,8	0,6	2,5
2014-07-03 19:15		7,1				-0,4	-0,2	-0,2	-0,1	0,2	0,2	1,0
2014-08-09 00:10		8,7				-0,1	-0,1	-0,2	-0,2	5,6	3,4	5,0
2014-08-11 20:25		10,0				0,0	0,0	-0,1	-0,2	277,0	2,2	3,0
2014-08-12 20:10		10,3				0,0	0,0	0,0	-0,1	252,8	2,0	4,5
2014-08-14 21:10		11,4				0,0	0,0	0,0	-0,1	268,9	1,6	5,0
2014-08-16 20:40		12,9				0,3	0,4	0,2	-0,1	259,9	2,0	4,0
2014-08-21 18:25		22,4				0,0	0,3	0,3	0,1	263,1	4,5	8,0
2014-08-23 16:25		17,2				-0,1	-0,1	0,0	0,1	260,9	3,0	6,5
2014-10-19 23:10	17,4	20,2	5,9	5,8	**1,6**	2,7	4,0	5,0	5,4	265,7	2,4	4,0
2014-10-21 00:25	16,1	19,6	5,5	5,6	**1,6**	3,2	4,8	6,0	6,6	186,0	0,0	0,5
2014-11-05 00:25	24,8	37,4	-1,5	-1,4	**-0,1**	1,5	3,3	4,5	5,5	216,7	7,0	10,1
2014-11-15 19:10	24,1	30,2	-1,7	-1,7	**0,1**	2,8	6,0	7,9	8,7	278,0	8,4	11,6
2014-11-16 19:25	23,8	29,3	-2,7	-2,7	**0,3**	2,8	5,8	7,2	7,6	115,5	1,3	2,0
2014-11-17 19:40	23,5	28,3	-0,3	-0,5	**2,2**	4,8	7,6	8,8	8,8	63,1	0,0	0,0
2014-11-19 02:25	22,7	27,5	2,0	2,1	**0,6**	2,0	4,1	5,7	6,9	249,9	3,6	6,0
2014-11-20 02:55	21,9	26,5	3,9	3,9	**1,0**	2,4	4,6	6,2	7,4	249,0	3,5	6,5
2015-01-17 03:55	25,1	31,5	-2,3	-1,9	**0,2**	2,9	6,5	8,9	10,5	211,6	1,3	3,0
2015-04-07 02:25	25,9		3,0	3,0	**2,0**							
2015-04-09 02:55	25,0		1,8	1,8	**1,2**							
2015-04-09 22:10	24,6		5,0	4,9	**2,1**							
2015-04-11 23:55	23,8		5,4	5,3	**1,9**							
2015-04-15 03:10	23,5		0,4	0,4	**1,0**							
2015-04-15 18:40	23,2		-0,4	-0,4	**1,3**							
2015-04-16 18:40	22,9		-1,4	-1,3	**1,8**							
2015-04-17 18:25	22,4		-2,8	-2,6	**0,7**							
2015-04-18 18:40	22,1		-0,5	-0,5	**0,5**							
2015-04-19 16:55	22,1		3,1	3,2	**1,1**							
2015-04-20 18:25	21,7		1,2	1,2	**0,5**							
2015-04-21 18:10	21,5		2,5	2,6	**1,3**							
2015-04-26 21:25	20,6		3,0	2,9	**1,2**							
2015-04-27 18:25	20,4		3,4	3,4	**1,8**							
2015-04-29 23:25	19,8		3,7	3,7	**1,8**							
2015-04-30 20:10	19,6		0,0	0,0	**0,5**							
2015-05-10 21:10	21,3		0,1	0,2	**1,1**							
2015-05-11 23:40	20,6		-0,3	-0,2	**0,6**							
2015-05-12 22:55	20,0		0,6	0,7	**0,5**							

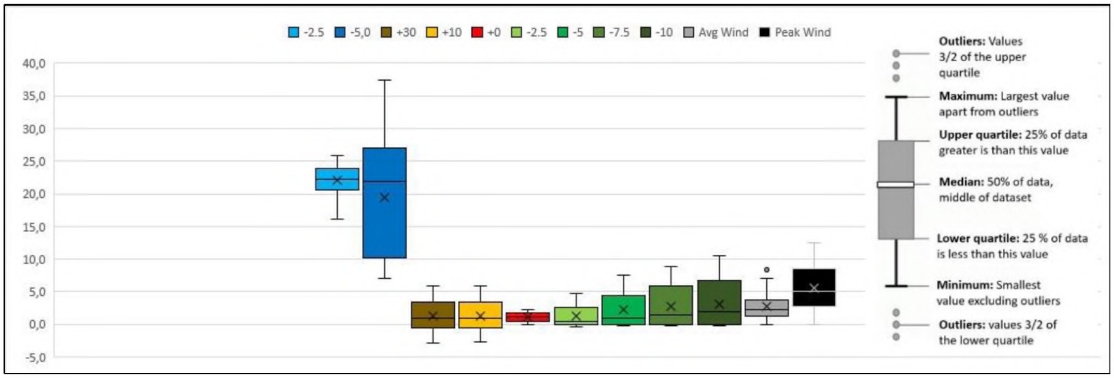

Figure 5.11. Box - Whisker diagram summarising environmental data at the moment of growth initiation from Site 1.

A noteworthy observation is that a majority of events display positive surface temperatures during needle ice growth initiation. Events on the 19th and 21st of October and 19th and 20th of November show no negative air, surface or ground temperatures at the moment of initiation. Needle ice growth at positive temperatures will be analysed in subsequent sections.

Site 1 displayed 28 needle ice events with available air and surface temperatures during initiation of needle ice growth, 15 showed a positive temperature gradient from the air towards the ground, while the remaining 13 displayed the opposite. Ten needle ice events had both air, surface and ground temperatures available, all displaying a positive soil temperature gradient, not necessarily below freezing, with depth beneath the surface. Of the 16 events without air or surface temperatures at initiation, nine displayed decreasing temperatures with depth (by ca 0,1°Cper 2.5cm) and the remaining seven showed increasing temperatures with depth. Four of the nine needle ice events with available air, surface and ground temperatures show the surface temperature to be lower than both air and ground measurements.

Measurements of environmental parameters were also collected at the moment of visual needle ice decay initiation, denoted in the imagery by the image sequence showing maximum ice needle extent, followed by an image of ice needles weakening. Results are presented in Table 5.2. Subtracting the initial environmental values of Table 5.1 from Table 5.2 created Table 5.3, which displays change in environmental parameters from initiation of needle ice growth to initiation of decay. Table 5.3 shows that the majority of soil moisture readings had lowered following a night of needle ice growth. Changes in soil moisture content ranged from a minimum change of 0,0% to a maximum of -7.4%, with an average change of -0.7% for both the -2.5cm and -5cm soil moisture sensors. However, the 7.4% change in soil moisture seen in the event on the 17th of January 2015 (Table 5.3) at the -5cm sensor is statistically an outlier. Average change for the -5cm sensor became -0.4% when excluding the outlier.

Air temperatures increased in all measurements but one at the point of decay, with an average temperature increase of 4.4°C and 4.7°C for the +30 and +10cm sensors. Surface readings displayed

lower temperatures in 23 out of the 28 available measurements with an average decrease of -0.7°C. Similar to the surface readings, the majority of subsurface temperatures had decreased at the onset of needle ice decay.

Table 5.2. Environmental measurements from Site 1 at the point of visual needle ice decay initiation. Blank cells indicate sensor failure. Box-Whisker plot with statistics below the table.

Site 1												
	Soil moisture		Temperature							Wind speed/Direction		
	%		°C							°	m/s	
	May 2014 - May 2015											
Date	-2.5	-5,0	+30	+10	+0	-2.5	-5	-7.5	-10	Direction	Avg Wind	Peak Wind
2014-05-31 19:31		23,0				1,5	2,0	2,3	2,6	301,6	6,8	12,6
2014-06-01 18:30		23,0				2,1	2,8	3,1	3,1	300,9	2,3	7,0
2014-06-02 18:01		22,6				0,7	1,4	1,9	2,3	360,0	4,1	9,6
2014-06-03 15:32		21,9				0,4	0,9	1,4	1,9	327,7	4,1	10,1
2014-06-04 20:13		21,9				0,4	0,7	1,2	1,6	292,1	3,1	9,1
2014-06-30 21:44		8,0				-0,1	-0,1	-0,1	-0,1	319,4	0,6	2,0
2014-07-01 17:58		8,2				0,0	-0,1	-0,1	-0,1	235,9	1,2	3,5
2014-07-02 18:30		7,8				-0,1	-0,1	-0,1	-0,1	298,8	0,6	2,5
2014-07-03 19:13		7,1				-0,4	-0,2	-0,2	-0,1	0,2	0,2	1,0
2014-08-09 00:10		8,7				-0,1	-0,1	-0,2	-0,2	5,6	3,4	5,0
2014-08-11 20:22		10,0				0,0	0,0	-0,1	-0,2	277,0	2,2	3,0
2014-08-12 20:08		10,3				0,0	0,0	0,0	-0,1	252,8	2,0	4,5
2014-08-14 21:08		11,4				0,0	0,0	0,0	-0,1	268,9	1,6	5,0
2014-08-16 20:40		12,9				0,3	0,4	0,2	-0,1	259,9	2,0	4,0
2014-08-21 18:23		22,4				0,0	0,3	0,3	0,1	263,1	4,5	8,0
2014-08-23 16:27		17,2				-0,1	-0,1	0,0	0,1	260,9	3,0	6,5
2014-10-19 23:11	17,4	20,2	5,9	5,8	**1,6**	2,7	4,0	5,0	5,4	265,7	2,4	4,0
2014-10-21 00:25	16,1	19,6	5,5	5,6	**1,6**	3,2	4,8	6,0	6,6	186,0	0,0	0,5
2014-11-05 00:26	24,8	37,4	-1,5	-1,4	**-0,1**	1,5	3,3	4,5	5,5	216,7	7,0	10,1
2014-11-15 19:12	24,1	30,2	-1,7	-1,7	**0,1**	2,8	6,0	7,9	8,7	278,0	8,4	11,6
2014-11-16 19:24	23,8	29,3	-2,7	-2,7	**0,3**	2,8	5,8	7,2	7,6	115,5	1,3	2,0
2014-11-17 19:41	23,5	28,3	-0,3	-0,5	**2,2**	4,8	7,6	8,8	8,8	63,1	0,0	0,0
2014-11-19 02:26	22,7	27,5	2,0	2,1	**0,6**	2,0	4,1	5,7	6,9	249,9	3,6	6,0
2014-11-20 02:53	21,9	26,5	3,9	3,9	**1,0**	2,4	4,6	6,2	7,4	249,0	3,5	6,5
2015-01-17 03:54	25,1	31,5	-2,3	-1,9	**0,2**	2,9	6,5	8,9	10,5	211,6	1,3	3,0
2015-04-07 00:26	25,9		3,0	3,0	**2,0**							
2015-04-09 02:56	25,0		1,8	1,8	**1,2**							
2015-04-09 22:11	24,6		5,0	4,9	**2,1**							
2015-04-11 23:56	23,8		5,4	5,3	**1,9**							
2015-04-15 03:11	23,5		0,4	0,4	**1,0**							
2015-04-15 18:41	23,2		-0,4	-0,4	**1,3**							
2015-04-16 18:41	22,9		-1,4	-1,3	**1,8**							
2015-04-17 18:26	22,4		-2,8	-2,6	**0,7**							
2015-04-18 18:41	22,1		-0,5	-0,5	**0,5**							
2015-04-19 16:56	22,1		3,1	3,2	**1,1**							
2015-04-20 18:26	21,7		1,2	1,2	**0,5**							
2015-04-21 18:11	21,5		2,5	2,6	**1,3**							
2015-04-26 21:26	20,6		3,0	2,9	**1,2**							
2015-04-27 18:26	20,4		3,4	3,4	**1,8**							
2015-04-29 23:21	19,8		3,7	3,7	**1,8**							
2015-04-30 20:11	19,6		0,0	0,0	**0,5**							
2015-05-10 21:11	21,3		0,1	0,2	**1,1**							
2015-05-11 23:41	20,6		-0,3	-0,2	**0,6**							
2015-05-12 22:56	20,0		0,6	0,7	**0,5**							

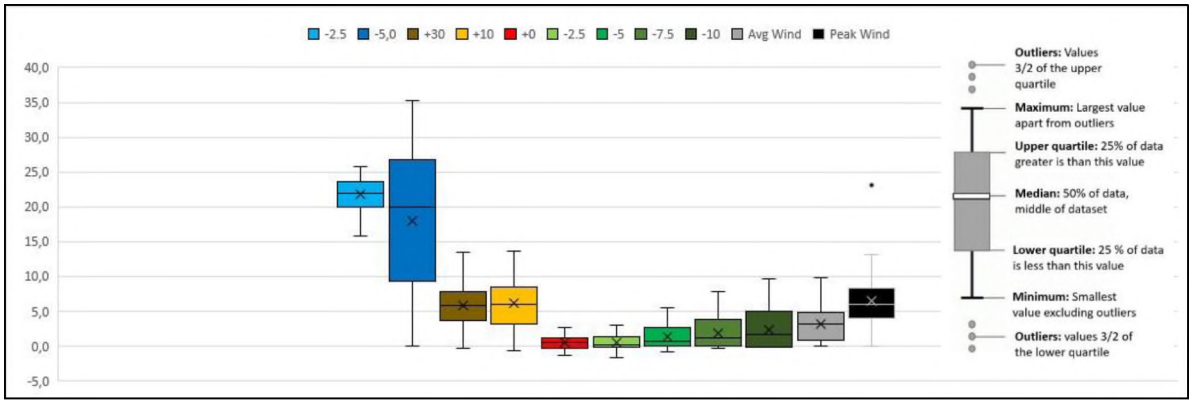

Figure 5.12. Box - Whisker diagram summarising environmental data at the moment of decay initiation from Site 1.

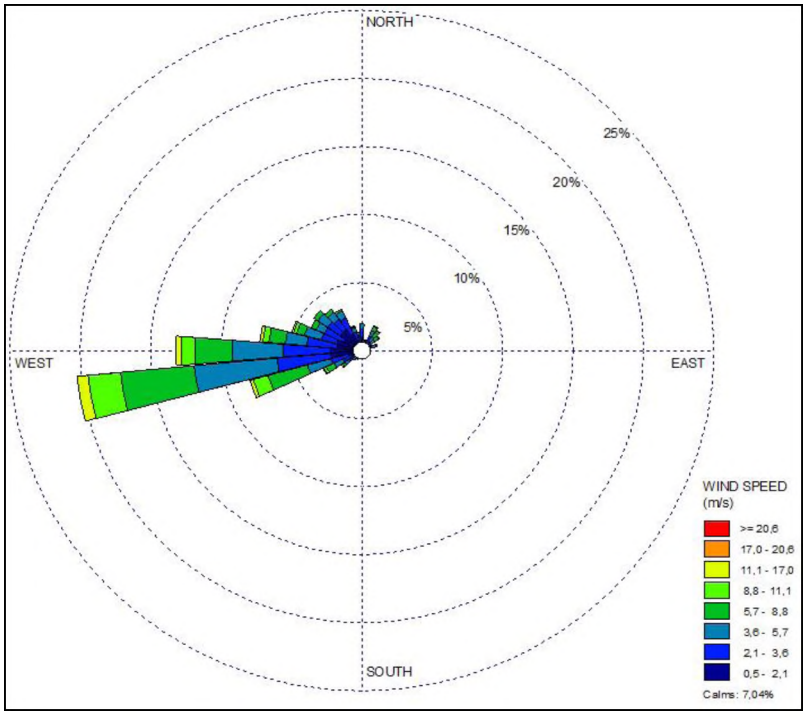

Figure 5.13. Wind rose plot for the period June 2014 - June 2015 from Site 1 showing an prevailing wind direction of west south-west.

The four ground temperature sensors combined showed 84 of the 96 readings to have decreased with an average of -1.1°C with the remaining 12 readings showed an average increase of 0.1°C. Most of the readings showing a temperature increase after the needle ice event occurred on August 9-14 2014.

Figure 5.13 displays the prevailing wind direction being from the west, indicating that the wind blew from the left in all of the imagery from Site 1.

Table 5.3. Changes in Site 1's environmental conditions from the point of growth initiation to the point of decay initiation. Blue, green and red cells indicate a reduction, a non-change or an increase of the measurement. Blank cells indicate sensor failure.

Site 1											
Soil moisture		Temperature							Wind speed/Direction		
%		°C							°	m/s	
May 2014 - May 2015											
-2.5	-5,0	+30	+10	+0	-2.5	-5	-7.5	-10	Direction	Avg Wind	Peak Wind
	-0,1				-0,1	-0,3	-0,3	-0,2	-36,8	3,0	10,6
	-0,6				-1,4	-1,4	-1,1	-0,7	-96,7	3,5	5,0
	-0,9				-0,9	-0,7	-0,5	-0,4	-128,2	0,1	-0,5
	-0,4				-0,2	-0,2	-0,2	-0,2	-132,2	-1,0	-4,0
	-0,3				-0,1	0,0	0,0	0,0	-70,2	-0,2	0,0
	-1,1				-0,3	-0,1	0,0	0,0	180,1	-0,7	-1,0
	-1,3				-0,8	-0,6	-0,3	-0,1	-69,6	4,1	4,5
	-0,5				-0,2	-0,3	-0,2	-0,1	160,1	0,6	3,0
	0,1				0,1	0,0	0,0	0,0	-10,4	-2,5	-0,5
	0,1				0,1	0,0	0,0	0,0	-31,8	0,3	1,5
	0,2				0,5	0,1	0,0	0,0	130,6	3,1	8,6
	0,1				0,3	0,0	0,0	0,0	119,0	-0,2	1,0
	0,0				-0,1	-0,3	-0,2	0,0	55,1	-0,2	1,0
	0,2				-0,5	-0,3	-0,2	0,0	-12,7	2,6	2,0
	-7,4				-1,6	-0,8	-0,4	-0,1	-93,2	1,3	0,5
-0,7	-0,3	4,7	4,8	0,2	-0,8	-1,4	-1,5	-1,2	-8,2	1,1	2,0
-0,3	0,1	7,9	8,1	-0,8	-1,3	-1,6	-1,6	-1,4	-0,1	0,0	0,0
-0,7	-2,1	7,2	6,5	0,6	-0,2	-0,6	-0,8	-0,8	-144,5	-3,9	-4,5
0,3	-0,6	6,4	8,4	-0,8	-2,8	-3,8	-4,0	-3,3	-16,4	-8,2	-9,6
-0,2	-0,6	6,6	5,0	-1,1	-3,0	-3,8	-3,7	-2,7	216,2	0,7	2,5
-0,4	-0,3	8,1	8,9	-1,6	-3,5	-4,7	-4,4	-3,2	392,6	5,3	8,0
-0,1	-0,1	4,8	3,5	0,4	-0,2	-0,6	-0,8	-0,7	-10,2	2,0	2,5
0,0	-0,1	1,8	2,0	1,6	0,5	-0,5	-0,9	-0,9	43,5	-1,6	-2,5
-0,1	-0,1	7,4	7,8	1,0	-0,2	-1,0	-1,1	-0,9	-280,4	3,1	3,0
-0,2		4,6	5,1	-0,2							
-0,1		6,3	7,1	0,0							
-0,2		2,8	4,7	-0,8							
-0,1		3,3	5,6	-0,3							
-0,3		0,8	2,5	-0,4							
-0,3		2,5	2,5	-0,9							
-0,9		1,1	0,6	-3,2							
-0,5		8,6	9,2	-1,7							
-0,1		2,2	2,2	-0,4							
-0,6		1,4	1,1	-1,4							
-0,4		5,6	9,2	-1,1							
-0,3		1,2	1,4	-1,0							
-0,5		3,7	5,0	-0,7							
-0,6		3,1	2,1	-1,6							
-0,4		-0,3	-1,1	-1,8							
-1,1		7,3	8,4	-0,9							
-0,8		8,0	6,3	-0,5							
-0,9		5,0	4,5	-0,4							
-0,9		1,8	1,2	-0,9							

5.3.2 Site 2

At Site 2, 22 needle ice events were identified during the three-month recording period from March to June 2015. Environmental conditions at the onset of needle ice initiation, seen in Table 5.4, show needle ice to initiate at surface temperatures from -1.3°C to 1.5°C (range of 2.8°C), and at soil moisture values from 14.4% to 25.4% (range of 11%) and 2.8% to 24% (range of 21.2%) at -2.5 and -5cm depth, respectively. Furthermore, needle ice measurements show needle ice to initiate at no wind up to wind speeds of 10.1m/s.

At the moment of initiation, 20 of the 22 needle ice events show ground surface temperatures to be lower than air temperatures, with the remaining two showing the opposite. Of the seven events, which have measurements for air, surface and ground temperatures, the surface temperatures were consistently lower than both air and ground temperatures.

Table 5.4. Environmental measurements from Site 2 at the point of visual needle ice initiation. Blank cells indicate sensor failure. Box-Whisker plot with statistics below the table.

Site 2												
	Soil moisture		Temperature							Wind speed/Direction		
	%		°C							°	m/s	
	March - June 2015											
	-2.5	-5,0	+30	+10	+0	-2.5	-5	-7.5	-10	Direction	Avg Wind	Peak Wind
2015-04-09 23:10	25,4	24,0	2,5	2,2	**0,4**	1,2	2,4	3,5	5,3	236,4	1,4	2,0
2015-04-11 23:40	24,7	23,2	4,3	3,8	**0,3**	1,1	2,3	3,4	5,0	305,0	1,6	3,0
2015-04-15 04:25	24,4	22,9	1,3	1,2	**0,2**	0,7	1,7	2,7	4,3	102,4	5,4	8,6
2015-04-15 19:25	23,8	22,1	0,8	0,8	**0,2**	1,0	2,0	2,9	4,3	106,6	3,9	5,5
2015-04-16 18:25	21,9	20,1	-0,4	-0,4	**0,5**	0,9	1,9	2,6	3,4	122,3	2,4	4,0
2015-04-17 17:55	18,9	13,3	-1,9	-1,8	**0,0**	0,1	1,3	1,9	2,5	35,1	0,3	1,0
2015-04-18 17:25	17,6	6,3	2,7	2,8	**1,1**	1,4	2,2	2,6	2,6	133,0	1,5	3,0
2015-04-19 18:10	16,5	7,8	1,6	1,5	**-0,3**					109,3	3,6	5,5
2015-04-20 18:25	15,5	2,8	2,1	2,0	**0,0**					127,6	1,6	2,0
2015-04-21 19:10	15,5	3,5	4,1	4,0	**0,2**					234,1	1,4	3,0
2015-04-27 00:25	15,0	3,1	4,8	4,6	**1,1**					113,9	3,7	5,5
2015-04-27 22:10	14,8	3,1	1,9	1,5	**0,0**					134,8	1,5	2,0
2015-04-30 01:10	14,7	3,0	3,6	3,5	**1,5**					112,4	6,6	10,1
2015-04-30 19:10	14,5	3,3	0,2	0,3	**0,7**					122,6	1,1	2,5
2015-05-02 01:55	14,6	2,8	2,8	2,7	**0,7**					109,4	6,5	10,1
2015-05-06 22:10	14,4	2,8	-0,5	-0,8	**-1,3**					78,2	0,0	0,0
2015-05-10 20:40	17,4	6,9	0,3	0,3	**0,7**					307,9	1,1	1,5
2015-05-11 21:10	17,2	6,0	0,3	0,3	**0,3**					142,0	1,1	1,5
2015-05-12 23:10	16,8	6,5	2,0	1,9	**-0,1**					118,3	3,8	6,0
2015-05-14 02:10	16,6	5,9	2,9	2,8	**0,3**					125,5	6,2	8,6
2015-05-14 20:10	15,8	5,2	5,4	5,2	**1,5**					156,9	5,8	8,6
2015-05-16 23:40	15,5	4,9	3,7	3,6	**1,0**					158,4	3,1	5,0

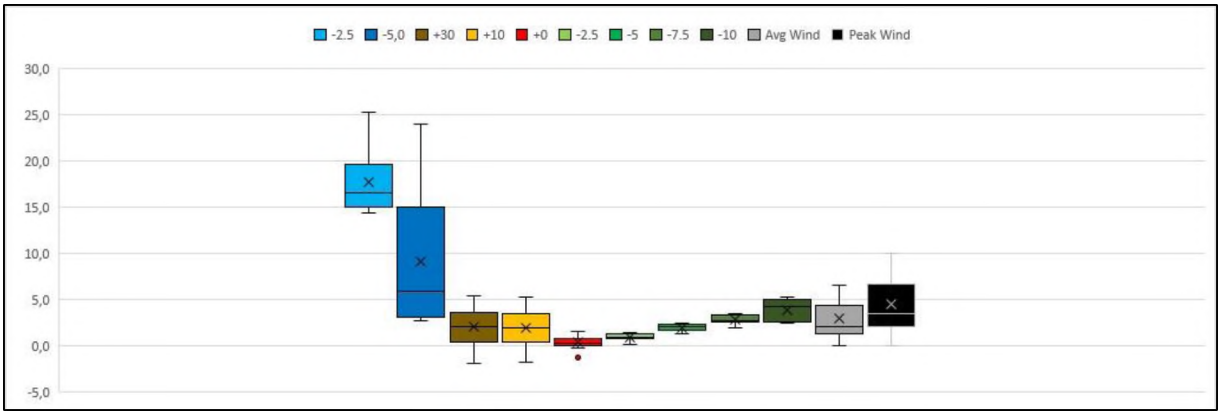

Figure 5.14. Box - Whisker diagram summarising environmental data at the moment of growth initiation from Site 2

Table 5.5. Environmental measurements from Site 2 at the point of visual needle ice decay initiation. Blank cells indicate sensor failure. Box-Whisker plot with statistics below the table.

Site 2												
	Soil moisture		Temperature							Wind speed/Direction		
	%		°C							°	m/s	
	March - June 2015											
	-2.5	-5,0	+30	+10	+0	-2.5	-5	-7.5	-10	Direction	Avg Wind	Peak Wind
2015-04-10 06:40	25,1	23,4	3,4	3,1	**0,2**	0,8	1,4	2,0	3,1	144,2	3,9	4,5
2015-04-12 06:40	24,5	22,8	4,9	4,7	**0,1**	0,7	1,3	1,9	3,1	324,5	3,3	4,5
2015-04-15 09:55	23,4	21,3	4,5	4,2	**0,0**	0,5	1,1	1,8	3,0	165,6	3,3	5,0
2015-04-16 09:55	20,0	17,1	2,8	2,8	**-0,4**	-0,1	0,5	1,0	1,8	106,8	3,4	7,0
2015-04-17 09:55	15,3	-0,1	3,0	3,4	**-1,0**	-0,6	-0,2	0,2	1,0	21,0	2,7	4,5
2015-04-18 09:55	13,4	-2,0	4,8	4,6	**-0,8**	-0,5	-0,2	0,2	0,9	114,3	3,4	5,5
2015-04-19 06:55	14,9	4,6	1,2	1,2	**0,1**	0,2	0,4	0,7	1,1	114,4	6,7	10,1
2015-04-20 10:10	12,9	-3,6	4,7	4,6	**0,0**					153,7	6,5	9,6
2015-04-21 09:55	13,5	-4,4	9,4	8,7	**-0,3**					142,2	0,8	2,5
2015-04-22 10:25	15,3	3,4	10,0	9,8	**3,0**					121,2	3,7	7,5
2015-04-27 10:25	14,9	3,2	8,9	8,7	**2,7**					125,6	3,4	7,5
2015-04-28 10:25	14,8	2,8	11,3	11,0	**2,0**					57,3	1,6	3,5
2015-04-30 10:40	14,5	2,3	7,2	7,0	**0,4**					95,0	1,8	4,0
2015-05-01 10:25	14,5	-2,9	9,3	8,8	**1,3**					112,4	2,2	4,5
2015-05-02 08:40	14,6	2,6	3,7	3,5	**0,9**					131,3	4,7	8,6
2015-05-07 10:40	14,3	-5,3	12,4	12,2	**2,1**					275,0	1,5	3,0
2015-05-11 10:10	17,1	6,4	5,6	5,7	**4,0**					344,0	2,7	3,5
2015-05-12 09:55	16,6	5,0	6,5	5,9	**0,7**					46,8	1,4	3,5
2015-05-13 10:55	16,3	4,3	5,9	5,6	**0,1**					156,0	3,3	6,0
2015-05-14 10:40	16,2	5,5	7,3	7,0	**1,1**					130,8	6,6	10,6
2015-05-15 08:25	15,9	5,2	5,9	5,7	**2,5**					94,0	10,4	14,1
2015-05-17 07:55	15,6	5,0	4,9	4,7	**1,6**					159,4	5,4	8,0

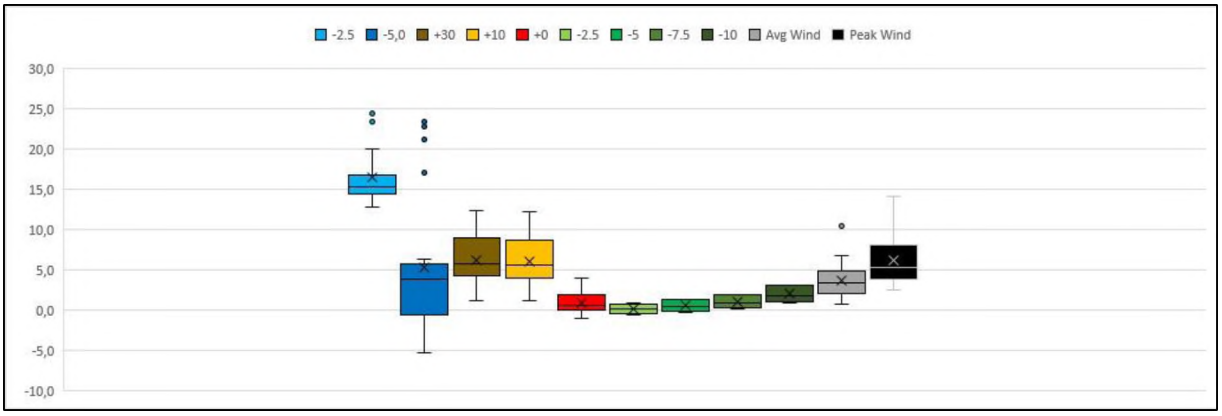

Figure 5.15. Box - Whisker diagram summarising environmental data at the moment of decay initiation from Site 2.Figure

Table 5.6. Changes in Site 2's environmental conditions from the point of growth initiation to the point of decay initiation. Blue, green and red cells indicate a reduction, a non-change or an increase of the measurement. Blank cells indicate sensor failure.

Site 2												
	Soil moisture		Temperature							Wind speed/Direction		
	%		°C							°	m/s	
	March - June 2015											
	-2.5	-5,0	+30	+10	+0	-2.5	-5	-7.5	-10	Direction	Avg Wind	Peak Wind
2015-04-10 06:40	-0,3	-0,6	0,9	0,9	-0,2	-0,4	-1,1	-1,6	-2,1	-92,2	2,5	2,5
2015-04-12 06:40	-0,2	-0,4	0,7	0,9	-0,2	-0,4	-1,0	-1,5	-1,9	19,5	1,6	1,5
2015-04-15 09:55	-1,0	-1,6	3,2	3,1	-0,2	-0,2	-0,6	-0,9	-1,3	63,2	-2,1	-3,5
2015-04-16 09:55	-3,8	-5,0	2,0	2,0	-0,6	-1,0	-1,6	-2,0	-2,5	0,3	-0,5	1,5
2015-04-17 09:55	-6,6	-20,2	3,4	3,7	-1,5	-1,5	-2,1	-2,4	-2,4	-101,3	0,3	0,5
2015-04-18 09:55	-5,5	-15,3	6,7	6,4	-0,9	-0,6	-1,4	-1,7	-1,6	79,2	3,1	4,5
2015-04-19 06:55	-2,7	-1,7	-1,4	-1,6	-1,0	-1,3	-1,9	-1,9	-1,5	-18,6	5,2	7,0
2015-04-20 10:10	-3,6	-11,3	3,1	3,1	0,3					44,4	2,9	4,0
2015-04-21 09:55	-2,0	-7,2	7,3	6,7	-0,2					14,7	-0,8	0,5
2015-04-22 10:25	-0,2	-0,1	5,9	5,9	2,8					-112,9	2,3	4,5
2015-04-27 10:25	-0,1	0,1	4,1	4,1	1,6					11,8	-0,3	2,0
2015-04-28 10:25	0,1	-0,3	9,5	9,5	1,9					-77,5	0,1	1,5
2015-04-30 10:40	-0,2	-0,7	3,6	3,5	-1,1					-17,4	-4,7	-6,0
2015-05-01 10:25	-0,1	-6,2	9,1	8,5	0,6					-10,3	1,1	2,0
2015-05-02 08:40	0,0	-0,3	0,9	0,8	0,1					22,0	-1,8	-1,5
2015-05-07 10:40	-0,1	-8,1	12,9	13,0	3,4					196,8	1,5	3,0
2015-05-11 10:10	-0,4	-0,5	5,3	5,3	3,4					36,1	1,6	2,0
2015-05-12 09:55	-0,5	-1,0	6,2	5,7	0,4					-95,2	0,2	2,0
2015-05-13 10:55	-0,5	-2,2	3,8	3,8	0,2					37,6	-0,5	0,0
2015-05-14 10:40	-0,4	-0,4	4,4	4,2	0,8					5,4	0,3	2,0
2015-05-15 08:25	0,1	0,1	0,5	0,5	1,1					-62,9	4,6	5,5
2015-05-17 07:55	0,1	0,1	1,2	1,1	0,6					1,0	2,3	3,0

Measurements taken at the point of needle ice decay initiation (Table 5.5) were compared to the readings collected at growth initiation (Table 5.4). Changes in each measured parameter was thereafter calculated and is displayed in Table 5.6. Table 5.6 shows that surface temperatures increased by an average of 1.3°C in 13 of the 22 events while in the remaining 9 events temperatures decreased by an average of -0.6°C from the point of needle ice growth to initiation of decay. Furthermore, the combined soil moisture readings decreased in 36 of the 44 measurements by an average of 3.0%. In the remaining 6 events where soil moisture increased, it increased by an average of 0.1%. Seven of the 22 events had soil temperature readings, all of which showed decreased temperatures by the end of the event.

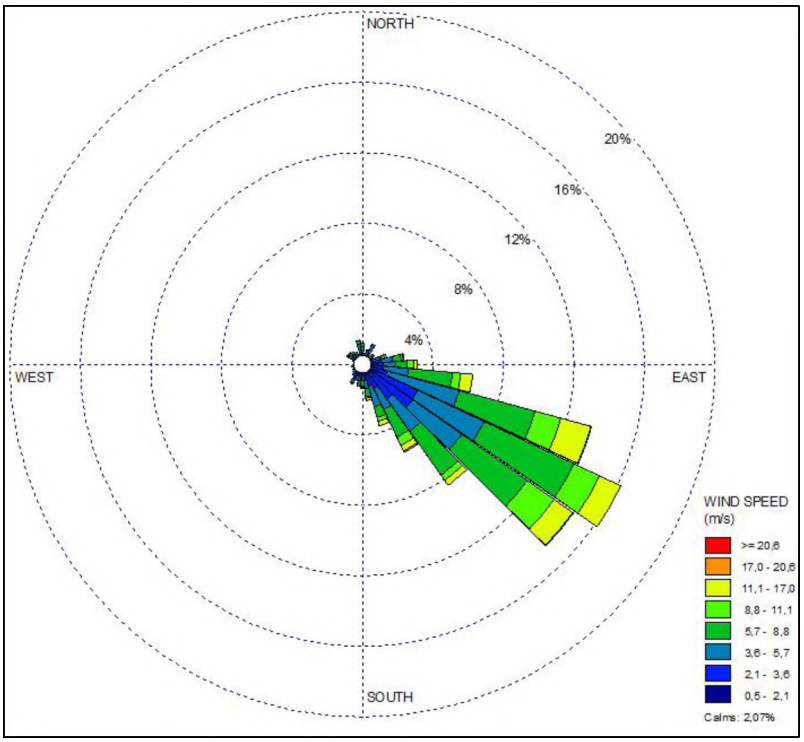

Figure 5.16. Wind rose plot between March 2015 and June 2015 from Site 2 showing an prevailing wind direction of south-east.

Figure 5.16 shows the incoming wind direction at Site 2 being south-east or from behind on the right side in the recorded imagery.

5.3.3 Site 3

A total of 15 needle ice events were identified from Site 3 between late April 2014 and early May 2015. Environmental conditions at the point of initiation ranged from surface temperatures at -2.0°C to 4.3°C (range of 6.3°C), soil moisture of 0.4% to 12.5% (range of 12.1%) and 1.4% to 18.2% (range of 16.8%) at -2.5cm and -5cm respectively (Table 5.7). Wind measurements, although only available in 4 out of the 15 events, ranged from calm to 7.5m/s.

Table 5.7. Environmental measurements from Site 3 at the point of visual needle ice initiation. Blank cells indicate sensor failure. Box-Whisker plot with statistics below the table.

Site 3											
	Soil moisture		Temperature						Wind speed/Direction		
	%		°C						°	m/s	
	April 2014 - April 2015										
	-2.5	-5,0	+10	+0	-2.5	-5	-7.5	-10	Direction	Avg Wind	Peak Wind
2014-04-27	12,4	18,2	-2,7	**-0,2**	0,4	0,7	1,3	1,5	158,4	2,3	7,5
2014-05-13	12,5	17,5	-3,0	**-0,3**	0,2	0,4	0,9	1,1	51,5	0,0	0,0
2014-05-15	3,8	10,3	-1,7	**-0,9**	0,0	0,0	0,3	0,4	254,9	2,3	7,0
2014-05-16	0,4	3,6	0,5	**-0,4**	0,0	-0,1	0,0	0,0	348,4	0,2	2,0
2015-03-01		10,5	-0,8	**-0,7**	-0,3	0,0	0,5	0,7			
2015-03-11		9,2	1,3	**1,4**	0,6	0,1	0,5	0,7			
2015-03-12		8,0	-0,4	**-0,6**	-0,3	-0,1	0,8	1,3			
2015-03-14		8,1	0,2	**0,0**	-0,1	0,0	0,7	1,0			
2015-03-20		9,9	0,7	**0,1**	0,3	0,9	2,6	3,1			
2015-03-27		7,1	-0,2	**-0,4**	-0,3	-0,2	0,2	0,3			
2015-03-30		8,6	-0,1	**-0,3**	-0,3	-0,3	0,0	0,1			
2015-03-31		5,4	-1,3	**-2,0**	-1,7	-1,1	-0,6	-0,6			
2015-04-02		7,7	-0,5	**-0,7**	-0,5	-0,4	0,0	-0,1			
2015-04-03		4,5	-0,9	**-1,9**	-1,5	-1,2	-0,9	-0,9			
2015-04-11		1,2	0,5	**0,1**	0,4	0,3	0,4	0,3			

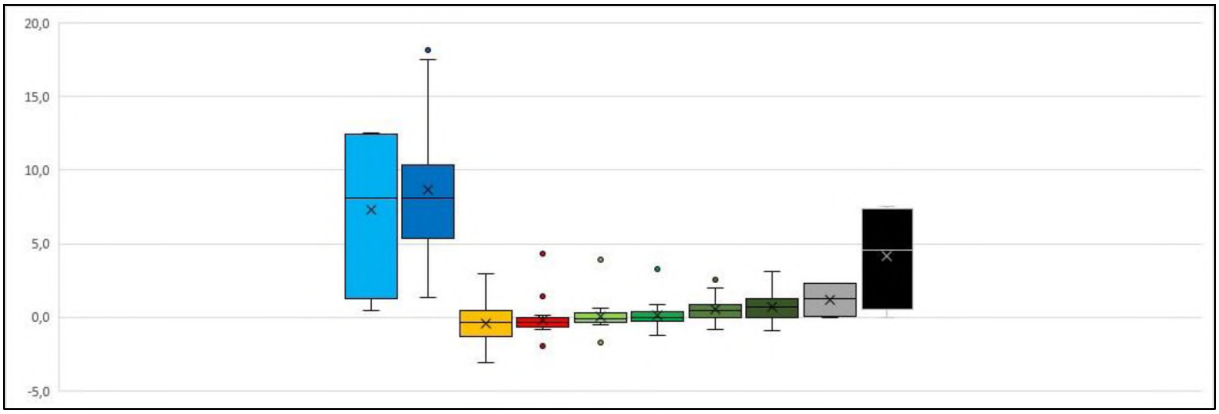

Figure 5.17. Box - Whisker diagram summarising environmental data at the moment of growth initiation from Site 3.

In 12 of the 15 needle ice events captured at Site 3, temperatures closer to the surface were consistently lower than subsurface temperatures at the point of initiation, by an average of 0.3°C. In the 3 events where surface temperatures were higher than the subsurface, the average temperature difference was 0.4°C. Air measurements showed higher temperatures at +10cm compared to the soil surface in 9 of the 15 events, with an average increase of 0.5°C. Six events displayed lower surface compared to air temperatures, the average difference was 1.3°C.

Table 5.8. Environmental measurements from Site 3 at the point of visual needle ice decay initiation. Blank cells indicate sensor failure. Box-Whisker plot with statistics below the table. Only one measurement of soil moisture and wind speeds was available for needle ice events at Site 3, hence, no statistical summary is presented.

Site 3											
	Soil moisture		Temperature						Wind speed/Direction		
	%		°C						°	m/s	
	April 2014 - April 2015										
	-2.5	-5,0	+10	+0	-2.5	-5	-7.5	-10	Direction	Avg Wind	Peak Wind
2014-04-27	3,2	5,7	-0,6	**-0,2**	-0,2	-0,2	0,1	0,0	526,4	5,8	11,1
2014-05-13	N/A	N/A	N/A	**N/A**	N/A	N/A	N/A	N/A	N/A	N/A	N/A
2014-05-15	N/A	N/A	N/A	**N/A**	N/A	N/A	N/A	N/A	N/A	N/A	N/A
2014-05-16	N/A	N/A	N/A	**N/A**	N/A	N/A	N/A	N/A	N/A	N/A	N/A
2015-03-01		7,6	0,7	**4,2**	1,1	-0,1	0,1	0,3			
2015-03-11		8,9	0,2	**0,8**	0,7	0,0	0,2	0,2			
2015-03-12		7,4	1,1	**1,2**	1,0	0,2	0,2	0,3			
2015-03-14		7,3	-0,4	**0,0**	-0,1	-0,1	0,4	0,7			
2015-03-20		4,1	-0,2	**-0,5**	-0,1	-0,4	-0,1	0,2			
2015-03-27		3,6	0,2	**4,2**	0,9	0,0	-0,1	-0,2			
2015-03-30		5,1	-0,6	**0,3**	0,0	-0,1	-0,2	-0,2			
2015-03-31		3,3	-1,4	**-1,1**	-0,8	-0,7	-0,2	-0,1			
2015-04-02		-2,5	-0,3	**0,3**	0,1	0,0	-0,2	-0,3			
2015-04-03		-2,8	-1,0	**-1,0**	-0,5	-0,5	-0,3	-0,6			
2015-04-11		-1,1	0,0	**1,6**	1,3	1,0	0,5	-0,1			

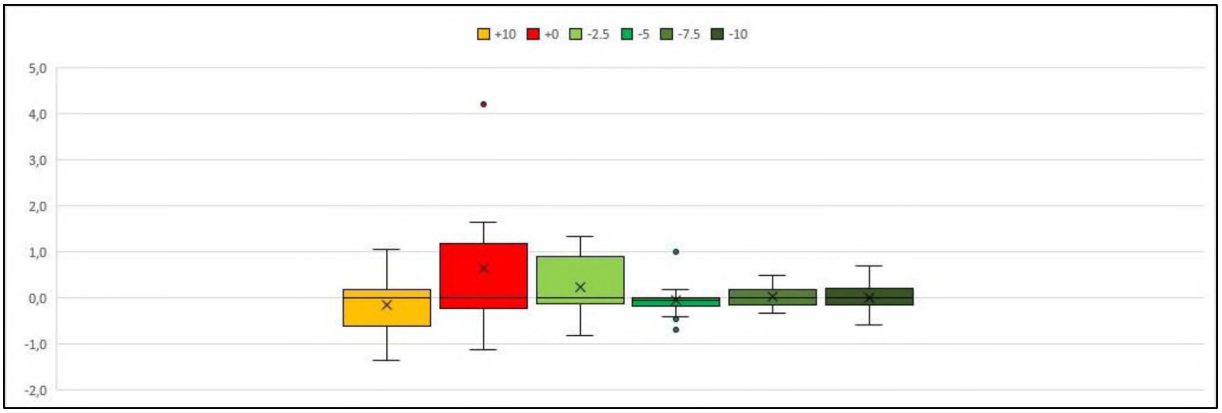

Figure 5.18. Box - Whisker diagram summarising environmental data at the moment of decay initiation from Site 3.

An analysis of change in environmental parameters between the moment of growth initiation to the onset of decay is presented in Table 5.9. Due to harsh weather obscuring images, decay initiation was unavailable for three events at Site 3. Site 3 shows 29 of the 48 combined ground temperature measurements to have decreased values by an average of -0.9°C, while in 19 events temperatures increased by an average of 0.5°C. A majority of surface and -2.5cm measurements showed increased temperatures at decay initiation, while deeper sensors recorded a temperature decrease at decay

initiation. Air temperatures showed an even split between increasing and decreasing temperatures. Site 3 displayed a general cooling of the deeper -7.5 and -10cm sensors and warming of the surface and -2.5cm sensors while air measurements had no clear trend.

Only one soil moisture measurement was available from the -2.5cm soil moisture sensor, which displayed a decrease during the needle ice event. All measured events at the -5cm sensor indicate reduced soil moisture at the moment of decay initiation compared to growth initiation by an average of -4.3%.

Table 5.9. Changes in Site 3's environmental conditions from the point of growth initiation to the point of decay initiation. Blue, green and red cells indicate a reduction, a non-change or an increase of the measurement. Blank cells indicate sensor failure.

Site 3											
	Soil moisture		Temperature						Wind speed/Direction		
	%		°C						°	m/s	
	April 2014 - April 2015										
	-2.5	-5,0	+10	+0	-2.5	-5	-7.5	-10	Direction	Avg Wind	Peak Wind
2014-04-27	-9,2	-12,5	2,1	-0,1	-0,6	-0,9	-1,3	-1,5	368,0	3,5	3,5
2014-05-13											
2014-05-15											
2014-05-16											
2015-03-01		-2,9	1,5	4,9	1,4	-0,1	-0,3	-0,5			
2015-03-11		-0,3	-1,0	-0,6	0,1	-0,2	-0,3	-0,5			
2015-03-12		-0,6	1,4	1,8	1,2	0,3	-0,6	-0,9			
2015-03-14		-0,8	-0,5	0,1	0,0	-0,1	-0,3	-0,3			
2015-03-20		-5,7	-0,8	-0,6	-0,5	-1,3	-2,6	-2,9			
2015-03-27		-3,5	0,4	4,7	1,2	0,2	-0,3	-0,5			
2015-03-30		-3,6	-0,5	0,6	0,4	0,2	-0,2	-0,3			
2015-03-31		-2,0	-0,1	0,8	0,9	0,4	0,4	0,5			
2015-04-02		-10,2	0,2	0,9	0,6	0,4	-0,1	-0,2			
2015-04-03		-7,3	0,0	0,9	0,9	0,7	0,5	0,3			
2015-04-11		-2,5	-2,9	-2,7	-2,6	-2,3	-1,5	-1,6			

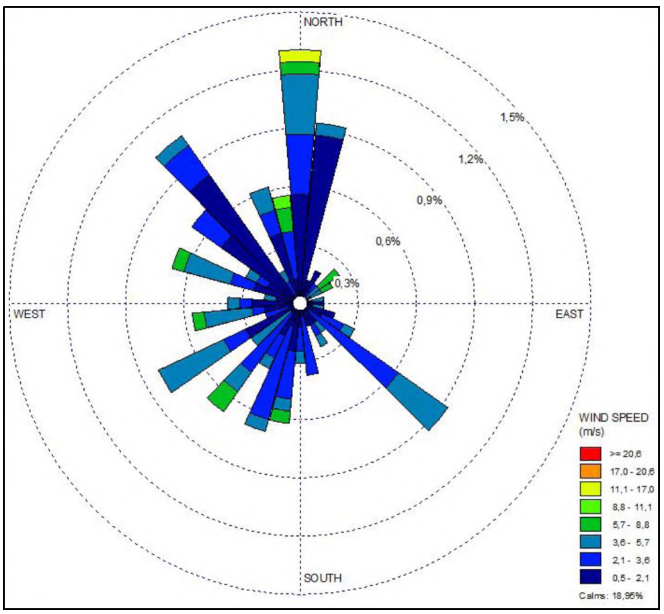

Figure 5.19. Wind rose plot between April 2015 and April 2015 from Site 3 showing wind to occur from several directions, although most often from the north.

The incoming wind at Site 3 occurred from several directions as seen in Figure 5.19. The prevailing wind direction was from the north, marking the incoming angle of wind as into the camera lens from the right in images from Site 3.

Section 2.1.3 and Chapter 3 identifies the physical prerequisites of a needle ice growth environment; hence, the following section displays results a soil analysis at Site 1, 2 and 3.

5.3.4 Soil properties

Soil textural controls on needle ice growth are viewed as a part of the environmental setting at each study site, and their relation to needle ice sediment movement will be the focus of Chapter 6. Hence, analyses of the physical soil aspects of the study sites were performed. Soil samples were collected from each study site, and subjected to analyses detailed in Section 4.5. Organic content and porosity of collected soil samples are presented in Table 5.10, while grain size distribution from the same samples are presented in Figure 5.20, 5.21 and 5.22.

Table 5.10. Soil organic content and porosity calculated for each site.

Site	**Soil samples**	
	Organic content (%)	Porosity (%)
Site 1	3.6	45.1
Site 2	4.4	31.3
Site 3	0.7	29.5

Particle size distribution from Site 1 and 2 resulted in a fine fraction of 17% and 22% respectively. Such fine fraction percentages places both sites within suggested frost susceptible limits of 7-57% fines (particles smaller than 0.064mm) proposed in literature (e.g. Beskow, 1935; Gradwell, 1957; Higashi and Corte, 1971; Meentemeyer and Zippin, 1981; Outcalt, 1971; Soons and Greenland, 1970). Results from Site 3 displays a fine fraction of 6%, being less than 7% fines, suggesting non-frost susceptible soils, yet, as evident from imagery, needle ice growth was observed at Site 3.

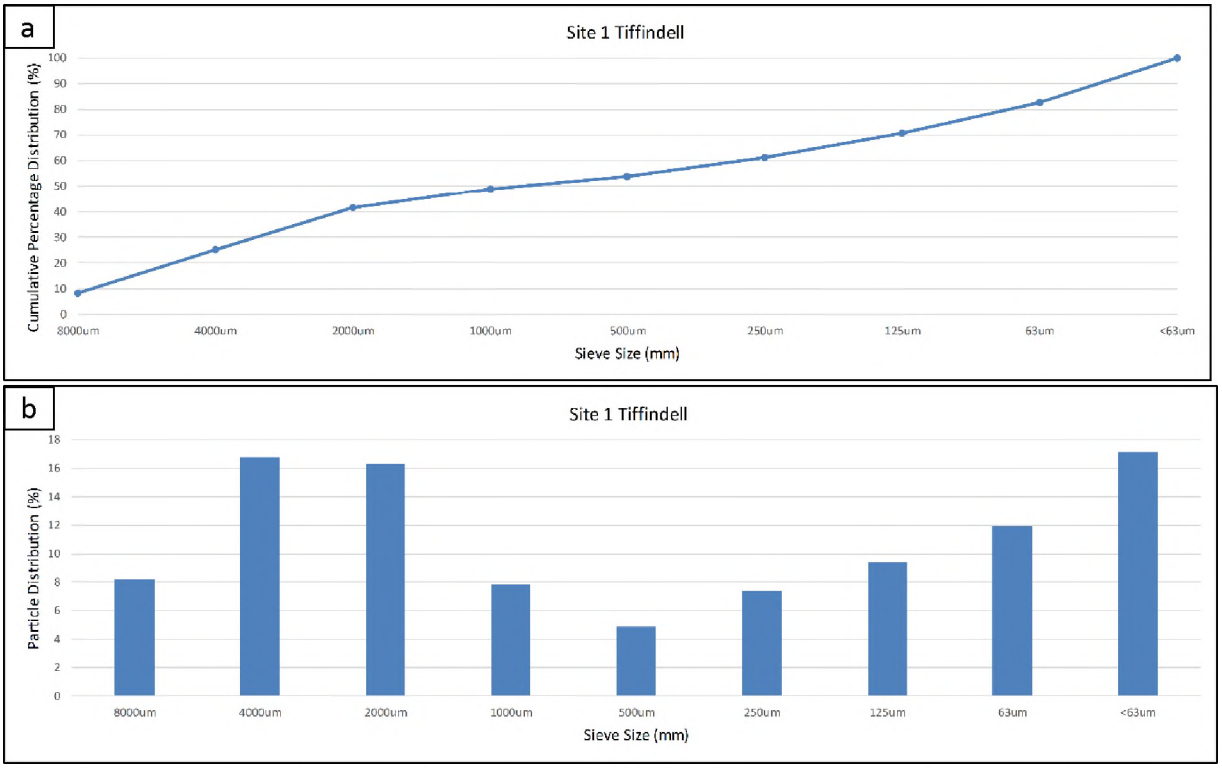

Figure 5.20. Cumulative percentage (a) and particle size (b) distribution of a soil sample from Site 1 at Tiffindell.

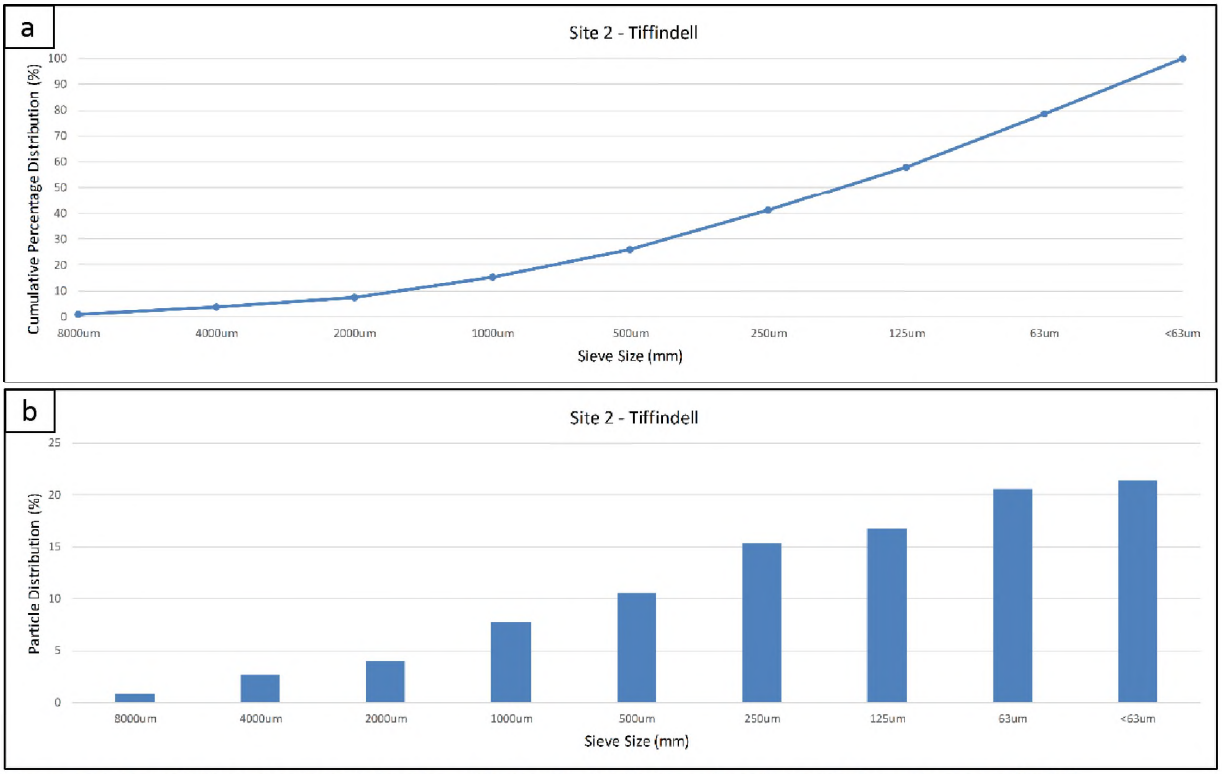

Figure 5.21. Cumulative percentage (a) and particle size (b) distribution of a soil sample from Site 2 at Tiffindell.

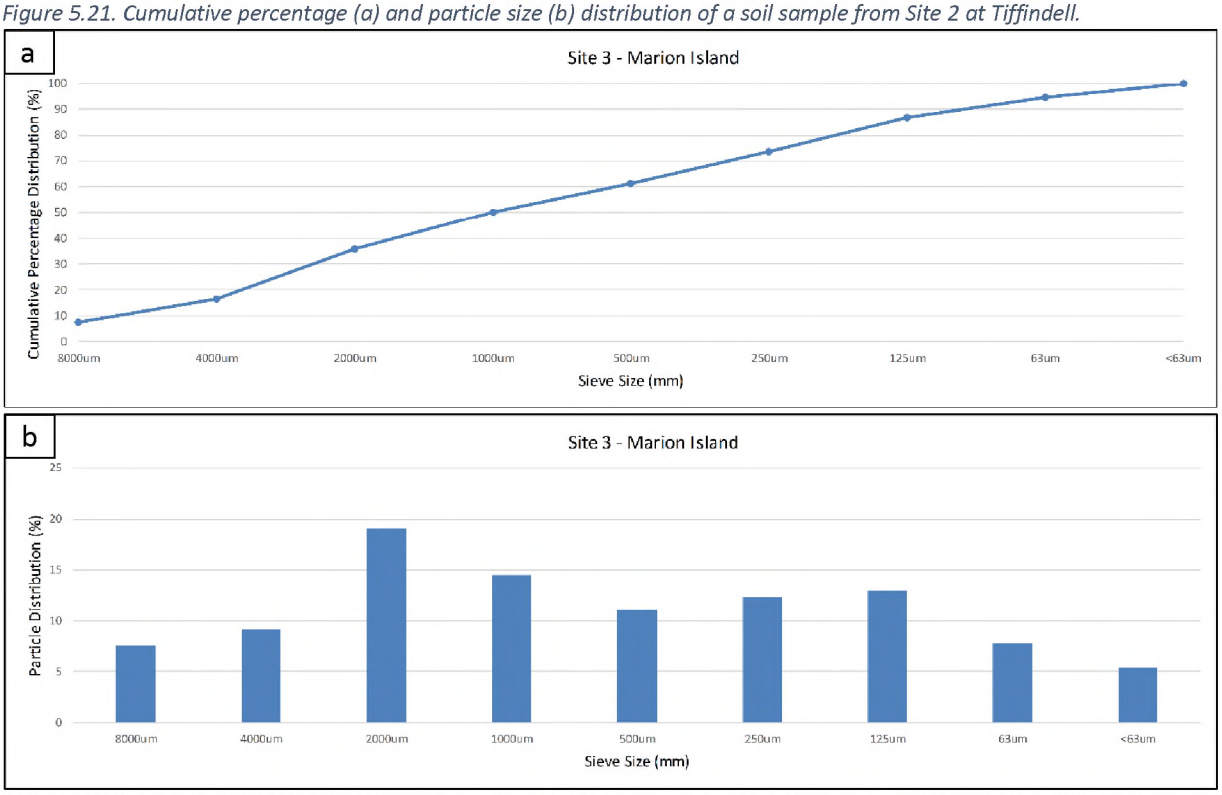

Figure 5.22. Cumulative percentage (a) and particle size (b) distribution of a soil sample from Site 3 on Marion Island

5.4 Environmental signatures of needle ice growth

The following section attempts to identify the environmental signatures indicating needle ice growth in the measurement data. Detailed analysis of individual events with visually proven needle ice growth from each site will stand as a basis for signature recognition.

During analysis of the temperature record several peculiar sudden increases in temperature were noted in conjunction with initiation of needle ice events. Paterson (1994) considers the importance of the latent heat of fusion for water being 334J/g (Section 2.1.4). Consequently, when water changes phase into ice, that amount energy must be expelled. As a result of the energy output, a sudden warming should occur at that moment. The following section will analyse identified temperature spikes occurring in close temporal proximity to needle ice initiation.

5.4.1 Identifying temperature spikes.

Rapid temperature increases (spikes) were compared to imagery of needle ice growth initiation. Spikes were found to occur within an average of 2 hours 22 minutes and 1 hour and 12 minutes of growth initiation for Site 1 and 2 respectively. Site 3 showed more complex regime, where latent heat release events were noted and are detailed in Section 5.4.2.3. Site 1 had 24 of 44, Site 2 had 20 of 22 and Site 3 had 11 of 16 events showing distinct spikes during needle ice initiation. Table 5.11 presents all temperature spikes identified from the 81 analysed needle ice events and the maximum temperature change induced by the spike, measured in degrees Celsius. The average temperature change induced by the spikes at Site 1 and 2 were both 0.3°C, while Site 3 showed double that at 0.6°C. Table 5.11 also includes timing of the spikes as well as the moment of visual growth initiation.

Three spike events were randomly chosen from each site for further analysis, identifying the change in cooling rate, soil moisture, and air and ground temperature before and after identified spike in temperature data. Each figure in addition display the time period in which needle ice was visually observable with a yellow line on the X-axis (Figure 5.23).

Table 5.11. Observed needle ice growth initiation time, latent heat release spikes, timing of spikes, occurrence of the zero-curtain effect, and temperature at spiking for all needle ice events captured at Site 1, 2 and 3. Red numbers indicate that the surface temperature sensor was unavailable and the -2.5cm was used as proxy data.

Site 1						Site 2						Site 3				
Date	Initiation	Spike	Timing of spike	Zero-curtain	Temp	Date	Initiation	Spike	Timing of spike	Zero-curtain	Temp	Date	Initiation	Spike	Zero-curtain	Temp
2014-06-01	19:30					2015-04-10	23:10	0,2	00:36	Yes	0,1	2014-04-27	17:11	1,0		
2014-06-02	18:30					2015-04-12	23:40	0,4	00:51	Yes	0,2	2014-05-13	14:11		Yes	
2014-06-03	18:00					2015-04-15	04:25	0,4	05:10	Yes	-0,2	2014-05-15	17:21			
2014-06-04	15:30					2015-04-16	19:25	0,4	20:07	Yes	0,1	2014-05-16	17:11		Yes	
2014-06-05	20:15	0,1				2015-04-17	18:25	0,4	18:44		0,1	2015-03-01	19:11	0,7		
2014-07-01	21:45					2015-04-18	17:55	0,1	19:00		-0,2	2015-03-11	22:31	0,5		
2014-07-02	18:00					2015-04-19	17:25	0,4	18:49		-0,2	2015-03-12	20:01	0,9		
2014-07-03	18:30			Yes		2015-04-20	18:10	0,8	18:38		-0,6	2015-03-14	21:31	0,5		
2014-07-04	19:15			Yes		2015-04-21	18:25	0,5	19:00		-0,5	2015-03-20	16:21	0,7		
2014-08-09	00:10			Yes		2015-04-22	19:10	0,8	20:40		0,0	2015-03-27	22:21	0,5		
2014-08-12	20:25			Yes		2015-04-27	00:25	0,2	23:26		1,5	2015-03-30	23:11	0,2		
2014-08-13	20:10			Yes		2015-04-28	22:10	0,4	23:11		0,0	2015-03-31	18:21	1,0	Yes	
2014-08-15	21:10	0,3				2015-04-30	01:10	0,3	03:40		-0,3	2015-04-02	18:31		Yes	
2014-08-17	20:40			Yes		2015-05-01	19:10	0,3	22:09		-0,4	2015-04-03	01:11	0,3	Yes	
2014-08-22	18:25					2015-05-02	01:55	0,5	21:24		0,3	2015-04-11	18:01	0,5		
2014-08-24	16:25					2015-05-07	22:10	0,3	23:17		-1,4	2015-04-30	22:41			
2014-10-20	23:10	0,3	23:29		1,5	2015-05-11	20:40	0,2	19:03		1,8					
2014-10-21	00:25	0,4	23:30		2,6	2015-05-12	21:10	0,3	21:29		0,0					
2014-11-05	00:25					2015-05-13	23:10	0,3	00:13		-0,1					
2014-11-16	19:10					2015-05-14	02:10	0,2	02:10		0,2					
2014-11-17	19:25	0,1	19:35		0,1	2015-05-15	20:10									
2014-11-18	19:40	0,1	19:21		1,4	2015-05-17	23:40			Yes						
2014-11-19	02:25	0,1	23:24		0,8											
2014-11-20	02:55	0,7	02:57		0,8											
2015-01-17	03:55	0,6	02:24		0,2											
2015-04-07	02:25	0,1	02:16		1,2											
2015-04-09	02:55	0,5	03:06	Yes	1,0											
2015-04-10	22:10	0,2	23:10		1,5											
2014-04-12	23:55															
2015-04-15	03:10	0,6	03:10		1,0											
2015-04-16	18:40	0,2	18:28		1,2											
2015-04-17	18:40	0,2	17:59		1,7											
2015-04-18	18:25	0,1	16:17		0,8											
2015-04-19	18:40															
2015-04-20	16:55															
2015-04-21	18:25	0,2	17:23		0,5											
2015-04-22	18:10															
2015-04-27	21:25	0,3	20:43		1,0											
2015-04-28	18:25															
2015-04-30	23:25	0,1	02:40		0,3											
2015-05-01	20:10															
2015-05-11	21:10	0,2	23:18		0,7											
2015-05-12	23:40	0,2	20:30		0,8											
2015-05-13	22:55	0,3	19:24	Yes	0,7											

5.4.1.1 Site 1

Figure 5.23, 5.24 and 5.25 show the spike at Site 1 on the 15th of November 2014 and on the 16th and 30th of April 2015. All three events show a distinct increase in surface temperature during ongoing cooling of the soil surface, a spike, occurring just after 21:00 in Figure 5.23 and at ca 18:00 in Figure 5.24 and 5.25 (indicated by black arrow). In addition, Figure 5.23 shows that the spike seen in surface temperatures at ca 21:00, also affects temperatures at -2.5cm depth ca one hour later compared to surface temperatures. The temperature spike at depth was however of less amplitude.

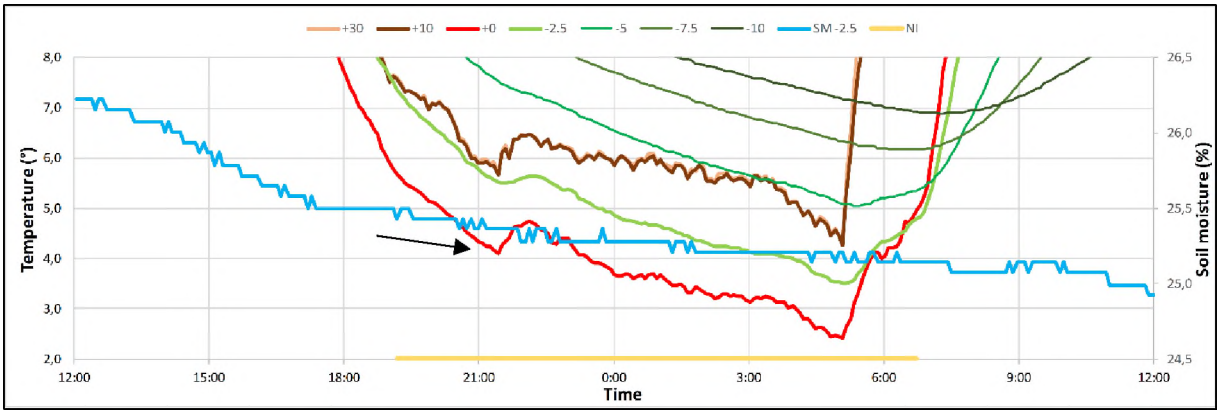

Figure 5.23. Soil moisture and air, surface and ground temperature recorded at Site 1 on the 15th of December 2014. Temperature spiking is marked by the arrow and needle ice duration is depicted by the yellow line.

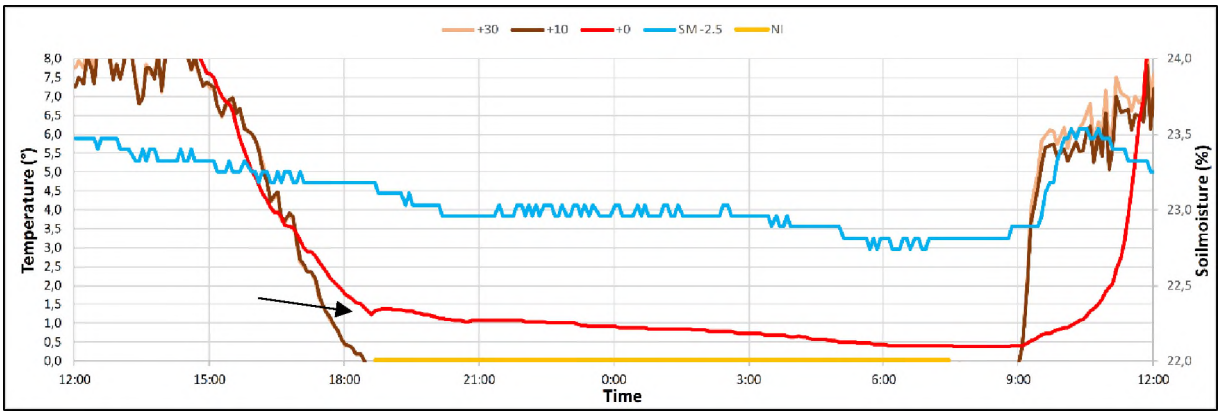

Figure 5.24. Soil moisture and air and surface temperature recorded at Site 1 on the 16th of April 2015. Temperature spiking is marked by the arrow and needle ice duration is depicted by the yellow line.

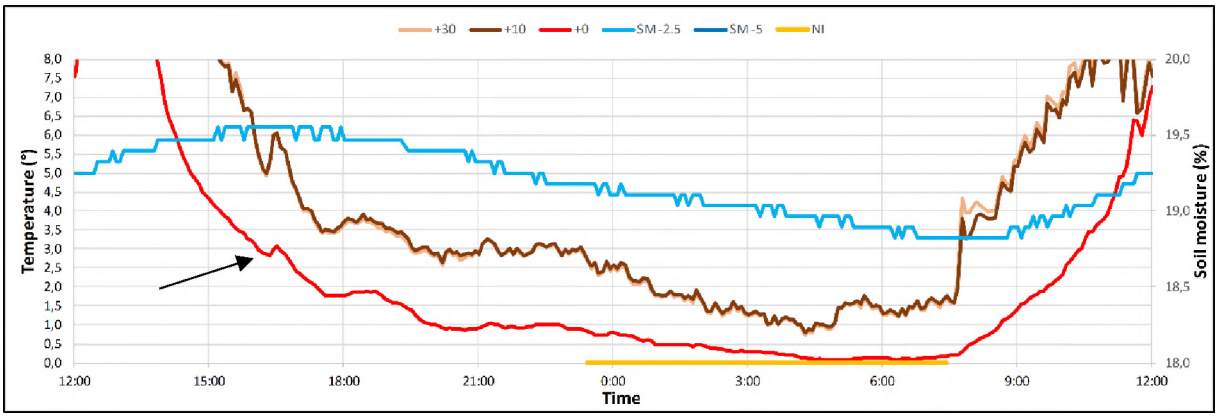

Figure 5.25. Soil moisture and air and surface temperature recorded at Site 1 on the 30th of April 2015. Temperature spiking is marked by the arrow and needle ice duration is depicted by the yellow line.

Temperatures during the spike increased by 0.5°C, 0.2°C and 0.1°C and the rate of temperature decline was reduced from 1.0 and 0.2, 1.9°C/h to 0.05 and 0.85 to 0.05°C/h after the initial spike for Figure 5.23 , 5.24 and 5.25 respectively, when averaging the periods three hours before and after the spike.

Soil moisture levels in the figures were sufficiently high (Branson *et al., 1996)* to sustain needle ice growth through each event, with the lowest soil moisture levels seen in Figure 5.25 at 18.7%. Soil moisture was expected to decrease during growth of ice needles, and increase after melt, which can be seen in Figure 5.24 and 5.25. However, Figure 5.23 shows a constant decline in soil moisture even after the onset of melt. Figure 5.24 and 5.26 show that the decrease in soil moisture is accelerated after the onset of freeze and inverted at melt.

5.4.1 Site 2

Figure 5.26, 5.27 and 5.28 show needle ice initiation from Site 2 on the 12th and 20th of April and on the 2nd of May, 2015. Distinct spikes are seen close to midnight in Figure 5.26 and at ca 18:00 (Figure 5.27 and 5.28). Surface temperatures after the spike increased by 0.4°C, 0.8°C, 0.5°C (Figure 5.26, 5.27 and 5.28), before temperature lowering continued. After the release spike, the rate of temperature decline decreased from 1.7 to 0.06°C/h, 3.3 to 0.27°C/h and from 2.9 to 0.24°C/h (Figure 5.26, 5.27 and 5.28). Ground temperature measurements are only shown in Figure 5.26, which shows a small temperature spike simultaneously at -2.5cm. No spikes were recorded by the deeper sensors. However, a decrease in the rate of temperature lowering is visible in all ground temperature after the initial surface spike.

Soil moisture levels at Site 2 (Figure 5.26 and 5.27) show increased rates of decrease following the observed spike, while Figure 5.28 displays drying in relation to the spike, followed by an increase in soil moisture from ca 19:00. The lowest soil moisture was seen in Figure 5.27 displaying soil moisture levels of ca 13%.

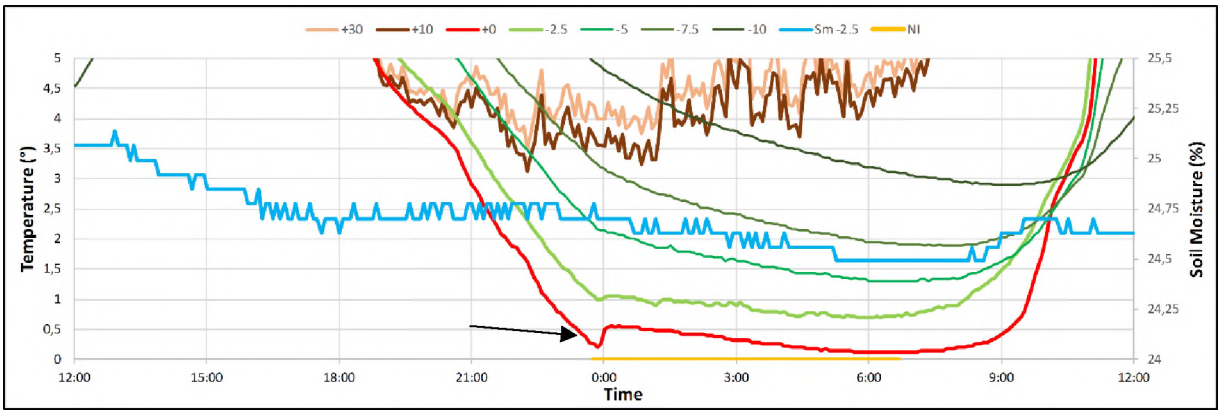

Figure 5.26. Soil moisture and air, surface and ground temperature recorded at Site 2 on the 12th of April 2015. Temperature spiking is marked by the arrow and needle ice duration is depicted by the yellow line.

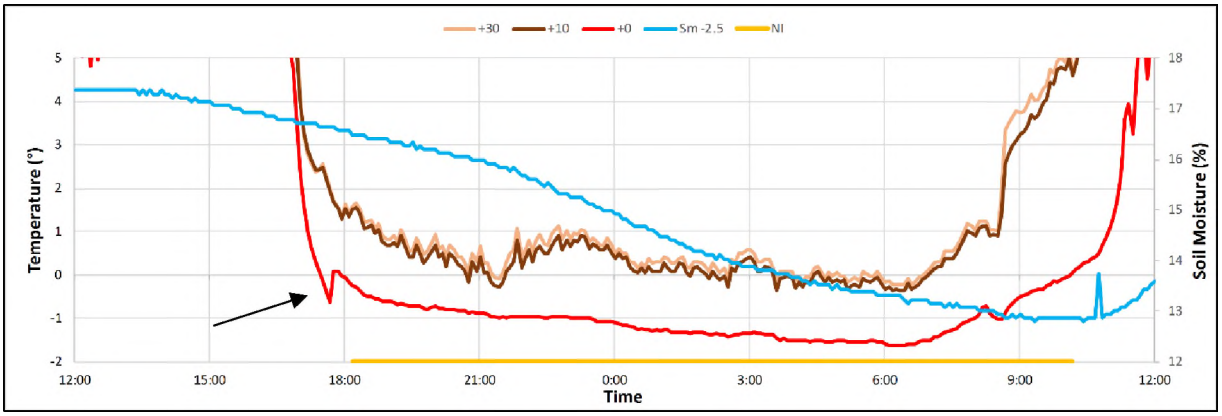

Figure 5.27. Soil moisture and air and surface temperature recorded at Site 2 on the 20th of April 2015. Temperature spiking is marked by the arrow and needle ice duration is depicted by the yellow line.

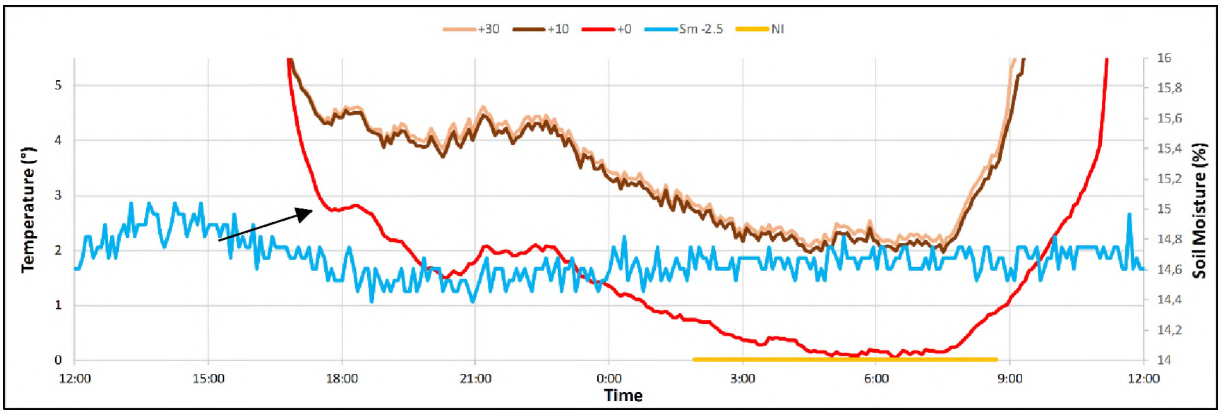

Figure 5.28. Soil moisture and air and surface temperature recorded at Site 2 on the 2nd of May 2015. Temperature spiking is marked by the arrow and needle ice duration is depicted by the yellow line.

Notable in Figure 5.28 is that although the rate of temperature decline is impacted in a similar way as seen in the previous events, needle ice growth is only visible ca seven hours later.

5.4.1 Site 3

Temperature spikes were observed on the 27th of April 2014, on the 14th of March 2015 and on the 11th on April 2015 from Site 3 and are displayed in Figure 5.29, 5.30 and 5.31. As previously mentioned, the temperature figures from Site 3 are more complex. Several spike occasions during a single needle ice growth event, are displayed as peaks and troughs in the surface temperature sensor curve (Figure 5.29, 5.30 and 5.31). Temperature change averaged over three of these temperature spikes during each event display an increase in temperature of 1.0°C, 0.5°C and 0.5°C before reinitiated cooling, while the rate of cooling changed from 1.5 to 0.2°C/h, 3.5 to 0.1°C/h and 1.3 to 0.3°C/h after the spike.

Soil moisture readings were only available for the -5cm sensor at Site 3. The rate at which soil moisture declined was constant until melt in Figure 5.29, while Figure 5.30 and 5.31 show an increase in soil moisture reduction during the night. Noteworthy are the low soil moisture levels during and

toward the end of each event, with Figure 5.31 displaying negative soil moisture for a period of time. All three events had visually confirmed needle ice growth.

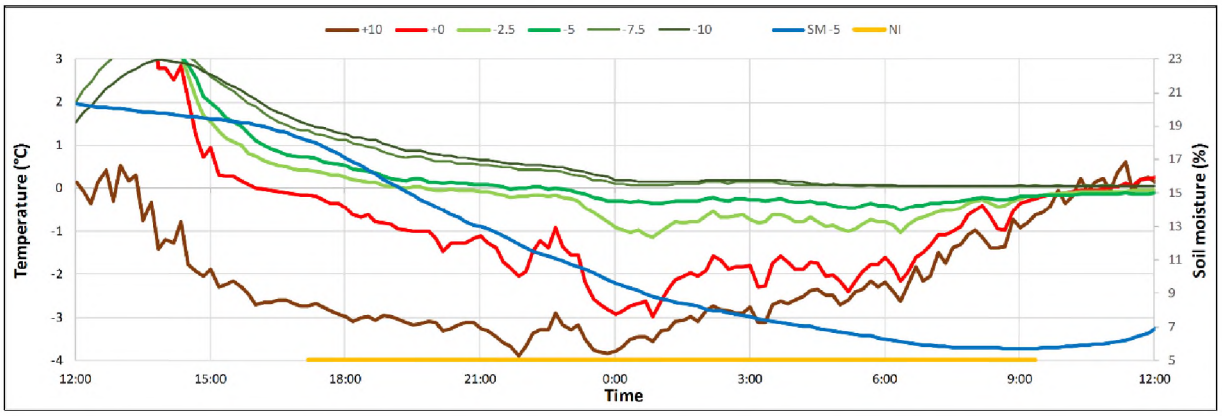

Figure 5.29. Soil moisture and air, surface and ground temperature recorded at Site 3 on the 27th of April 2014. Temperature spiking is marked by the arrow and needle ice duration is depicted by the yellow line.

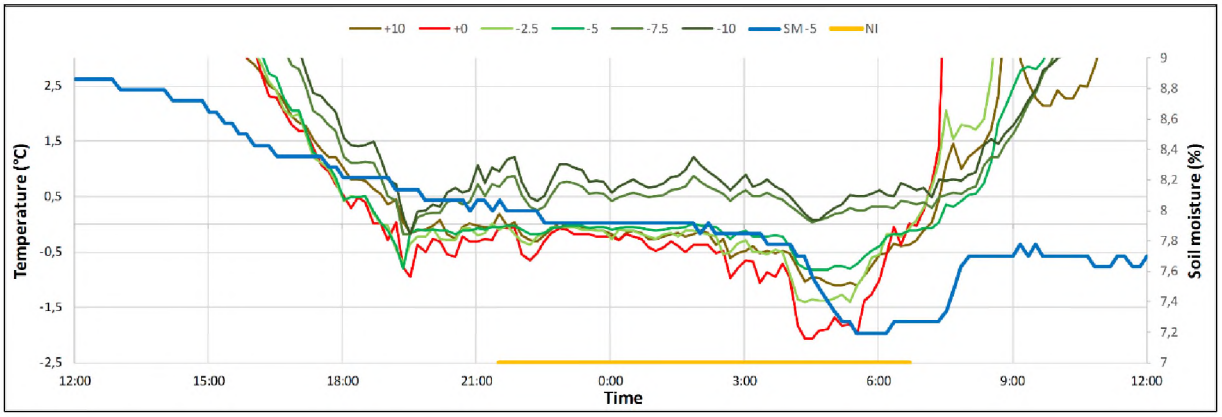

Figure 5.30. Soil moisture and air, surface and ground temperature recorded at Site 3 on the 14th of March 2015. Temperature spiking is marked by the arrow and needle ice duration is depicted by the yellow line.

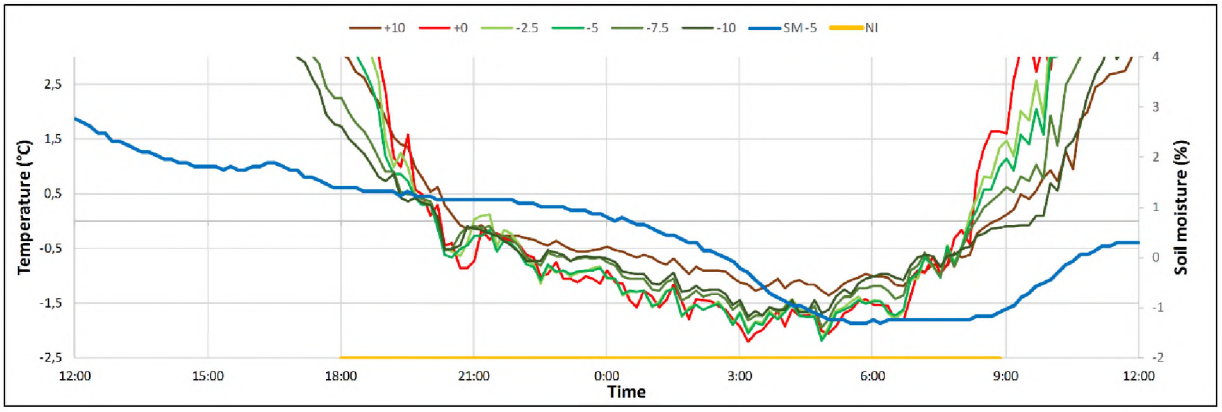

Figure 5.31. Soil moisture and air, surface and ground temperature recorded at Site 2 on the 11th of April 2015. Temperature spiking is marked by the arrow and needle ice duration is depicted by the yellow line.

Section 5.2 and the previous section display the different characteristics of several needle ice events. Hence, the following section analyses several needle ice events in close temporal proximity.

5.4.2 Environmental influence on latent heat release dynamics

Detailed in Chapter 2 are the circumstances required for needle ice growth, which are below zero temperatures, sufficient soil moisture content and a surface texture capable of transport moisture to the freezing front. The following section will show results regarding several needle ice events occurring within a few days of each other, highlighting the influence that local scale environmental differences exert on needle ice growth.

Section 5.4.1 identified spikes (sudden increases) in temperature at the onset of needle ice growth. In the same section, a distinct change in the rate of temperature decline after the observed spikes was noted (Figure 5.24, 5.27 and 5.31). Previous work strongly suggests that such identified rapid increases in temperature relate to the release of latent heat during phase transition of water to ice (e.g. Outcalt et al., 1990; Branson et al., 1996; Kozlowski, 2009, 2016). The spikes will henceforth be identified as latent heat release events. Section 5.4.1 also identified two phases during several of the needle ice events, which include an initial spike phase and a subsequent lowering of the rate of cooling phase.

5.4.2.1 Site 1

Four needle ice events and their environmental details are presented in Figure 5.32. Events were selected based on the occurrence of several needle ice events within a short, a few days to a little more than a week, period. The initiation of needle ice growth was evident in the short inversion in temperature marked by the arrows. Said inversions can similarly be seen in air temperatures and in the -2.5cm sensor in the second event from the left in the same figure. Two of the four events show no temperatures in air, surface or ground going below zero, although needle ice formation was seen in the imagery. Noted are the positive temperatures at which initiation starts at the surface.

The point of ice nucleation did not occur at a constant air, surface or ground temperature or at a specific soil moisture for these four consecutive events, despite using the same equipment at the same location. The results are, thus clearly not a reflection of the recording equipment. Nucleation initiation temperature increases with each consecutive day while soil moisture becomes progressive lower. Figure 5.32 shows soil moisture to decrease over the full four-day period. Notable is that soil moisture levels are consistently higher at 5cm depth compared to at -2.5cm.

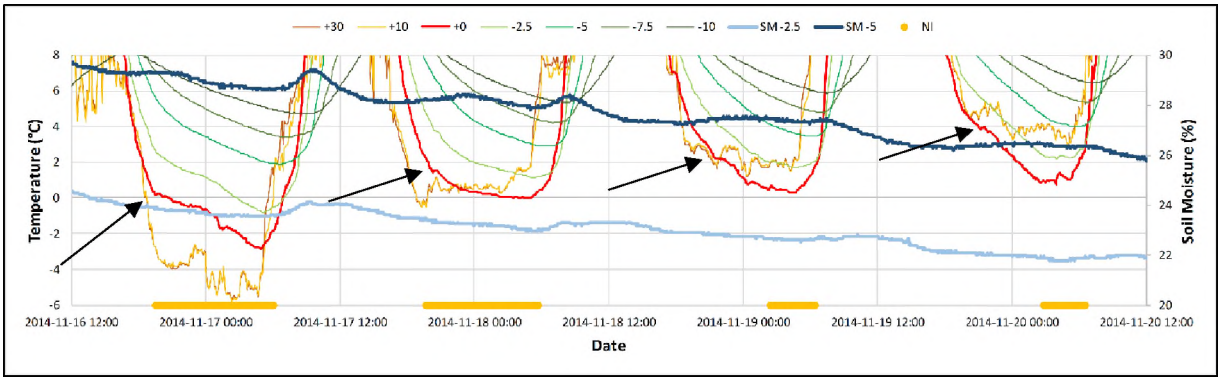

Figure 5.32. Soil moisture and air, surface and ground temperature recorded at Site 1 from the 16th of November 2014 to the 20th of November 2014. Temperature spikes are marked by arrows and needle ice duration is depicted by the yellow lines.

The rate at which temperature declines at the surface is markedly lower after the initial latent heat release event. The two needle ice events on the right in Figure 5.32 show needle ice to initiate several hours after the initial spike.

5.4.2.2 Site 2

Seven needle ice events at Site 2 are evident in Figure 5.33, marked by the yellow bars. Each event is initiated by a latent heat release spike, followed by a decline in the rate of temperature decrease. The spike is most visible in the surface temperature, but also visible at -2.5 cm and in the air temperature at +30 and +10 cm above the ground. Furthermore, Figure 5.33 displays surface and air temperatures that are above zero (0.15°C and 1.4°C) during the initial release spike for the two events on the left, while the two events on the right never show below zero temperatures at the surface, although imagery confirms the growth of needle ice.

Air temperature in Figure 5.33 shows differences in the freezing regime between the analysed events. Temperatures at +30 and +10 never go below zero during the first two events while the latter three show a minimum temperature of -6.0°C. The rate of temperature decline is seen to be reduced after the initial temperature spike in all five events; however, the rate of decline is steeper in event 4 and 5 (counted from the left in Figure 5.33).

Soil moisture is seen to slightly decrease in a linear manner over the first six days only displaying smaller diurnal fluctuations mostly during growing and melting of needle ice. However, on the night of the 15 May 2015, larger fluctuation is seen following visually identifiable moisture input at 20:00h the previous evening. During the next needle ice growth events, air temperatures and ground temperatures go below zero with a marked lowering of soil moisture levels. Minimum soil moisture from the -5cm sensor was recorded at -5% (negative soil moisture readings are explained in Section 4.3.4) with a maximum of 13.5% 12 hours earlier on the 18th, while the -2.5cm sensor dropped to 13% from 19% on the same day.

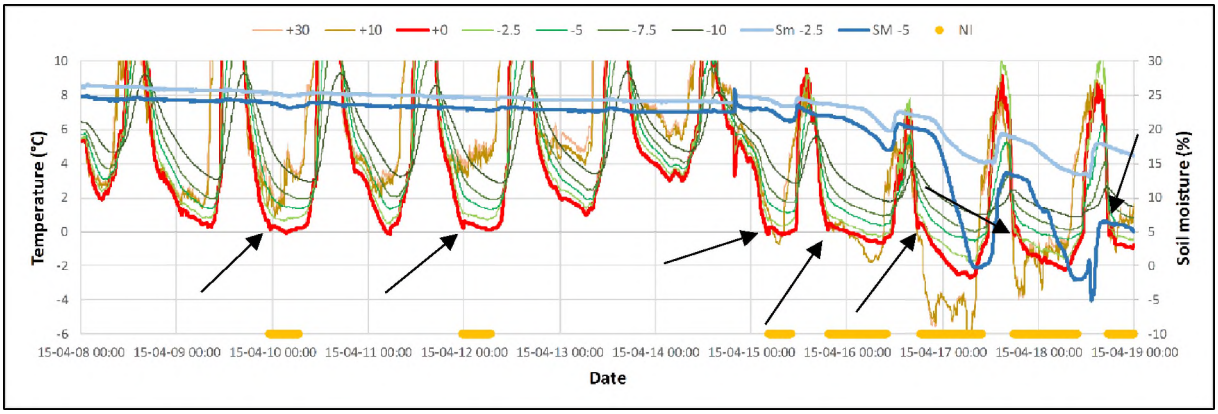

Figure 5.33. Soil moisture and air, surface and ground temperature recorded at Site 2 from the 8th of April 2015 to the 19 of April 2015. Temperature spikes are marked by arrows and needle ice duration is depicted by the yellow lines.

5.4.2.3 Site 3

Figure 5.34 shows three days with visually observed needle ice growth. Several spikes in soil surface temperature are seen within each event (marked by boxes in Figure 5.34). Unlike the small-scale temperature undulations seen in events from Site 1 and 2, Site 3 displays spikes of a larger amplitude, with several temperature changes ranging from 0.4°C to over 1°C in a single event. Furthermore, spikes can be seen to affect temperatures to a depth of -5cm at a reduced amplitude with increasing depth. Surface temperatures on the evening of the 12th, 14th and 15th go well below zero while, on the evening of the 13th, temperatures cross below zero, however, only for ca five hours.

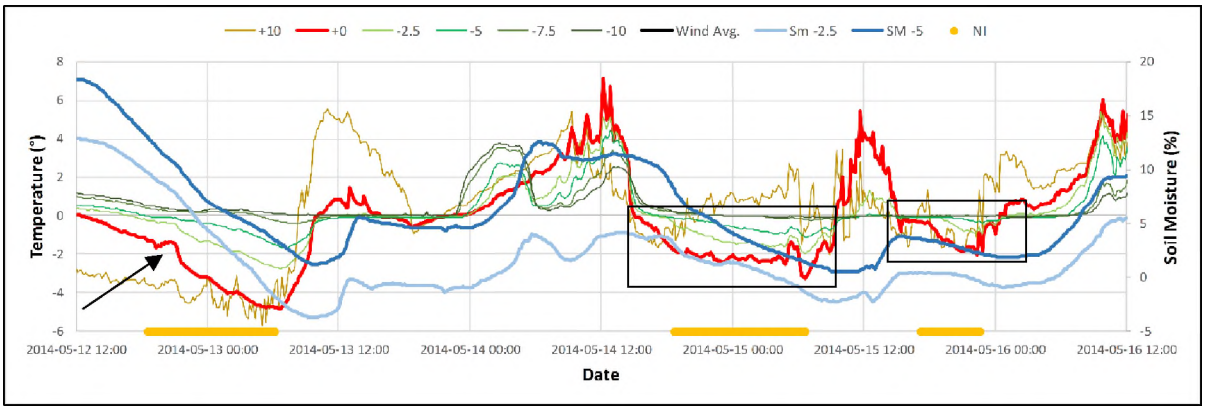

Figure 5.34. Soil moisture and air, surface and ground temperature recorded at Site 3 from the 12th of May 2014 to the 16th of May 2014. Temperature spike is marked by the arrow and periods of many spikes are enclosed in the boxes. Needle ice duration is depicted by the yellow lines.

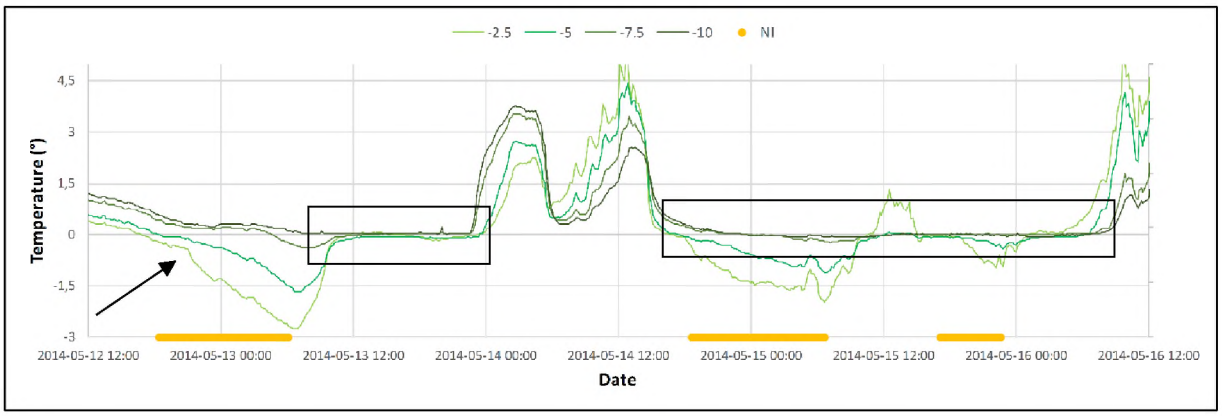

Figure 5.35. Ground temperatures recorded at Site 3 from the 12th of May 2014 to the 16th of May 2014. Temperature spike is marked by the arrow and periods of many spikes are enclosed in the boxes. Needle ice duration is depicted by the yellow lines.

Soil moisture measurements show decreases when needle ice growth is observed and increases with melt. Similarly, the rates at which soil moisture levels change coincide with growth and decay initiation.

Ground temperatures show two periods where they are close to zero for extended periods (Figure 5.35). The first instance had all ground sensors at close to zero for ca 11 hours, while the second showing only the deeper -7.5cm and -10cm sensors at zero degrees for ca 31h. The arrow in Figure 5.35 shows the temperature spike penetrating down to -5cm depth.

Visual analysis, in the form graphs, in this section show a notable change in the rate of temperature change after the initiation of needle ice growth. The following section will analyse potential zero-curtain effects found during measured needle ice events.

5.4.3 Cooling rate change as a result of latent heat release and zero-curtain effects

Section 2.1.4 identifies the circumstances occurring during the phase shift from water to ice. In addition to the release of latent heat, and the resulting temperature spike, the characteristics of a zero curtain is described. Described in the following section are occurrences of what can be described as zero curtains (Figure 5.36), however, the terminology, based on how it is used in literature by Outcalt *et. al. (1990) and* Van Everdingen (1998) was considered restrictive. What was seen in Section 5.4.1 and 5.4.2 and is subsequently described is not always a zero curtain, but instead a balance between cooling and the release of latent heat, affecting the rate at which temperatures change.

Observations relating to the coincidence of decreases in soil moisture with the initiation of needle ice growth and followed by a constant decrease in soil moisture during growth will be presented. Two events showing changes in cooling rate associated with latent heat release from each site will subsequently be presented.

5.4.3.1 Site 1

Figure 5.36 shows a zero-curtain event occurring on the 9th of April 2015 at Site 1. At 20:16h a sharp increase in temperatures is visible in surface temperatures. However, no needle ice production was seen in the imagery. Seven hours later an additional, but much smaller, spike is notable, followed by four hours of little temperature change.

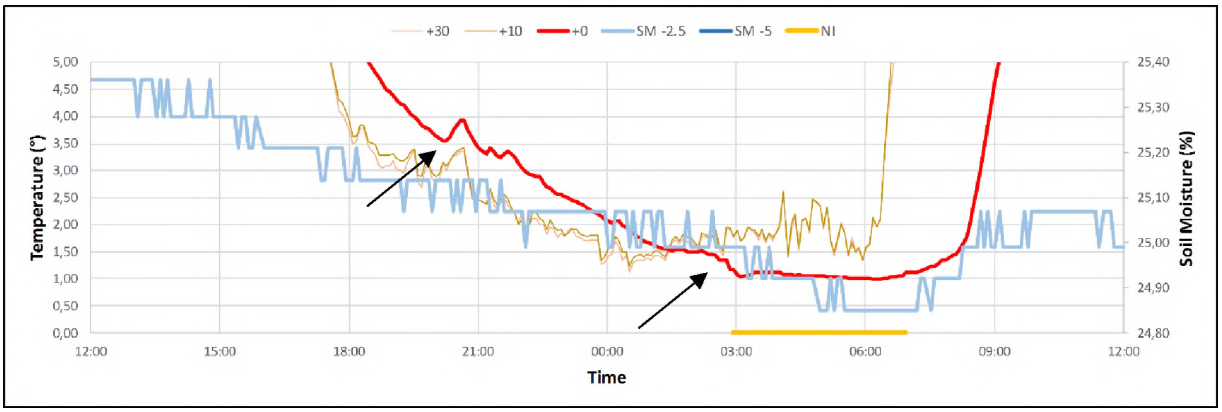

Figure 5.36. Soil moisture and air and surface temperature recorded at Site 1 on the 9th of April 2015. Temperature spiking is marked by the arrow and needle ice duration is depicted by the yellow line.

Comparably, the rate of temperature decrease between 00:00 to 03:00 was 0.3°C/h and between 03:00 and 06:00, 0.02°C/h. Temperatures increased after 07:00, marking the end of needle ice growth and the start of melt. The soil moisture sensor recorded a decrease from 12:00 on the 8th to 07:00 on the 9th when they began increasing, coinciding with melt.

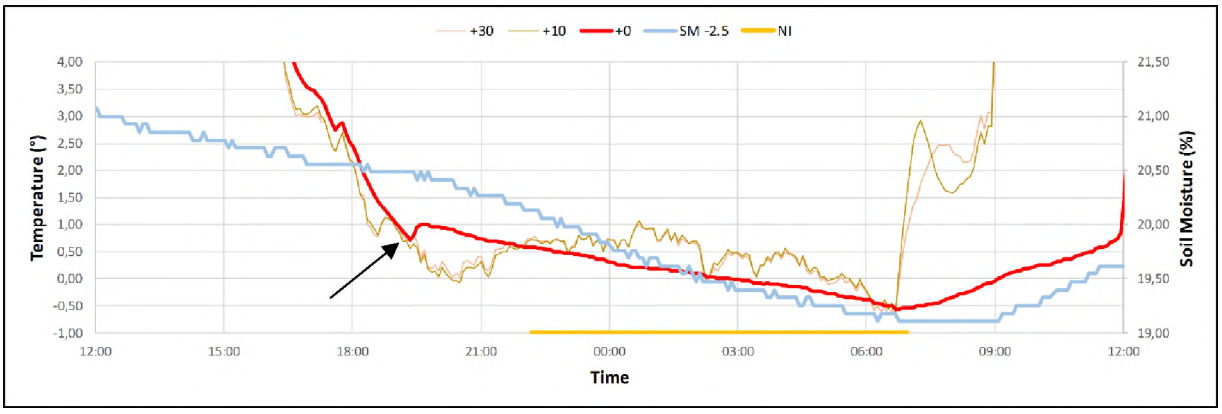

Figure 5.37. Soil moisture and air and surface temperature recorded at Site 1 on the 13th of May 2015. Temperature spiking is marked by the arrow and needle ice duration is depicted by the yellow line.

A spike in temperatures is noted at 19:20 on the 13th of May 2015 (Figure 5.37). No needle ice growth was observable before 22:20, when a distinct change in the rate of temperature decline is apparent after the spike. The rate of temperature decline changes from ca 1.0°C/h to 0.17°C/h before and after the initial temperature spike. Surface temperatures display a constant lowering from 19:40 to 06:40 the following morning showing little variation, while air temperature during the same time

period fluctuates. Soil moisture decreases from the point of the spike to 06:40 where air temperatures are seen to sharply increase. At 09:00, ca two hours later, soil moisture is seen to increase.

5.4.3.2 Site 2

On the 12th of April 2015 at Site 2 ground temperatures remain close to zero with little fluctuation for an extended period of time (Figure 5.38). At 23:50 surface temperatures are seen to spike, subsequently, surface temperatures show little change until 09:00 where they increase sharply. The rate of temperature decline changes from ca 1°C/h to 0,03°C/h after the spike.

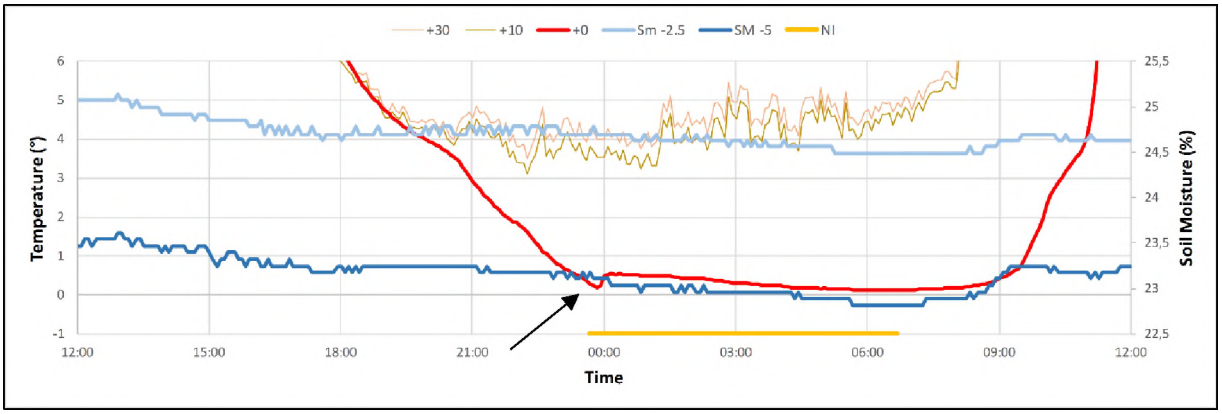

Figure 5.38. Soil moisture and air and surface temperature recorded at Site 2 on the 12th of April 2015. Temperature spiking is marked by the arrow and needle ice duration is depicted by the yellow line.

Air temperatures fluctuate between 3 and over 6°C during the same time period while surface temperatures are relatively stable at ca 0.5°C. Soil moisture decreases in conjunction with the spike and melt within ca 0.5% change.

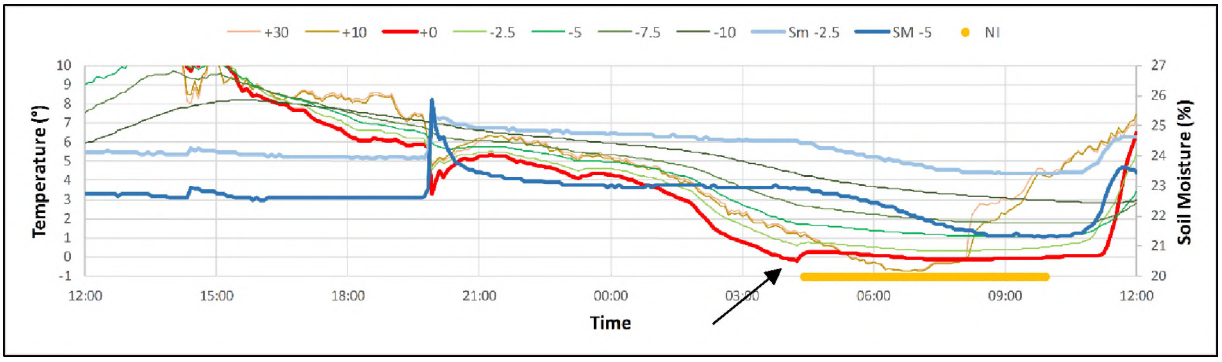

Figure 5.39. Soil moisture and air, surface and ground temperature recorded at Site 2 on the 15th of April 2015. Temperature spiking is marked by the arrow and needle ice duration is depicted by the yellow line.

A needle ice event was observed at Site 2 on the 15th of April 2015, which displays constant temperatures after a brief temperature spike at 04:15 (Figure 5.39). Prior to the temperature spike, a rapid increase in soil moisture and decrease in temperatures occurred at ca 20:00 (Figure 5.39). Imagery was used to show that rainfall fell, following which, temperatures decreased until 04:15 when

a spike is seen and needle ice was observed to grow. Subsequent to the spike, the rate of temperature decline changes from ca 1.1 to 0.04°C/h after the spike. Concurrently with the spike, soil moisture levels at both -2.5 and -5cm decrease until 10:45. Air temperatures increase sharply at ca 08:00 while surface temperature rises at 11:15.

5.4.3.3 Site 3

A spike in temperatures is seen at 18:41 on 30March 2015 at Site 3(Figure 5.40), followed by isothermal conditions on the 31. The reversal in temperature trends seen at the point of needle ice initiation marks a change in rate from 1.2 to 0.04°C/h. Although the surface temperatures are relatively stable at ca -2.25°C, soil moisture is seen to constantly decline. Air temperatures at +10cm show a similar curve to that of surface temperature during most of the event, only displaying marked differences after 06:00 in the morning of the 31st.

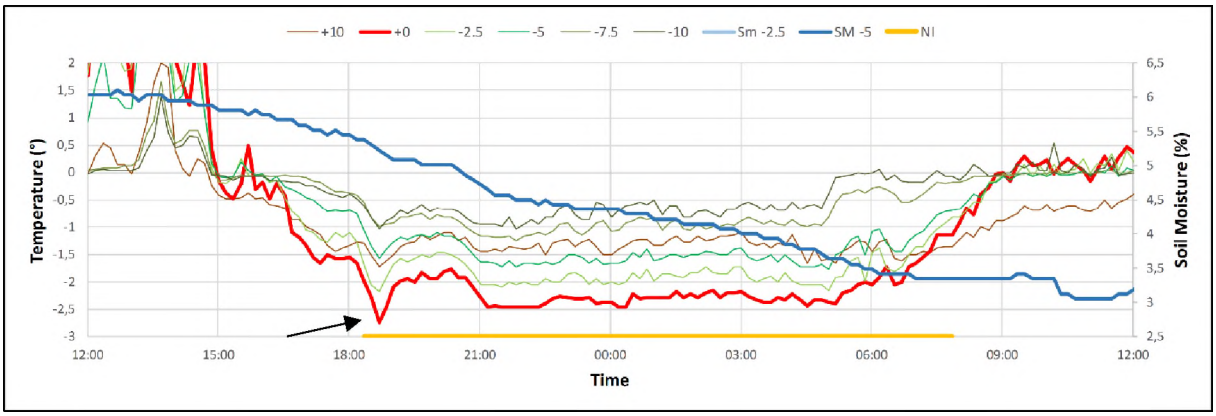

Figure 5.40. Soil moisture and air, surface and ground temperature recorded at Site 3 on the 31th of March 2015. Temperature spiking is marked by the arrow and needle ice duration is depicted by the yellow line.

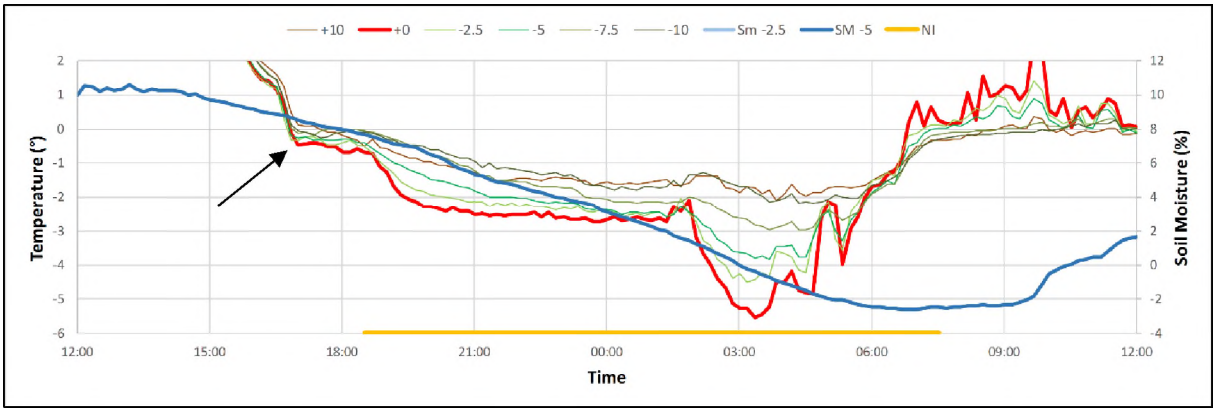

Figure 5.41. Soil moisture and air, surface and ground temperature recorded at Site 3 on the 2nd of April 2015. Temperature spiking is marked by the arrow and needle ice duration is depicted by the yellow line.

The needle ice event on the 2nd of April 2015 shown in Figure 5.41 displays a spike at 17:00h followed by several changes in the rate of temperature decline. First, at 18:30, coinciding with the initiation of needle ice growth, temperatures decline more rapidly, almost at the rate of before the

spike. Second, a period of almost six hours with very little temperature change. Third, at 02:00, after a short period of temperature increase, surface temperatures drop to -5.5°C. After the last drop, temperatures increase inconsistently until melting takes place at 07:30. Noteworthy is that the reading for the soil moisture sensor at -5cm drops to a minimum of -2.6%, displaying well below levels associated with needle ice growth.

Section 5.4.3 displays several events with a latent heat release spike followed by a change in rate of cooling. Figure 5.36 and Figures 5.39-5.42 display events which, at least partially, could be described as zero curtain events. However, Figure 5.37 presents an event where cooling and the release of latent heat do not appear to be in equilibrium.

5.4.4 Signatures of needle ice growth

Section 5.4 analyses several events from each study site that has observable needle ice from imagery and describes temperature characteristics, identifying both latent heat release and zero curtain effects. Several events were presented in Section 5.4 where no temperature sensor displayed sub-zero temperatures. However, both temperature spikes and needle ice were observed. Furthermore, Section 5.4.2 shows several needle ice events within a few days of measurements displaying different characteristics of needle ice growth. Events occurring show unsynchronised timing of the onset of needle ice, needle ice height (see Chapter 6 for further detail) and event duration (Section 5.8).

Identification of the signature of needle ice growth required further analysis. Hence, the immediate change induced at initiation of needle ice growth and initiation of needle ice decay was analysed.

5.5 Environmental fluxes and gradients

The following section will describe changes in environmental parameters (temperature, soil moisture and wind speed) over a short time-scale. Logger data was extracted 10 and 60 minutes before and after start of visual growth of needle ice. Table 5.12, 5.13 and 5.14 present changes in readings for particular sensors before and after the onset of needle ice growth was observed. The results are displayed graphically, where colours are used for indicating change with red indicating an increase, green indicating no change, and blue indicating a decrease in values before and after needle ice initiation.

The summarisation of results (Table 5.12, 5.13 and 5.14) indicate an increase in soil moisture and temperatures 10 and 60 minutes before needle ice initiation for all sites, except for the -2.5cm soil moisture sensor at Site 2. The greatest change in measured values occurred increasing surface temperatures before needle ice initiation. In addition, ground temperatures were seen to increase at a higher rate closer to the surface at needle ice initiation, when compared to 10 and 60 minutes prior

Table 5.12. Change in environmental parameters 10 and 60 minutes prior and past visual needle ice initiation from Site 1. Blue indicates a lowering, green equals no change and red shows an increase in the measured parameter.

Differences 10 minutes before needle ice initiaiton												
Date	SM -2.5	SM -5	+30	+10	+0	-2.5	-5	-7.5	-10	Direct	wind avg	wind peak
2014-05-31 19:31		0,1				0,0	0,0	0,0	0,0	-18,4	1,4	-3,0
2014-06-01 18:30		0,0				-0,1	-0,1	0,0	0,0	113,0	-0,6	0,5
2014-06-02 18:01		0,0				0,0	0,0	0,0	0,0	230,9	0,8	1,5
2014-06-03 15:32		0,0				0,0	0,0	0,0	0,0	157,4	-1,7	-1,5
2014-06-04 20:13		-0,1				0,0	0,0	0,0	0,0	-121,5	1,0	3,5
2014-06-30 21:44		0,0				0,0	0,0	0,0	0,0	-1,0	-3,6	-5,5
2014-07-01 17:58		0,1				0,0	0,0	0,0	0,0	-127,0	0,1	0,5
2014-07-02 18:30		0,0				0,0	0,0	0,0	0,0	29,3	0,2	1,0
2014-07-03 19:13		-0,1				0,0	0,0	0,0	0,0	0,0	-0,3	0,0
2014-08-09 00:10		0,0				0,0	0,0	0,0	0,0	-6,1	-1,7	-1,5
2014-08-11 20:22		0,0				0,0	0,0	0,0	0,0	1,4	-0,2	-0,5
2014-08-12 20:08		-0,1				0,0	0,0	0,0	0,0	-73,5	1,4	2,5
2014-08-14 21:08		0,0				0,0	0,0	0,0	0,0	-115,3	0,5	1,5
2014-08-16 20:40		0,1				0,0	0,0	0,0	0,0	0,1	-0,2	1,0
2014-08-21 18:23		-0,1				0,0	0,0	0,0	0,0	14,6	-0,5	-0,5
2014-08-23 16:27		0,0				-0,1	0,0	0,0	0,0	18,5	0,7	2,0
2014-10-19 23:11	0,0	0,0	0,2	0,2	-0,1	0,0	-0,1	0,0	0,0	-4,6	-0,2	0,0
2014-10-21 00:25	0,0	-0,1	0,0	0,0	0,0	-0,1	-0,1	0,0	-0,1	0,1	0,0	0,0
2014-11-05 00:26	0,0	-0,1	-0,1	-0,2	0,0	-0,2	0,0	0,0	0,0	-22,2	1,0	0,5
2014-11-15 19:12	0,0	0,1	-0,1	-0,1	-0,1	-0,1	-0,1	-0,1	-0,1	22,7	0,2	0,5
2014-11-16 19:24	-0,1	0,0	-0,6	-0,7	-0,1	-0,2	-0,2	-0,1	0,0	-50,4	-0,1	-0,5
2014-11-17 19:41	0,1	0,1	-0,2	-0,4	-0,2	-0,2	-0,2	-0,2	-0,1	0,0	-1,7	-2,5
2014-11-19 02:26	0,0	0,0	0,3	0,3	0,1	0,0	0,0	0,0	0,0	-21,8	2,0	2,5
2014-11-20 02:53	0,0	0,0	-0,2	-0,2	0,0	-0,1	-0,1	-0,1	-0,1	-46,1	0,4	-1,5
2015-01-17 03:54	0,0	0,0	0,3	0,3	-0,1	-0,1	-0,1	-0,1	-0,1	-7,6	0,3	1,0
2015-04-07 00:26	-0,1		-0,2	-0,1	-0,1							
2015-04-09 02:56	0,0		-0,2	-0,2	-0,2							
2015-04-09 22:11	0,0		0,0	0,0	-0,1							
2015-04-11 23:56	0,0		0,4	0,4	0,0							
2015-04-15 03:11	-0,1		-0,3	-0,3	-0,2							
2015-04-15 18:41	0,0		-0,2	-0,2	0,0							
2015-04-16 18:41	0,1		0,0	0,0	0,0							
2015-04-17 18:26	0,0		-0,2	-0,3	0,0							
2015-04-18 18:41	0,0		-0,1	-0,3	0,0							
2015-04-19 16:56	0,0		-0,5	-0,5	0,0							
2015-04-20 18:26	0,0		0,0	0,0	0,0							
2015-04-21 18:11	0,0		-0,5	-0,4	-0,1							
2015-04-26 21:26	-0,1		0,0	-0,1	0,0							
2015-04-27 18:26	0,0		-0,4	-0,4	-0,1							
2015-04-29 23:21	0,0		-0,5	-0,5	-0,1							
2015-04-30 20:11	0,0		0,4	0,3	0,0							
2015-05-10 21:11	0,0		0,1	0,1	-0,1							
2015-05-11 23:41	0,0		0,0	0,1	0,0							
2015-05-12 22:56	0,0		-0,1	0,0	0,0							

Differences 10 minutes after needle ice initiaiton												
Date	SM -2.5	SM -5	+30	+10	+0	-2.5	-5	-7.5	-10	Direct	wind avg	wind peak
2014-05-31 19:31		0,0				0,0	0,0	0,0	0,0	70,2	2,6	5,0
2014-06-01 18:30		0,1				0,1	0,0	0,0	0,0	601,4	-0,7	1,5
2014-06-02 18:01		0,1				0,0	0,0	0,0	0,0	79,5	0,6	2,0
2014-06-03 15:32		0,1				0,0	0,0	0,0	0,0	-25,7	1,5	3,0
2014-06-04 20:13		-0,1				0,1	0,0	0,0	0,0	-58,9	1,1	3,0
2014-06-30 21:44		0,0				0,0	0,0	0,0	0,0	73,5	-1,2	-2,5
2014-07-01 17:58		0,0				0,0	0,0	0,0	0,0	-130,1	0,6	1,5
2014-07-02 18:30		0,0				0,0	0,0	0,0	0,0	-51,4	0,6	2,5
2014-07-03 19:13		0,0				0,0	0,0	0,0	0,0	0,0	0,1	0,0
2014-08-09 00:10		0,0				0,0	0,0	0,0	0,0	-23,0	0,0	0,0
2014-08-11 20:22		0,0				0,0	0,0	0,0	0,0	29,9	-0,4	-1,5
2014-08-12 20:08		0,0				-0,1	0,0	0,0	0,0	7,2	-1,9	-0,5
2014-08-14 21:08		0,0				0,0	0,0	0,0	0,0	-75,0	0,7	1,5
2014-08-16 20:40		0,1				0,1	0,0	0,0	0,0	0,0	1,4	2,0
2014-08-21 18:23		0,1				0,0	0,0	0,0	0,0	27,6	0,8	0,5
2014-08-23 16:27		0,0				0,0	0,0	0,0	0,0	-51,8	1,4	1,5
2014-10-19 23:11	0,0	0,0	0,7	0,7	0,3	0,1	0,1	0,0	0,1	-0,4	0,8	1,5
2014-10-21 00:25	-0,1	-0,1	-0,2	0,0	0,1	0,1	0,1	0,1	0,0	0,1	0,0	0,5
2014-11-05 00:26	0,0	0,1	-0,1	-0,1	-0,1	0,0	0,1	0,0	0,0	-19,3	-0,2	-0,5
2014-11-15 19:12	0,1	0,1	0,3	0,3	0,1	0,1	0,1	0,1	0,1	59,8	0,2	-1,0
2014-11-16 19:24	-0,1	0,0	0,1	0,1	0,2	0,2	0,2	0,1	0,1	0,0	0,0	-0,5
2014-11-17 19:41	0,1	0,1	-0,9	-0,8	0,1	0,3	0,2	0,1	0,1	0,0	0,0	0,0
2014-11-19 02:26	0,0	0,0	-0,1	0,0	0,0	-0,1	0,0	0,1	0,0	3,3	0,5	1,0
2014-11-20 02:53	0,0	0,0	-0,1	-0,1	-0,1	0,1	0,1	0,0	0,0	31,6	-0,9	-1,0
2015-01-17 03:54	0,1	0,0	0,5	0,6	0,2	0,1	0,1	0,1	0,1	-42,9	-1,4	-1,5
2015-04-07 00:26	0,0		-0,9	-0,7	0,1							
2015-04-09 02:56	0,0		0,1	0,1	0,1							
2015-04-09 22:11	0,0		0,1	0,0	0,1							
2015-04-11 23:56	0,0		-0,1	-0,1	0,0							
2015-04-15 03:11	0,0		0,2	0,2	-0,1							
2015-04-15 18:41	0,1		0,2	0,2	0,0							
2015-04-16 18:41	0,1		0,3	0,3	0,1							
2015-04-17 18:26	0,0		0,5	0,6	0,1							
2015-04-18 18:41	0,0		-0,1	-0,1	0,1							
2015-04-19 16:56	0,1		0,7	0,6	0,1							
2015-04-20 18:26	0,1		-0,1	-0,1	0,0							
2015-04-21 18:11	0,0		-0,3	-0,2	0,0							
2015-04-26 21:26	-0,1		-0,2	-0,2	0,0							
2015-04-27 18:26	0,0		0,3	0,2	0,1							
2015-04-29 23:21	0,0		0,5	0,5	0,2							
2015-04-30 20:11	0,0		0,2	0,2	0,0							
2015-05-10 21:11	0,1		0,0	0,0	0,1							
2015-05-11 23:41	0,0		-0,3	-0,2	0,0							
2015-05-12 22:56	0,0		0,1	0,1	0,0							

Differences 60 minutes before needle ice initiaiton												
Date	SM -2.5	SM -5	+30	+10	+0	-2.5	-5	-7.5	-10	Direct	wind avg	wind peak
2014-05-31 19:31		0,0				-0,1	-0,1	-0,1	0,0	89,9	1,2	0,5
2014-06-01 18:30		0,0				-0,1	-0,1	0,0	0,0	113,0	-0,6	0,5
2014-06-02 18:01		0,0				0,0	0,0	0,0	0,0	230,9	0,8	1,5
2014-06-03 15:32		0,0				0,0	0,0	0,0	0,0	157,4	-1,7	-1,5
2014-06-04 20:13		-0,1				0,0	0,0	0,0	0,0	-121,5	1,0	3,5
2014-06-30 21:44		0,0				0,0	0,0	0,0	0,0	-1,0	-3,6	-5,5
2014-07-01 17:58		0,1				0,0	0,0	0,0	0,0	-127,0	0,1	0,5
2014-07-02 18:30		0,0				0,0	0,0	0,0	0,0	29,3	0,2	1,0
2014-07-03 19:13		-0,1				0,0	0,0	0,0	0,0	0,0	-0,3	0,0
2014-08-09 00:10		0,0				0,0	0,0	0,0	0,0	-6,1	-1,7	-1,5
2014-08-11 20:22		0,0				0,0	0,0	0,0	0,0	1,4	-0,2	-0,5
2014-08-12 20:08		-0,1				0,0	0,0	0,0	0,0	-73,5	1,4	2,5
2014-08-14 21:08		0,0				0,0	0,0	0,0	0,0	-115,3	0,5	1,5
2014-08-16 20:40		0,1				0,0	0,0	0,0	0,0	0,1	-0,2	1,0
2014-08-21 18:23		-0,1				0,0	0,0	0,0	0,0	14,6	-0,5	-0,5
2014-08-23 16:27		0,0				-0,1	0,0	0,0	0,0	18,5	0,7	2,0
2014-10-19 23:11	0,0	0,0	0,2	0,2	-0,1	0,0	-0,1	0,0	0,0	-4,6	-0,2	0,0
2014-10-21 00:25	0,0	-0,1	0,0	0,0	0,0	-0,1	-0,1	0,0	-0,1	0,1	0,0	0,0
2014-11-05 00:26	0,0	-0,1	-0,1	-0,2	0,0	-0,2	0,0	0,0	0,0	-22,2	1,0	0,5
2014-11-15 19:12	0,0	0,1	-0,1	-0,1	-0,1	-0,1	-0,1	-0,1	-0,1	22,7	0,2	0,5
2014-11-16 19:24	-0,1	0,0	-0,6	-0,7	-0,1	-0,2	-0,2	-0,1	0,0	-50,4	-0,1	-0,5
2014-11-17 19:41	0,1	0,1	-0,2	-0,4	-0,2	-0,2	-0,2	-0,2	-0,1	0,0	-1,7	-2,5
2014-11-19 02:26	0,0	0,0	0,3	0,3	0,1	0,0	0,0	0,0	0,0	-21,8	2,0	2,5
2014-11-20 02:53	0,0	0,0	-0,2	-0,2	0,0	-0,1	-0,1	-0,1	-0,1	-46,1	0,4	-1,5
2015-01-17 03:54	0,0	0,0	0,3	0,3	-0,1	-0,1	-0,1	-0,1	-0,1	-7,6	0,3	1,0
2015-04-07 00:26	-0,1		-0,2	-0,1	-0,1							
2015-04-09 02:56	0,0		-0,2	-0,2	-0,2							
2015-04-09 22:11	0,0		0,0	0,0	-0,1							
2015-04-11 23:56	0,0		0,4	0,4	0,0							
2015-04-15 03:11	-0,1		-0,3	-0,3	-0,2							
2015-04-15 18:41	0,0		-0,2	-0,2	0,0							
2015-04-16 18:41	0,1		0,0	0,0	0,0							
2015-04-17 18:26	0,0		-0,2	-0,3	0,0							
2015-04-18 18:41	0,0		-0,1	-0,3	0,0							
2015-04-19 16:56	0,0		-0,5	-0,5	0,0							
2015-04-20 18:26	0,0		0,0	0,0	0,0							
2015-04-21 18:11	0,0		-0,5	-0,4	-0,1							
2015-04-26 21:26	-0,1		0,0	-0,1	0,0							
2015-04-27 18:26	0,0		-0,4	-0,4	-0,1							
2015-04-29 23:21	0,0		-0,5	-0,5	-0,1							
2015-04-30 20:11	0,0		0,4	0,3	0,0							
2015-05-10 21:11	0,0		0,1	0,1	-0,1							
2015-05-11 23:41	0,0		0,0	0,1	0,0							
2015-05-12 22:56	0,0		-0,1	0,0	0,0							

Differences 60 minutes after needle ice initiaiton												
Date	SM -2.5	SM -5	+30	+10	+0	-2.5	-5	-7.5	-10	Direct	wind avg	wind peak
2014-05-31 19:31		0,1				0,1	0,1	0,0	0,0	53,8	2,5	1,5
2014-06-01 18:30		0,0				0,3	0,3	0,2	0,1	-114,0	0,2	0,5
2014-06-02 18:01		0,1				0,1	0,0	0,0	0,0	245,5	-0,2	-3,5
2014-06-03 15:32		0,0				0,1	0,0	0,0	0,0	-14,6	1,1	0,0
2014-06-04 20:13		0,1				0,1	0,1	0,0	0,0	84,2	1,1	2,5
2014-06-30 21:44		0,0				0,0	0,0	0,0	0,0	89,0	-1,3	-3,0
2014-07-01 17:58		0,0				0,0	0,0	0,0	0,0	-161,4	0,8	1,5
2014-07-02 18:30		0,0				0,1	0,1	0,0	0,0	40,8	0,5	1,5
2014-07-03 19:13		0,1				0,2	0,0	0,0	0,0	-14,0	0,2	1,0
2014-08-09 00:10		-0,1				-0,1	0,0	0,0	0,0	-512,7	-0,4	0,0
2014-08-11 20:22		0,1				0,0	0,0	0,0	0,0	27,1	1,9	1,0
2014-08-12 20:08		-0,1				0,0	0,0	0,0	0,0	-31,3	0,7	1,0
2014-08-14 21:08		0,0				0,1	0,1	0,0	0,0	-64,8	0,9	2,0
2014-08-16 20:40		0,1				0,2	0,2	0,1	0,0	-2,7	1,8	2,5
2014-08-21 18:23		0,3				0,1	0,1	0,1	0,0	34,7	-1,3	-1,5
2014-08-23 16:27		0,2				0,1	0,0	0,0	0,0	40,3	0,7	1,0
2014-10-19 23:11	0,2	0,0	-0,4	-0,4	0,1	0,4	0,4	0,3	0,2	4,4	-1,5	-1,5
2014-10-21 00:25	0,0	-0,1	-0,5	0,0	1,0	0,6	0,5	0,4	0,3	0,1	0,0	0,5
2014-11-05 00:26	0,2	0,6	-0,3	-0,3	-0,1	0,1	0,2	0,2	0,2	0,9	0,5	1,0
2014-11-15 19:12	0,1	0,2	0,6	0,6	0,3	0,5	0,7	0,8	0,5	21,3	-0,9	-1,0
2014-11-16 19:24	0,1	0,0	1,0	1,0	0,3	0,6	0,9	0,7	0,4	15,0	0,1	0,0
2014-11-17 19:41	0,1	0,0	-1,2	-1,4	0,7	1,1	1,1	0,8	0,4	0,0	-1,0	-2,0
2014-11-19 02:26	0,0	0,0	0,2	0,2	0,1	0,1	0,3	0,3	0,2	-10,5	0,4	0,0
2014-11-20 02:53	0,1	0,1	0,6	0,7	0,2	0,2	0,3	0,4	0,3	20,7	2,3	2,0
2015-01-17 03:54	0,1	0,0	-2,7	-2,3	-0,1	0,3	0,6	0,5	0,4	-44,0	0,5	1,5
2015-04-07 00:26	0,1		-0,2	-0,1	0,5							
2015-04-09 02:56	0,1		-0,1	-0,1	0,1							
2015-04-09 22:11	0,1		-0,8	-0,4	0,6							
2015-04-11 23:56	0,1		0,1	0,1	0,1							
2015-04-15 03:11	0,1		0,7	0,7	-0,1							
2015-04-15 18:41	0,1		1,0	1,0	0,1							
2015-04-16 18:41	0,2		3,1	3,1	0,7							
2015-04-17 18:26	0,1		0,7	0,8	0,2							
2015-04-18 18:41	0,1		-0,1	0,0	0,3							
2015-04-19 16:56	0,1		2,6	2,6	0,5							
2015-04-20 18:26	0,1		-0,5	-0,5	0,1							
2015-04-21 18:11	0,1		-0,2	0,0	0,3							
2015-04-26 21:26	0,1		-0,5	-0,5	0,1							
2015-04-27 18:26	0,1		0,7	0,8	0,4							
2015-04-29 23:21	0,1		1,7	1,7	0,6							
2015-04-30 20:11	0,1		-0,1	-0,1	0,1							
2015-05-10 21:11	0,1		-0,2	-0,1	0,4							
2015-05-11 23:41	0,1		-0,6	-0,4	0,1							
2015-05-12 22:56	0,1		-0,1	0,0	0,2							

Table 5.13. Change in environmental parameters 10 and 60 minutes prior and past visual needle ice initiation from Site 2. Blue indicates a lowering, green equals no change and red shows an increase in the measured parameter.

Differences 10 minutes before needle ice initialton												
Time	Sm -2.5	SM -5	+30	+10	+0	-2.5	-5	-7.5	-10	Direction	Wind Avg.	Wind Peak
2015-04-09 23:00	-0,1	-0,1	0,7	0,6	-0,1	-0,1	-0,1	-0,1	-0,1	11,4	0,1	0,5
2015-04-11 23:30	0,0	0,0	0,2	0,2	-0,1	-0,1	-0,1	-0,1	-0,1	-3,5	0,1	0,5
2015-04-15 04:15	-0,1	0,0	-0,1	-0,1	0,4	0,1	0,0	0,0	-0,1	-9,1	0,5	1,0
2015-04-15 19:15	0,0	0,0	0,0	0,1	0,1	0,0	-0,1	-0,1	-0,1	0,1	0,2	-0,5
2015-04-16 18:15	0,0	0,1	0,0	0,0	0,0	0,0	-0,1	-0,1	-0,1	0,5	0,9	-0,5
2015-04-17 17:45	0,1	0,0	-1,1	-1,3	-0,5	-0,4	-0,3	-0,2	0,0	-15,9	-0,3	0,0
2015-04-18 17:15	0,0	0,0	-0,4	-0,5	-0,8	-0,7	-0,5	-0,3	0,0	7,3	0,5	1,0
2015-04-19 18:00	-0,1	0,0	0,0	-0,1	-0,2					-2,8	0,8	0,5
2015-04-20 18:15	-0,1	0,0	-0,1	-0,1	-0,1					23,7	0,4	0,0
2015-04-21 19:00	0,0	0,0	0,4	0,3	0,0					67,7	0,1	-0,5
2015-04-27 00:15	0,2	0,0	0,0	0,1	-0,1					-34,1	-0,5	-1,0
2015-04-27 22:00	-0,1	0,0	0,3	0,2	0,0					-9,0	-0,3	-0,5
2015-04-30 00:00	0,2	-0,1	0,0	-0,1	-0,1					10,2	1,7	2,0
2015-04-30 19:00	-0,2	0,1	-0,1	0,0	-0,1					41,7	0,0	0,5
2015-05-02 01:45	0,1	-0,1	-0,2	-0,2	0,0					-36,0	0,5	1,5
2015-05-06 22:00	-0,1	0,0	-0,8	-0,7	-0,3					0,0	-0,3	-1,5
2015-05-10 20:30	0,0	0,0	0,1	0,1	0,2					-13,5	0,0	0,0
2015-05-11 21:00	0,1	-0,1	-0,4	-0,4	0,0					18,8	0,5	0,0
2015-05-12 23:00	-0,2	0,0	-0,1	-0,1	0,0					-33,5	0,2	1,0
2015-05-14 02:00	0,2	-0,1	-0,1	-0,1	0,0					30,5	-0,1	0,0
2015-05-14 20:00	-0,1	0,1	-0,1	0,0	0,0					15,5	0,7	1,0
2015-05-16 23:30	0,1	0,0	0,0	0,0	-0,1					22,3	-0,2	-0,5

Differences 10 minutes after needle ice initialton												
Time	Sm -2.5	SM -5	+30	+10	+0	-2.5	-5	-7.5	-10	Direction	Wind Avg.	Wind Peak
2015-04-09 23:20	0,0	0,0	-0,8	-0,5	0,1	0,1	0,1	0,1	0,1	-20,2	0,1	0,0
2015-04-11 23:50	0,0	0,1	0,3	0,3	0,1	0,1	0,1	0,1	0,1	15,0	0,1	0,5
2015-04-15 04:35	0,0	0,1	0,3	0,3	-0,1	0,0	0,0	0,1	0,0	-1,2	0,8	0,0
2015-04-15 19:35	0,0	0,1	0,2	0,3	-0,3	0,0	0,1	0,1	0,1	26,8	0,3	0,0
2015-04-16 18:35	0,0	0,0	0,1	0,1	0,0	0,0	0,0	0,1	0,1	46,4	1,3	1,5
2015-04-17 18:05	0,1	0,1	0,8	0,9	-0,3	-0,1	0,1	0,1	0,0	8,2	-0,3	-0,5
2015-04-18 17:35	0,1	0,1	0,6	0,5	0,6	0,5	0,4	0,2	0,0	5,7	0,4	1,0
2015-04-19 18:20	0,0	0,0	0,1	0,1	0,1					-8,4	0,2	0,0
2015-04-20 18:35	0,0	0,0	-0,2	-0,1	0,0					-33,6	-0,3	-1,0
2015-04-21 19:20	0,0	0,1	-0,7	-0,6	0,0					95,0	-0,5	-2,0
2015-04-27 00:35	0,1	0,0	0,1	0,1	0,1					-36,0	0,0	0,0
2015-04-27 22:20	-0,1	0,0	0,1	0,1	0,0					-3,3	-0,2	-0,5
2015-04-30 00:20	0,1	0,0	0,2	0,2	0,1					-9,1	0,2	1,5
2015-04-30 19:20	0,0	0,0	0,3	0,4	0,2					-0,5	-0,7	0,0
2015-05-02 02:05	-0,1	0,0	0,1	0,1	0,1					5,5	0,3	1,0
2015-05-06 22:20	0,0	0,0	0,1	0,0	-0,3					0,0	-0,2	-1,0
2015-05-10 20:50	0,0	0,0	-0,1	-0,1	0,1					27,5	0,3	0,0
2015-05-11 21:20	0,0	0,1	0,1	0,0	0,0					-67,0	0,0	0,0
2015-05-12 23:20	-0,2	0,1	0,2	0,2	-0,1					-23,3	0,3	0,5
2015-05-14 02:20	0,0	0,1	0,2	0,2	0,0					-5,1	0,4	0,0
2015-05-14 20:20	0,0	0,1	0,0	0,1	0,1					43,8	0,2	-0,5
2015-05-16 23:50	0,1	0,0	0,1	0,1	0,0					20,9	-0,2	0,0

Differences 60 minutes before needle ice initialton												
Time	Sm -2.5	SM -5	+30	+10	+0	-2.5	-5	-7.5	-10	Direction	Wind Avg.	Wind Peak
2015-04-09 22:10	-0,1	-0,1	-1,3	-0,7	-0,5	-0,5	-0,6	-0,7	-0,6	-30,3	0,4	0,5
2015-04-11 22:40	-0,1	0,0	0,3	0,3	-0,8	-0,8	-0,8	-0,8	-0,6	5,5	-0,1	-1,0
2015-04-15 03:25	-0,1	-0,1	-0,6	-0,6	-0,2	-0,5	-0,7	-0,7	-0,6	-41,6	1,2	2,0
2015-04-15 18:25	0,0	0,0	-0,4	-0,4	-0,8	-0,8	-0,9	-0,8	-0,6	-17,5	1,1	0,5
2015-04-16 17:25	-0,1	-0,1	-0,6	-0,6	-0,7	-1,0	-1,2	-0,9	-0,4	32,7	-1,2	-2,5
2015-04-17 16:55	0,1	-0,2	-7,4	-6,6	-6,3	-7,2	-3,7	-1,6	0,0	8,2	0,1	0,5
2015-04-18 16:25	-0,2	-0,1	-4,4	-4,2	-5,3	-7,3	-3,7	-1,3	0,2	33,1	-0,7	-1,0
2015-04-19 17:10	-0,2	-0,1	-1,2	-1,4	-1,3					-6,6	1,4	2,0
2015-04-20 17:25	-0,1	-0,1	-1,6	-1,6	-0,7					9,0	-0,7	-2,0
2015-04-21 18:10	0,0	-0,2	0,6	0,4	-0,7					23,4	0,5	1,5
2015-04-26 23:25	0,1	0,0	-0,7	-0,6	-0,5					-3,2	-0,9	-1,0
2015-04-27 21:10	-0,1	0,0	-0,2	-0,2	-0,7					-0,6	-0,3	-1,0
2015-04-29 23:10	0,3	0,0	-1,8	-1,8	-1,0					-5,2	0,2	1,0
2015-04-30 18:10	-0,1	0,1	-0,4	-0,5	-0,9					40,3	0,0	0,5
2015-05-02 00:55	0,1	0,0	-0,4	-0,3	-0,2					-39,8	0,4	1,5
2015-05-06 21:10	-0,1	0,0	-2,1	-2,2	-1,9					-47,7	-1,8	-2,5
2015-05-10 19:40	0,4	0,6	-1,0	-1,1	-1,8					-9,1	-0,6	-1,0
2015-05-11 20:10	-0,1	-0,2	0,0	0,1	0,0					-150,9	0,2	0,0
2015-05-12 22:10	-0,2	0,1	-0,2	-0,2	-0,2					-9,9	0,5	0,5
2015-05-14 01:10	0,0	0,0	-0,1	-0,1	0,1					11,4	0,8	0,5
2015-05-14 19:10	-0,1	0,0	-0,4	-0,4	-0,3					28,9	-0,1	-2,0
2015-05-16 22:40	-0,1	0,1	0,3	0,4	0,0					28,3	0,5	1,0

Differences 60 minutes after needle ice initialton												
Time	Sm -2.5	SM -5	+30	+10	+0	-2.5	-5	-7.5	-10	Direction	Wind Avg.	Wind Peak
2015-04-10 00:10	0,0	0,2	0,0	0,1	0,1	0,3	0,4	0,5	0,5	-2,4	0,2	0,5
2015-04-12 01:20	0,1	0,1	-0,7	-0,7	-0,2	0,1	0,5	0,6	0,7	-18,4	-0,3	-0,5
2015-04-15 06:05	0,4	0,4	1,6	1,5	0,1	0,2	0,3	0,4	0,6	-24,9	1,7	3,0
2015-04-15 21:05	0,2	0,3	0,2	0,2	0,0	0,2	0,4	0,6	0,7	-9,3	0,1	-0,5
2015-04-16 20:05	0,2	0,3	3,5	3,4	0,6	0,9	0,8	0,8	0,6	87,0	1,3	1,5
2015-04-17 19:35	0,4	0,3	1,9	1,7	0,6	0,5	0,8	0,7	0,3	192,9	-0,7	-0,5
2015-04-18 19:05	0,4	0,2	3,2	3,3	1,6	1,7	1,6	1,2	0,4	-97,0	0,5	1,5
2015-04-19 19:50	0,3	0,2	1,1	1,1	0,6					-9,9	1,2	1,5
2015-04-20 20:05	0,2	0,2	0,3	0,4	0,4					0,0	-0,3	-1,0
2015-04-21 20:50	0,1	0,0	-1,3	-1,2	-0,3					106,1	-4,3	-6,5
2015-04-27 02:05	0,0	0,1	0,5	0,5	0,1					5,2	-0,6	-0,5
2015-04-27 23:50	0,0	0,2	-0,8	-0,8	-0,3					11,1	-1,5	-2,5
2015-04-30 01:50	0,2	0,0	1,4	1,4	1,2					-26,3	1,7	3,0
2015-04-30 20:50	0,0	0,1	-0,5	-0,3	1,0					0,7	-1,4	-1,0
2015-05-02 03:35	-0,1	-0,1	0,3	0,4	0,3					-7,0	0,1	1,5
2015-05-06 23:50	-0,1	0,2	-0,7	-0,5	0,5					-228,8	-1,1	-2,0
2015-05-10 22:20	0,2	0,7	-0,3	-0,2	0,4					177,3	-0,3	-0,5
2015-05-11 22:50	0,1	0,3	0,0	0,0	0,2					-69,6	0,2	0,0
2015-05-13 00:50	0,1	0,4	0,4	0,4	-0,1					-7,3	-0,1	-0,5
2015-05-14 03:50	0,2	0,3	0,4	0,4	0,1					8,4	0,8	1,5
2015-05-14 21:50	-0,3	0,1	0,2	0,2	0,1					50,2	-1,2	-2,0
2015-05-17 01:20	-0,1	0,0	0,0	0,0	-0,1					36,0	-0,7	-0,5

Table 5.14. Change in environmental parameters 10 and 60 minutes prior and past visual needle ice initiation from Site 3. Blue indicates a lowering, green equals no change and red shows an increase in the measured parameter.

Differences 10 minutes before needle ice initialton												
Time	Sm -2.5	SM -5	+10	+0	-2.5	-5	-7.5	-10	Direction	Wind Avg.	Wind Peak
2014-04-26 17:01	-0,1	-0,1	0,0	0,0	0,0	0,0	0,0	-0,1	-48,4	-0,4	1,0
2014-05-12 14:01	-0,1	-0,1	0,0	-0,1	0,0	0,0	0,0	0,0	0,0	0,0	0,0
2014-05-14 17:01	0,1	-0,1	-0,1	-0,2	0,0	0,0	0,0	0,0	173,7	0,1	1,0
2014-05-15 17:01		0,0	0,2	0,0	0,0	0,0	0,0	0,0	180,4	0,1	1,0
2015-02-28 19:01		0,0	0,0	0,0	0,0	0,0	0,0	0,0			
2015-03-10 22:21		0,0	0,3	0,5	-0,2	0,0	0,0	0,0			
2015-03-11 19:51		-0,1	0,0	0,1	0,1	0,1	0,0	0,0			
2015-03-13 21:21		0,1	0,2	0,2	-0,1	0,0	0,0	-0,1			
2015-03-19 16:11		-0,1	-0,8	-0,9	-0,6	-0,9	-1,2	-1,1			
2015-03-26 22:11		0,1	-0,1	0,0	-0,1	-0,1	0,0	0,0			
2015-03-29 23:01		-0,1	-0,1	-0,1	-0,1	-0,1	0,0	0,0			
2015-03-30 18:11		0,0	0,0	-0,3	-0,4	-0,3	-0,1	-0,1			
2015-04-01 18:21		-0,1	-0,2	-0,1	0,0	0,0	0,0	0,0			
2015-04-03 01:01		-0,1	0,0	0,0	0,0	0,1	0,0	0,0			
2015-04-10 18:01		0,0	0,1	-0,1	-0,5	0,4	-0,3	-0,2			

Differences 10 minutes before needle ice initialton												
Time	Sm -2.5	SM -5	+10	+0	-2.5	-5	-7.5	-10	Direction	Wind Avg.	Wind Peak
2014-04-26 17:21	0,1	0,1	-0,1	0,0	0,0	0,0	0,1	0,1	66,3	-0,1	1,0
2014-05-12 14:21	0,1	0,1	0,3	0,0	0,0	0,0	0,0	0,0	-0,1	0,0	0,0
2014-05-14 17:21	0,0	0,1	-0,2	0,2	0,0	0,1	0,0	0,0	-26,4	0,1	2,0
2014-05-15 17:21	0,0	0,1	-0,2	0,0	0,0	0,0	0,0	0,0	208,4	0,1	0,5
2015-02-28 19:21		0,0	-0,3	0,0	0,0	0,0	0,0	0,0			
2015-03-10 22:41		0,1	0,2	0,4	0,0	0,1	0,1	0,1			
2015-03-11 20:11		-0,1	-0,1	-0,1	0,0	-0,1	-0,1	-0,2			
2015-03-13 21:41		0,1	0,2	0,0	-0,1	0,0	-0,2	-0,2			
2015-03-19 16:31		0,1	0,4	0,3	0,3	0,5	0,7	0,6			
2015-03-26 22:31		0,0	0,3	0,5	0,3	0,1	0,0	0,0			
2015-03-29 23:21		0,1	0,1	0,1	-0,2	-0,1	0,0	0,0			
2015-03-30 18:31		0,1	0,2	0,3	0,4	0,3	0,3	0,2			
2015-04-01 18:41		0,1	-0,2	0,0	0,2	0,2	0,0	0,0			
2015-04-03 01:21		0,2	0,1	0,1	0,3	0,5	0,4	0,4			
2015-04-10 18:21		0,0	0,2	0,6	0,2	0,2	0,2	0,1			

Differences 60 minutes before needle ice initialton												
Time	Sm -2.5	SM -5	+10	+0	-2.5	-5	-7.5	-10	Direction	Wind Avg.	Wind Peak
2014-04-26 16:11	-0,4	-0,8	-0,1	-0,1	-0,2	-0,3	-0,4	-0,5	225,4	-0,6	0,0
2014-05-12 13:11	-0,2	-0,6	0,1	-0,2	-0,1	-0,1	0,0	-0,1	0,0	0,0	0,0
2014-05-14 16:11	0,3	-0,4	-0,4	-0,5	-0,1	-0,1	-0,2	-0,2	509,0	-0,4	0,5
2014-05-15 16:11	0,0	-0,1	2,1	0,0	0,0	0,0	0,0	0,0	206,8	0,0	0,5
2015-02-28 18:11		-0,1	-0,2	-0,1	0,0	0,0	-0,1	-0,3			
2015-03-10 21:31		-0,1	0,0	0,3	-0,1	0,1	0,0	-0,1			
2015-03-11 19:01		-0,2	0,1	0,2	0,2	0,1	0,4	0,6			
2015-03-13 20:31		0,0	0,4	0,5	0,2	0,1	0,2	0,3			
2015-03-19 15:21		-0,4	2,7	-8,6	-7,2	5,3	-3,3	2,6			
2015-03-26 21:21		0,0	-0,5	-0,3	-0,3	-0,1	-0,3	-0,4			
2015-03-29 22:11		-0,7	-1,2	-0,5	-0,3	-0,2	-0,3	-0,5			
2015-03-30 17:21		-0,1	-0,2	-0,3	-0,5	-0,5	-0,4	-0,3			
2015-04-01 17:31		-0,5	-0,5	-0,3	-0,2	-0,1	0,0	0,2			
2015-04-03 00:11		-0,7	-0,2	0,0	0,1	0,0	-0,3	-0,2			
2015-04-10 17:11		-0,2	-0,8	0,3	-1,1	-1,3	-1,4	-1,4			

Differences 60 minutes after needle ice initialton												
Time	Sm -2.5	SM -5	+10	+0	-2.5	-5	-7.5	-10	Direction	Wind Avg.	Wind Peak
2014-04-26 18:11	0,5	1,3	0,4	0,5	0,2	0,3	0,3	0,3	-85,0	-0,2	0,5
2014-05-12 15:11	0,4	1,0	0,5	0,3	0,1	0,1	0,1	0,1	0,0	0,0	0,0
2014-05-14 18:11	0,2	1,3	-1,0	0,7	0,1	0,1	0,1	0,1	-156,8	-0,1	1,0
2014-05-15 18:11	0,1	0,1	1,7	0,3	0,0	0,0	0,0	0,0	515,0	0,1	1,0
2015-02-28 20:11		0,2	0,2	0,6	0,3	0,1	0,1	0,2			
2015-03-10 23:31		0,1	0,5	1,0	0,1	0,1	0,3	0,4			
2015-03-11 21:01		0,1	0,1	0,5	0,5	0,4	0,5	0,6			
2015-03-13 22:31		0,1	0,4	0,3	0,1	0,1	0,4	0,5			
2015-03-19 17:21		0,4	0,9	0,6	0,6	0,9	1,9	2,2			
2015-03-26 23:21		-0,1	0,6	1,2	0,7	0,3	0,2	0,3			
2015-03-30 00:11		0,8	0,2	0,3	0,1	0,0	0,0	0,0			
2015-03-30 19:21		0,3	0,0	0,0	-0,1	0,2	0,3	0,1			
2015-04-01 19:31		0,7	0,3	1,4	1,2	0,8	0,4	0,4			
2015-04-03 02:11		1,3	0,4	0,0	0,5	0,8	1,0	0,8			
2015-04-10 19:11		0,1	1,4	3,2	3,0	2,5	1,1	0,7			

to the growth. The same trend in increased soil moisture and temperature was seen 10 and 60 minutes after initiation of needle ice growth at all three sites.

Imagery was used to identify synchronicity in the growth of needle ice with temperature spikes. During the examination of such imagery, it was noted that the needle ice growth initiation depth varied in the captured imagery throughout the study sites and study period. Some ice needles grew at the surface, while other needle ice events showed growth to have originated from deeper ice nucleation.

5.6 Surface and subsurface growth of needle ice

Historically, little research has been published on the initiation depth of needle ice (Outcalt, 1971; Matsuoka, 1996; Peterson and Krantz, 2003). Results from this study show a more dynamic needle ice growth environment than previously thought, with initiation depth ranging from visible ice crystals at surface level to suggested initiation at several centimetres depth.

Image analysis of the 81 needle ice events observed from camera imagery identified events with visible ice needles on the surface, as well as events where no ice was seen at the surface, and only heaving of the soil was observed. An analysis of the depth of needle ice initiation follows.

Images of events in the following section are presented at the time of maximum heave (tallest ice needles) taken one camera image (15 minutes) before initiation of melt. The following section displays events from each site illustrating shallow and deep ice nucleation. Terminology described in Section 4.3.3.3 referring to Image-Logger Discrepancy (ILD) will be used in the following section.

5.6.1 Ice nucleation depth at Site 1

Needle ice nucleation depth was analysed for two events at Site 1 visually displaying differences in needle ice growth depth. Figure 5.39 shows two images of needle ice events from Site 1, split between two frames (a, b). The shallow event was recorded on January 17 2015 and the deeper event on November 18 2014.

Shallow ice nucleation is observable in the lower left corner (red oval) in Figure 5.42a. Needle ice nucleation was seen to occur at a surface temperature of -0.1°C with a positive ILD of 20 minutes, indicating that the surface temperature crossed to below 0°C 20 minutes after visual identification of needle ice growth.

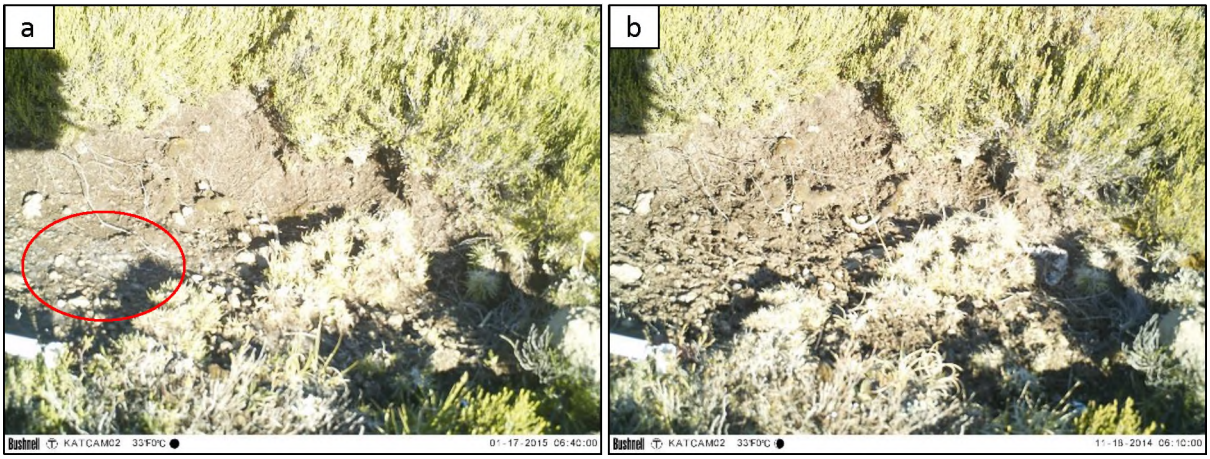

Figure 5.42. Shallow (a) and deep (b) nucleation of ice at Site 1. See text for more information.

Deeper ice nucleation is suggested in an event captured on 18 November 2014 (Figure 5.42b). The event shows no surface ice or ice needles visible in the imagery during growth or decay. Surface temperatures during visual identification of growth were 2.2°C, with a positive ILD (further detailed in Section 5.7) of 7h44min, meaning surface temperatures reached below 0°C 7h44min (31 images) after needle ice initiation was observable in imagery. The time-span from below zero temperatures to visually observable needle ice was 7h24min longer on November 18 2014 than on January 17 2015.

5.6.2 Ice nucleation depth at Site 2

Events demonstrating shallow and deep needle ice growth from Site 2 occurred on 15 April 2015 and 27 April 2015. Shallow needle ice growth was observed in the background and in the lower right (red ovals) in Figure 5.43a, while deep, non-visible, segregation ice is suggested to be represented in Frame b. Frame a shows the side of ice needle lifting material within the red circles, as well as tips of ice surfacing in the general surface area. Frame b shows only heaving of the surface material and at no point is ice visibly present at the surface. Surface temperatures during needle ice initiation on the April 15 event were measured to be -0.2°C with a positive ILD of 30 minutes. Surface measurements during the night prior to Frame 2 showed no negative values; however, minimum surface temperatures reached 0.4°C at 05:50, 4h25min after visual initiation of growth. Surface temperature during initiation of growth on April 27 was 1.1°C.

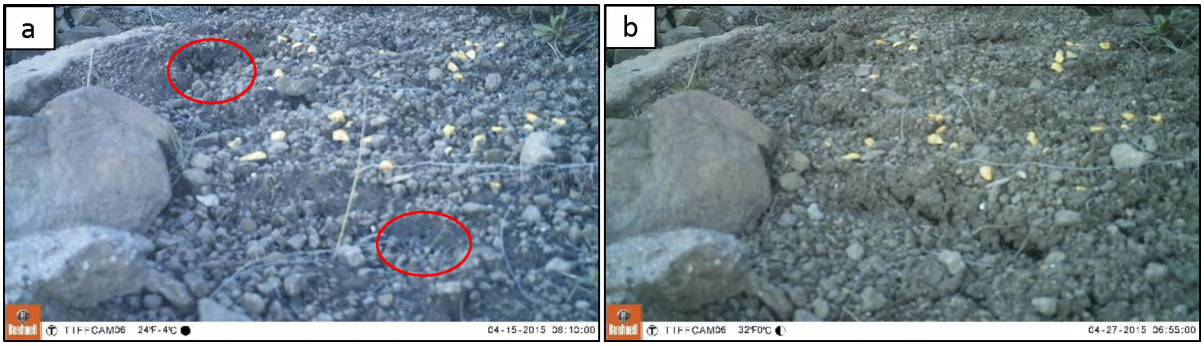

Figure 5.43. Shallow (1) and deep (2) nucleation of ice from Site 2.

5.6.3 Ice nucleation depth at Site 3

None of the 16 needle ice events captured from Site 3 showed shallow needle ice initiation. While several images taken with a hand-held camera during filed studies on Marion Island, in addition to personal observations that indicate that needle ice grows at the boundary between a subsurface layer of fine material overlain by scoria (Figure 5.44, Figure 3.12 in Section 3.3.2 and Figure 4.17 in Section 4.5).

Figure 5.44. Ice needles growing close to Site 3 showing supporting coarse material and growing out of a finer substrate.

Figure 5.45. Ice needles growing close to Site 3 supporting coarse material and growing out of a finer substrate

Figure 5.46. Ice needles growing close to a Azorella Selago plant. Needles emerged from the fine, wet and unfrozen material.

Results from Section 5.6 show that not only is there a varying spatial component to needle ice growth initiation but also a temporal one. The following section analyses timing of needle ice growth and decay in addition to needle ice event duration.

5.7 Timing of needle ice growth and decay

Needle ice growth and decay initiation observations showed marked differences within, and between, study sites. This section describes timings of visually observed needle ice growth and decay initiation based on camera images, focusing on how needle ice initiation, decay and duration is affected by location and diurnal/seasonal change in temperature, soil moisture, wind speeds and timing of sunrise and sunset.

Results from the following section will be presented as tables and graphs that display event timings of growth and decay, as well as histograms displaying event duration. Needle ice growth and decay initiation will be compared to the timing of sunrise and sunset. A table displaying timing of sunrise and sunset from each study location during each needle ice event is presented in Appendix A (Table 9.1).

5.7.1 Duration and timing of needle ice growth, decay and duration at Site 1

5.7.1.1 Growth

Site 1 registers the largest number of needle ice events of the three study sites, 44 in total. However, due to logger failure, described in Chapter 3, near surface (+0cm) temperature data is missing for 14 of the identified events. Data from next shallowest sensor, the -2.5cm temperature sensor, was used as a proxy for temperatures related to needle ice growth during these events (Section 4.7.2).

The span of visual identification of needle ice growth initiation from camera images at Site 1 range from 15:30 prior, to 03:55 after midnight of the event, ranging 12h25min between earliest and latest initiation (Figure 5.50). The average event at Site 1 started at 21:06 and lasted 13h27min, with 71% of events occurring within one standard deviation (3h13min) of 21:00 (Figure 5.47, 5.52 and Table 5.1)

ILD measurements for Site 1 are presented in Figure 5.47. Fourteen of the 44 events had available data from the +0cm sensor, and showed below 0°C minimum event temperatures. The average ILD of these 14 events was 2h43min. The ten events for which proxy data from the -2.5cm temperature sensor was used (Table 5.1), showed an average ILD of 2h56min. ILD was based on temperatures reaching 0°C, but for 12 events the +0cm sensor temperature did not go below 0°C. For these 12 events the average minimum surface temperature reached was 0.62°C, with an absolute minimum of 0.09°C and an absolute maximum of 1.25°C. These events displayed an average ILD of 6h16min. Furthermore, ground temperature during four events never exceed 0°C during growth, they displayed an average maximum temperature of -0.02°C with an ILD of 2h50min between growth and the reached minimum temperatures.

Initiation of needle ice growth before and after sunset is shown in Figure 5.49. Initiation of growth compared to sunset was seen from 26min to 9h54min after sunset, while a majority of needle ice

events initiated growth within three hours after sunset. Only one needle ice event was observed to initiate before sunset.

5.7.1.2 Decay

Visual identification of the initiation of decay and end of melt range from 05:55 to 10:00 and 06:55 to 12:55 respectively at Site 1. The average melt started at 07:40 and ended at 10:33 and lasted 2h53min, with 64% of melting events starting and ending within one standard deviation (1h05min and 1h29min) of average melt start and end, respectively.

At Site 1 all 44 needle ice events showed distinguishable initiation of needle ice decay from the imagery (Figure 5.48). Twenty-three of these 44 events occurred when the surface temperature was below 0°C during decay initiation. However, the analysis of eight of the 23 events that showed sub-zero temperatures at decay initiation, relied on the -2.5cm sensor for proxy. Average ILD for these 22 events was 1h51min. The average ILD for the eight proxy events was 3h13min. The remaining 14 events with available +0cm sensor data showed an average ILD of 1h03min.

Figure 5.49 shows initiation of decay in relation to sunrise. The delay at Site 1 varied between 22min to 3h20min between the earliest and latest onset of decay after sunrise. A majority of events started melting within 1h30min of sunrise and no events decayed before sunrise.

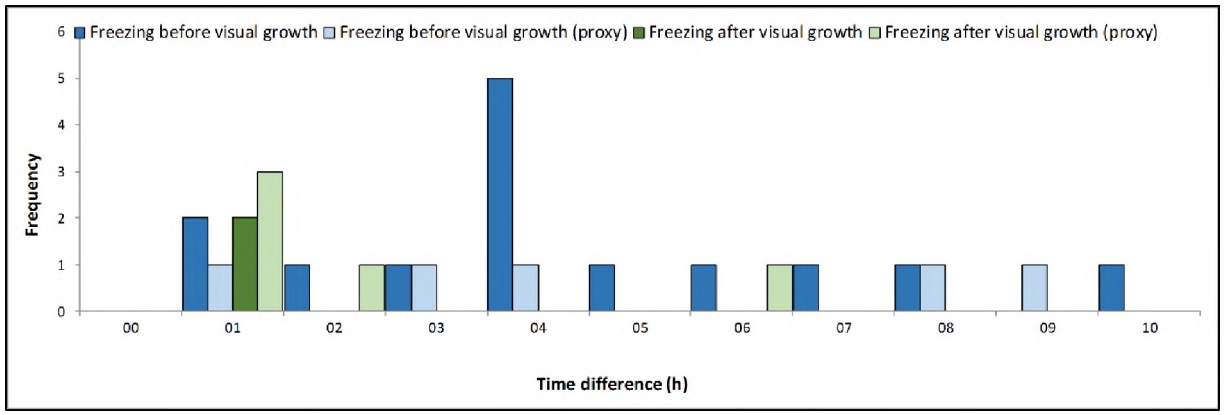

Figure 5.47. Image-logger discrepancy in growth for the 24 events with measurable ILD captured from Site 1. Measurements using proxy data from the -2.5cm sensor, due to a malfunctioning +0cm sensor, are shown in light green and light blue.

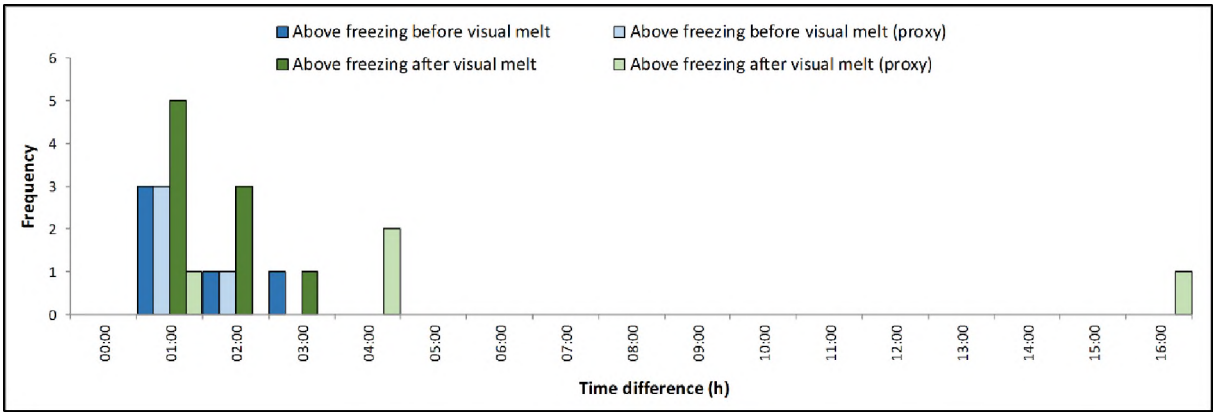

Figure 5.48. Image-logger discrepancy for melt of 22 events with measurable ILD from Site 1. Measurements using proxy data from the -2.5cm sensor, due to a malfunctioning +0cm sensor, are shown in light green and blue

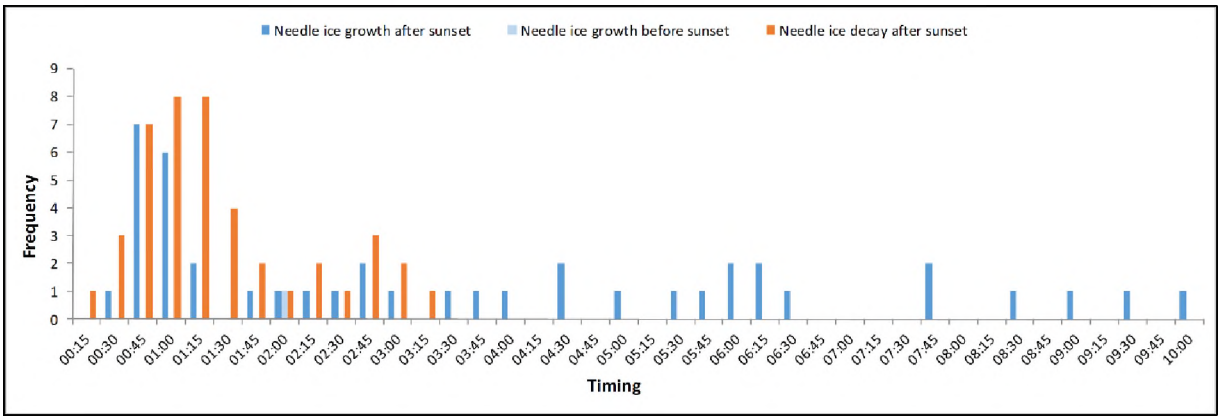

Figure 5.49. Initiation of growth or decay of needle ice relative to sunset/sunrise at Site 1.

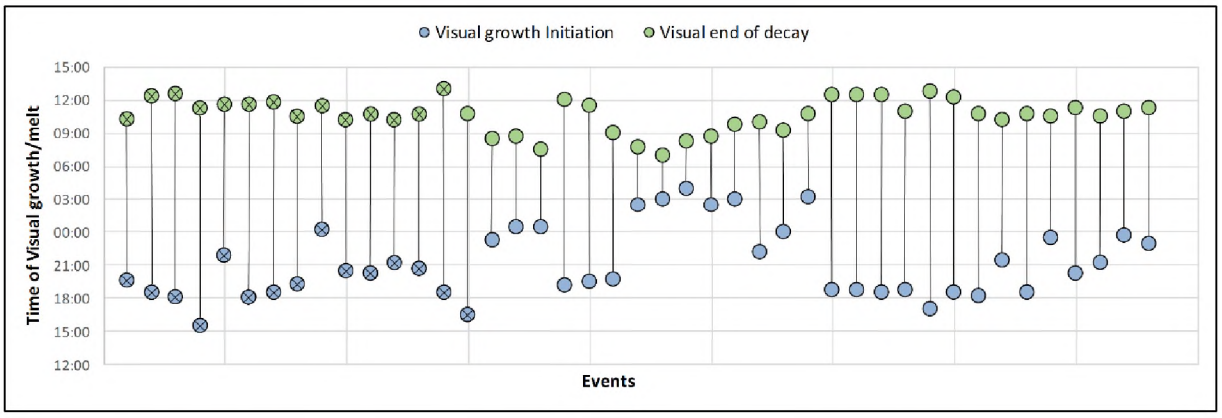

Figure 5.50. Visualization of initiation and decay timing of the 44 needle ice events captured at Site 1. Markers which are crossed inside show data using the -2-5cm proxy for temperature.

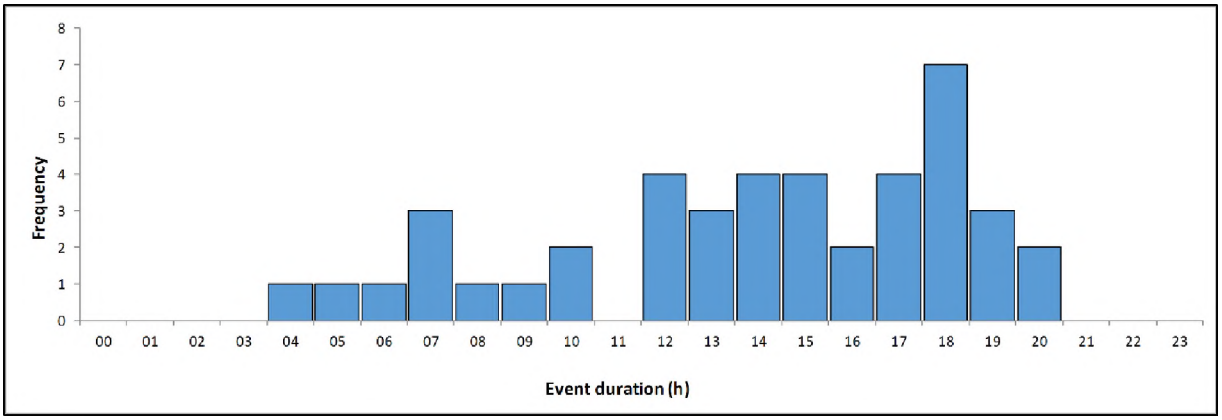

Figure 5.51. Frequency histogram of the 45 needle ice events durations captured at Site 1.

5.7.2 Duration and timing of needle ice growth, decay and duration at Site 2

5.7.2.1 Needle ice growth

Visual identification of needle ice growth initiation from Site 2 ranged from 17:25 to 04:25 in the 22 observed events, displaying a range of 11h from the earliest to the latest growth initiation. The average event started at 20:38 and lasted 15h33min; 68% of events occurred within one standard deviation (3h06min) of 20:38.

The 22 analysed needle ice events from Site 2 had an average ILD of 2h15min (Table 5.15). Sub-grouped into below zero and above zero temperature events, the average ILD varied from 1h20min in the former to 3h52min in the latter. During eight events, surface temperatures did not go below freezing. Average minimum temperature reached during these eight events were 0.49°C, with an absolute minimum of 0.01°C and an ILD of 6h14min during the reached minimum.

Timing of needle ice initiation, before or after sunset, is visualized in Figure 5.53. Growth initiated from 6 minutes to 6h15min after sunset. In addition, six events showed growth initiation before sunset in a span from 22minutes to 10h33minutes. No clear grouping of timing between the 22 events was observed.

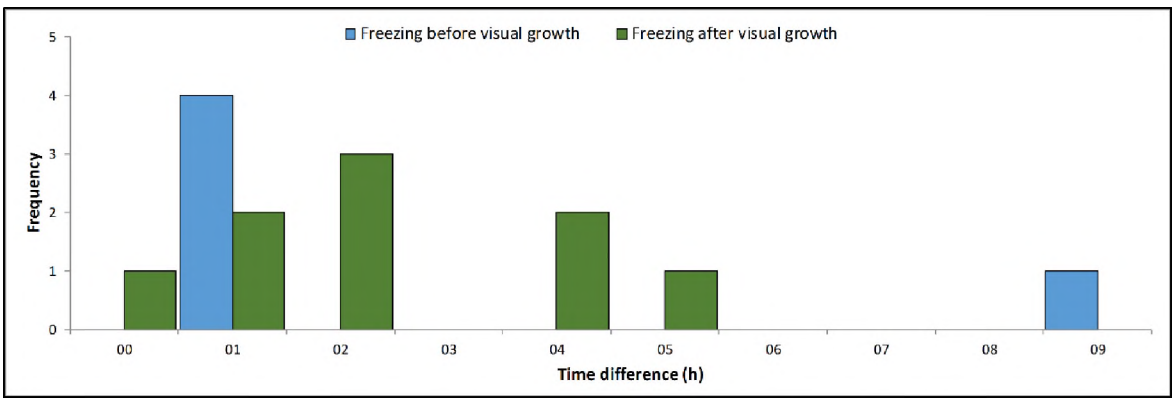

Figure 5.52. Image-logger discrepancy for growth of the 14 events with measurable ILD from Site 2.

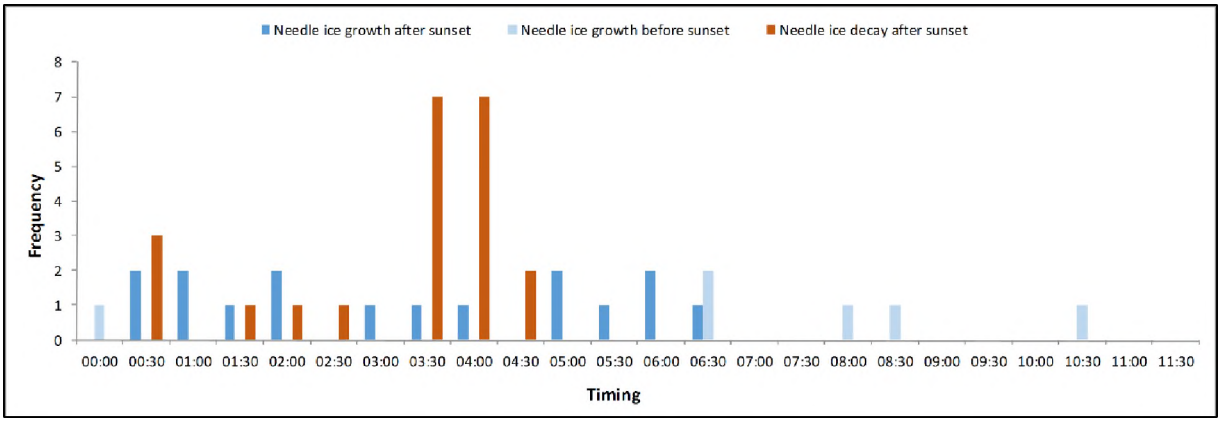

Figure 5.53. Initiation of growth and decay of needle ice measured in time after or before sunset/sunrise at Site 2.

5.7.2.2 Decay

Visual identification of decay initiation and end of melt from Site 2, ranged from 06:40 to 10:55 and 09:40 to 16:55 respectively. The average melt at Site 2 started at 09:31 and ended at 13:17, lasting 3h45min. Eighty-two percent of melting started, and 59% of melting ended within one standard deviation (1h21min and 2h13min) of average. Average ILD for the 13 events that showed below zero temperatures during decay initiation at Site 2 lasted for 1h08min, while non-below zero events average ILD was 6h14min hours (Figure 5.54).

The timing of melt initiation and sunrise/sunset at Site 2 is seen in Figure 5.53. Decay initiation ranged from 14 minutes to 4h10min after sunrise. A majority of events started needle ice decay 3 to 4 hours after sunrise, and no events were seen to initiate decay before sunrise.

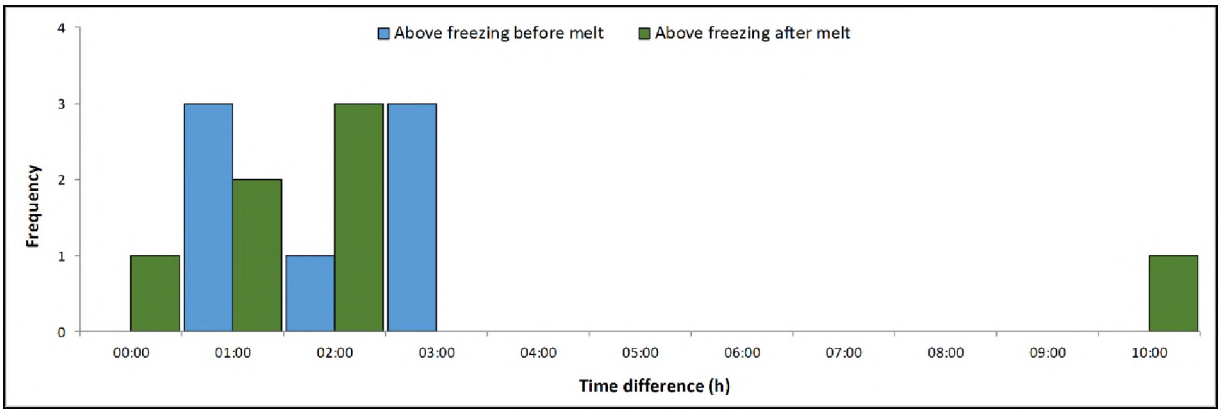

Figure 5.54. Image-logger discrepancy for melt of the 14 events with measurable ILD from Site 2.

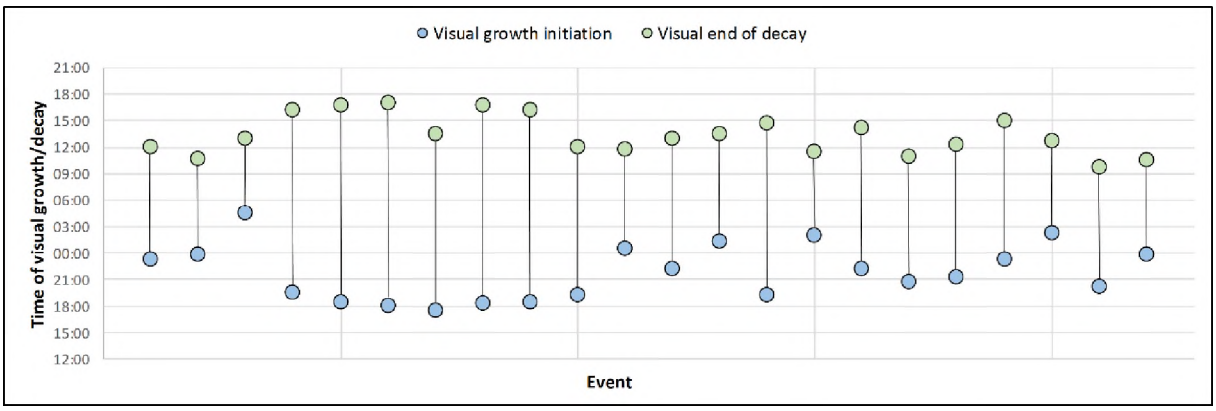

Figure 5.55. Visual identification of initiation and decay from all needle ice events captured at Site 2

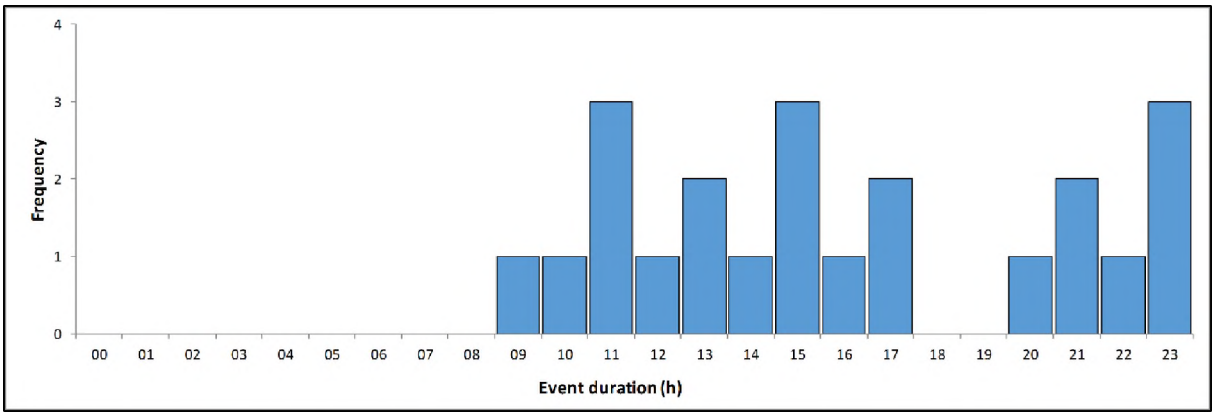

Figure 5.56. Frequency histogram of event duration in hours of the 22 needle ice events captured at Site 2.

5.7.3 Duration and timing of needle ice growth, decay and duration at Site 3

5.7.3.1 Needle ice growth

Visual identification of needle ice growth ranged from 16:21 to 01:11 (a range of 9h10min) for 16 observed significant events at Site 3. The average event started at 19:36 and lasted 13h42min, with 69% of events occurring within one standard deviation (3h00min). Average ILD for the 16 needle ice events from Site 3 was 1h55min (Figure 5.57 and Table 5.15).

Timing of growth and decay relative to the sunset/sunrise at Site 3 is displayed in Figure 5.58. Growth initiation was seen to occur from 2min to 4h49min after sunset and from 7min to 4h49min before sunset from Site 3.

5.7.3.2 Needle ice decay

Visual identification of initiation of decay and end of melt from Site 3 ranged from 04:31 to 09:21 and 08:41 to 23:41 respectively. The average time of the initiation of melting was 07:42 and ended at 13:47 lasting 6h04min, with 77% of melts starting and 69% of melts ending within one standard deviation (1h26min and 4h47min) of the average.

Average ILD for 12 of the 16 events showing observable melt was 0:53 hours (Figure 5.59), while four events did not have observable melt, due to obstruction of the camera melt by frost, and hence an ILD could not be calculated.

Decay was seen to initiate from 19min to 2h48min after sunrise and at two events within 18min before sunrise. The majority of needle ice events initiated decay within 2h to 2h and 30min from sunrise.

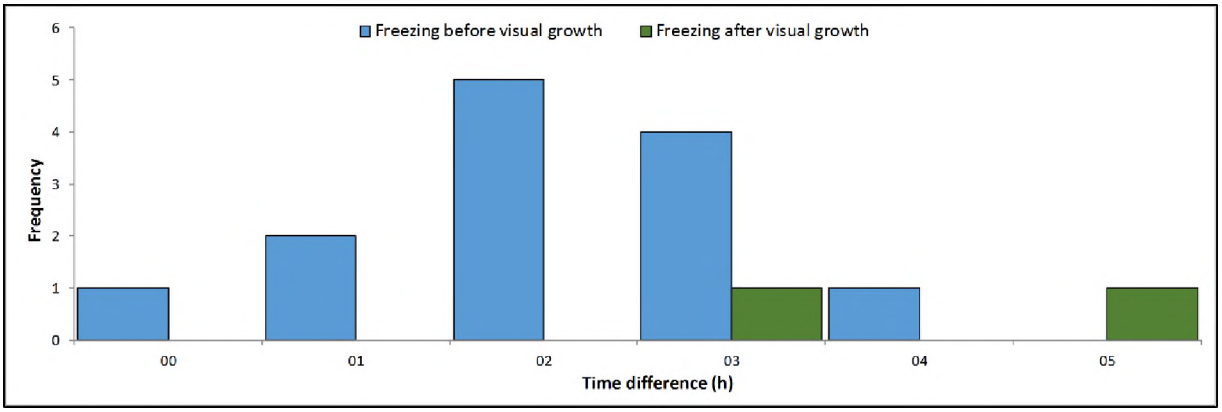

Figure 5.57. Image-logger discrepancy for growth of the 15 events with measurable ILD from Site 3.

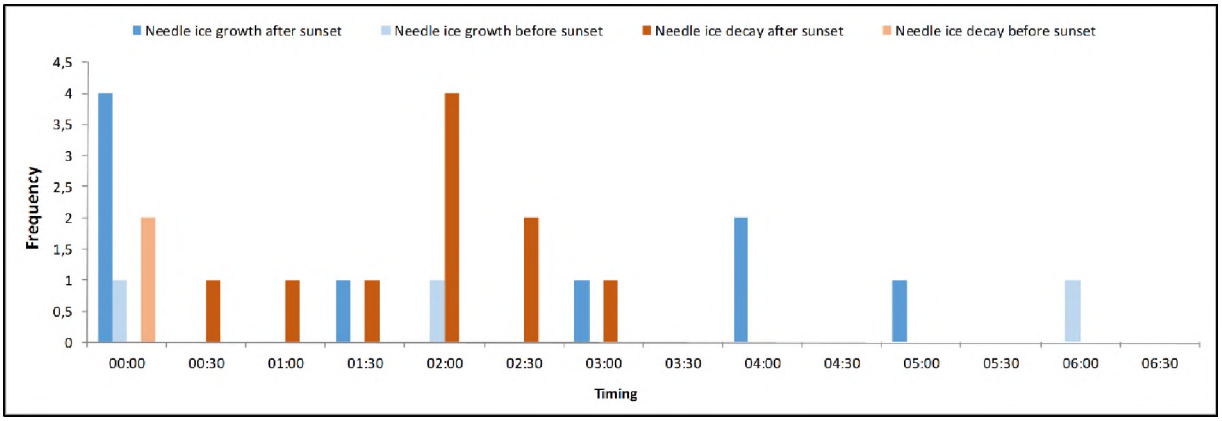

Figure 5.58. Initiation of growth and decay of needle ice measured in time after or before sunset/sunrise at Site 3.

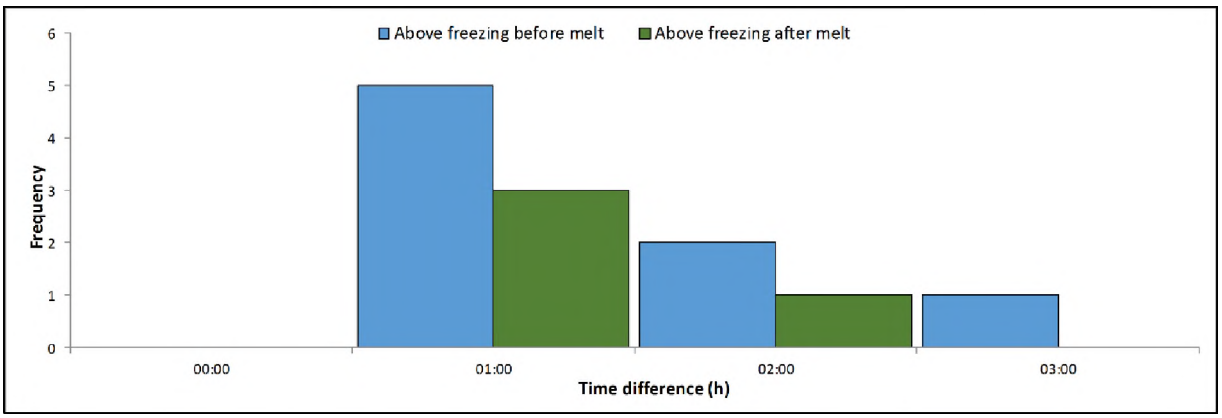

Figure 5.59. Image-logger discrepancy for melt of the 12 events with measurable ILD from Site 3.

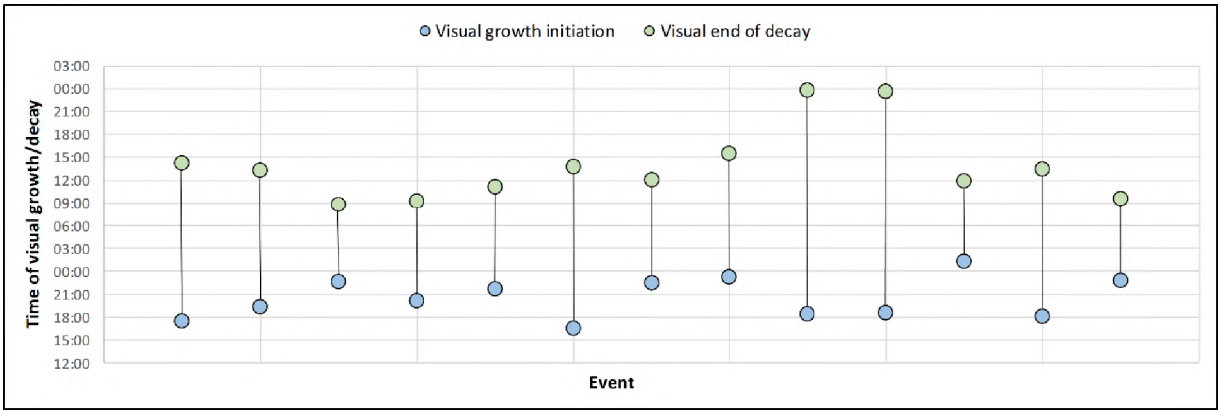

Figure 5.60. Visual identification of initiation and decay from all needle ice events captured at Site 3

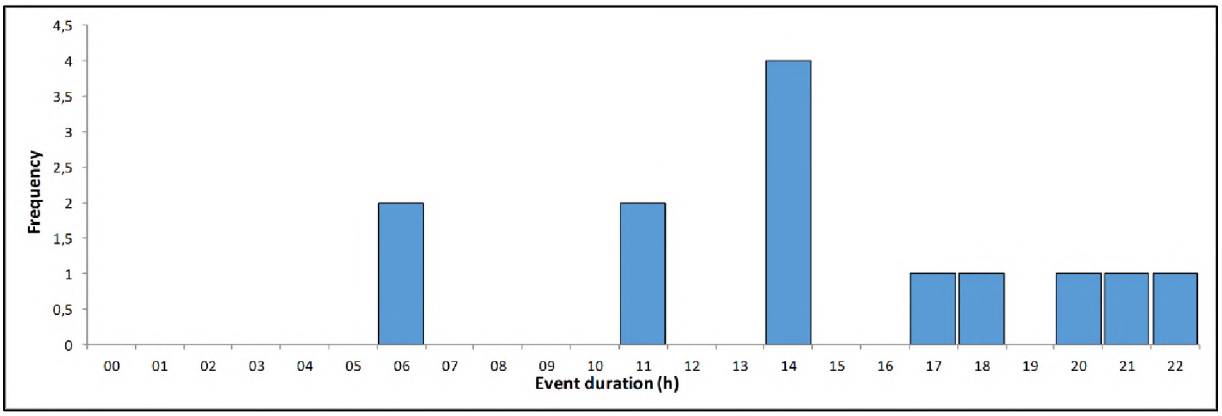

Figure 5.61. Frequency histogram of event duration in hours of the 16 needle ice events captured at Site 3.

Table 5.15.Summarised data of initiation of growth and decay as well as the average needle ice event duration and decay duration.

	Growth timing			Duration	Decay timing			Final decay timing			Duration
	Time			h:min	Time			Time			h:min
	Initiation (min)	Initiation (avg)	Initiation (max)		Initiation (min)	Initiation (avg)	Initiation (max)	Final melt (min)	Final melt (avg)	Final melt (max)	
Site 1	15:30	21:06	03:55	13:27	05:55	07:40	10:00	06:55	10:33	12:55	02:53
Site 2	17:25	18:27	04:25	15:33	06:40	09:31	10:55	09:40	13:17	16:55	03:45
Site 3	16:21	19:20	01:11	13:42	04:31	07:58	09:21	08:41	14:08	23:41	06:04

Table 5.16.Summary of Image Logger Discrepancy (ILD) from analysis of timing of needle ice growth initiation. The number within parenthesis is the number of measurements.

Site	Avg Positive ILD	Avg Negative ILD	Avg Positive ILD Proxy	Avg Negative ILD Proxy	Min	Average	Max	Range
	Time (h:min)							
Site 1	00:26 (13)	05:28 (1)	00:13 (4)	03:50 (5)	00:05	03:13	09:43	09:38
Site 2	01:47 (9)	02:05 (5)	N/A	N/A	00:00	01:53	08:20	08:20
Site 3	01:43 (13)	03:15 (2)	N/A	N/A	00:00	01:55	04:20	04:20

Table 5.17. Summary of Image Logger Discrepancy (ILD) from analysis of timing of needle ice decay initiation. The number within parenthesis is the number of measurements.

Site	Avg Positive ILD	Avg Negative ILD	Avg Positive ILD Proxy	Avg Negative ILD Proxy	Min	Average	Max	Range
	Time (h:min)							
Site 1	00:45 (9)	05:41 (5)	01:08 (4)	01:00 (4)	00:08	01:50	15:32	15:24
Site 2	01:28 (7)	01:56 (7)	N/A	N/A	00:00	01:42	09:12	09:12
Site 3	01:07 (8)	00:26 (4)	N/A	N/A	00:03	00:53	02:17	02:14

Table 5.15, 5.16 and 5.17 present the summarised image-logger discrepancy (ILD) during growth and decay from all three study sites, while Table 5.18 presents data on growth and decay of needle ice in relation to sunset and sunrise. Average positive and negative ILDs are displayed in Table 5.17 with the number of observations of each within parenthesis next to each value.

Table 5.18. Summarised data of the average timing of growth and sunset in addition to decay and sunrise. Red text displays events of growth before sunset and decay before sunrise.

	Timeing sunset-growth			Timeing sunrise-decay		
	h:min			h:min		
	Growth after/before sunset (min)	Growth after/before sunset (avg)	Growth after/before sunset (max)	Decay after/before sunrise (min)	Decay after/before sunrise (avg)	Decay after/before sunrise (max)
Site 1	00:25	03:26	09:54	00:22	01:18	03:20
Site 2	00:06	03:00	06:15	00:14	02:55	04:10
	00:22	06:53	10:33			
Site 3	00:02	01:50	04:49	00:19	01:34	02:48
	00:07	02:47	05:56	00:02	00:13	00:18

5.8 Non-growth events

In screening needle ice measurements from all sites, 53 days with similar temperature conditions to days displaying needle ice were identified, but no heave by any form of segregation ice was observed. Chapter 3 suggests suitable textural conditions for needle ice growth and all sites demonstrate the occurrence of needle ice growth. However, these 53 events did not display needle ice growth during favourable temperature conditions. Non-growth must be limited by an additional factor(s). Meentemeyer and Zippin (1981), Lawler (1989), Branson *et. al* (1996) and Matsuoka (1996) all suggest the importance of available soil moisture for needle ice growth. Hence, air, surface and ground temperature, in addition to soil moisture were compared between visually confirmed needle ice events and days displaying suggested appropriate environmental conditions for needle ice growth.

Table 5.19 and 5.20 show data from Site 1 and 2 over their full record period (Section 5.3) in addition to environmental averages of days showing needle ice and the days not showing needle ice growth.

Comparing needle ice growth days and non-growth days from Site 1 and Site 2, show that during non-growth days both Site 1 and 2 experience below zero surface or air temperatures. However, non-growth days had consistently less soil moisture. Average and maximum soil moisture levels at -2.5 and at -5cm are markedly lower for non-growth days than for needle ice growth days, especially at the -

5cm sensor. Site 1 shows on average 13.1% and Site 2 3.2% lower soil moisture at -5cm comparing needle ice growth days and non-growth days. The soil moisture limits of 15% presented by Branson *et al.* (1996) suggest conditions at -2.5cm during non-growth events from Site 1 and 2 to be within growth limits, however, both sites show soil moisture levels markedly below 15% at -5cm.

Screening of imagery from Site 3 provided no clear events where environmental conditions were favourable for needle ice growth, but growth was not observed.

Table 5.19. Environmental conditions during non-growth events from Site 1, compared to 24-hour data from needle ice events and long-term conditions

Site 1												
	Soil moisture		Temperature							Wind speed/Direction		
	%		°C							°	m/s	
	-2.5	-5,0	+30	+10	+0	-2.5	-5	-7.5	-10	Direction	Avg Wind	Peak Wind
	Needle ice growth event											
Minimum	16,1	6,3	-7,3	-7,2	**-2,9**	-2,7	-1,1	-0,5	-0,3	0,2	0,0	0,0
Average	22,6	19,3	4,6	4,5	**4,5**	0,4	0,4	0,5	0,6	249,4	3,4	6,7
Maximum	27,5	46,0	19,4	19,6	**32,0**	7,7	4,0	3,4	3,2	360,0	16,4	23,6
	Non-growth event											
Minimum	17,1	4.9	1,4	1,5	**-1,0**	-7,8	-5,7	-4,4	-3,4	0,2	0,0	0,0
Average	18,1	6,2	5,7	5,7	**3,2**	-1,7	-1,3	-1,0	-0,7	256,4	5,2	8,9
Maximum	19,0	7,8	16,8	16,1	**18,4**	0,9	-0,1	-0,1	0,1	360,0	18,4	29,7

Table 5.20. Environmental conditions during non-growth events from Site 2, compared to 24-hour data from needle ice events and long-term conditions

Site 2												
	Soil moisture		Temperature							Wind speed/Direction		
	%		°C							°	m/s	
	-2.5	-5,0	+30	+10	+0	-2.5	-5	-7.5	-10	Direction	Avg Wind	Peak Wind
	Needle ice growth event											
Minimum	12,8	-8,7	-6,8	-7,0	**-2,7**	-1,8	-0,6	0,0	0,9	0,1	0,0	0,0
Average	17,3	7,6	4,3	4,2	**2,8**	3,7	3,4	3,3	3,5	141,8	3,3	5,4
Maximum	25,9	25,9	15,6	15,8	**17,1**	16,4	13,4	11,6	9,3	360,0	11,4	16,1
	Non-growth event											
Minimum	14,1	3,4	1,1	1,0	**-1,0**					0,1	0,0	0,5
Average	14,8	4,4	5,5	5,4	**3,9**					144,0	3,4	5,6
Maximum	15,3	4,9	15,1	14,8	**14,6**					360,0	10,8	17,1

5.9 Single needle ice event analysis

A total of 82 unique needle ice events with 24-hour environmental and visual monitoring were captured and analysed within the study. To observe documented effects and properties of needle ice growth shown in section 5.4-5.8, a single event from each site was analysed in great detail. Events

which incorporated several of the identified characteristics of growth, decay, temperature spike and changes in cooling rate due to latent heat release were chosen. The aim was to focus on the dynamics of needle ice growth and decay, connected to environmental conditions, initiation depth and latent heat release in high detail, in an empirical example.

Environmental conditions were analysed in detail over 24 hours, between 12:00 and 12:00 the following day, in the following sections. Imagery is shown within the thesis, while videos of events are attached in digital form in Appendix B. Video 1, 2 and 3 and Figure 5.43 – 5.55 correspond to the detailed study that follows.

5.9.1 Site 1

At 12:00 on the 16th of November 2014, surface temperatures peaked at 23.2°C, while air temperatures were 10.2°C. During the following 3 hours and 30 minutes temperatures fluctuated between 21°C and 10°C at the surface and 9°C and 4°C for air until 15:40, when surface temperatures dropped markedly and air temperatures slowly decreased. At 16:55 air and surface temperature were the same and followed a similar decline. A sudden drop in air temperatures was seen at 18:15, subsequent sub-zero measurements were recorded at 18:30. The surface sensor had a less steep decline and displayed below 0°C temperatures at 20:40, coinciding with the onset of needle ice growth.

Air sensors showed stable temperatures at ca -4°C until 22.30 where fluctuations began during the night. Minimum air temperatures of -5.4°C were reached at 02:20. Surface temperatures followed a more constant cooling trend after 0°C, with isothermal conditions between 18:30 and 00:00, after which temperatures decrease slightly (Figure 5.62). Minimum surface temperatures of -2.9°C were reached at 04:50 (Figure 5.62).

A rapid air temperature increase from -5.6°C to 1.5°C was observed between 04:40 and 05:50, followed by a constant increase to 12.2°C at 12:00. Ground temperatures increased at a slower rate for the first hours of morning, until 06:40 when ground temperatures drastically increased, reaching 24.5°C at 12:00 (Figure 5.63).

Sub-surface temperatures were synchronous with the surface temperature, but showed decreasing amplitude with depth. Two points of inversion were seen during evening and morning. The inversion points occurred when deeper sensors displayed warmer conditions during night, and *vice versa*. The points of inversion occurred at 16:30, 17:00 and 18:30 during the evening, and at 08:30, 09:30 and 10:15 in the morning for the -2.5, -5 and -7.5cm sensors respectively. The -2.5cm sensor was the only ground sensor that recorded sub-zero temperatures, crossing below zero at 02:50, while the remaining three sensors never showed sub-zero temperatures.

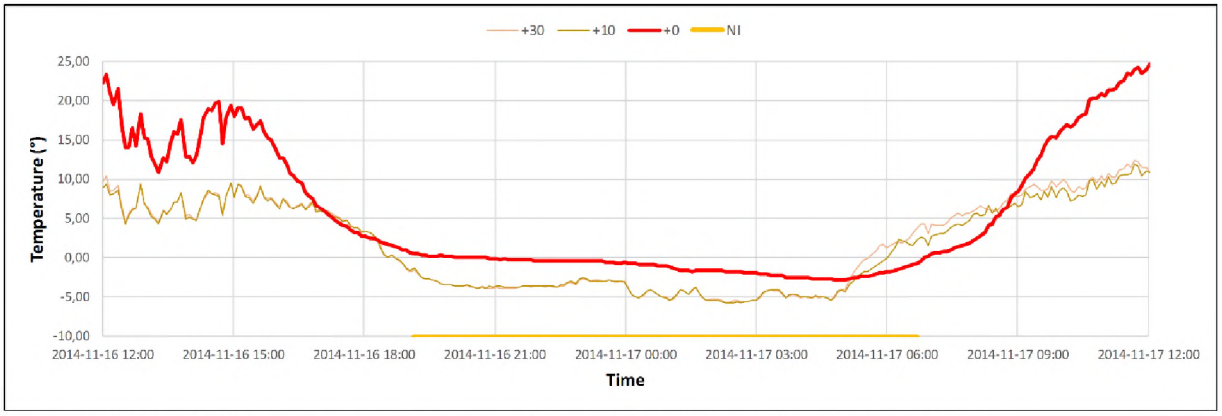

Figure 5.62. Air and surface temperature measurements from the 16th to the 17th of November 2014.

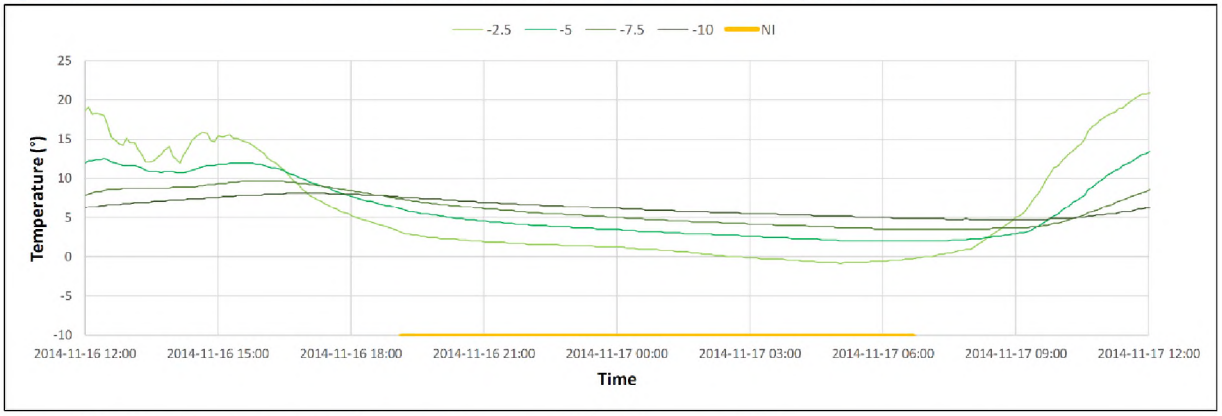

Figure 5.63. Ground measurements from the 16th to the 17th of November 2014

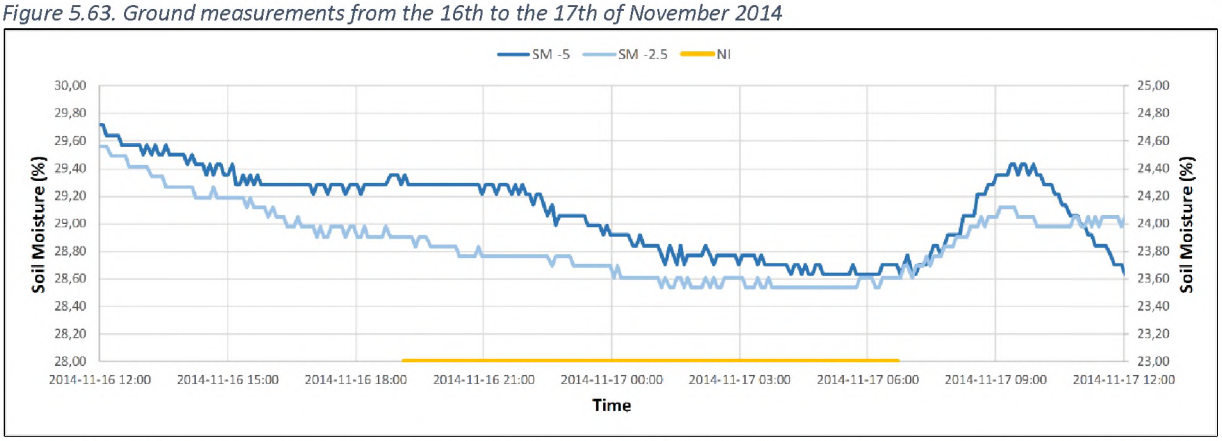

Figure 5.64. Soil moisture measurements from the 16th to the 17th of November 2014. Primary axis shows -5cm depth and secondary axis -2.5cm, note they are on a different scale.

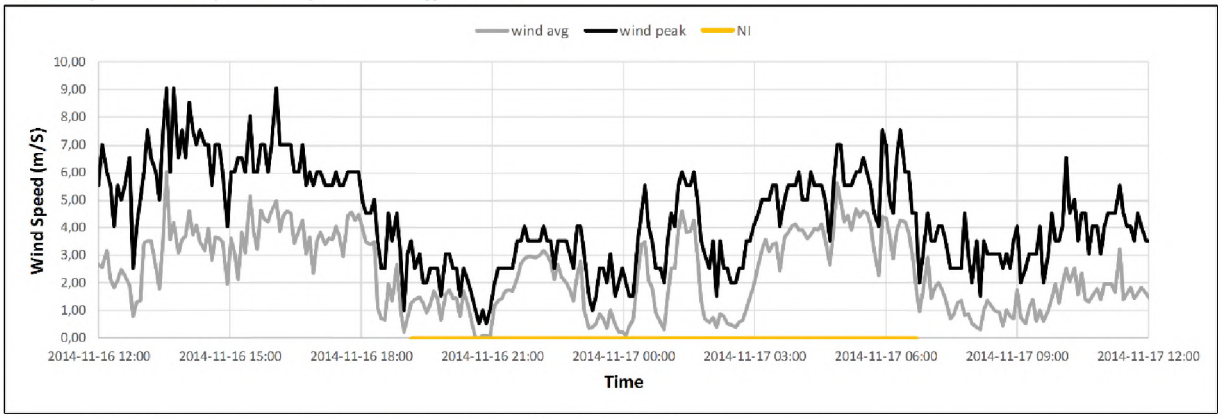

Figure 5.65. Wind measurements from Site 1 for the 16th and 17th of November 2014.

Soil moisture showed constant lowering during both day and night from both sensors. However, the -5cm sensors recorded, on average, 5.2% lower soil moisture than the -2.5cm sensor.

The -2.5cm soil moisture sensor displays a small increase in soil moisture lowering at 19:10 during needle ice initiation. Soil moisture at -5cm initiated decreased approximately two hours later. During melting, notable increases in soil moisture were measured at 05:40 for both soil moisture sensors. Maximum and minimum soil moisture readings measured 24.6% and 23.5% for the -2.5cm sensor and 29.7% and 28.6% for the -5cm sensor (Figure 5.64).

Wind average and peak speeds are displayed in Figure 5.45. Weak correlations exist (R^2<0.3) with other measured environmental (temperature and soil moisture) parameters and wind speed. Average wind direction was from the south east (140°) between the 16th and 17th of November 2014.

Needle ice initiation was observed at 19:10, followed by a constant growing until 06:40, when the start of decay was noted. No more resettling was evident after 11:10. Material was seen to heave by several centimetres and sediment was observably reworked. Heaving and sediment movement are the focus of the following chapter. Ice crystals were seen to heave soil and rocks, but additionally vegetation was influenced by heave. Fringes of the vegetation patch located roughly in the centre of the pictures in Figure 5.46, were, like the surface clasts, seen to be heavily influenced by heaving. No needle ice was observable at the surface but individual aggregates lifted on the lower left side suggest relatively shallow needle ice growth.

Rates of temperature decline and increase were seen to influence needle ice growth. Surface temperatures were drastically lower during the evening of the 16thNovember, while the rate of decrease of surface and ground temperatures was observed to be markedly slower reaching sub-zero conditions at 18:30. Air temperature increased rapidly after sunrise, while a lag in surface temperature increase until 06:40, when the rate of surface warming increased. At ca 09:00 the absorption of radiation at the surface warmed the ground surface to higher temperatures than the ambient air.

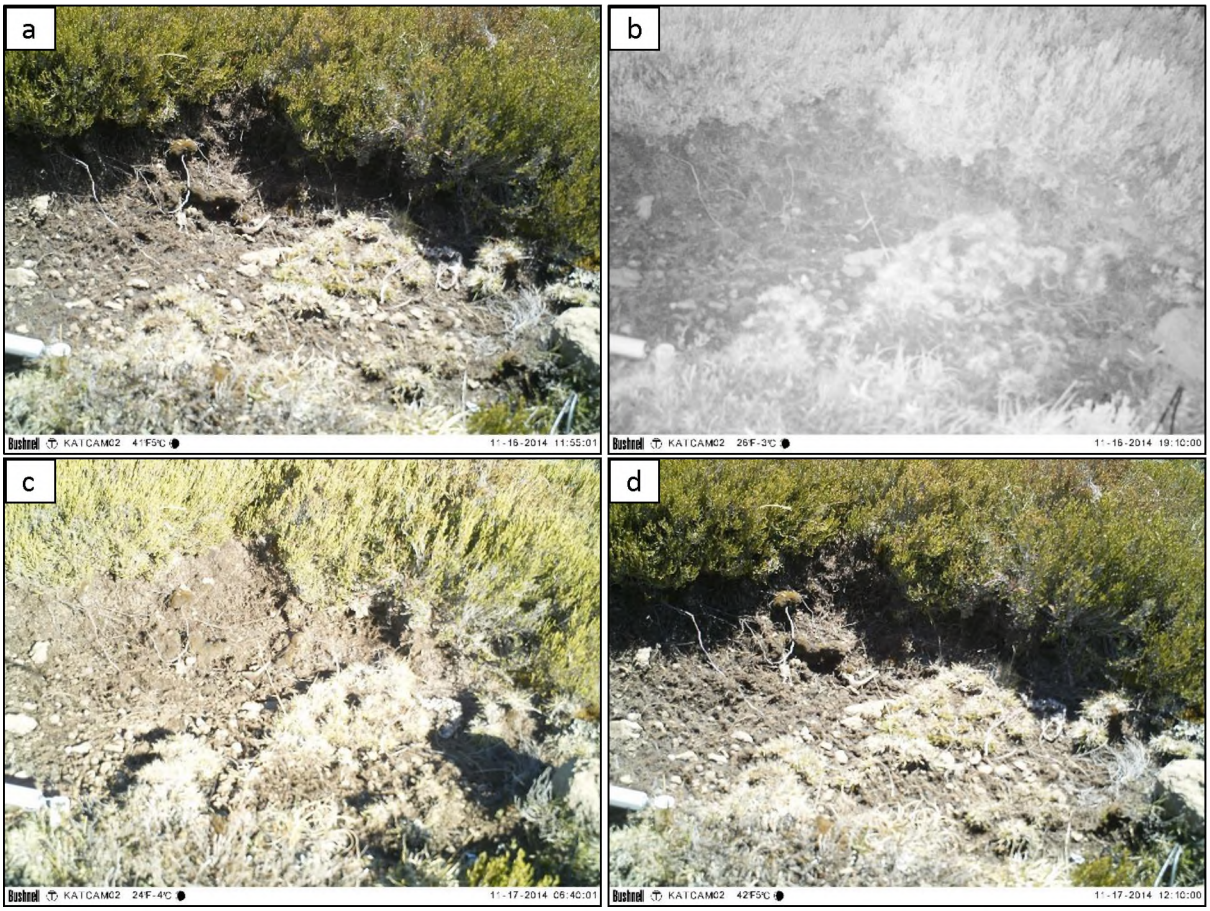

Figure 5.66. Phases of needle ice growth from November 16-17 at Site 1. Pre-growth (a), initiation of growth (b), initiation of decay (c) and final melt (d). The event is seen in Video 1.

5.9.2 Site 2

Due to prolonged melt noted from the event studied on the April 17 to April 18 2015 at Site 2, 24h monitoring was extended to 28h. Surface temperatures reached 3.6°C at 12:00 on the 17th, while air temperatures were constant at ca 2°C higher. Afternoon surface temperatures peaked at 9.0°C at 14:55 with air temperatures ca 2°C cooler. A steady decline in both air and surface temperatures was recorded between 14:55 and 16:50, when both declined drastically. Air temperatures dropped from 5.3°C to 0°C in 25min, crossing the zero-degree boundary at 17:25 and 17:35 for the +30 and +10cm sensors respectively, while surface temperature dropped below 0°C at 18:00. Surface temperatures rose by ca 0.5°C for 10 minutes after crossing the 0°C boundary and subsequently continued declining. Air temperatures fluctuated between a minimum of -4.0°C at 19:10 and -0.2°C during the night, and positive temperatures ensued at 07:45 and 08:00 for the +30cm and +10cm sensors. Negative surface temperatures followed at 18:55, steadily declining until 06:40, where a minimum of -2.3°C was recorded. Surface temperatures increase moderately between 06:40 and 11:05, after which a more notable increase in temperature occurred. Positive surface temperatures were recorded at 11:10 reaching 4.7°C at 12:00 (Figure 5.67). Soil moisture initially increased from 15.3% to 19.2% at -2.5cm depth and from 1.0% to 11.8% at -5cm between 12:00 and 14:30. Thereafter both sensors recorded a

decrease in soil moisture levels until 10:30 on the 18th April. The temperature at -5cm then decreased at a higher rate, from 13.5% to -2.2%, compared to 19.2% to 13.3% at -2.5cm depth during the night. Subsequently, at 11:55 and 12:45 respectively, the soil moisture at the -2.5 and -5cm temperature dropped markedly. The -2.5cm temperature dropped by 0.8% while at -5cm it dropped by 5.9%. Following the reduction, soil moisture levels rapidly increased and stayed stable until 18:00 (Figure 5.68).

Ground temperatures followed a similar trend to the surface temperatures; however, the amplitude of the change was diminished with increasing depth of the sensor. Similar to Site 1, two inversions can be noted at ca 17:30 and 10:15, all four sensors inverted within 10 minutes. The -2.5 and -5cm sensor showed a similar increase in temperatures to that of the surface sensors after reaching zero. The -2.5 and -5cm temperatures were below zero during the night, while sub-zero conditions never reached to the -7.5 and -10 sensors. Spikes in temperature, related to latent heat release were observable in both surface and sub-surface temperature sensors. An increase in temperature was recorded prior to 18:00 at the +0, -2.5, -5 and -7.5cm sensors and subsequent cooling rates were seen to attenuate (Figure 5.69).

Figure 5.49 shows wind speed averages and peaks over the high-frequency study from Site 2. Wind speeds and soil moisture showed a moderate negative correlation (R^2=-0.64 and -0.63) with the -2.5 and -5cm sensors. Hence, increased wind speeds showed moderate correlation to lowering of the soil moisture of Site 2 during the studied event.

The initial observations at Site 2 (Figure 5.71a) on the 17th of April 2015, showed that melting from the previous night's needle ice event was still in progress. No more melting from this previous event could be identified after 16:25. The first heaving from needle ice growth was noted at 18:25. Needle ice growth was continuous until 09:25, with initial melt observed 30 minutes later. Melting from Site 2 on the 18th did not terminate until 17:55.

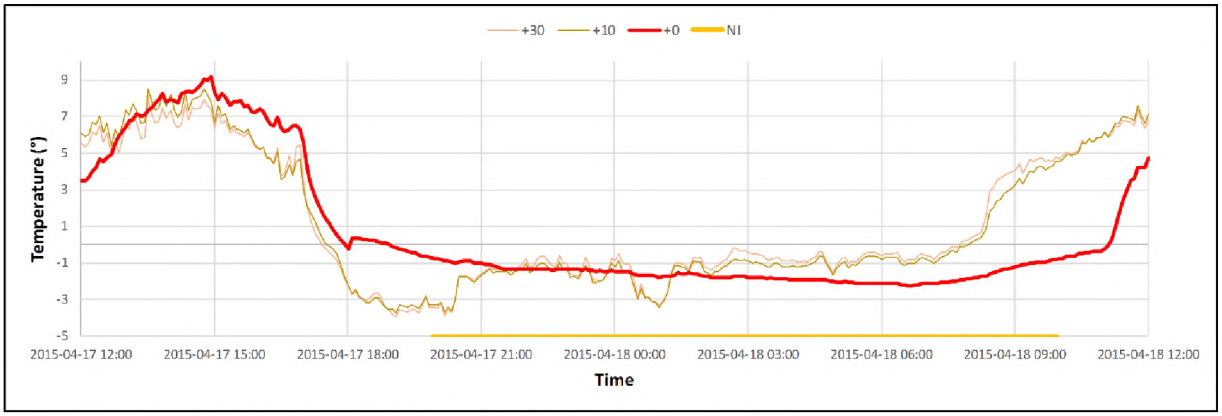

Figure 5.67. Air and surface measurements from the 17th to the 18th of April 2015.

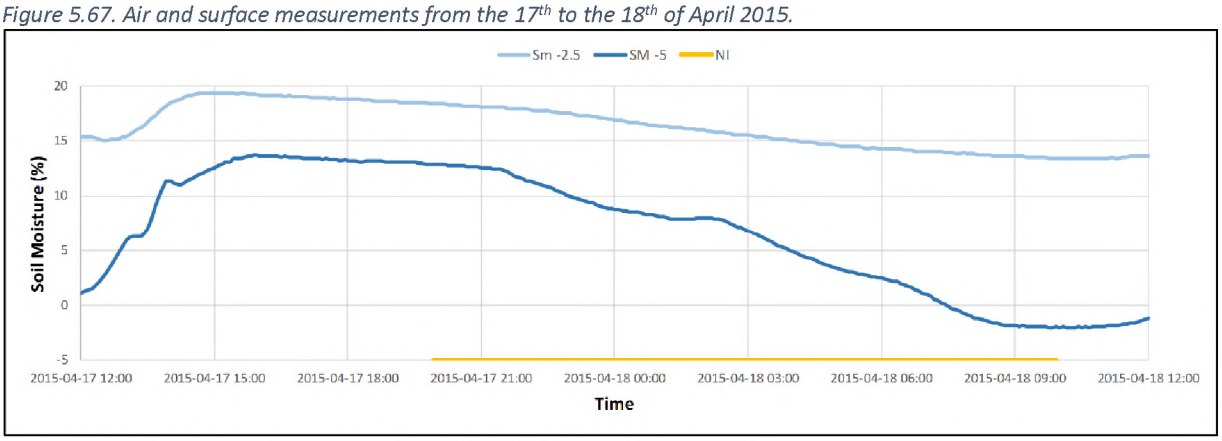

Figure 5.68. Soil moisture measurements from the 17th to the 18th of April 2015

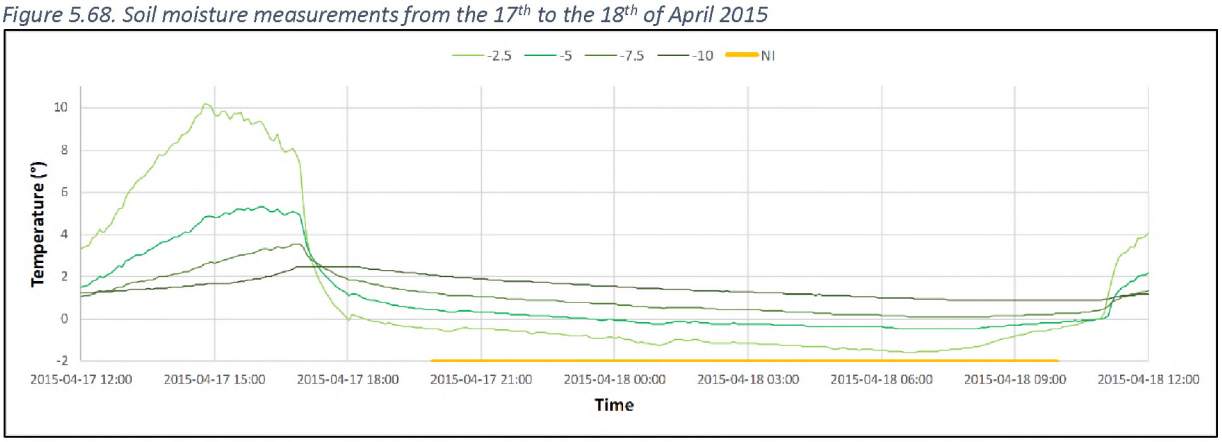

Figure 5.69. Ground measurements from the 17th to the 18th of April 2015.

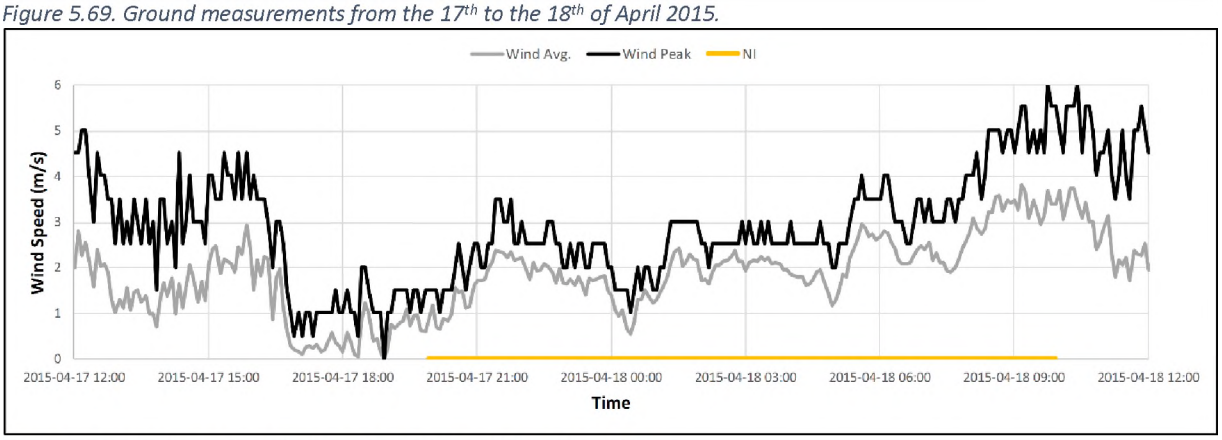

Figure 5.70. Wind speed at Site 2 for the 17th and 18th of April 2015.

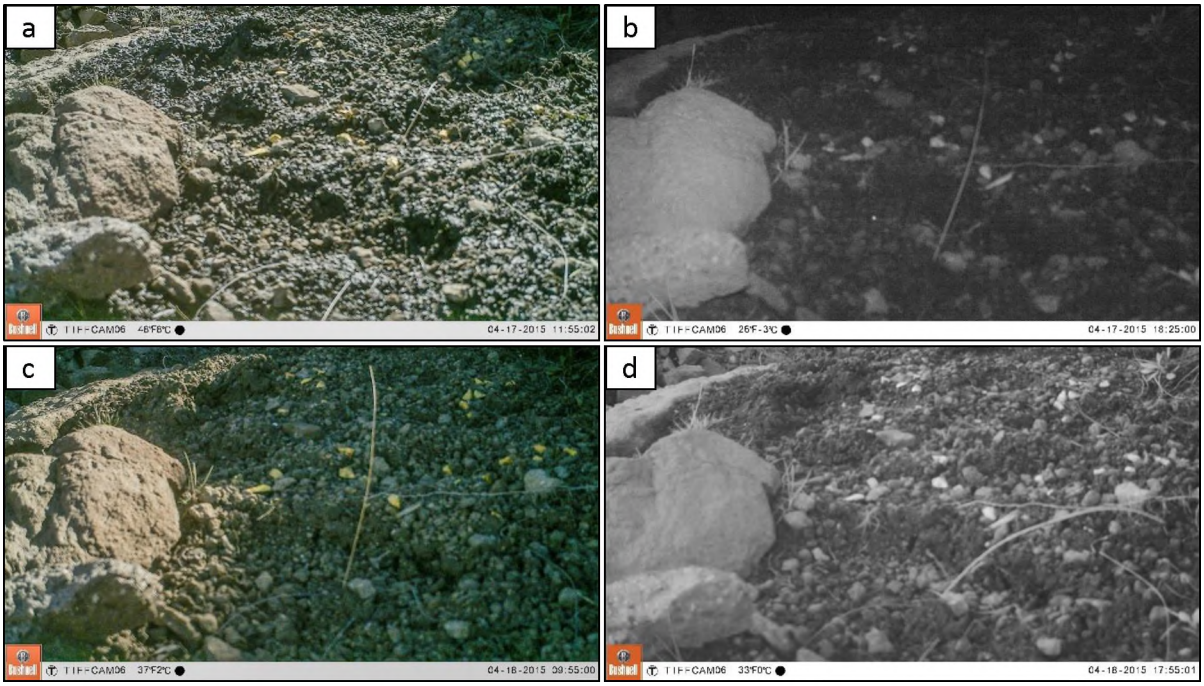

Figure 5.71. Phases of needle ice growth from April 17-18 at Site 2. Pre-growth (a) (with previous night´s needle ice not melted out), initiation of growth (b), initiation of decay (c) and final melt (d) (later than 12:00). The events are seen in Video 2.

Similar to Site 1, surface material was seen to be markedly reworked with even a large stone, seen in the lower left side of pictures in Figure 5.71, measuring over 30 x 25 x 15 cm, distinctly heaving and resettling (Video 2). No needle ice was observed at surface of Site 2 in Video 2 but movement of individual clasts in the centre of the study site suggests support of individual ice needles close to the surface.

5.9.3 Site 3

At 12:00 on the 14th June 2014, surface and air temperatures were 7.1°C and 3.5°C respectively. Subsequently, at 13:00, air, ground and surface temperatures declined until sub-zero values were reached at 14:30 for the air sensor and at 15:00 at the ground surface. Air temperatures fluctuated during the night, and after 20:00 showed mostly positive values until 06:15, when two periods in the early morning displayed negative air temperatures. Surface temperatures remained below zero throughout the night, with positive temperatures first recorded at 09:30 the morning of the 15th. A sudden increase in air and surface temperatures was seen at 05:10, followed by a similarly sudden decrease in temperatures at 06:00. Minimum air temperatures of -1.5°C were reached at 06:20, while a surface minimum of -3.3°C was recorded at 06:40. Temperatures increased in both the air and ground from 06:40, with surface temperatures steadily rising, while air readings fluctuated more. Surface and air maxima was reached at 11:40 with values of 5.3°C and 2.7°C respectively (Figure 5.72).

Soil moisture at 12:00 was 3.8% and 11.1% at -2.5 and -5cm respectively. Both sensors showed constantly declining soil moisture levels from 12:00 to 10:40 the following morning. However, an

increase at 17:10 in conjunction with initiation of needle ice growth, is seen at both -2.5 and -5cm. Subsequently, at 19:30, the rate of soil moisture decline decreases and lowers constantly at -5cm while the -2.5cm sensor displays increased lowering at 01:10. The soil moisture at -2.5cm dropped from 3.8% to -2% and the -5cm from 11.1% to 0.6% during the event. A slight increase in soil moisture levels were recorded between 10:40 and 12:00 from both sensors (Figure 5.73).

Ground temperatures at Site 3 showed very similar trends to the surface sensor, but with amplitudes decreasing with increasing depth. An inversion in ground temperatures occurred at 14:40, with all sensors inverting within 10 minutes of each other. Sub-zero temperatures were seen at all ground sensors after 23:10, and all, but the -2.5cm sensor, stay below zero for the remainder of the study period. The -2.5cm sensor shows positive readings at 10:50 on the 15th June. Isothermal conditions are seen in ground temperature data from the -7.5 and -10cm sensors after 22:00, while the -2.5 and -5cm sensors display non-changing temperatures from 16:00 till 18:00, when temperature decline recommences (Figure 5.74).

Wind speeds averaged 1.5 m/s between the 14th and 15th June, with average gusts of 3.9 m/s. Correlation between wind speeds and moisture from the -2.5 and -5cm sensor showed a strong correlation of R^2-values of 0.89 and 0.88 respectively.

Needle ice initiated at 17:10 and continuous growth was seen until 06:30. Melting commenced at 09:20 and persisted for 4:40 hours, until no more resettling was noted at 14:00.

Noteworthy observations from Site 3 during needle ice growth were the preferential growth ridges located in the fore- and background of the imagery. Only readily distinguishable in an animated video (Video 3) (Figure 5.77). Preferential growth patterns will be further analysed in Chapter 6 and discussed in Chapter 7. Figure 5.75 shows wind speed averages and peaks over the high-frequency study from Site 3. Wind speeds and soil moisture showed a strong positive correlation (R^2=0.89 and 0.88) with the -2.5 and -5cm moisture contents. Hence, increased wind speeds strongly correlated to an increase in soil moisture of Site 3 during the studied event. Only heaving and resettling of surface material as seen in Video 3 suggests deeper needle ice initiation.

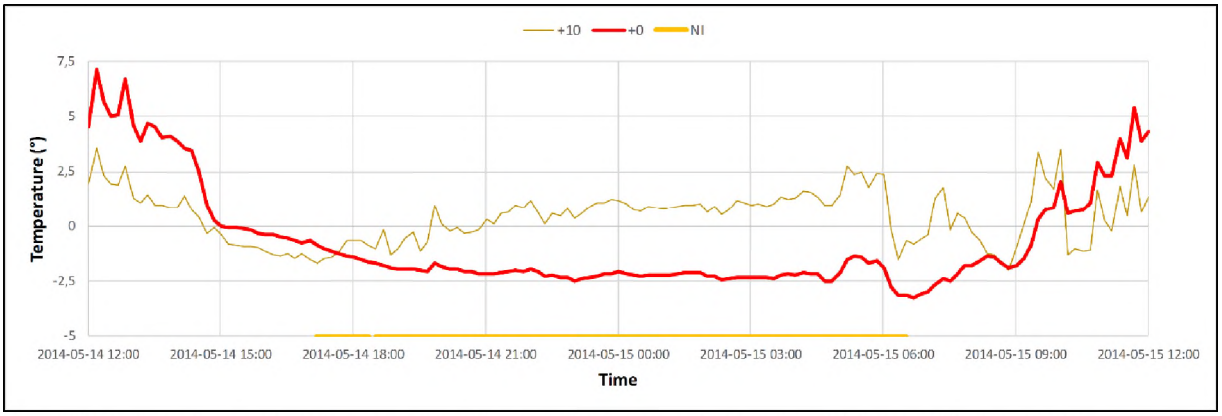

Figure 5.72. Air, surface and soil moisture (secondary axel) measurements from the 14th to the 15th of June 2014.

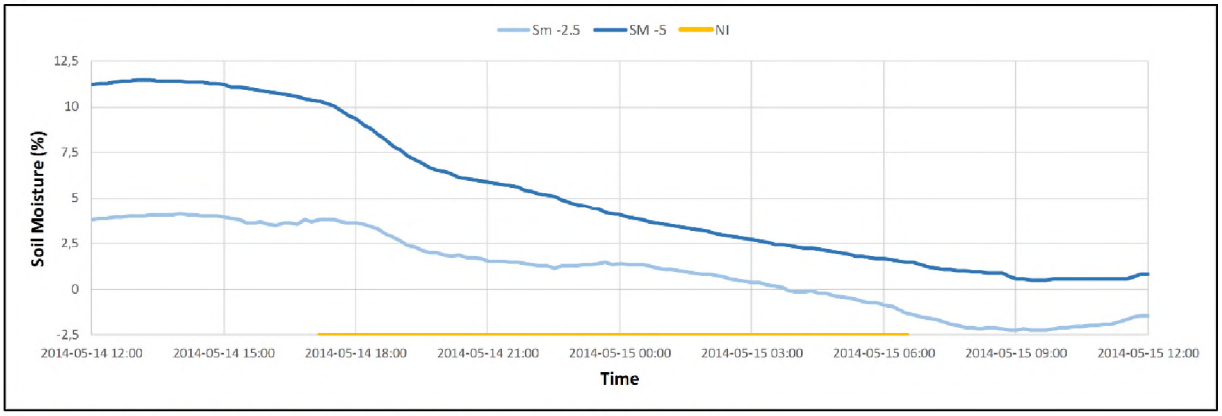

Figure 5.73. Soil moisture measurements from the14th to the 15th of June 2014.

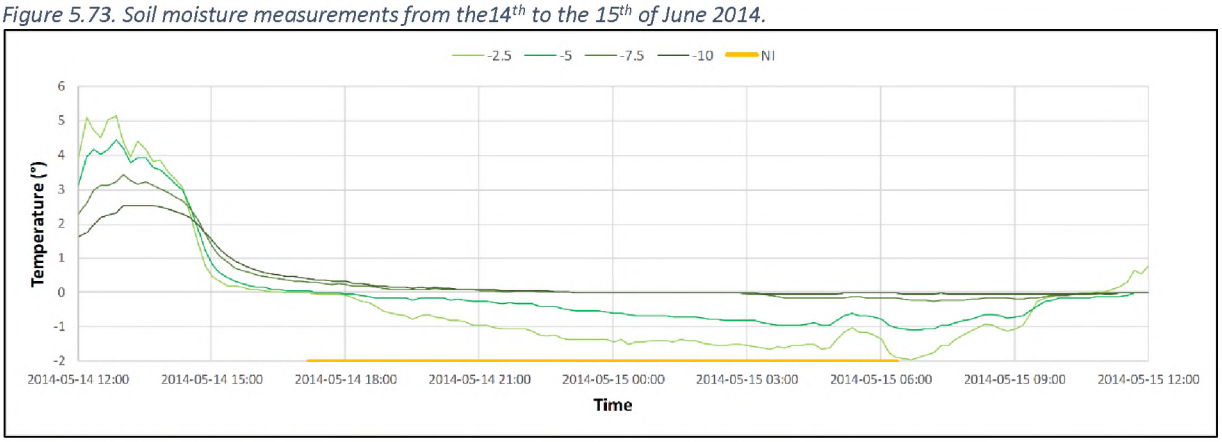

Figure 5.74. Ground temperature measurements from the 14th to the 15th of June 2014.

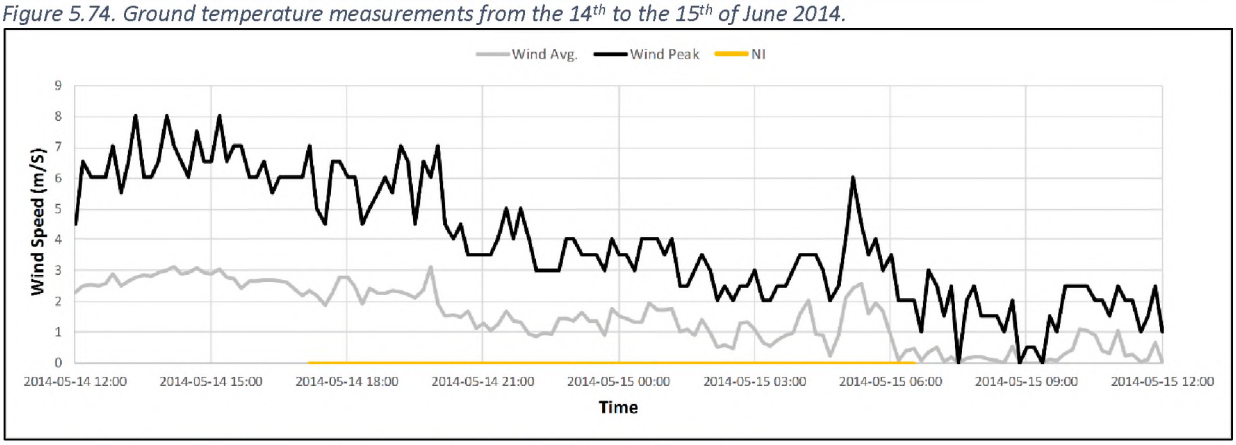

Figure 5.75. Wind measurements from Site 3 for the 14th and 15th of June 2014.

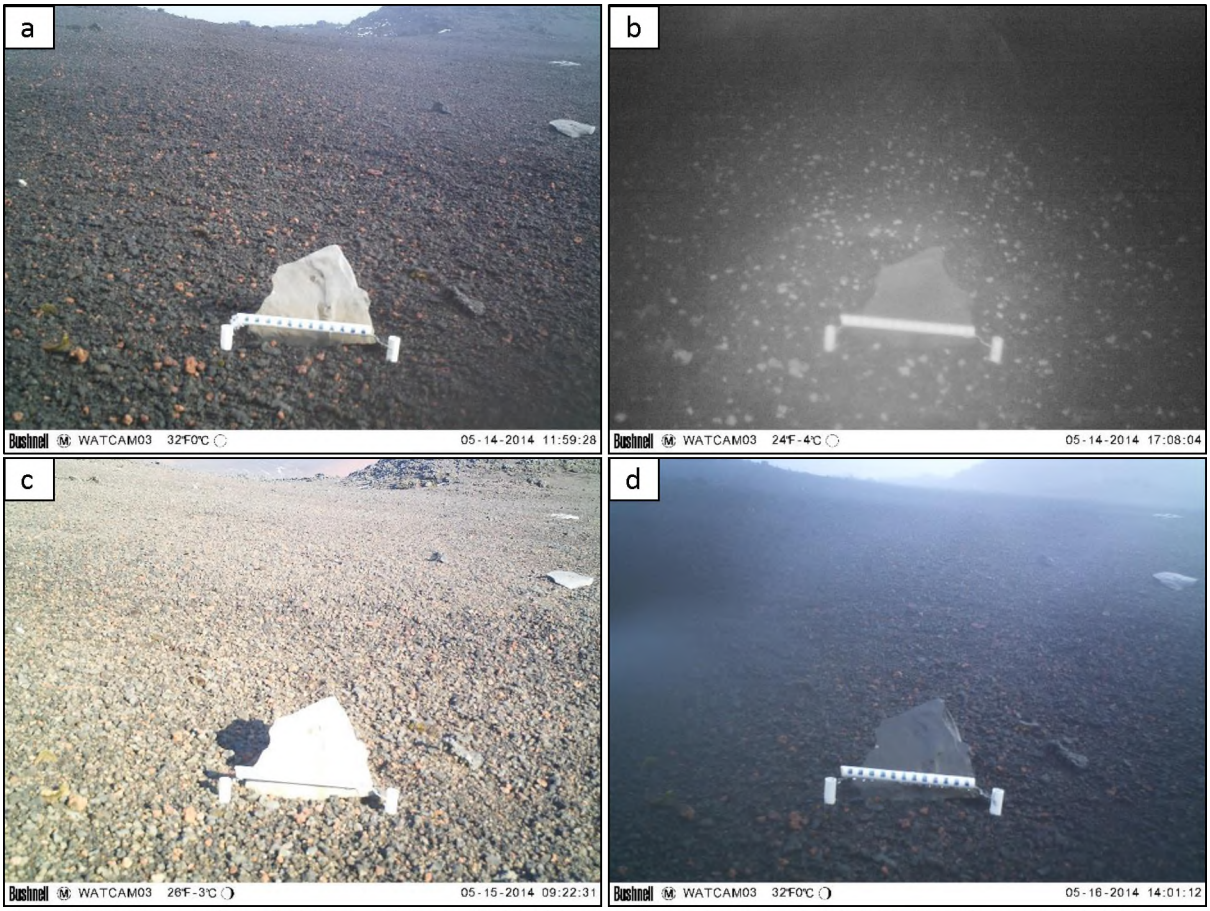

Figure 5.76. Phases of needle ice growth from 15-16 of June at Site 3. Pre-growth (a), initiation of growth (b), initiation of decay (c) and final melt (d) (later than 12:00). The event is seen in Video 3.

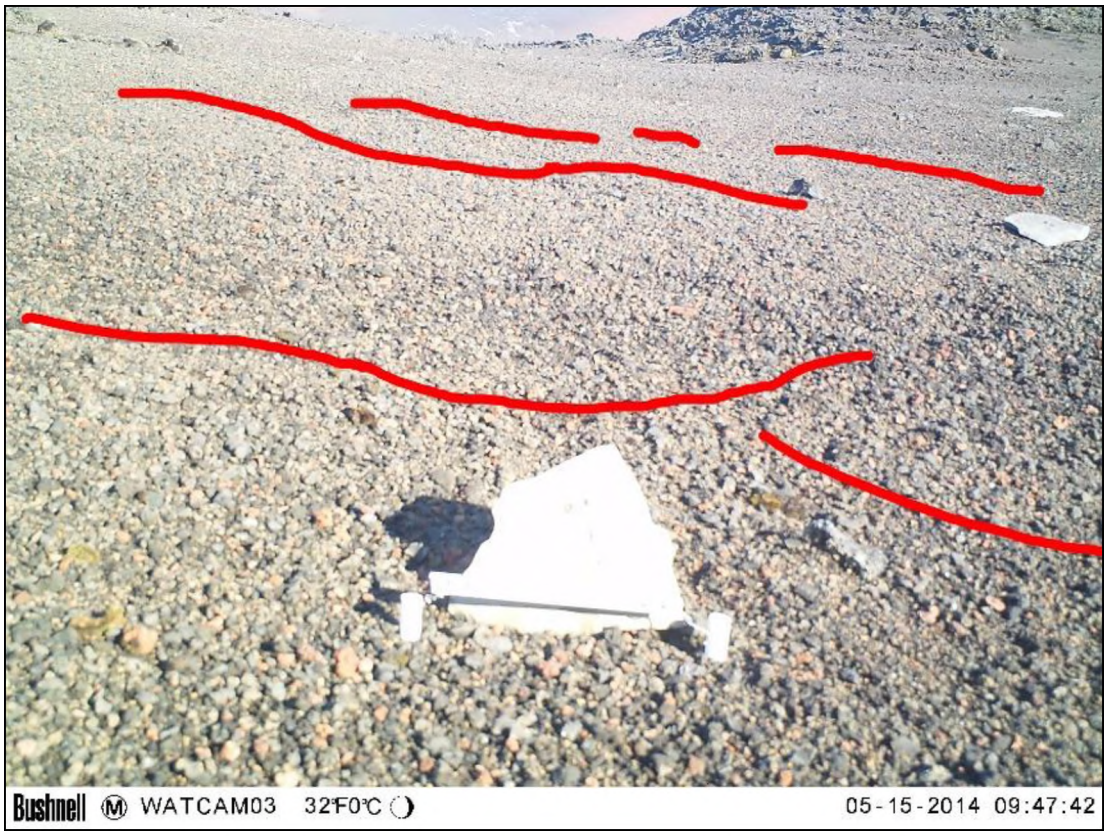

Figure 5.77. Preferential growth patterns of needle ice seen both during growing and decaying of needle ice.

Chapter 6 – Results: Transport and mechanisms of sediment movement

Chapters 1 and 2 outline the need for additional observations of mechanisms involved in sediment movement by needle ice. The following chapter presents results from imagery and video clips of needle ice heaving and transporting sediment, identified from the three study sites. The aim was to identify and classify sediment movement based on camera imagery. In addition, single particle displacement by each mechanism and total movement by needle ice and non-needle ice events over the 12-month study will be presented. Methods on how particle displacement and spatial changes were measured are described in section 4.3.3.

In addition to the analysis of needle ice as a transport process, other factors inducing surface displacement were also analysed. Section 6.4 and 6.5 focus on non-needle ice displacement as well as how to differentiate between the two.

6.1 Needle ice event videos

Five needle ice events from each study site are presented in the following sub-sections. Events have attached video files displaying sediment movement as well as images tracing particle movement by trajectory and movement distance. Image analysis displayed movement trajectory for select particles as well as local slope and suggested differences in soil moisture impacting needle ice sediment displacement. Additionally, results from spatial variability analysis of needle ice growth on the surface of the study sites will be presented.

Fifteen videos showing NISD were selected from the 82 captured events, with the purpose of presenting events showing little, moderate, and extensive needle ice heave from each site. Selected events provide an overview of needle ice event variability, portraying different properties of NISD. Hence, events showing small, moderate and extensive needle ice growth were purposefully chosen. Small events were classified as having vertical heave of less than 0.5cm, and are visible in Video 4, 12 and 16 from Site 1, 2 and 3 respectively. Events that showed moderate heave of 0.5 to 1.5cm are displayed in Video 5, 6, 7, 9, 13, 14, 15 and 18. The events which displayed the most heave from each site are seen in Video 8, 9, 10, 11 and 17, showing heave of 3, 3.5 and 3cm from Site 1, 2 and 3. Needle ice events are analysed in ascending order based on corresponding video with date and environmental parameters presented in Table 6.1, 6.2 and 6.3. Video 4-8 show events from Site 1, Video 9-13 show events from Site 2 and Video 14-18 show events from Site 3.

The following sections display analysis of these 15 videos focusing on environmental conditions, intra-site heave variability and movement relating to particle size of NISD.

6.1.1 Environmental details of needle ice videos

Table 6.1, 6.2 and 6.3 show environmental data for the 15 selected events in a similar layout as data from needle ice events seen in section 5.1.4 and 5.3. Data is presented as averages over 24 hours, 12h prior to, and 12h after midnight on the night of the needle ice growth event. For some needle ice events the air temperature sensor did not function, so for analysis of events 4 and 5, the built-in camera temperature sensor was used as a proxy for air temperature.

Table 6.1. Environmental details for the five needle ice events from Site 1 covered in Video 4-8

Environmental data for Video 4-8													
Event	Date	Soil moisture		Temperature							Wind speed/Direction		
		%		°C							°	m/s	
		-2.5	-5,0	+30	+10	+0	-2.5	-5	-7.5	-10	Direction	Avg Wind	Peak Wind
		Max											
4	2014-07-02		7,9				0,0	0,0	-0,1	-0,1	360,0	9,8	12,1
5	2014-08-22		23,3				0,7	0,5	0,4	0,1	353,3	10,9	16,1
6	2014-11-16	24,9	30,7	10,9	10,8	**23,3**	19,2	14,8	11,9	10,0	360,0	16,4	22,1
7	2014-11-18	24,1	28,7	15,7	14,8	**26,9**	22,4	16,3	12,2	9,5	290,6	7,8	10,6
8	2015-04-17	23,3		7,6	7,5	**13,9**							
		Average											
4	2014-07-02		7,9				-0,2	-0,1	-0,1	-0,1	287,0	1,0	3,5
5	2014-08-22		22,7				-0,3	0,1	0,2	0,1	263,5	6,4	10,5
6	2014-11-16	24,3	30,0	1,5	1,3	**5,0**	5,5	6,3	6,8	7,3	257,2	5,7	9,8
7	2014-11-18	23,4	28,2	5,2	5,1	**8,6**	8,5	8,0	7,6	7,2	190,2	3,6	5,7
8	2015-04-17	22,5		-1,1	-1,2	**1,7**							
		Min											
4	2014-07-02		6,3				-1,3	-0,7	-0,4	-0,2	0,2	0,0	0,0
5	2014-08-22		22,1				-1,2	-0,1	0,1	0,1	210,8	1,7	3,5
6	2014-11-16	24,0	29,4	-5,5	-5,5	**-2,5**	-0,5	2,2	3,8	5,1	13,5	0,3	2,0
7	2014-11-18	23,0	27,6	-0,5	-0,6	**0,0**	1,2	2,9	4,2	5,4	50,9	0,0	0,0
8	2015-04-17	21,9		-7,3	-7,2	**-1,8**							

Environmental data showed that for all needle ice events, minimum temperatures at +0cm were at or below 0°C. However, temperatures in air and ground vary markedly during the study period. Soil moisture levels during the captured events range from a maximum of 25.9% to -8.3%. Measurements from Video 12, 13 and 18 show minimum negative soil moisture values from the -5cm sensor. The average soil moisture from the events depicted in Video 12, 13 and 18 show only the deep sensor displaying negative values. Due to Camera 3 at Site 3 losing its internal “time-stamp”, in-picture dates seen in Video 16, 17 and 18 are incorrect, correct dates are presented in Table 6.3.

Table 6.2. Environmental details for the five needle ice events from Site 2 covered in Video 9-13

Environmental data for Video 9-13													
Event	Date	Soil moisture		Temperature							Wind speed/Direction		
		%		°C							°	m/s	
		-2.5	-5,0	+30	+10	+0	-2.5	-5	-7.5	-10	Direction	Avg Wind	Peak Wind
		Max											
9	2015-04-10	25,9	24,5	14,5	14,9	**17,1**	16,4	13,4	11,6	9,3	360,0	4,0	5,0
10	2015-04-12	25,4	24,1	14,8	15,2	**18,2**	17,1	13,5	11,6	9,3	360,0	3,5	6,0
11	2015-04-16	24,6	23,5	8,3	8,7	**9,5**	9,3	7,5	6,5	5,6	199,6	5,9	10,1
12	2015-04-22	16,1	4,1	11,8	12,3	**12,4**					338,2	7,5	12,1
13	2015-05-07	14,8	3,2	14,4	14,4	**17,0**					340,7	3,5	6,0
		Average											
9	2015-04-10	25,4	23,9	6,7	6,5	**4,9**	5,2	5,0	5,1	5,3	178,5	1,8	2,8
10	2015-04-12	25,1	23,6	7,2	7,2	**5,8**	5,9	5,7	5,7	5,7	121,1	1,2	2,4
11	2015-04-16	24,2	22,7	5,5	5,4	**4,3**	4,7	4,9	5,2	5,6	124,8	3,7	6,3
12	2015-04-22	15,4	2,8	6,7	6,6	**3,2**					125,8	3,9	6,6
13	2015-05-07	14,4	0,4	4,7	4,5	**3,3**					190,7	1,6	2,8
		Min											
9	2015-04-10	24,9	23,1	1,0	0,9	**-0,1**	0,6	1,4	2,0	2,9	0,1	0,0	0,0
10	2015-04-12	24,9	23,3	2,5	2,0	**-0,2**	0,4	1,3	2,1	3,3	0,1	0,0	0,0
11	2015-04-16	19,8	17,0	-1,8	-1,9	**-0,7**	-0,3	0,3	0,9	1,8	11,3	2,2	4,5
12	2015-04-22	14,0	-8,3	3,4	3,2	**0,0**					47,6	0,8	1,5
13	2015-05-07	14,1	-5,7	-0,7	-1,7	**-2,2**					9,8	0,0	0,0

Table 6.3. Environmental details for the five needle ice events from Site 3 covered in Video 14-18

Environmental data for Video 14-18												
Event	Date	Soil moisture		Temperature						Wind speed/Direction		
		%		°C						°	m/s	
		-2.5	-5,0	+10	+0	-2.5	-5	-7.5	-10	Direction	Avg Wind	Peak Wind
		Max										
14	2014-04-27	13,7	20,3	0,6	6,2	**4,9**	4,2	3,4	3,0	339,5	7,7	18,1
15	2014-05-15	4,1	11,5	3,6	7,2	**5,1**	4,4	3,5	2,6	356,3	3,1	8,0
16	2015-03-14			8,9	8,3	**16,9**	15,4	13,8	13,1	6,4		
17	2015-03-30			10,0	5,5	**5,8**	5,9	5,9	6,0	2,9		
18	2015-04-11			2,8	10,4	**11,6**	11,5	11,1	10,8	5,2		
		Average										
14	2014-04-27	8,0	11,5	-2,1	-0,5	**0,3**	0,5	0,8	0,8	223,8	3,7	8,7
15	2014-05-15	1,1	5,2	0,4	-0,6	**-0,3**	0,1	0,4	0,4	191,9	1,5	3,9
16	2015-03-14		8,0	1,8	2,9	**2,8**	2,5	2,8	3,0			
17	2015-03-30		7,2	1,7	1,9	**1,9**	1,8	2,0	2,0			
18	2015-04-11		0,6	1,7	2,2	**2,0**	1,8	1,6	1,4			
		Min										
14	2014-04-27	3,1	5,7	-3,9	-3,0	**-1,1**	-0,5	0,0	0,0	4,6	1,5	4,5
15	2014-05-15	-2,3	0,5	-2,0	-3,3	**-2,0**	-1,1	-0,3	-0,1	0,2	0,0	0,0
16	2015-03-14		7,2	-1,1	-2,1	**-1,4**	-0,8	-0,2	-0,2			
17	2015-03-30		5,1	-1,7	-2,2	**-2,0**	-1,8	-1,2	-0,8			
18	2015-04-11		-1,3	-1,4	-2,2	**-2,2**	-2,2	-2,0	-1,8			

6.1.2 Intra-site needle ice heave variability

Analysis of the 82 needle ice events showed that height and spatial distribution of needle ice is not constant within each site. The five events selected from each site were analysed for observed needle ice heave and spatial variability. Events in Video 4-18 were visually examined with the aim of providing average needle ice height classes (methods described in Section 4.3.3) over the whole study site. The three classes are defined as: heave less than 0.5cm, heave of 0.5 to 1.5cm, and heave greater than 1.5cm. These classes were used to display intra-site heave variability in Figure 6.1, 6.2 and 6.3 using overlays of 50% transparency. This means that increasing opaqueness in the overlays is a measure of increased frequency of needle ice growth at those locations. The position of the transition between classes was vague in the imagery, and, therefore, difficult to display accurately. The superimposed needle ice classes seen in Figure 6.1, 6.2 and 6.3 display areas of intra-site variability in needle ice growth height within the three study sites, based on the five documented needle ice events from each site. Intra-site heave variability is presented and described in the following section.

6.1.2.1 Intra-site heave variability of Site 1

Figure 6.1 shows needle ice growth to be more frequent in a band across the middle of the study area at Site 1. Similarly, heave was recorded to be greater in the same area. The most frequent and the tallest ice needles were produced in the middle to lower left portion of the study site, seen as opaque in Figure 6.1, which housed the largest portion of the above 1.5cm heave class (x in Figure 6.1). Ice needle distribution was homogenous across the central surface of the site.

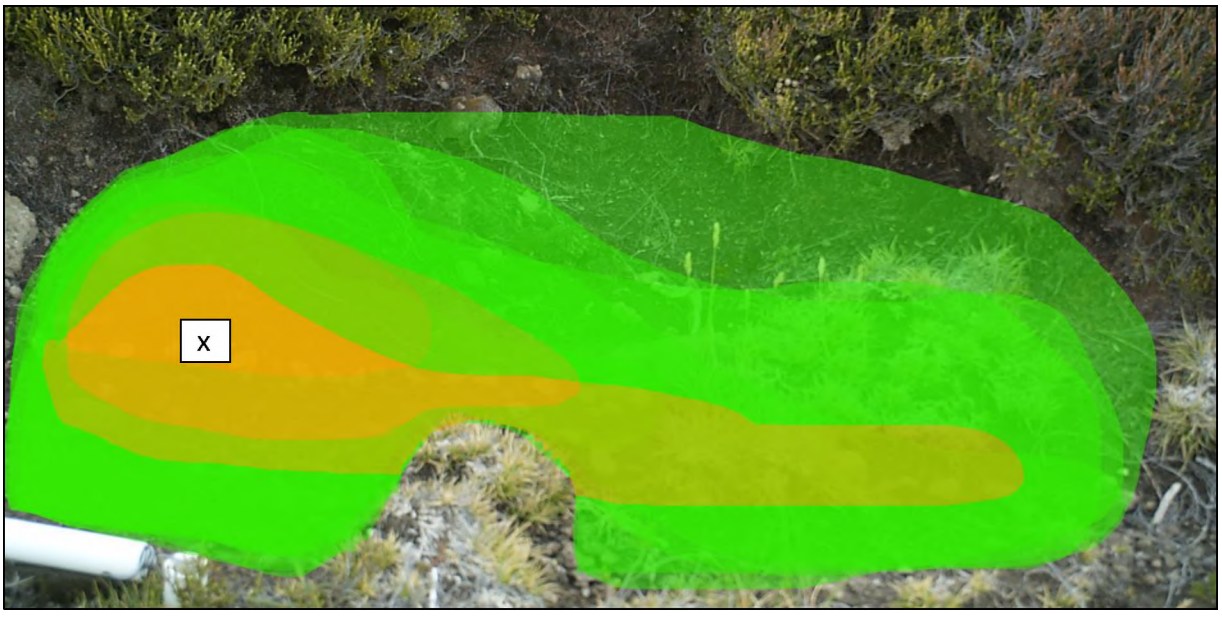

Figure 6.1.Composite needle ice activity on Site 1, based on five events (see Table 6.1). Green and orange areas display ice needle height of 0.5-1.5cm and over 1.5cm respectively. The area of most frequent and tall heaving is located at (x).

6.1.2.2 Intra-site variability of Site 2

Site 2 displayed more discontinuous needle ice growth. Low-intensity events were less homogenously influence by needle ice, producing patches of needle ice growth, while the general area was unaffected by heave. Similarly, the same areas that displayed localized heaving, coincided with areas showing increased needle ice heights during events where the general area was covered by shorter ice needles.

Two areas displayed especially active needle ice growth and were located in the middle of the study site (marked by x and y in Figure 6.2). Video 10 and 11 from Site 2 show tall ice needles (>2cm) covering the whole study area.

6.1.2.3 Intra-site variability of Site 3

Site 3 showed discontinuous patches of needle ice growth. The patches were elongated downslope to the right in Figure 6.3 (x, y and z), aligned with one of the two slope gradients presented in Section 3.3.2. Taller ice needles were seen in discontinuous patches in the general study area. The area surrounding Site 3, was observed to be influenced in a similar manner, though only one patch could be identified to heave in the background of Figure 6.3 (q).

Figures 6.1, 6.2 and 6.3 show ice needle heave heights were not consistent over the study site. Needle ice growth is shown to occur first at preferential locations within each study site during less suitable environmental conditions for needle ice development. Under such conditions, a high degree of intra-site spatial variability in growth is seen. During optimal conditions for needle ice with growth covering the general area, locations with preferential needle ice growth developed taller ice needles. The environmental characteristics of intra-site locations with preferential needle ice growth will be discussed in section 6.3. Areas prone to needle ice growth were seen to produce needle ice, when no needle ice was recorded in the sounding area, and produced taller ice needles. Areas that showed more intense needle ice growth were located on morphologically distinct surface topography, such as in depressions or on increased slope angles, this will be further analysed on in Section 6.3. The following section presents results on sediment displacement and its relations to particle size.

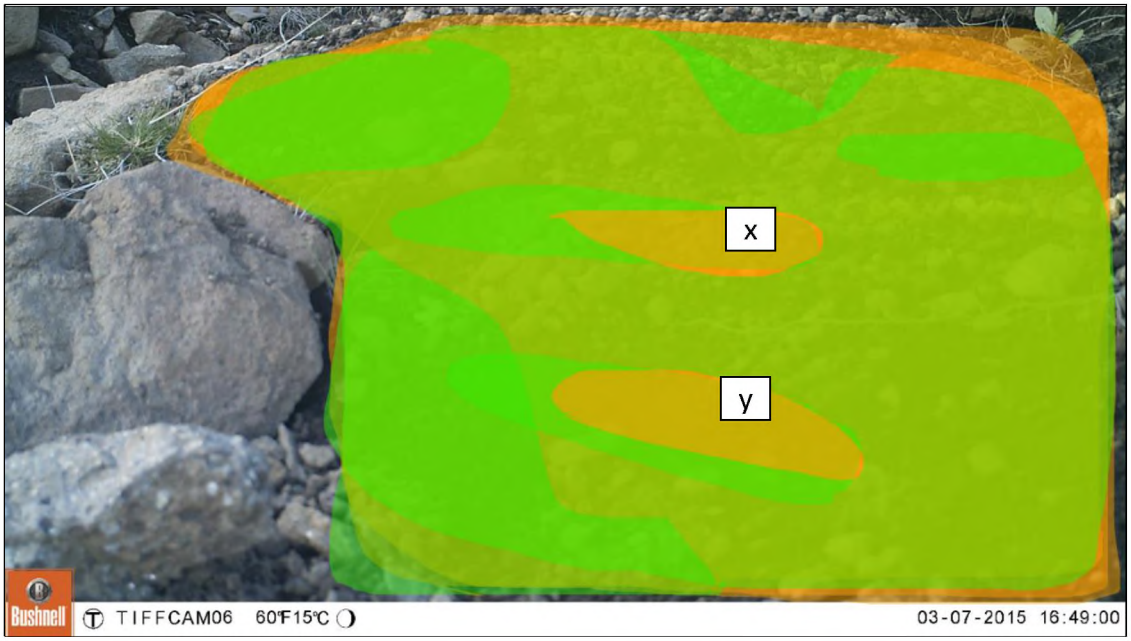

Figure 6.2. Composite needle ice activity on Site 2, based on five events (see Table 6.2). Green and orange areas display ice needle height of 0.5-1.5cm and over 1.5cm respectively. The area of most frequent and tall heaving is located at (x, z).

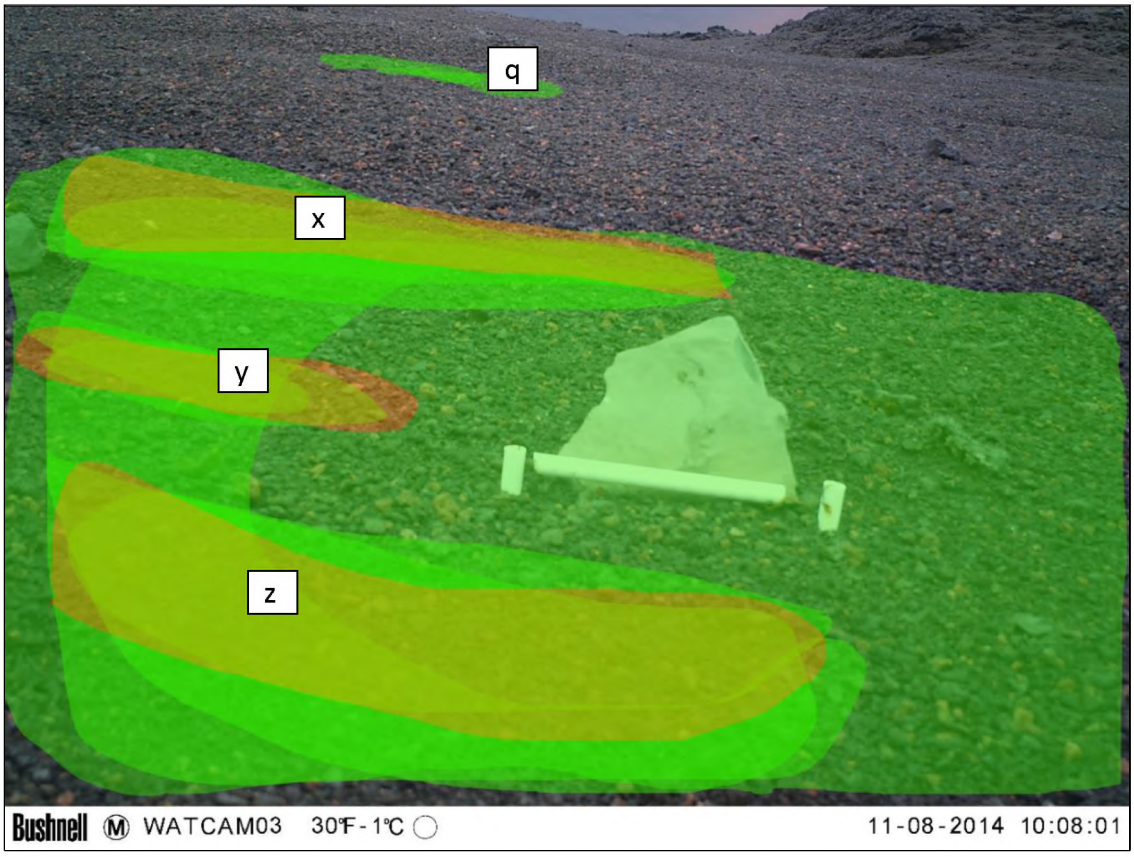

Figure 6.3. Composite needle ice activity on Site 3, based on five events (see Table 6.3). Green and orange areas display ice needle height of 0.5-1.5cm and over 1.5cm respectively. The area of most frequent and tall heaving is located at (a, b ,c). Heaving of surface material was seen in the background of Site 3 during the five events (d).

6.1.3 Sediment heave and movement relating to particle size

Displacement of surface material was sub-grouped into three material classes, consisting of the matrix (<2mm), small stones (2-20mm), and large stones (>20mm), represented by green, blue and yellow arrows respectively. Methods on how heave and displacement was measured is presented in Section 4.3. The corresponding videos to each event analysed below are represented with their corresponding number as frame number in Figures 6.4, 6.6 and 6.8.

6.1.3.1 Heave and sediment displacement at Site 1 (Video 4-8)

Video 4 - A large portion to the left of the study site was heaved by needle ice. However, no displacement of surface clasts was measurable apart from small changes in clast orientation.

Video 5 - Little heave and movement was seen across the study area. No visible movement of small stones was discernible, while only marginal movement of less than 0.5cm was noted from larger stones moved by heave and resettling. The matrix was additionally seen to be moved by less than 0.5cm downslope by heave and resettling, while a majority of the study site was not visually affected by needle ice growth.

Video 6 – Displacement of more than 1cm was observed from the top left portion of the study site, coinciding with areas of taller ice needles. Movement of large stones was seen to occur downslope to the right in the imagery by heaving and resettling, in a similar direction and distance as displacement observed in Video 5. However, movement of small stones over a distance of ca 1cm from the middle and right part of the study site was recorded, similarly only moved by the mechanisms of heaving and resettling could be identified. The fine matrix was displaced upslope by ca 0.5cm from the top left part of Site 1, possibly due to resettling after heave resulting in the surface matrix appearing less compact.

Video 7 – Needle ice heave was observed to influence a majority of the study site; although, more intense heave and movement was recorded in the top left most portion of the imagery. Displacement of small stones and a large stone of ca 0.5cm by heave and resettling occurred in the lower left part. Trampling by a human foot compacted the surface and created a ca 2cm deep depression. The trampling hindered quantification of surface movement by destroying ice needles from compaction instead of melting. A soil aggregate, observed in the back portion of the study site, was moved ca 4cm downslope after being trampled.

Video 8 – Tall ice needles (>1.5cm) were seen forming in a band across the middle portion of Site 1, while smaller ice needles covered most of the remainder of the study site. Large stones (> 20mm) moved ca 1.5cm in the top left part by heave and resettling, while smaller stones (2-20mm) were displaced by up to 2cm in the middle of the study site by heave and resettling and by toppling,

coinciding with the band displaying taller heave. The matrix in the middle of the study site was observed to move ca 2cm, resettling in various directions based on local topography. Matrix material in the lower right corner of the imagery moved upslope after heaving and resettling by ca 0.5cm. Similar to Video 6, the soil matrix in the lower right corner seemed less compacted after resettling.

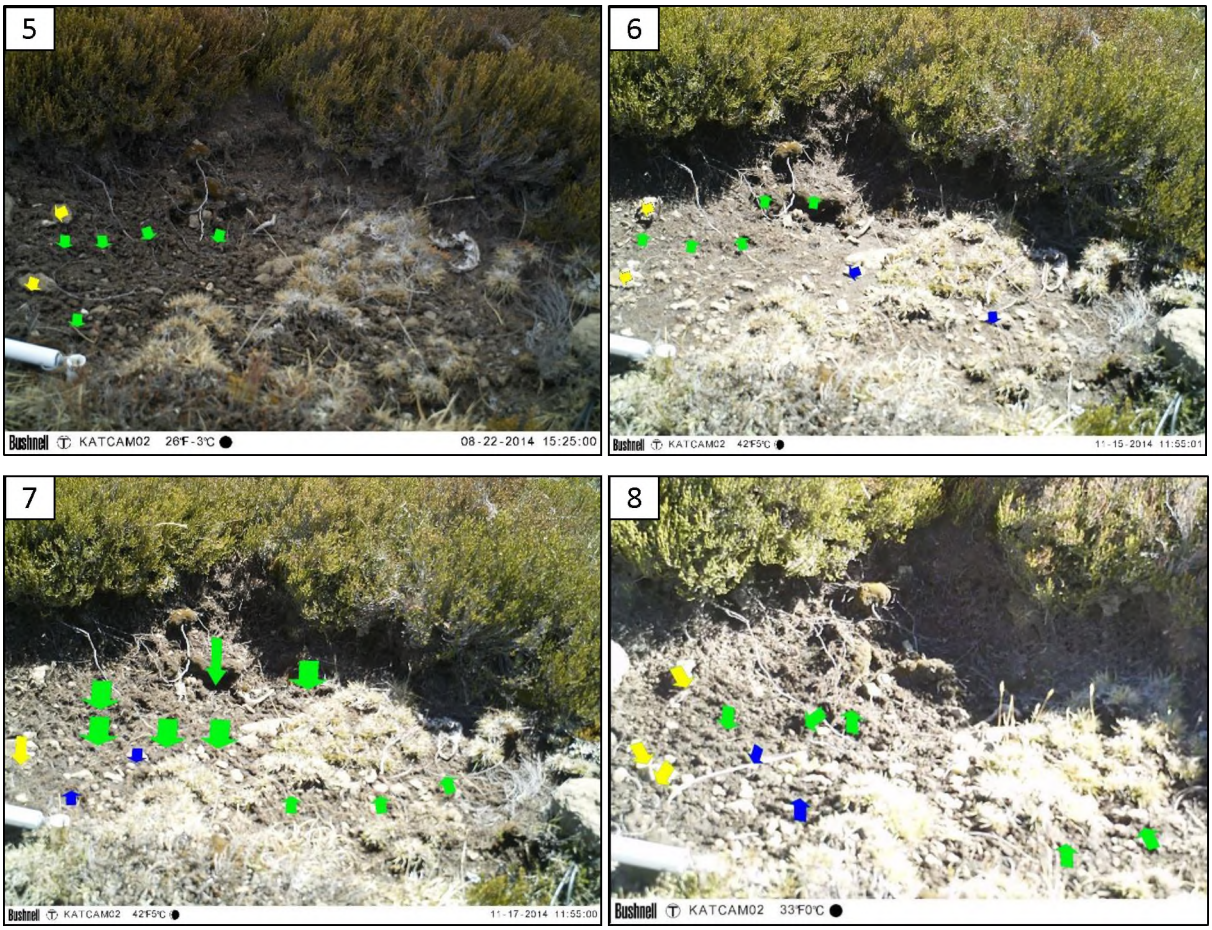

Figure 6.4. Movement of surface material sub-grouped into particle size from Videos 4-8 from Site 1. Video 4 did not show any discernible surface movement. Green, blue and yellow arrows show movement of the matrix, small stones and large stones respectively.

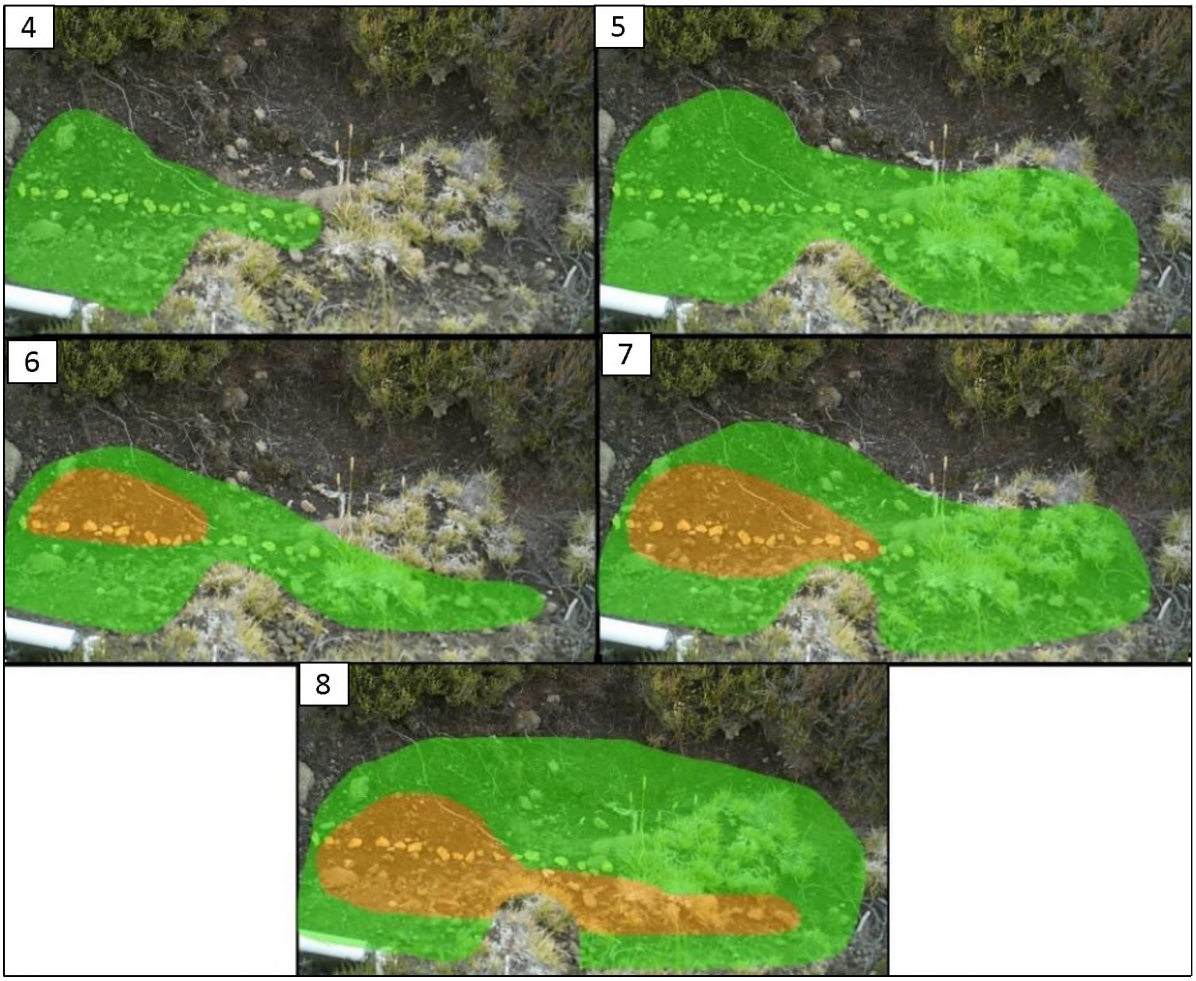

Figure 6.5. Needle ice height classes for the five events shown in Video 4-8 from Site 1. Green areas display heaving of 0.5-1.5cm and orange areas display heaving in excess of 1.5cm.

6.1.3.2 Heave and sediment displacement at Site 2 (Video 9-13)

Video 9 – The majority of the surface was seen to heave by more than 1.5cm during the event, and the lower left corner and the top middle portion was observed to heave less. Large stones were not heaved, however, both small stones and the soil matrix was seen to displace up to 3cm. Small stones moved downslope by heave and resettling and toppling in directions depending on local slope aspect and gradient to ca 3cm, although the majority of clasts moved by less than 1cm. The matrix was observed to predominantly be moved upslope by ca 1.5cm against the gradient of the slope angle, as a result of visible expansion.

Video 10 – Heave of 1.5cm or more covered the study site in Video 10, displacing most clasts. Marked differences in movement direction and distance was seen with varying particle size. Large stones were moved downslope by heave and resettling, toppling and rolling up to 5.5cm in a general left direction in the imagery, while smaller stones were displaced a maximum distance of 3.5cm by mostly toppling at steep slope angles and ca 1cm by heaving and resettling on flatter surfaces. The soil

matrix was seen to predominantly move upslope ca 1cm by heave and resettling, however, downslope movement of ca 4cm was measured in relation to steep surface topography.

Video 11 – A general heave of over 1.5cm covered the surface of Site 2 in Video 11. Large and small stones alike were seen to displace ca 3cm by toppling downslope, moving along the slope gradient and orientation. Video 11 displays the only large stone observed to topple. The matrix moved in a similar direction to the larger and smaller clasts for the majority of the study site, however, upslope movement of the matrix of ca 1cm was observed in the top left of the imagery, occurring after resettling.

Video 12 – Discontinuous patches of less than 1.5cm of heaving were noted in the mostly non-heaving needle ice surface seen in Video 12. No large or small stone movement were measurable, while the matrix was observed to move by less than a centimetre by heave and resettling in the top left and middle portion of the study site.

Video 13 - The surface was predominantly covered by needle ice of less than 1.5cm in height, although two locations of taller ice needles were observed close to the centre of the study site. Large stones were not observed to displace in Video 13, although small stones and the matrix were observed to move less than ca 0.5cm by heave and resettling downslope along the surface gradient, although locally enhanced in the top left and middle portions in the imagery, showing movement by heave and resettling of up to ca 3cm.

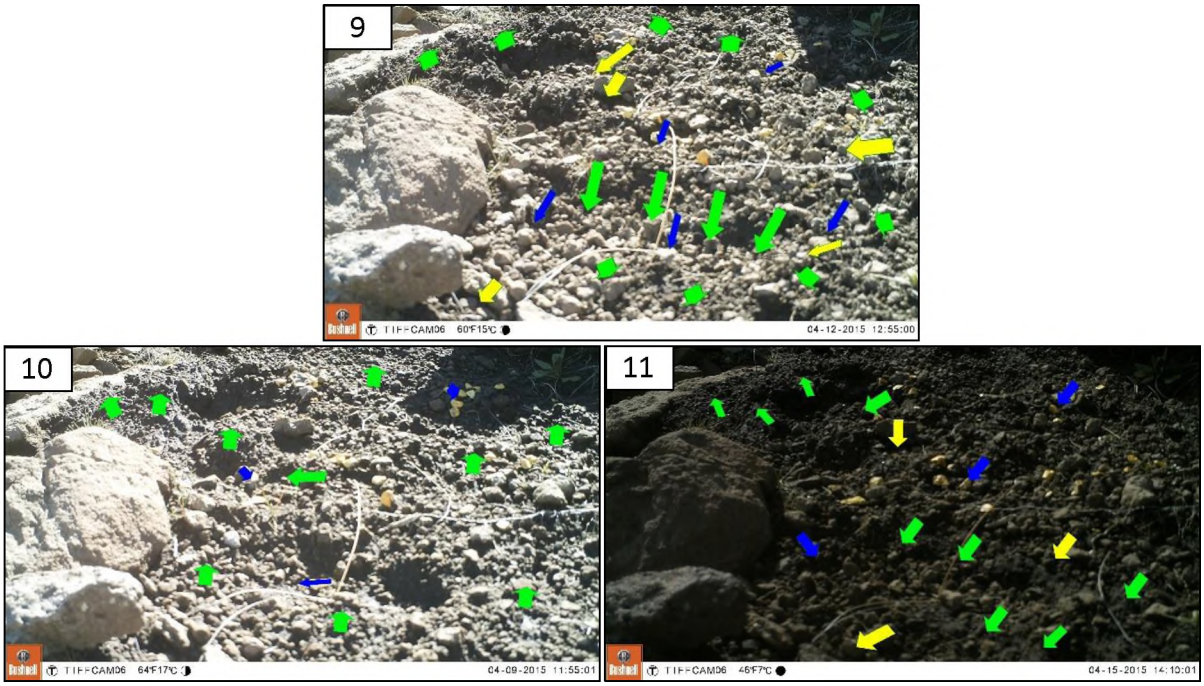

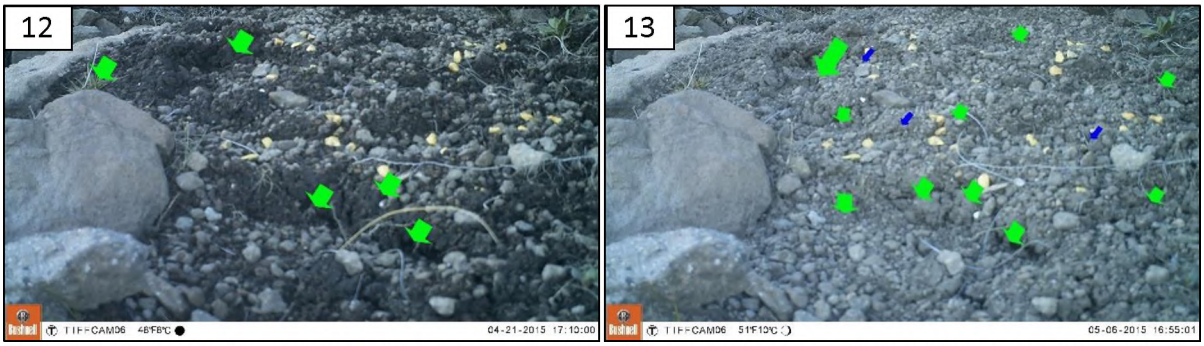

Figure 6.6. Movement of surface material sub-grouped into particle size from videos 9-13 from Site 2. Green, blue and yellow arrows show matrix, small stones and large stones respectively.

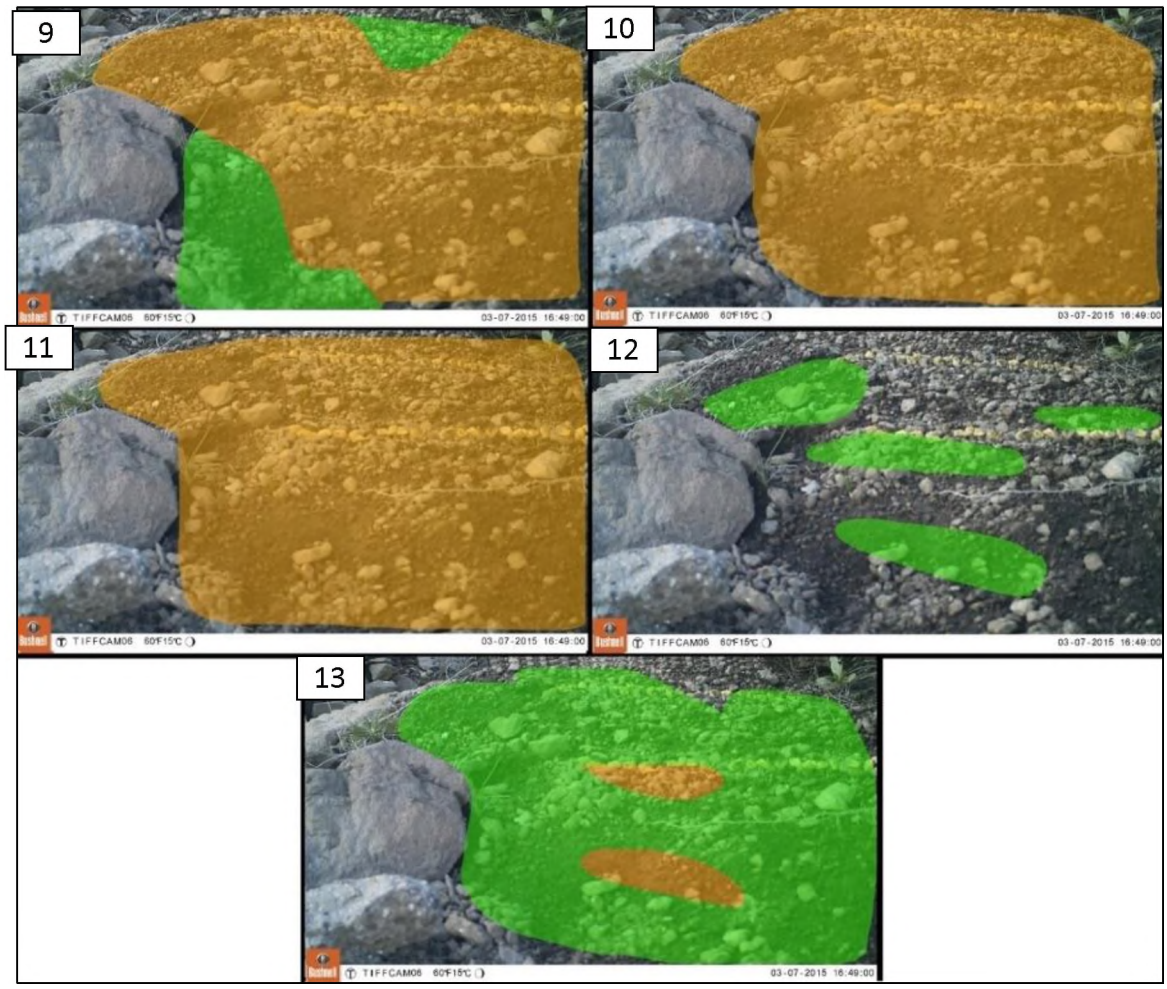

Figure 6.7. Needle ice height classes for the five events shown in Video 9-13 from Site 2.

6.1.3.3 Heave and sediment displacement at Site 3 (Video 14-18)

Video 14 – Discontinuous needle ice growth was seen to produce heaving in three areas on the left in the imagery. Small and large stones moved by heave and resettling ca 1cm on the left and foreground of the study site. Movement of the matrix was seen to be enhanced in a line in the back portion of the imagery displacing soil by ca 1cm by heave and resettling. Enhanced heave and displacement was observed following a depression in the background, which additionally was seen to accumulate snow.

Video 15 – Needle ice heave was observed in a crescent shape to the left and in the background of the imagery. Surface disturbance moved matrix by heave and resettling less than 0.5cm in the depression in the background and a similar distance by the same mechanisms in the foreground. Only one large stone was observed to move by ca 1cm by rolling due to destabilization after melt.

Video 16 –Surface heaved in discontinuous patches of roughly similar extent to observations in Video 15. Heave and resettling of ca 0.5cm is observable in the of the matrix coinciding with depressions in the back- and foreground. No displacement of large or small stones was visible, however disturbance of the soil in a patch in the far background was noted, however not measurable.

Video 17 – Needle ice covered the majority of the study site and was enhanced in three areas on the left side of the imagery. Small stones displaced up to 2cm by toppling and large stones ca 1cm by heave and resettling. The matrix moved ca 2cm in the depression in the back- and foreground of the video, displacing material by the mechanisms of toppling. Heaving and resettling of the matrix moved a large stone in the background, although not measurable.

Video 18 – Needle ice covered the majority of the study site in a similar manner as seen in Video 17. However, less heave and displacement was measurable. Only one small clast was seen to heave and resettle with measurable displacement. The matrix was displaced by heaving and resettling ca 0.5cm in the bottom left of the imagery. Snow was observed to cover the surface of the study site during the late night and early morning of Video 18.

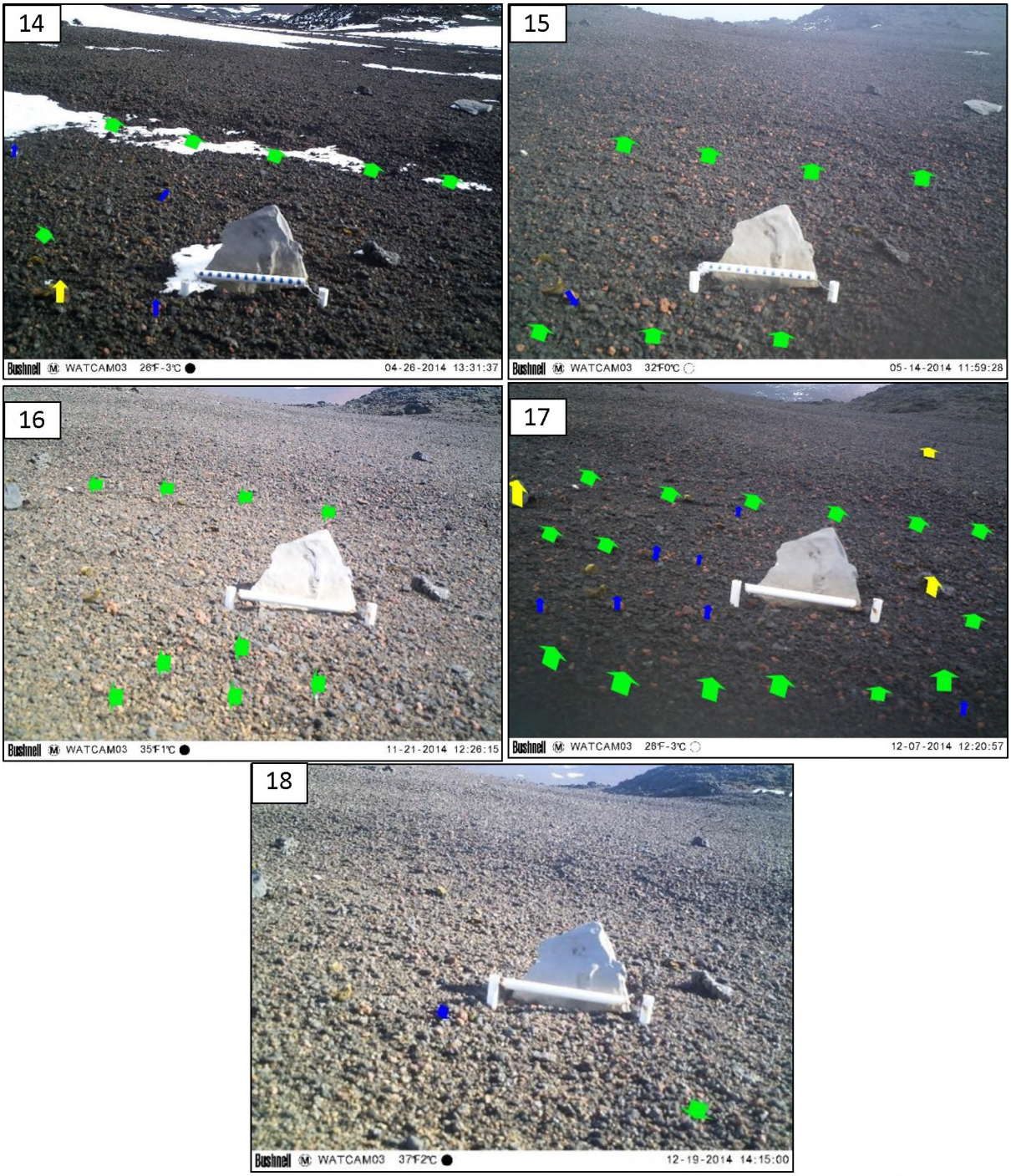

Figure 6.8. Movement of surface material sub-grouped into particle size from videos 14-18 from Site 3. Green, blue and yellow arrows show matrix, small stones and large stones respectively.

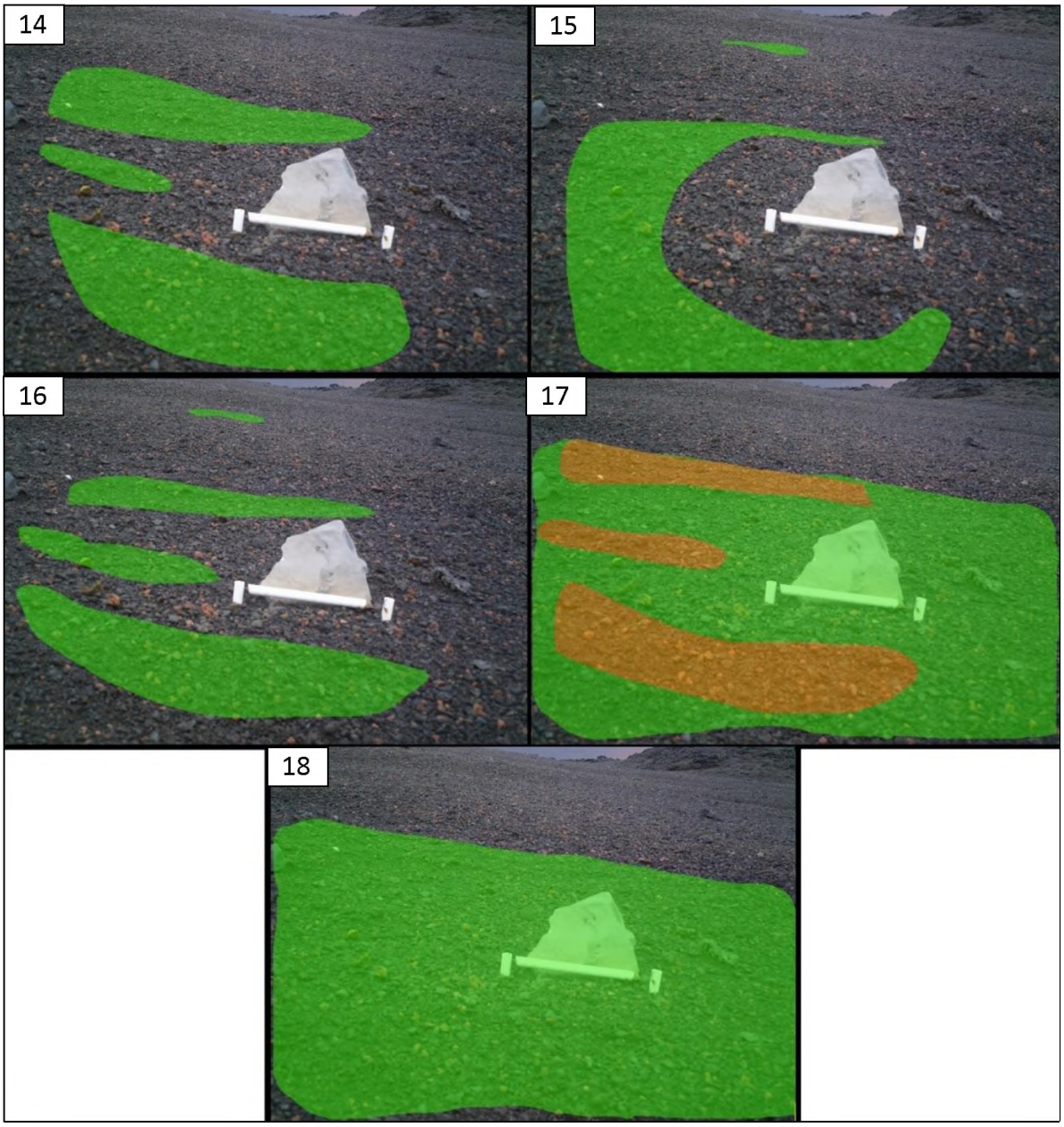

Figure 6.9. Needle ice height classes for the five events shown in Video 14-18 from Site 3.

Particle size analysis of the material shown in Video 4-18 showed clasts of different sizes moved in separate directions and displaced an uneven distance within each study site. Additionally, observations showed movement mechanisms affecting sediment displacement based on the particle size of the moved clasts. In addition to particle size, local surface morphology including slope angle and surface depressions were noted to affect sediment movement distance and displacement mechanisms.

6.2 Observed needle ice displacement mechanisms

Section 6.1 showed intra-site variability of NISD in relation to particle size and heave variability. Results showed intra-site areas with enhanced movement displayed in Figure 6.4, 6.6 and 6.8 from Site 1, 2 and 3 respectively. Understanding how heave height, particle size and slope morphology affect surface

displacement require analysis of movement mechanisms. Previous research (Higashi and Corte, 1971; Outcalt, 1971; Mackay and Mathews, 1974a) suggest needle ice height, slope angle and surface texture influence mechanism of displacement. With the addition of soil moisture and micro climate measurements the following section will analyse surface topography, texture and heave height and how they affect movement mechanisms and displacement.

To identify links between sediment displacement distance, the mechanisms of movement and surface texture the following section will analyse particle-sizes relation to observed movement. The same 15 events displaying intra-site heave variability in section 6.1, were additionally selected for this analysis, as they display a range of needle ice growth characteristics within each site.

The following section will display results of attained NISD by the mechanisms of heave and resettling, toppling and rolling (Figure 6.10) of surface clasts in relation to particle size and slope morphology.

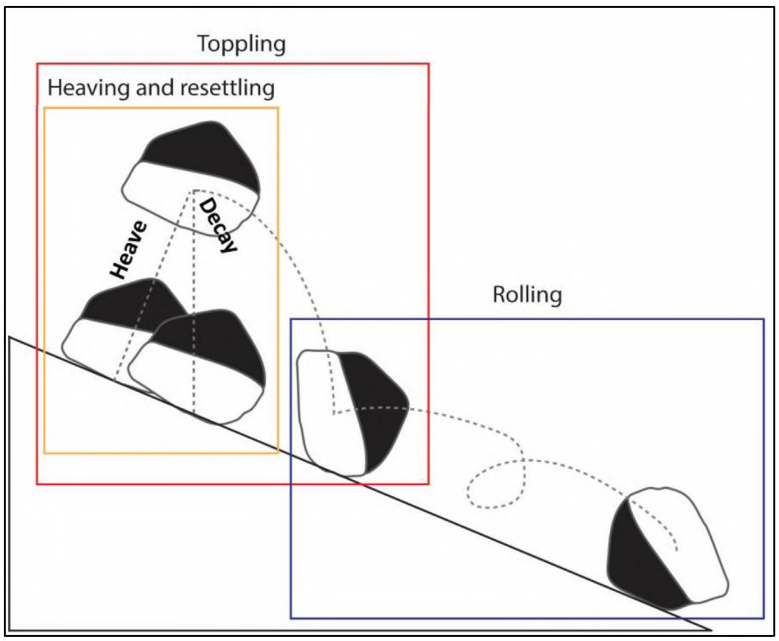

Figure 6.10. Schematic view of the three mechanisms of sediment displacement observed at the study sites. The three rectangles represent a simplified view how displacement is achieved by each mechanisms

Table 6.4. All 82 needle ice events captured from Site 1, 2 and 3 with measured heaving, surface displacement and displacement mechanisms. The first mechanisms indicate the most influential mechanism of that event.

Site 1			
Date of event	Avg heave (cm)	Max displacement (cm)	Mechanisms
2014-06-01	2	0	Resettling
2014-06-02	2	0	Resettling
2014-06-03	2	1	Resettling
2014-06-04	1	0	Resettling
2014-06-05	N/A	N/A	N/A
2014-07-01	N/A	N/A	N/A
2014-07-02	0,5	0	Resettling
2014-07-03	0,5	0	Resettling
2014-07-04	0,5	0	Resettling
2014-08-09	0,5	0	Resettling
2014-08-12	0,5	0	Resettling
2014-08-13	0,5	0	Resettling
2014-08-15	1	0	Resettling
2014-08-17	1	0	Resettling
2014-08-22	2	0,5	Resettling, Toppling
2014-08-24	0,5	0	Resettling
2014-10-20	1	0	Resettling
2014-10-21	0,5	0	Resettling
2014-11-05	1	0	Resettling
2014-11-16	2	1	Resettling
2014-11-17	2	0,5	Resettling
2014-11-18	2	2	Resettling
2014-11-19	0,5	0	Resettling
2014-11-20	0,5	0	Resettling
2015-01-17	0,5	0	Resettling
2015-04-07	0,5	0	Resettling
2015-04-09	0,5	0	Resettling
2015-04-10	0,5	0,5	Resettling
2014-04-12	1,5	1	Heave, Toppling
2015-04-15	1	0	Resettling
2015-04-16	3	1	Resettling, Toppling
2015-04-17	2	1	Resettling, Toppling
2015-04-18	1	0	Resettling
2015-04-19	1	0,5	Resettling
2015-04-20	1	0	Resettling
2015-04-21	1	0	Resettling
2015-04-22	1	0,5	Resettling
2015-04-27	0,5	0	Resettling
2015-04-28	0,5	0	Resettling
2015-04-30	0,5	0	Resettling
2015-05-01	0,5	0	Resettling
2015-05-11	N/A	N/A	N/A
2015-05-12	1	0	Resettling
2015-05-13	0,5	0	Resettling

Site 2			
Date of event	Avg heave (cm)	Max displacement (cm)	Mechanisms
2015-04-10	1,5	3	Resettling, Toppling
2015-04-12	2,5	5,5	oppling, Resettling, Rollin
2015-04-15	1	0,5	Resettling
2015-04-16	3	3	Resettling, Toppling
2015-04-17	2	1	Resettling
2015-04-18	1	1	Resettling, Toppling
2015-04-19	1	0	Resettling
2015-04-20	1	0,5	Resettling
2015-04-21	1,5	0,5	Resettling
2015-04-22	0,5	0	Resettling
2015-04-27	0,5	0	Resettling
2015-04-28	1	0	Resettling
2015-04-30	0,5	0	Resettling
2015-05-01	1	0,5	Resettling
2015-05-02	N/A	N/A	N/A
2015-05-07	0,5	0	Resettling
2015-05-11	0,5	0	Resettling

Site 3			
Date of event	Avg heave (cm)	Max displacement (cm)	Mechanisms
2014-04-27	2	0	Resettling
2014-05-13	N/A	N/A	N/A
2014-05-15	1	1,5	Resettling, Rolling
2014-05-16	0,5	0	Resettling
2015-03-01	2	1	Resettling
2015-03-11	0,5	0	Resettling
2015-03-12	1,5	0	Resettling
2015-03-14	1	0	Resettling
2015-03-20	1,5	1	Resettling, Toppling
2015-03-27	2	0	Resettling
2015-03-30	0,5	0	Resettling
2015-03-31	3	3	Resettling
2015-04-02	3	3	Resettling, Toppling
2015-04-03	N/A	N/A	N/A
2015-04-11	0,5	0	Resettling
2015-04-30	2	0	Resettling

6.2.1 Surface movement at Site 1

Table 6.4 presents heave, displacement and movement mechanisms of the 44 needle ice events analysed from Site 1. However, in three events displacement could not be measured due to camera obstruction. The studied events all displayed heave and resettling as the main mechanism of NISD, although most events did not show displacement in any direction, despite observable heaving. Although no lateral movement of any clast size was measurable in many of the events displayed, some spatial influence often showed in the form of minute differences in clast orientation occurred after heave.

Two events, shown in Video 4 and 8, were selected to display details of movement generated by heave and resettling and toppling mechanisms observed at Site 1, as they clearly displayed the different stages of heaving and resettling and heaving and toppling.

6.2.1.1 Heave and resettling mechanism at Site 1

Heaving and resettling of surface clasts was active in all of the 41 analysed events from Site 1. Observations of heave included ice needles of ca 3.5cm (Video 8), while other events showed heaving of less than 0.5cm (Video 4). Out of the 41 observed events, 78% showed negligible lateral displacement during heaving and resettling. Out of the 9 events that showed lateral movement, average event displacement measured ca 1 cm (Table 6.4).

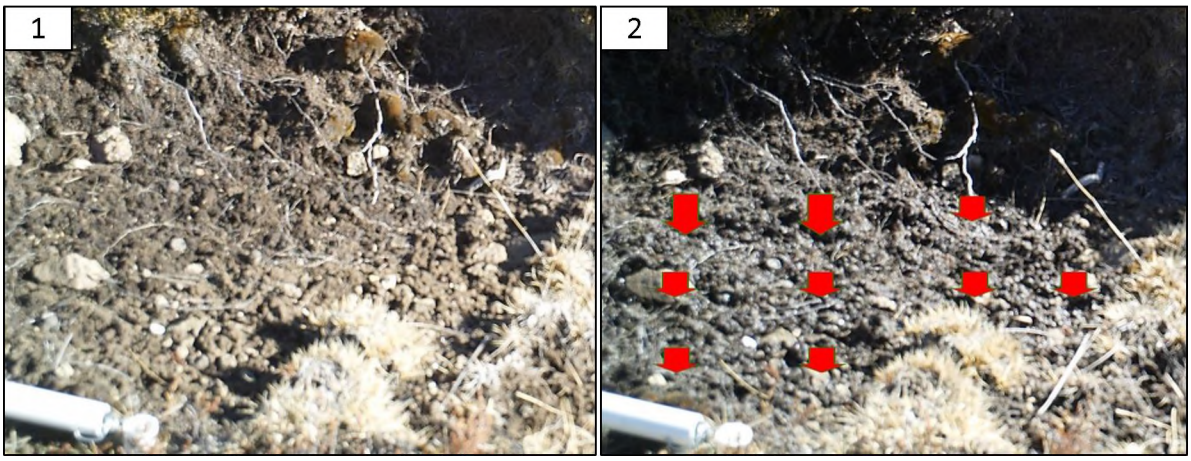

Figure 6.11. Heaving and resettling at 09:04 and 12:10 from Site 1 from Video 4 (a and b) show downslope movement of surface material at Site 1. The red arrows show a general lowering of ca 0.5cm while the top left two arrows show a lowering of ca 1cm.

Analysis of an event with little displacement is seen in Figure 6.11. Frame a and b respectively show maximum and minimum heave of the ground from Video 4. Heaving was seen to initiate from the subsurface and resettling began upon melting. The majority of the area was heaved by less than ca 0.5cm. However, heaving of ca 1cm was measured in the top left portion of the study site, close to the study site margin. The location showing enhanced heave coincides with steeper slope angles of ca 10-15°. No quantifiable lateral displacement post heaving and resettling was measurable from Video 4. Heaving and resettling in Video 4 show no ice needles exposed at the surface. The area heaves as a single mass, and clasts are observably supported by each other. Resulting in no displacement in any direction.

6.2.1.2 Toppling mechanisms at Site 1

Toppling of clasts from Site 1 were only recorded in four events of the 41 from Site 1. All toppling events coincided with heaving exceeding 1.5cm

Figure 6.12 shows two frames from at 08:25 and 08:40 from Video 8, with one clast toppling in the middle-left portion of the image. The studied clast was seen to heave ca 1.5cm and subsequent to melt, displace a particle downslope by ca 1.5cm. Only small stones were seen to topple and observations of movement distance from toppling aligned with the height of the ice needle which

supported the small stone previous to melting. Toppling was seen to not occur simultaneously between all clasts, hence only one clast was seen to topple in Figure 6.12. Melting was observed to correspond to the initiation of sunlight moving over the study site. Toppling was seen to occur within the area of enhanced heave showing steeper slope angles, positioned near the margin of Site 1.

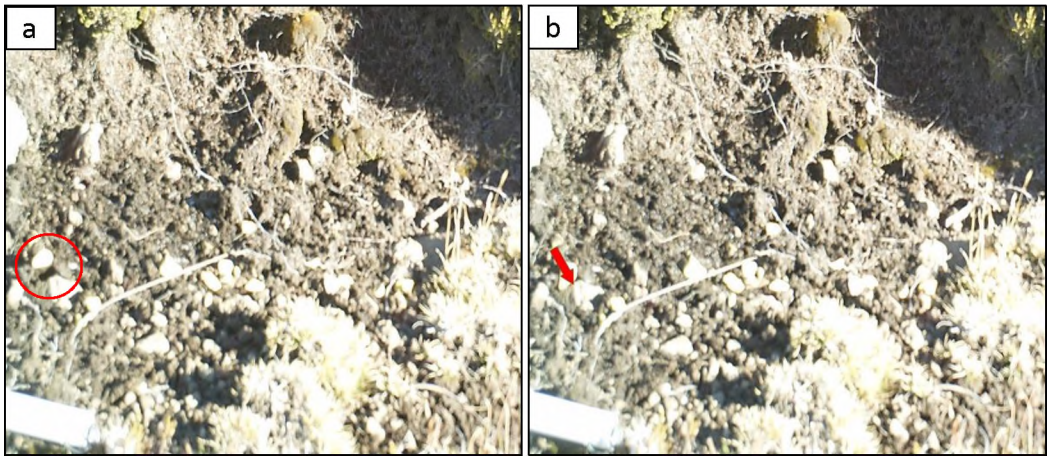

Figure 6.12. Toppling of an ice needle over 15 minutes in Video 8 from Site 1.

6.2.1.3 Displacement mechanisms of specific particle sizes at Site 1

Section 6.1.3.1 displays results from sediment movement as coloured arrows in Videos 4-8 from Site 1, sub-grouped into different particle sizes. Results show specific particle size classes, defined in section 4.5, to vary in displacement mechanisms and movement distance.

Movement measured in the five videos display events with less heave height (see Video 4 and 5), only being affected by heave and resettling. In Video 4 for example, although heave was visually identifiable, no surface displacement was measurable. In Video 5, heave and resettling resulted in a few clasts moving less than 0.5cm, while a majority only displayed slight orientation changes. Videos 6 and 7 show small parts of the area experiencing tall ice needles (>1.5cm), with the majority of the surface showing heave between 0.5 and 1.5cm (Figure 6.4 and 6.5). The smaller areas coincide with the location of taller ice needles in Video 4 and 5, located close to the site margin. All particle sizes in Video 6 and 7 are seen to displace a similar distance of ca 1cm. Although ice needles taller than 1.5cm were visible, only the effect of heave and resettling was observed to affect clasts movement of all sizes from both events. Video 6 displayed temperatures of -9°C during the night, suggesting a stabilizing effect of particles freezing together and the human tramping during melting in Video 7 partly obscured visual analysis of displacement.

Video 8 displays heaving and toppling of clasts from Site 1. A majority of the study area was covered by needle ice growth with a band across the centre showing heave of over 1.5cm. Areas showing increased needle ice height correspond with toppling of ice needles. In addition, the mechanisms

active were seen to relate to particle size, with large stones not toppling. The majority of the fine matrix was only affected by heave and resettling. Some small stones were seen to topple in the lower left portion of the study site. Furthermore, a single clast of what was identified as an aggregate of soil was also displaced by the topping mechanism. A majority of small stones were however only seen to be influenced by heave and resettling.

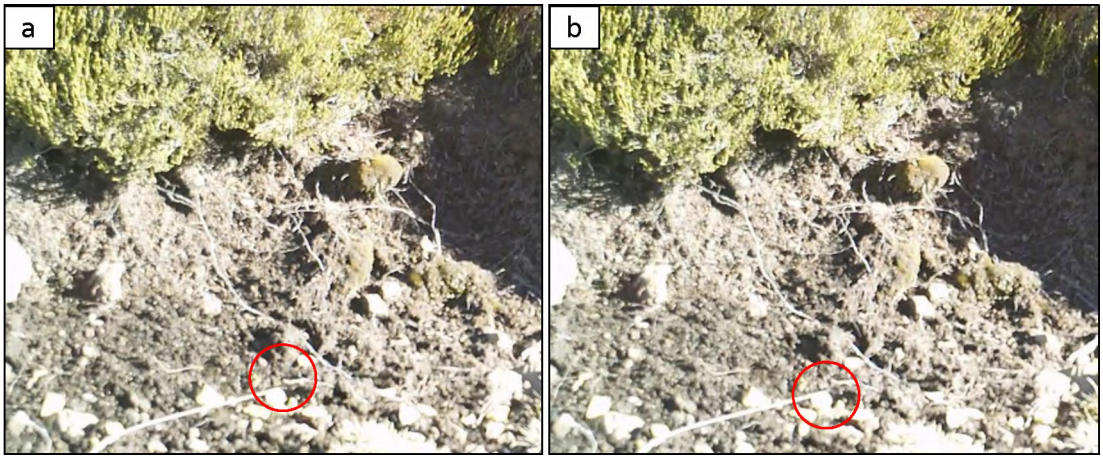

Figure 6.13. Toppling of an aggregate of soil in Video 8

6.2.1.4 Surface morphology and mechanisms of movement at Site 1

Site 1 displays increased slope angles in the areas located close to the margin to the top left (encircled in Figure 6.14).

Figure 6.14. Site 1 overview with the area showing enhanced needle ice growth encircled.

Locally enhanced growth of ice needles is displayed in Figure 6.1 from Section 6.1.2.1. Enhanced growth of needle ice and steeper slope angles coincided with the area of active needle ice toppling in Videos 4-8. The surface morphology of Site 1 was additionally seen to change after rain. Figure 6.15

shows surface clasts heaved out by needle ice after input of snow and snowmelt evening out the surface texture (Figure 6.15a). After a night of needle ice heaving surface material, the surface texture is notably rougher (Figure 6.15b). It is suggested that the effect increases erosivity.

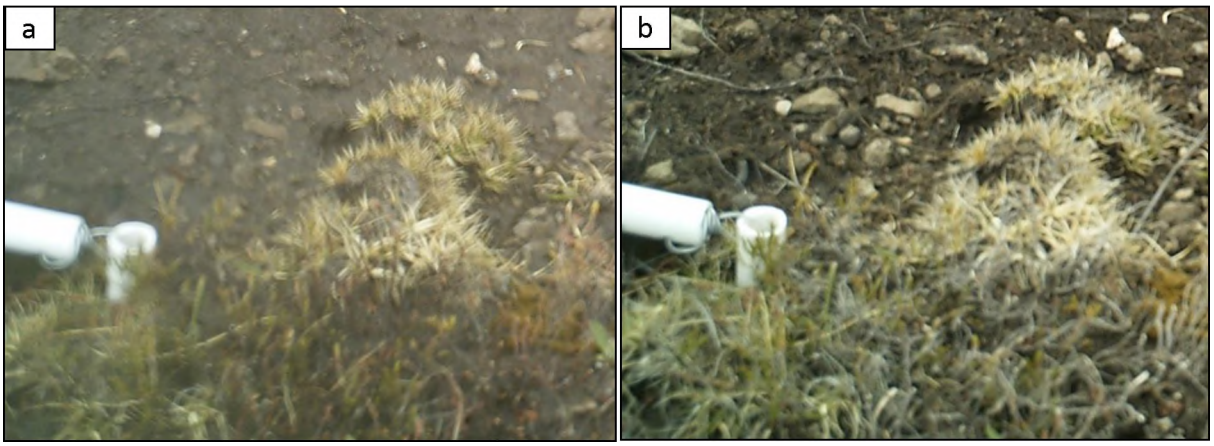

Figure 6.15. Heave out of clasts from needle ice over a 24h period on November 4-5 2014.

6.2.2 Surface movement at Site 2

Table 6.4 shows heave, displacement and movement mechanisms of the 17 needle ice events recorded at Site 2. Heave and resettling was observed as the main mechanism of NISD for most events, although several events did not show any lateral displacement. Two events, shown in Video 10 and 13, were selected to display details of movement generated by heave and resettling, toppling and rolling mechanisms observed at Site 2.

6.2.2.1 Heave and resettling mechanism at Site 2

Heaving and resettling of surface clasts was active in all of the 17 events analysed from Site 2. Observations of heave include tall ice needles of ca 3.5cm (Video 10) while other events showed heaving of less than 0.5cm (Video 12). Out of the 17 observed events, 41% showed negligible lateral displacement during heaving and resettling. Out of the nine events that showed lateral movement, eight showed heaving a resettling as the main mechanisms of movement and one displayed toppling to be most active in displacing soil. Average displacement of the nine events showing surface movement was ca 1.5 cm.

Figure 6.16 shows heaving and resettling from Site 2 in Video 13. A majority of the area was heaved by 0.5-1.5cm, however two locations of enhanced heave were noticed in the centre of the study site. The two locations of enhanced heaving showed ice needles of ca 3cm and were on locally steeper slope angles.

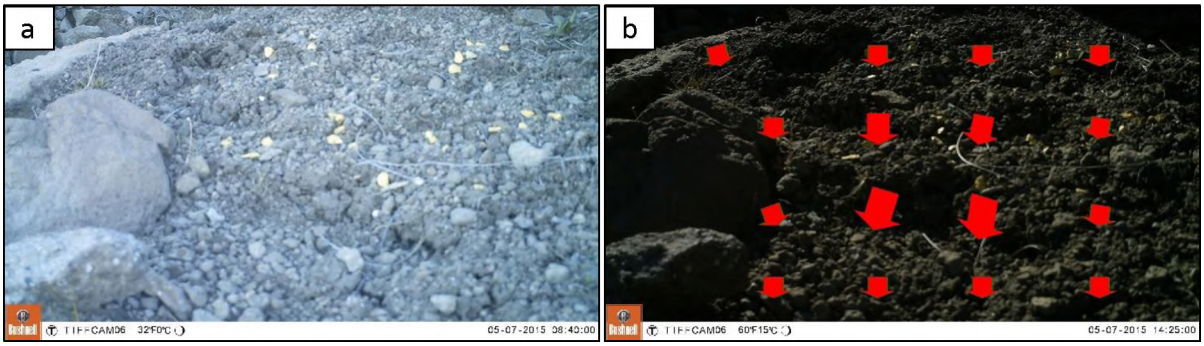

Figure 6.16. Heaving and resettling at 08:40 and 14:25 at Site 2 from Video 13 (1 and 2). The red arrows show a general vertical settlement of ca 1cm over the whole study site, although settling of ca 3cm in seen in the middle portion.

6.2.2.2 Toppling mechanism at Site 2

Four of the 17 events analysed had observable toppling of clasts. Toppling coincided with an average heaving of more than 1.5cm over the whole study site for three of the four events, however local heaving heights showed all clasts that toppled to initially heave more than 1.5cm.

Figure 6.17 shows two frames at 10:40 and 10:55 from Video 10, with four clasts toppling from the top left in a band to the bottom right of the image. The studied clasts were seen to heave ca 2-3cm and subsequent to melt, displace supported particles ca 2-3.5cm, with a trajectory downslope along the local slope gradient.

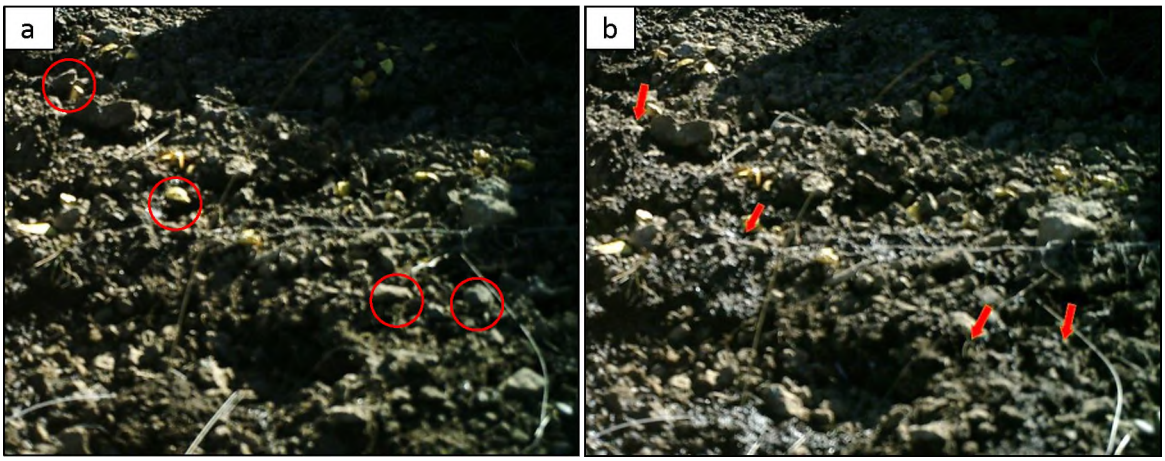

Figure 6.17. Toppling of an ice needle over 15 minutes in Video 10 from Site 2.

Several clasts were seen to topple in the same event and observations of clast movement distance from toppling compared, or exceeded, the height of the ice needle which supported the clast previous to melting. Toppling was not seen to occur simultaneously between all clasts heaved, hence only a few of the clasts were seen to topple in Figure 6.17 as melting corresponded to the sunlight moving over the study site. Video 10 shows toppling to generate most movement in the area with steeper slope angles in the lower centre of Site 2 (see Figure 6.21).

6.2.2.3 Rolling mechanism at Site 2

Rolling was observed in one clast from Site 2 in Video 10. The spherical to semi-spherical clasts were seen to be destabilized when lifted by ice needles, and subsequently roll during melt. Although the mechanism of rolling was not specifically recorded, it could be inferred, due to clast being spherical and the distance moved. The rolling occurred after toppling and resulted in further displacement. A change in the rotation of the clasts surface was observed after decay, which additionally suggests rolling, as a previously unexposed surface of the clast was seen (Figure 6.18). Displacement of ca 5.5cm was measured after rolling, which showed greater movement than any other clasts measured over 15 minutes in the 82 needle ice events.

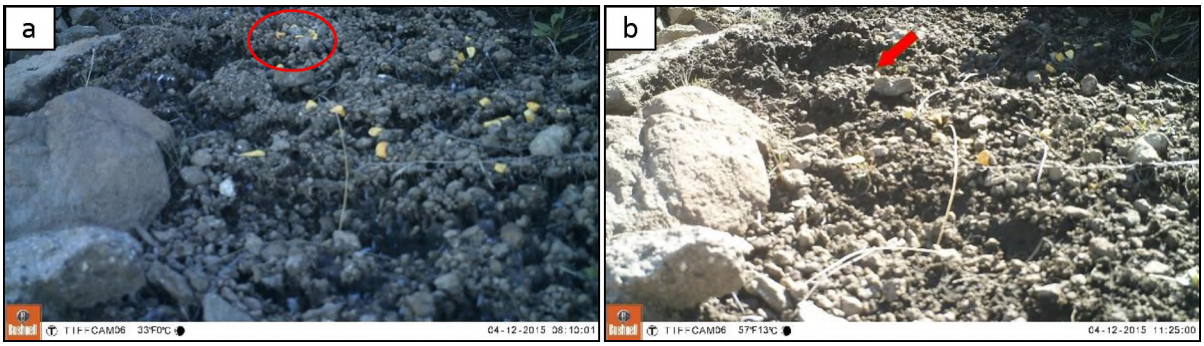

Figure 6.18. Rolling of a large stone (encircled) in Video 10 from Site 2. Although the event of rolling occurred within 15 minutes between 08:55 and 09:10, it is most visible in Frame 1 and 2 between 08:10 and 11:25.

6.2.2.4 Displacement mechanisms of specific particle sizes at Site 2

Section 6.1.3.2 showed results of sediment movement in the form of coloured arrows in frames extracted from Videos 9-13. These were sub-grouped into classes, based on particle sizes. Results showed specific particle size classes to vary in displacement mechanisms and movement distance.

Videos 9, 10 and 11 showed ice needles over 1.5cm tall that covered the majority of the study site, and showed the greatest surface displacement of the 82 needle ice events analysed. Video 10 displayed the only event where toppling of ice needles was the most prominent mechanism for surface displacement. Videos 9, 10 and 11 showed the matrix, small stones and large stones to move separately and by different mechanisms. The fine matrix predominantly moved through heaving and resettling while small stones moved by toppling. Although the majority of larger rocks were seen to move by heaving and resettling, Video 11 showed one large rock to toppling during decay (Figure 6.19). Videos 12 and 13 showed less heave than Videos 9, 10 and 11 and displayed sediment movement by only heave and resettling, except from the middle part of Site 2 that showed toppling of matrix soil aggregates in Video 12.

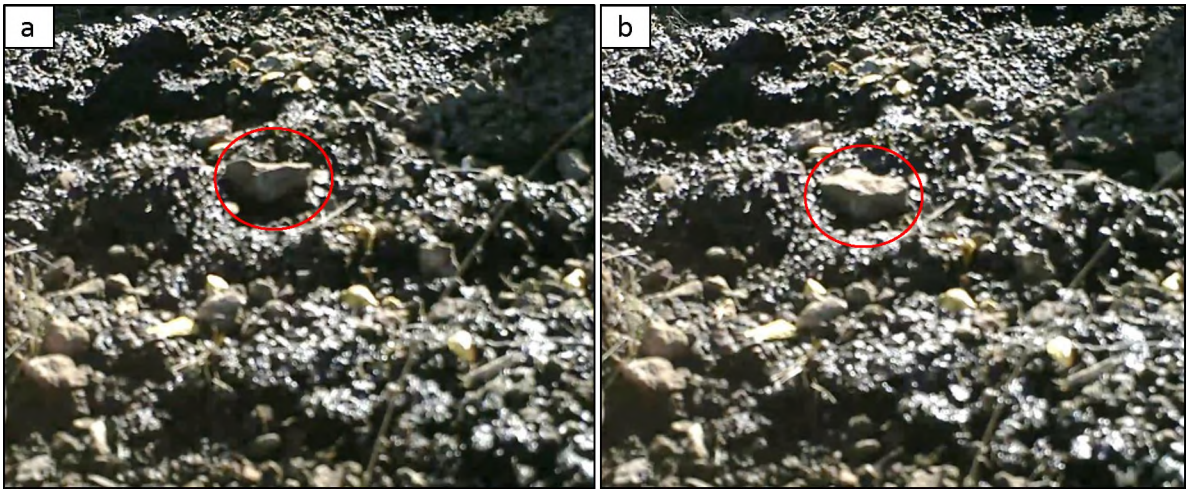

Figure 6.19. Toppling of a large stone between 11:25 and 11:40 from Site 2 in Video 11.

Site 2 showed greater heave and surface displacement by toppling compared to Site 1. Notable differences were seen in displacing particles of different sizes as well as the trajectory of said particle classes. Intra-site variability of heave and movement was as well noted to be extensive from Site 2, with enhanced heave and subsequent displacement noticed in locations of steeper slope angles.

6.2.2.5 Surface morphology and mechanisms of movement at Site 2

Similar to results from Site 1 in Section 6.2.1.4, Site 2 showed only heave and resettling during needle ice events that displayed heave of less than 1.5cm. Intra-site variability was greater at Site 2 than Site 1. In addition, Site 2 showed the notable impact slope angles on both active mechanism and sediment displacement distance. Site 2, showed enhanced heave height in the centre portion of the study site also coinciding with steeper parts of the study surface, noted in Figure 6.21 from Section 6.1.2.2. It is suggested that the steeper parts of Site 2 have enhanced moisture availability due to subsurface flow, however will be further discussed in Chapter 7.

The topography of Site 2 was seen to affect both mechanisms of movement and distance of sediment displacement. Video 12 showed no measurable movement in small or large stones. However, aggregates of fine matrix are seen to topple on steeper slope angles (>30°). Surface morphology at Site 2 was seen to change the mechanisms of sediment movement, as well as allow for particles of all sizes to displace.

Figure 6.20. Site 2 overview

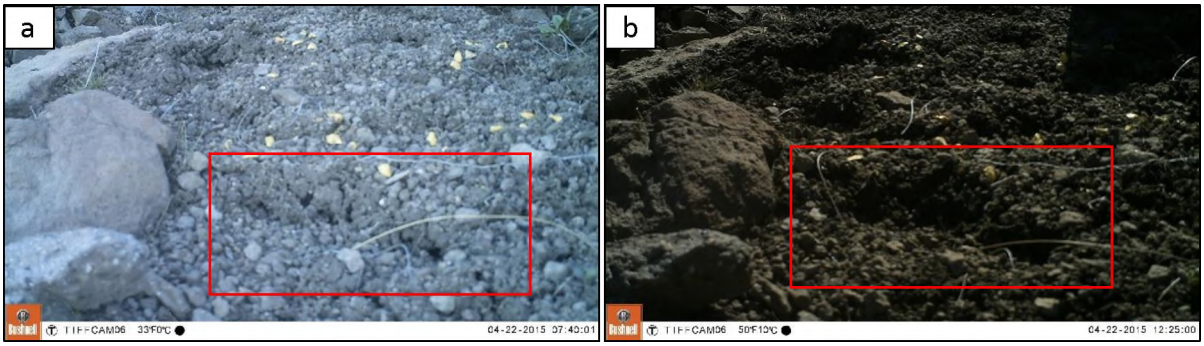

Figure 6.21. Steeper slope angles in the surface area of Site 2 impacting active needle ice movement mechanisms.

6.2.3 Surface movement at Site 3

Table 6.4 shows heave, displacement and movement mechanisms of the 16 needle ice events at Site 3. The studied events displayed heave and resettling as the main mechanism of NISD, however 64% of events did not show any lateral displacement, despite observable heaving. Three events, shown in Videos 15, 16 and 17 were selected to display details of movement generated by heave and resettling, toppling and rolling mechanisms observed from Site 3.

6.2.3.1 Heave and resettling mechanism at Site 3

Heaving and resettling of surface clasts was seen in all of the 16 events from Site 3. Observations of heave included tall ice needles of ca 3cm (Video 17), while other events showed heaving of less than 0.5cm (Video 16). Out of the 16 observed events, three had lens obstructions preventing analysis, eight showed negligible lateral displacement and four displayed movements. Of the four events that showed lateral movement, three were associated with heaving and resettling and one displayed heave and

resettling in addition to toppling. Average displacement from each of the four events that showed surface movement was ca 1.5 cm (Table 6.4).

Figure 6.22 displays heaving and resettling from Site 3 in Video 16. The majority of the area was heaved by 0.5cm, however, two locations of enhanced heave were visible in the back- and foreground of Video 16. Both areas showed enhanced needle ice heights corresponding with surface depressions.

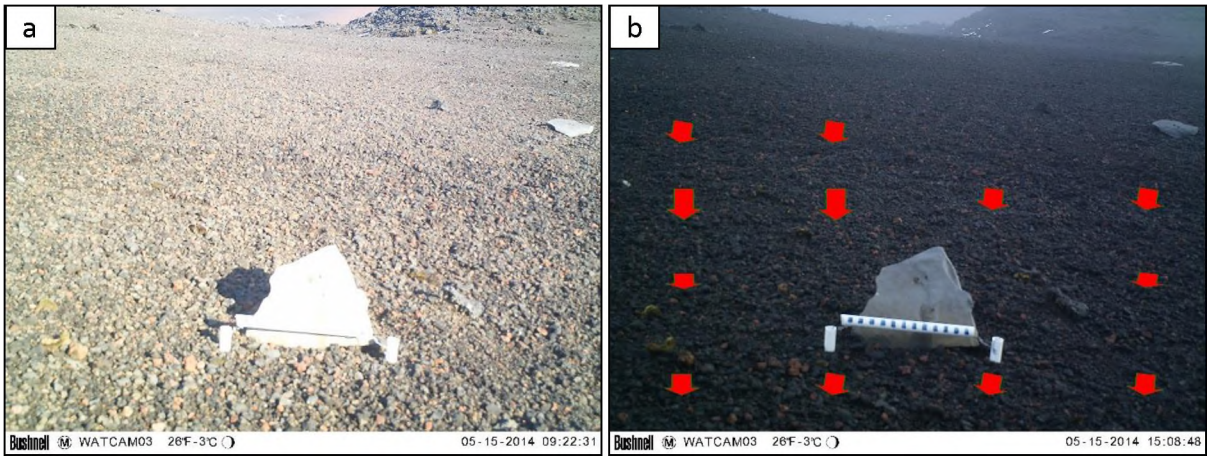

Figure 6.22. Heaving and resettling at 09:22 and 15:08 at Site 3 from Video 16 (1 and 2). The red arrows show a general lowering of ca 0.5cm over the whole study site.

6.2.3.2 Toppling mechanisms at Site 3

Only one event at Site 3 showed surface material to topple (Video 17). Average heave of ca 1.5cm was seen over the study site. However, local heave of ca 3cm was measured in the depressions that housed toppling ice needles.

Figure 6.23 shows two frames from at 11:33 and 11:46 from Video 17, with six clasts toppling from the bottom left area, circled in of Figure 6.23a. Ice needles were seen to topple in several directions throughout the melting period, moving clasts up to 3cm and reducing the density of the surface. Melting is seen to initiate simultaneously in the encircled area, not showing the time-lag in melting seen from Site 1 and 2 during preferential melting as the sun moves over the study sites. Particle sizes of material toppled in Video 17 was hard to distinguish, however, it is suggested that the majority of clasts are of small stone size, possibly with aggregates of soil also ranging between 2-20mm. Significant surface reworking is seen in the encircled area in Figure 6.23a.

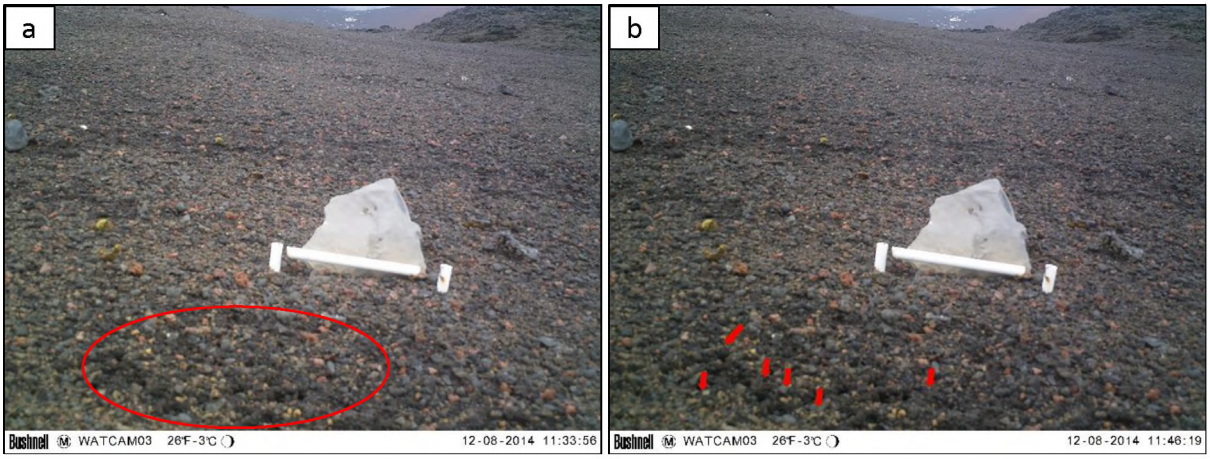

Figure 6.23. Toppling of an ice needle over 15 minutes in Video 17 from Site 3. The area encircled in Frame 1 shows the location of many toppling ice needle during the morning melt seen in Video 17.

6.2.3.3 Rolling mechanism at Site 3

Rolling of a single clast was observed from Site 3 in Video 15. The spherical to semi-spherical clasts were seen to destabilize when lifted by ice needles and rolled during melt. Displacement of ca 1.5cm was measured as well as rotation of the clast, further suggesting rolling. Similar to rolling of the clast from Site 2, rolling of the clast in Video 15 is suggested to be controlled by clast morphology.

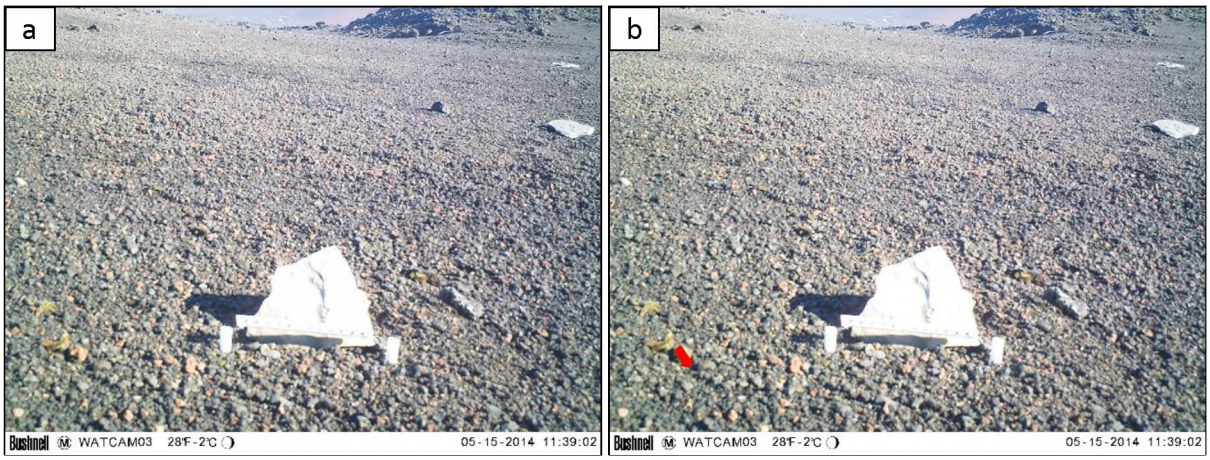

Figure 6.24. Rolling of a stone in Video 15 from Site 3.

6.2.3.4 Displacement mechanisms of specific particle sizes at Site 3

Section 6.1.3.3 displayed results from sediment movement as coloured arrows in Videos 14-18 from Site 3, sub-grouped into different particle sizes. Results showed displacement mechanisms and movement distance to vary with specific particle size classes.

Intra-site variability of NISD mechanisms from Site 3 showed a single toppling event, while the majority of the events were only affected by heave and resettling. Videos 14-16 showed heaving of the matrix to be most active in the depressions in the fore- and background, seen as opaque in Figure 6.3 from Section 6.1.2.3. Apart from toppling in the encircled area displayed in Figure 6.23a from Video 17

and the one clast observed rolling in Video 15, only heave and resettling was observed to be over the entire study area. Areas with active heave and resettling is delimited in Figure 6.3 to topographical depressions at the study site.

6.2.3.5 Surface morphology and mechanisms of movement at Site 3

Surface morphology at Site 3 was seen to influence the growth regimes of needle ice and hence, impacting sediment movement rates across the study site surface (Figure 6.25). Needle ice was seen to be concentrated in the fore- and background of the study site, coinciding with areas of lower relief. Frames 14-17 in Figure 6.8 from Section 6.1.3.2 showed enhanced movement in the depression in the background, while Frame 15-17 from the same figure shows enhanced movement in the fore- and background. The frequent inputs of snow at Site 3 were recorded as persisting in the described depressions.

Figure 6.25. Site 3 overview.

6.3 Long-term displacement at the study sites

The following section displays total sediment movement from each site over each respective corresponding study period. Site 1 and 2 displays twelve months of study while Site 3 displays imagery from three months (Section 4.4.1.1). Methods used for long term displacement measurements are detailed in Section 4.3.3.2.

6.3.1 Site 1

Sediment movement displayed in Frame a) and b) from Figure 6.26 show displacement of large stones a maximum of ca 2cm over the nine-month period. Conversely, movement of ca 5cm was measured for the painted markers (2 to 20mm) over the last three months of the study from Site 1. One of the

painted markers moved ca 1cm upslope from the middle of the painted marker line in during the same period (Frame d) of Figure 6.26).

Although individual needle ice events have shown decay up to 2cm from a single mechanism during one cycle, preferential movement vectors are only discernible at a longer timescale. Section 6.1.3.1 shows that particle movement occurred in several directions not always aligned downslope. Movement from several needle ice events at Site 1 suggest to produce counteracting displacement, where a single clast is moved in different directions between several needle ice events.

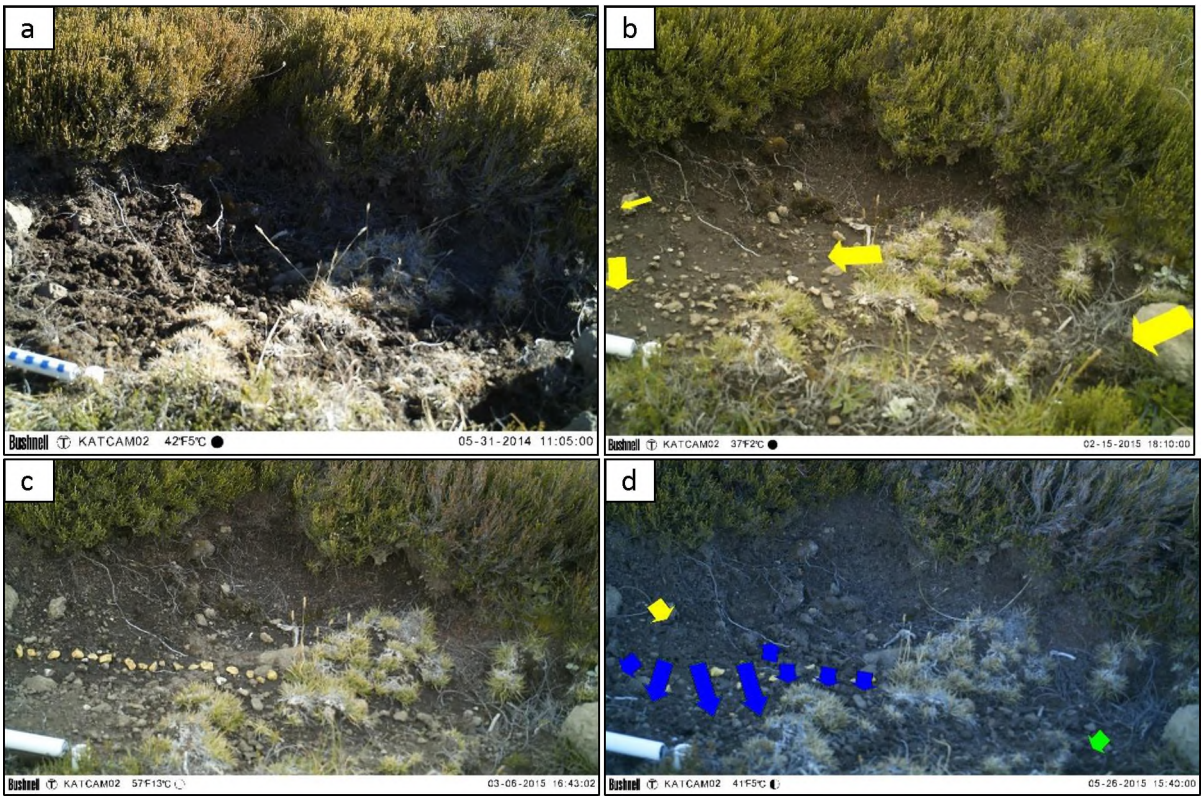

Figure 6.26. Long term displacement at Site 1. Frame a) and b) show displacement in significant features over nine months (May 2014 to February 2015), while Frame c) and d) show painted marker movement over three months (March to May 2015).

Although changes in the matrix of Site 1 were noticeable between Frame a) and b); and c) and d), measuring of displacement was not possible. The plastically deforming matrix makes comparison difficult as no point of reference are distinguishable between images. Some downslope deformation of the soil matrix is seen in the lower right of Frame d in Figure 6.26. However, the movement should be interpreted as a direction and not an absolute distance.

Figure 6.27. Image from early March with initial line of painted stones. The red polygon shows the area of painted stone propagation three months after the initial line was inserted.

The addition of painted stone markers, after the March 2015 downloading of data at Site 1, made measuring of sediment displacement of smaller particles more reliable. Before the painted markers, long term measurement of small stones was unreliable as identification of individual stones was difficult. After painted marker installation small stone movement was accurately discernible. The red polygon visible in Figure 6.27, shows the extent of marker propagation, three months after placement. Although long term displacement of small stones was not measurable for the full nine months, it is apparent from Figure 6.26 that the small stones class moves faster than large stones. However, analysis of the imagery from Site 1 enabled identification of the most impactful events on painted marker movement. Notable findings included substantial movement through non-frost related action. This will be further examined in section 6.4.

6.3.2 Site 2

Sediment displacement at Site 2 was comparably faster than Site 1. Movement distances of over 15 centimetres were measured from small clasts during the three-month study. Displacement distance is observably related to clast size as well as position on the slope surface. Movement of larger stones was seen to vary less compared to smaller stones. The three large stones measured in Figure 6.28b, moved an average of ca 4.5 to 5.5cm. Conversely, smaller particles from the same figure show a movement range of 1 to 16cm. Movement distance of the soil matrix over an extended period of time was difficult to measure, as points of reference for measuring were hard to assess between two images. The movement of the matrix in Figure 6.28 should only be interpreted as the movement direction and not as measured movement distance.

Similar to Site 1, Site 2 showed a marked portion of the surface displacement attained by processes not linking to needle ice (Section 6.4).

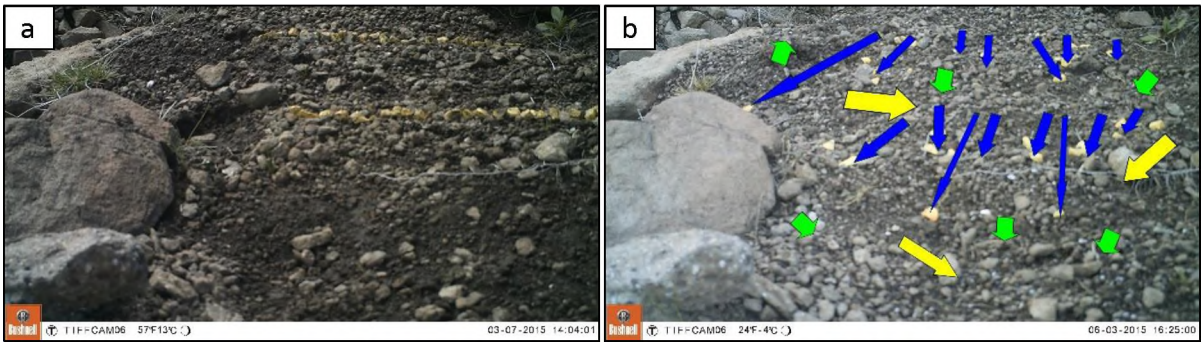

Figure 6.28. Long term displacement of surface material at Site 2 during the three-month study. Displacement of the soil matrix in Frame b) is to be considered as showing a direction and not displacement distance, as absolute distance was hard to quantify.

6.3.3 Site 3

Due to a positional change of the cameras as a result of the impact of weather and snow cover at Site 3, the viewing angle of the early and final images did not align. This made visual measurement of long term surface movement difficult and unreliable and are hence not included.

6.4 Sediment movement by non-frost related mechanisms

The positioning of painter markers at Site 1 and 2 in March of 2015 allowed for observations of marker movement during late South African summer. Sites 1 and 2 were positioned at close to 3000m.a.s.l., and freezing was a possibility even during summer. However, no sub-zero temperatures and no needle ice events were recorded at Site 1 or 2 before the 9th of April 2015, one month after painted marker installation in March. This allowed for ca one month's observation of painted marker movement without the influence of needle ice.

The following section shows visual evidence of surface clast displacement from Site 1 and 2 based on processes other than needle ice.

6.4.1 Rain

Although rain was noted on several days at both Site 1 and 2 over the one-month period, a visually measurable effect on clast movement was not observed. Rain was seen in some cases to smoothen the surface texture of the site by rain splash, slightly covering clasts in mud, but not producing any clast movement apart from slight changes in orientation. However, the erosive capacity of rain is suggested to be increased as a result of surface reworking by needle ice.

6.4.2 Hail

The effects of hail on surface particle displacement was noted at both Site 1 and Site 2. An observed single clast movement of ca 15cm was attributed to the effects of hail during the month without needle

ice at Site 2. Camera imagery captured surface movement from Site 1 and 2 during 4 and 3 hail events respectively. Results are displayed in Figure 6.29 and 6.30.

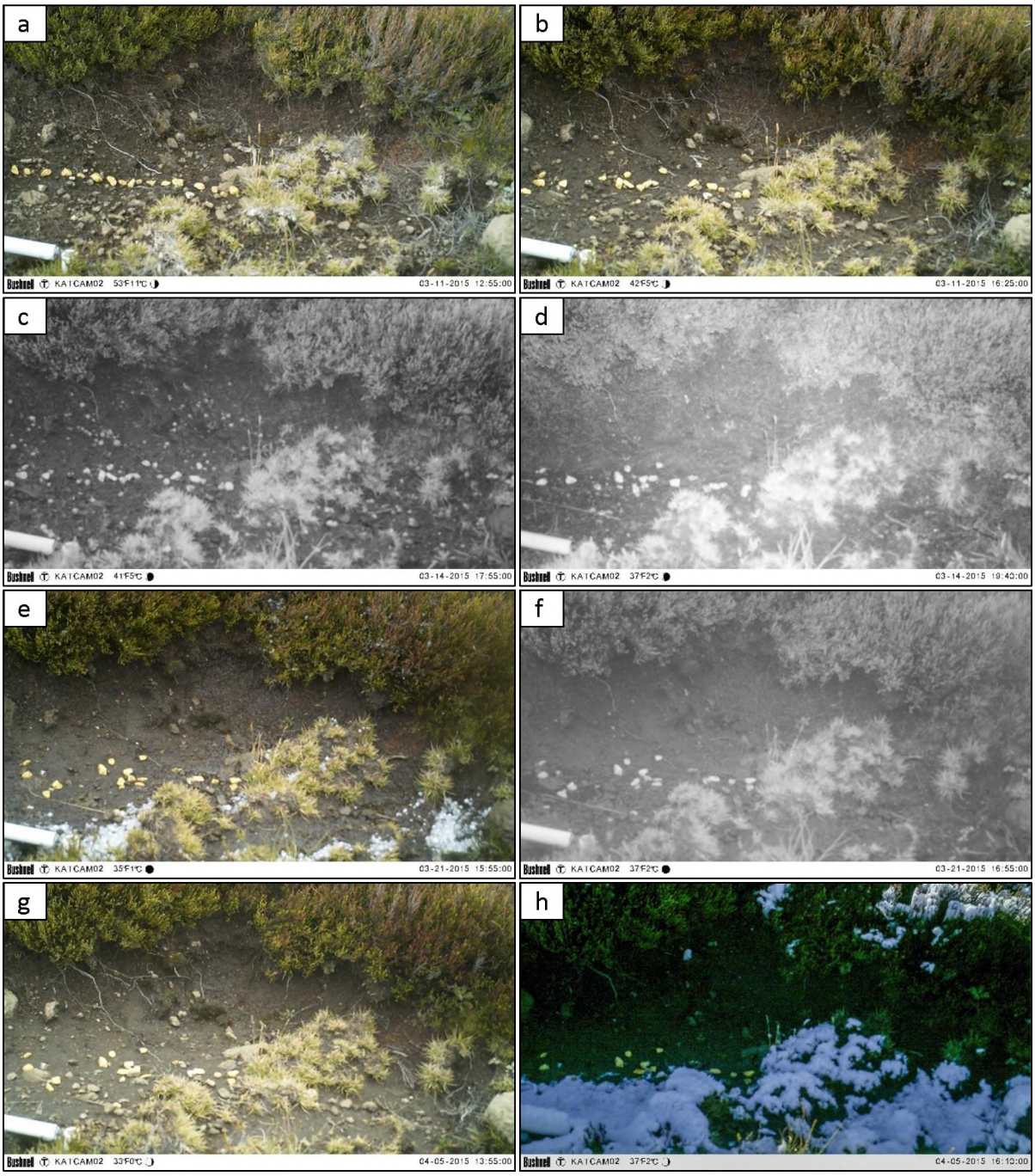

Figure 6.29. Painted marker displacement by hail over four events during March and April of 2015.

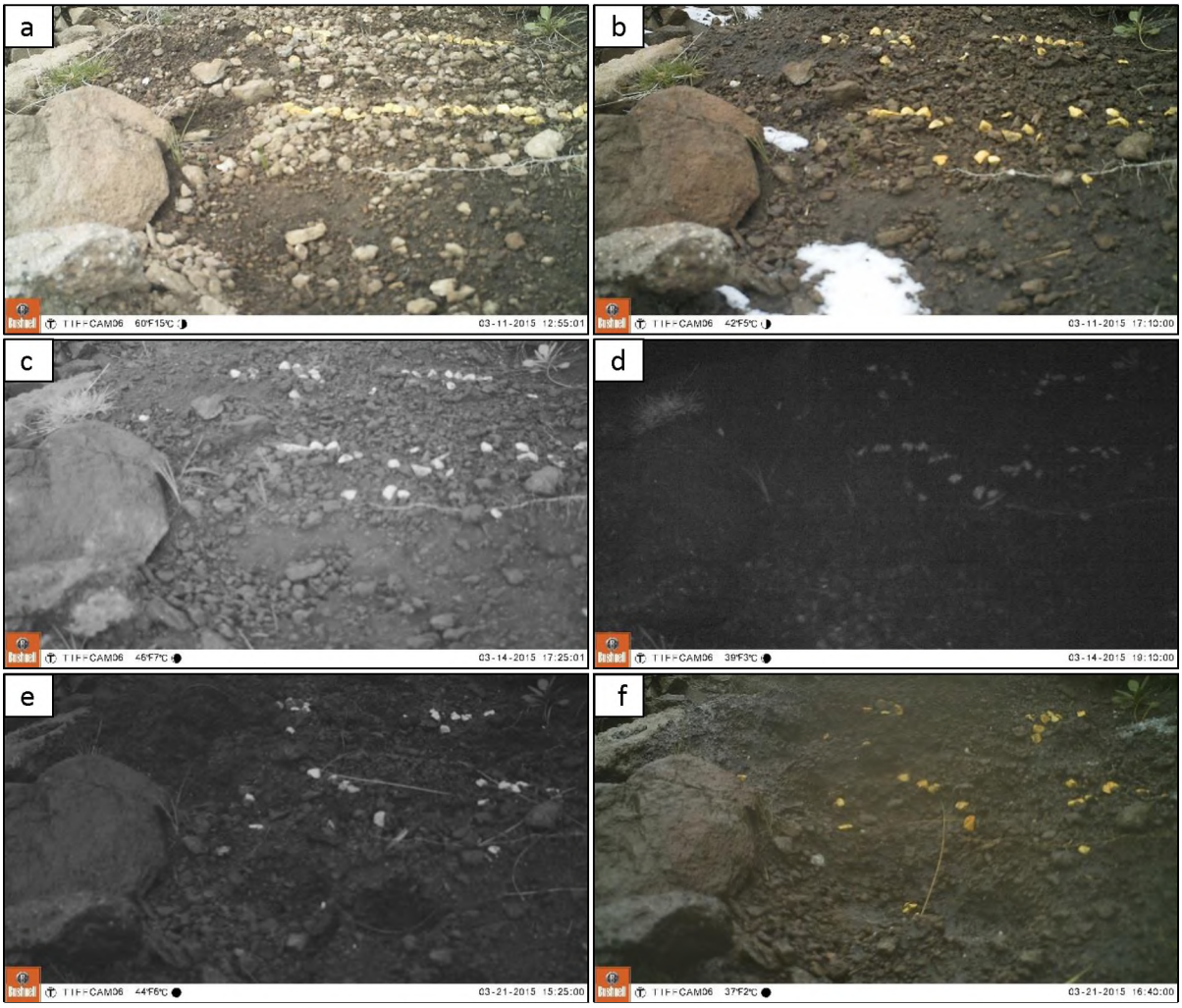

Figure 6.30. Painted marker displacement by hail four events during March 2015.

Painted marker displacement by hail is displayed in Frame a-h from Site 1, and in Frame a-f from Site 2 (Figure 6.29 and 6.30).

6.4.3 Animal influence

The study sites were influenced by humans and roaming animals, which, in some cases, were captured in the camera imagery. Site 1 was impacted by one event of human interference, while Site 2 displayed two events of animal influence during the three-month study period.

A person walked over the study area at Site 1, compacting ice needle during morning decay. Although, no quantifiable sediment movement from the foot was noted, compaction ca 2cm deep and changes of the surface environment were observable (Figure 6.31).

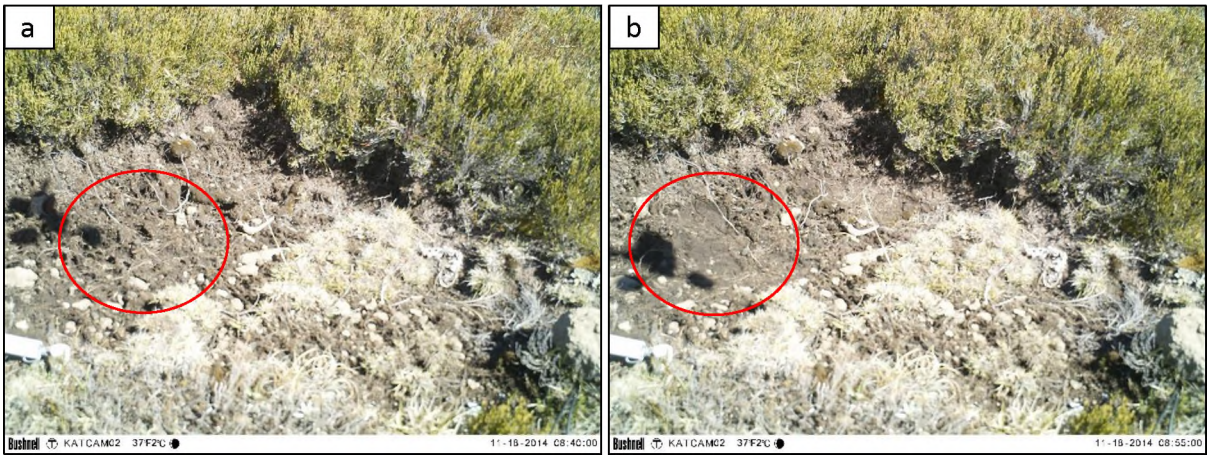

Figure 6.31. Foot-print compacting ice needles from Site 1 during March 2015.

Figure 6.32. Two events of sheep crossing the study area at Site 2, displacing surface material.

Two events of trampling by sheep is seen in to disrupt the surface of Site 2 in Figure 6.32, and one of the culprits was observed trampling at Site 2 in Figure 6.33.

Figure 6.33. Sheep standing at the surface of Site 2.

External factors contributing to sediment movement were visually significant. Total displacement of material by the effects of hail can be seen in Figure 6.29 and 6.36 from Site 1 and 6.30 and 6.37 from Site 2. Furthermore, total displacement during the full period with painted stones can be seen in Figure 6.34 and 6.35. Although the specific influence by animal trampling is hard to quantify, animal trampling was seen to burry clasts, thereby preventing influence from the effects of needle ice. Additionally, trampling of animals is suggested to be important in terrace formation and to initiate turf-exfoliation by needle ice (Pérez, 1993; Haussmann et al., 2009; Eriksson, 2011; Borg, 2012).

No animals were seen to influence surface displacement at Site3.

The following section compares sediment movement of the month without needle ice activity to that of sediment displacement seen from first needle ice influence on the 9th of April to the end of the study at Site 1 and 2.

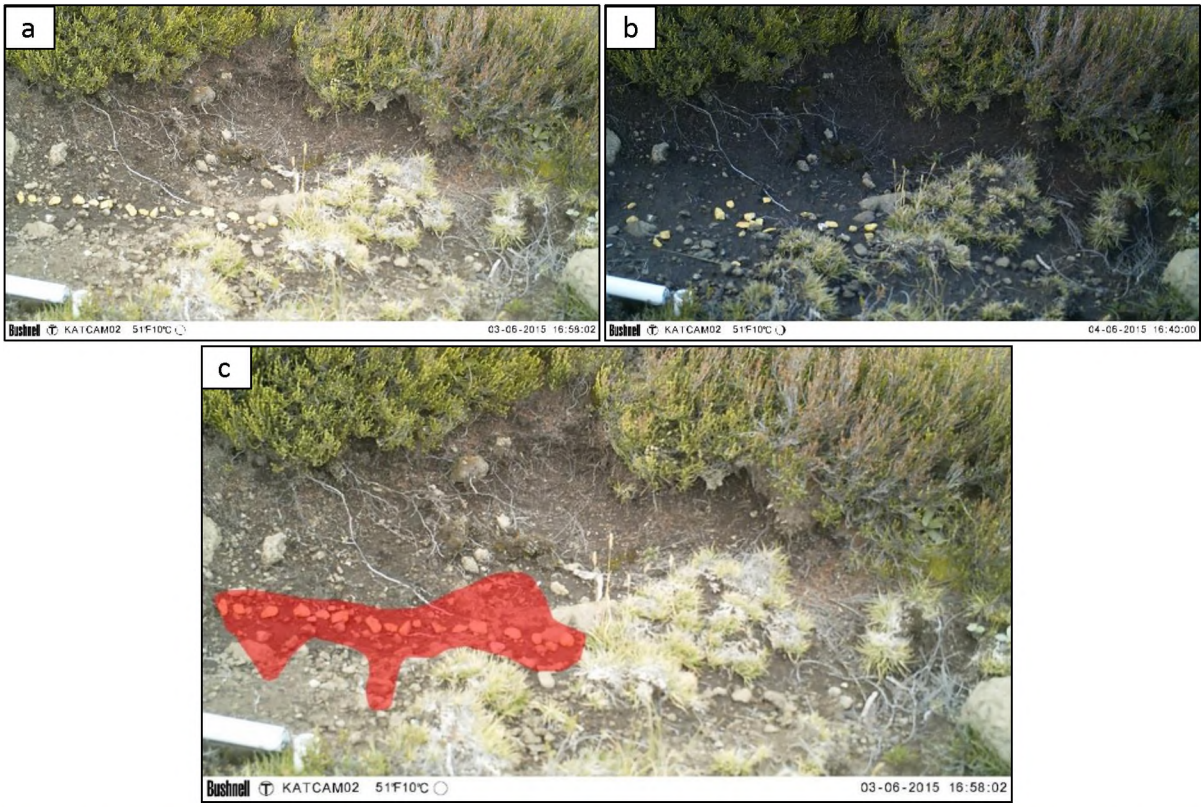

Figure 6.34. Frame a) and b) shows the initial and final displacement of non-needle ice related movement, while Frame c) shows the area of influence of painted marker movement compared to initial position from Site 1.

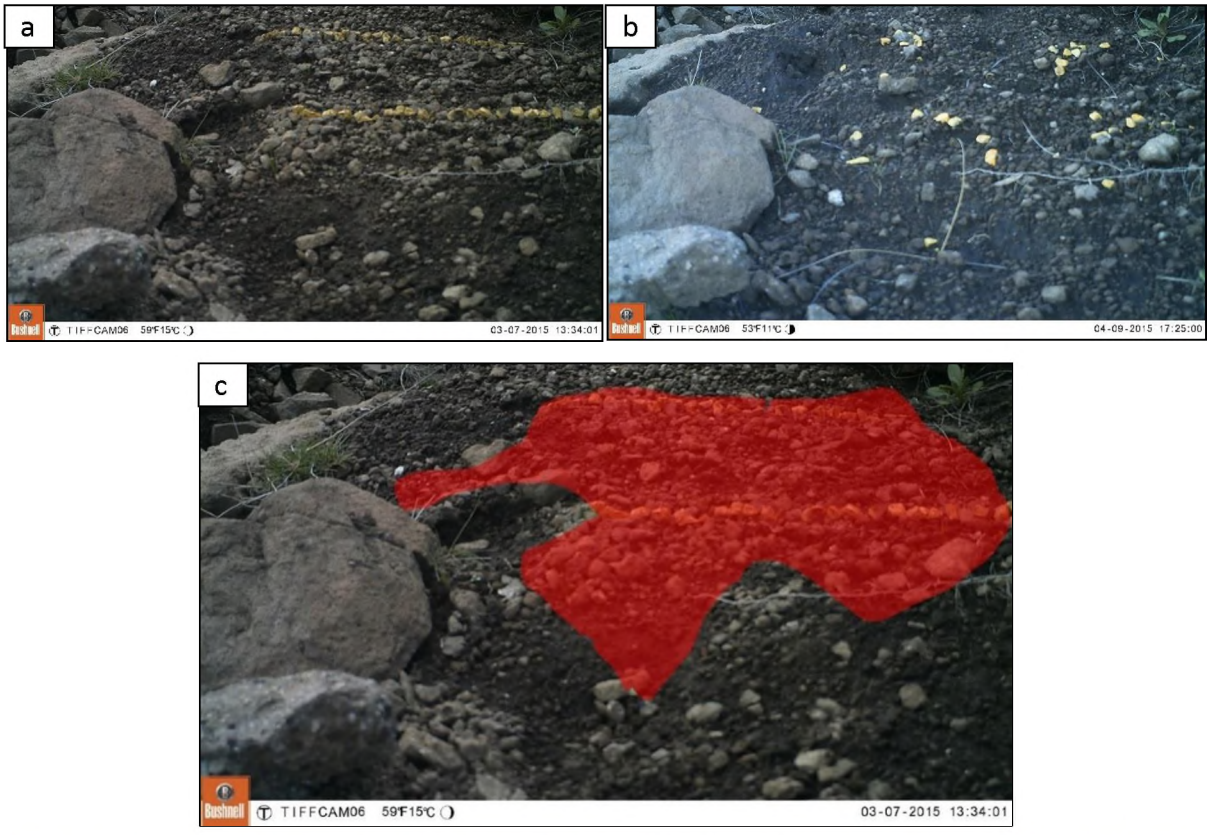

Figure 6.35. Frame a) and b) shows the initial and final displacement of non-needle ice related movement, while Frame c) shows the area of influence of painted marker movement compared to initial position from Site 2.

6.5 Differentiating movement generated by needle ice and non-needle ice events

Section 6.4 identified surface displacement by hail and animal influence was substantial. The two months following first needle ice observations on April 9 at Site 1 and Site 2 did not experience any hail or animal influence. As a comparison, the following section presents sediment displacement differences between the one month having impacts by hail and animal trampling and the two months of NISD.

6.5.1 Displacement at Site 1

Frame a-d in Figure 6.36 shows sediment displacement between the two periods of March 6 to April 8, [Frame a) and b)] and April 8 - June 3 [Frame c) and d)] of 2015. Four events of hail were seen to influence Site 1 between Frame a) and b) in Figure 6.29 (Section 6.4.2). Marked movement was only seen to influence small clasts, which were displaced between 1.5 and 5.5cm. Displacement occurred in a general downslope movement in all clasts except for one, which moved upslope. Most movement was seen from the centre left part of the painted marker line.

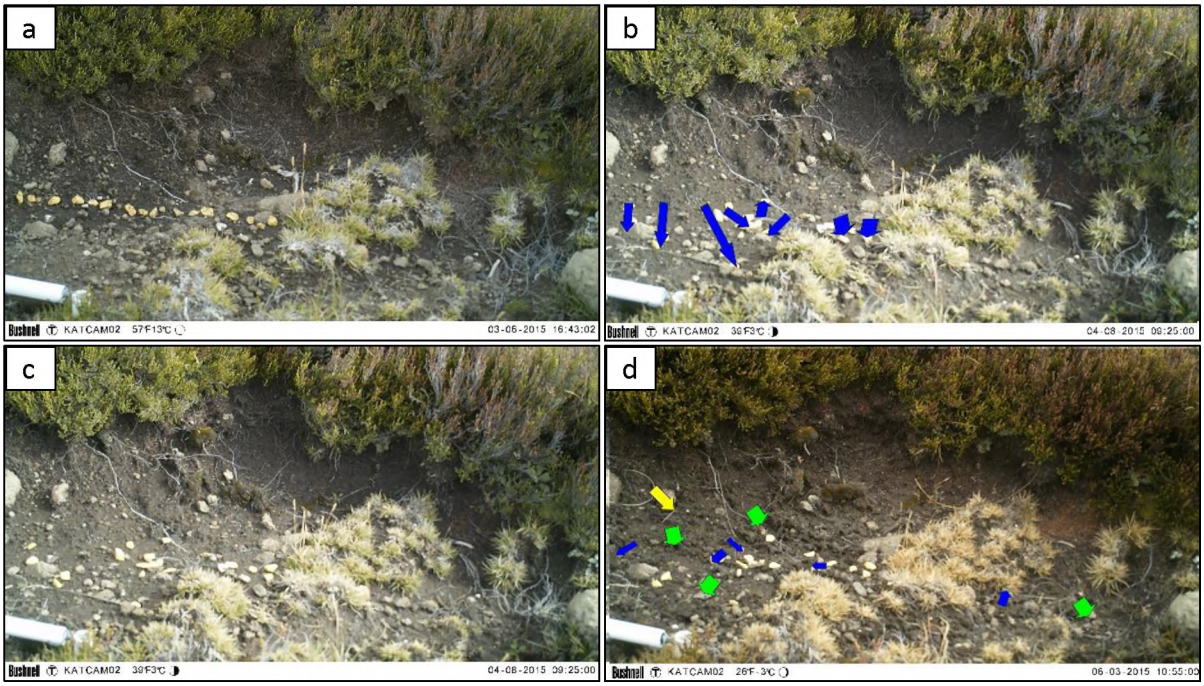

Figure 6.36. Frame a) and b) show displacement by four hail events, while Frame c) and d) shows NISD of 19 events post April 9 from Site 1.

Frame c) and d) display movement from Site 1 at the pre-initiation of needle ice growth after the warmest summer months. Frame c) shows disruption of the painted line by non-needle ice related processes and Frame d) shows displacement attributed only to NISD as no events of hail was seen from April 8 to June 3. Movement of surface material form needle ice is seen in Frame d) of Figure 6.36 to influence all material, regardless of clast size, although to different extent. One large stone is seen to

be moved ca 1cm while small clasts move between 1 and 1.5cm. Movement of the matrix is, as presented in Section 6.2 and 6.3, hard to quantify over longer time-spans, hence, the green arrows in Figure 6.35 should be interpreted as an indication of direction and not as displacement distance.

Comparing movement from four hail events and 19 needle events shows that hail movement induces more displacement of smaller clasts, while NISD influences surface movement of all particle sizes, although a shorter distance. The effect of hail displacement versus NISD will be discussed in Chapter 7.

6.5.2 Displacement at Site 2

Frame a) and b) in Figure 6.36 show sediment movement caused by three hail events and two events of animal trampling at Site 2. Similar to Site 1, Site 2 shows that hail events, displayed in Section 6.4.2, predominantly influence smaller clasts, while animal tramping, displayed in Section 6.4.3, influences all clasts sizes. One large stone is observed to be displaced ca 6cm by the trampling of a sheep. The trampling is additionally suggested to burrow clasts in the centre of the two painted marker lines, as many clasts disappear after the trampling events. Movement of most of the smaller clasts is attributed to hail displacement between Frame a) and b) in Figure 6.29. Movement of small clasts are measured between 1.5cm and 16cm.

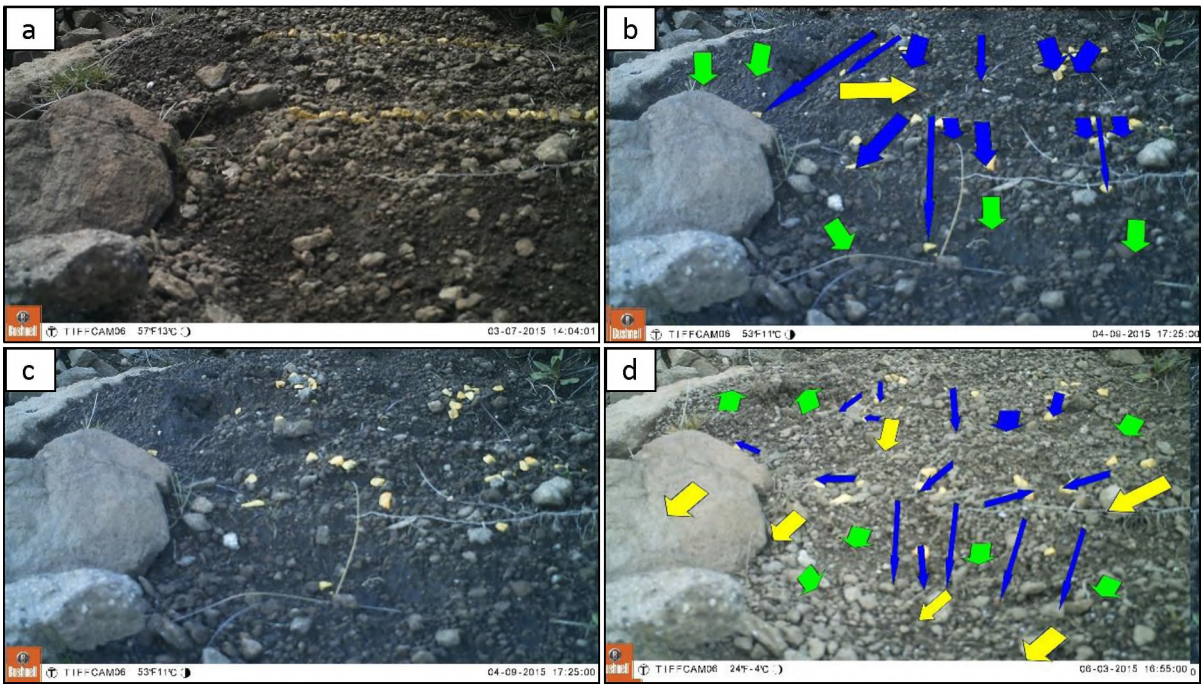

Figure 6.37. Frame a) and b) show displacement by three hail events and two events of animal trampling, while Frame c) and d) shows NISD of 22 events post April 9 from Site 2.

Displacement of the matrix is seen, however, the distance is, as previously noted, hard to quantify. The green arrows in Figure 6.36 are used to predominantly indicate direction and not distance.

Frame c) and d) in Figure 6.36 show sediment displacement over the 22 needle ice events at Site 2. Particles of all sizes are seen to be displaced in a range of directions at Site 2. Large stones are seen to displace between 2 and 5cm, with the very large stone on the left-hand part of the site displaying movement of ca 0.5-1cm. Small clasts movement is observed in a general downslope direction, however, a few clasts close to the top of the steeper part is seen to move upslope, related to low slope angles. The steep part of Site 2 (Figure 6.20) in Section 6.2.2.5 displayed small stones to move further at the steep parts. Movement of 5-6cm was measured from the steep part, while the rest of the study area showed movement of ca 1.5-4cm. The soil matrix is, similarly to Site 1, difficult to measure, however, the vector of movement can be seen. Most of the matrix is seen to displace downslope, although the top left part of Site 2 is seen to displace upslope, possibly due to less compaction after heave.

Comparing movement observed in Frame a-b and Frame c-d in Figure 6.36 shows that hail and animal trampling influences the surface to a greater degree than NISD over the three months studied. Hail is noted to impact smaller clasts while animal trampling influences surface material where the feet of the animal happens to land. Needle ice sediment movement was however seen to impact all surface material, although movement distance was seen to be increased in small stones compared to large stones, while the displacement of the matrix was hard to quantify.

6.6 Heaving of a very large stone

Heaving of a very large rock was observed in Video 11. Using a 3D mesh generated in PhotoScan® from the same camera imagery as the 3D surface models of Site 2 was created, the size the large rock heaved (marked by an X in Figure 6.37) was estimated at ca 38 x 30 x 15cm. The rocks sub-surface measurements were assumed to be consistent with the surface measurements, and with the use of a volumetric calculation using PhotoScan®, the rocks volume was calculated to be ca 8200 cm^3. Using a general Lesotho basalt density of 2,75g/cm^3 from Burley *et. al.* (1982), the rocks weight was estimated to be between 25 and 35kg, depending on the sub-surface measurements of the rock. Soil surrounding the rock was seen to be disturbed, which additionally suggests that the rock moves. The area influenced by suggested rock movement is visualized in Figure 6.38. Movement of this rock shows needle ice to displace clasts 10kg heavier than any previously documented in literature (Mackay and Mathews, 1974b).

Figure 6.38. The very large rock (X) position in the 3D surface plot and in imagery from Site 2.

Figure 6.39. Pushed sediment by rock movement due to needle ice heave. The area of influence highlighted in red in the left picture.

This concludes the result section of the thesis, the following chapters present the discussion, conclusions and avenues of future needle ice related research.

Chapter 7 – Discussion

Literature reviewed in Chapter 2 identified gaps in the current understanding of growth, decay, sediment transport rates and sediment transport mechanisms of needle ice. Gaps were related to a methodological inadequacy in i) confidently identifying the process of needle ice growth with simultaneous measurements, and ii) a lack of continuous long-term studies (months to years) at the same location. Without visual monitoring, results from environmental measurements may not relate to the specific process of needle ice. Visual identification of needle ice growth and mechanisms involved in needle ice sediment displacement is key in resolving the aims and objectives stated in Section 1.4. The methodology used in this study removes the uncertainties stated above and allows confidence in attributing processes to needle ice. Visual recording identified particle movement in increments of ca 5 minutes and not in increments of initial and final displacement over a period of months, which was identified as a weakness in reviewing literature in Chapter 2.

Analysis of sensor and image data in Chapter 5 and 6 resulted in previously undocumented observations on needle ice, including:

- Temperature exotherms during growth initiation;
- Observations on needle ice initiation depth;
- Documentation of the timing of the needle ice phenomenon;
- Visually observed mechanisms of needle ice sediment displacement.

Initially, the discussion will focus on the processes involved in needle ice growth and decay. This is followed by a discussion of sediment displacement rates and movement mechanisms as a consequence of growth and decay properties. Discussing growth and decay will naturally evolve to include sediment displacement and the mechanisms from which sediment transport results.

7.1 Criteria for needle ice growth

For accurate identification of environmental conditions (temperature, soil moisture and wind speeds) during needle ice initiation, growth and decay, evidence of each phase needed visual confirmation. In addition, examination of needle ice events with detailed environmental monitoring (5min interval) over a time-span of months allowed for identification of thresholds, extremes and averages of needle ice growth conditions as well as event duration. Linking visual observations and measured environmental data provided a level of certainty in deducing needle ice growth initiation temperature and timing.

As a point of departure for the analysis of needle ice growth initiation in Chapter 5, Outcalt's (1971a) publication suggested a surface temperature of -2°C needed for needle ice initiation to occur. In a more

recent publication by Nel and Boelhouwers (2014), empirical measurement of needle ice growth presents an estimate of initiation temperature at -0.2°C. Although Outcalt (1971a), Nel and Boelhouwers (2014) and several other publications (Chapter 2) show a set needle ice initiation temperature, results from this thesis display needle ice initiation to occur at a range of measured surface temperatures. Chapter 5 presents surface temperatures ranging from -2.0°C to 2.2°C at the time of needle ice initiation (Table 5.1, 5.4 and 5.7 in Chapter 5). Initial analysis suggests that local scale variability in environmental factors impact the threshold temperature for needle ice growth initiation. In addition, needle ice was observed to grow at *measured* surface temperatures above 0°C.

7.1.1 Temperature variability during needle ice growth initiation

Results presented in Table 5.1, 5.4 and 5.7 in Section 5.3 display a range of surface temperatures at which needle ice observably initiated. Surprisingly, a majority of events from Site 1 and 2, and 4 out of 15 at Site 3 displayed positive surface temperatures at the moment of needle ice initiation. Initially, this was thought to be attributed to sensor calibration error, however, sensors were calibrated using manufacturers specifications. Regardless of a potential sensor error, the error would not account for the 2.2°C above 0°C observed temperature during initiation (Section 4.3.4). Needle ice growing during positive surface temperatures initiated a search for possible explanations.

Fundamental physics explains that ice cannot grow in a natural environment at temperatures above zero degrees centigrade (Paterson, 1994; Rempel, 2007; Kozlowski, 2009). Therefore, ice needles were either not growing at the surface, or, temperatures at +10 and +0cm did not accurately portray the needle ice growth surface. Positive surface temperatures, which were recorded in 49 of the 65 events, with available measurements from the +0cm sensors during needle ice initiation, showed that the sensors used in this thesis were not recording temperatures at the right location of ice nucleation. Even when incorporating the accuracy (± 0.15°C) and resolution (0.02°C at 25°C) of the sensors, a majority (40 of 65) of events measured positive surface temperatures at initiation of growth (Section 4.3.4). Authors, including Branson *et.al. (*1996), Grab (2001) and Nel and Boelhouwers (2014), measured temperature at -1cm, as needle ice initiation was suggested to emanate below the surface. However, variability seen in Section 5.6, and aforementioned initiation temperatures suggest that the location of ice nucleation does not occur at a specific depth, rather, the point of nucleation varies within the near-surface soil column (this observation will be elaborated on later in the discussion). Another possible aspect of the measurement of positive surface temperature during needle ice growth was the loss of energy at an *active surface*.

Three energy exchanges between surface and air during cooling have been explained, namely: sensible heat flux, latent heat flux and radiative heat flux (Outcalt, 1971; Oke and Cleugh, 1987;

Paterson, 1994) (Section 2.1.4). To attain needle ice growth at positive air and ground temperatures, as seen in results from Section 5.3 and in Figure 5.27, it is suggested that the cooling of the ground surface is not by sensible heat exchange, but rather is dominated by radiative heat loss from the material surface. For example, Figure 5.37, 5.38 and 5.39 show how ice needles grow out of the substrate, while the substrate remains unfrozen. Personal observations by Boelhouwers (personal communication) from Marion Island and from Uppsala, Sweden, as well as laboratory experiments by Ozawa and Kinosita (1989) have indicated a similar growth environment. Such a needle ice growth environment would allow for air and ground temperatures to remain above 0°C while the energy removed by radiative loss permits freezing to take place only at the material surface. Such a surface is described by Oke (2002) as the *active surface*.

Apart from initiation at positive surface temperatures, several needle ice events showed growth initiating below 0°C (e.g. Table 5.1, 5.4 and 5.7). For ice nucleation to occur at temperatures below 0°C, the chemistry or physical surroundings of the water have to be altered (Beskow, 1935b; Paterson, 1994; Kozlowski, 2009; 2016). Kozlowski (2009) describes the phenomenon of supercooling (in this case only relating to water). Supercooling is the effect of water requiring temperatures below 0°C for ice to nucleate from liquid water. Solutes in the water can push the freezing temperature of water below 0°C but also pressure and the parent soil texture (esp. pore size distribution) can change water's freezing temperature (freezing point depression) (Beskow, 1935b; Outcalt, 1971; Rempel, 2007). Supercooling of soil water commonly occurs in water that is not chemically pure and restricted by spatial constraints (i.e. pore size) and decreases the nucleation temperature beyond that of the freezing point depression (Kozlowski, 2009; 2016). Supercooling of water can account for the negative surface temperatures measured at all three sites during needle ice initiation. In addition, a subsurface location of the freezing plane will also result in surface temperatures below 0°C at the time of initial ice nucleation (see below under 7.3).

Section 5.5 and Table 5.3, 5.6 and 5.9 show that measured parameters change before and after the moment of needle ice initiation. Temperature and soil moisture measurements followed a change in trend from growth initiation to decay initiation. Table 5.12, 5.13 and 5.14 show a majority of soil moisture, air, surface and ground temperatures increasing from before to after the moment of needle ice initiation. Resulting increases in temperature and soil moisture, 10 and 60 minutes after the initiation of needle ice growth, relate to the effect of latent heat release and moisture migration, which will be expanded on later in the discussion.

Table 5.3, 5.6 and 5.9 from Section 5.3 show environmental changes from the onset of needle ice growth to initiation of needle ice decay. The trends shown in these tables illustrate a general lowering

of soil moisture levels, as well as surface and ground temperatures, while a vast majority of air temperatures increased. Results from Section 5.3 and 5.5 show needle ice growth to desiccate the ground at both -2.5cm and -5cm and that most melting occurs due to increases in air temperature at initiation of decay.

7.1.2 Soil moisture controls on needle ice growth

To explain increases in soil moisture after the moment of needle ice initiation and the desiccation of the soil measured at onset of decay, results from Section 5.3 are discussed below. Moisture measurements at -2.5cm and -5cm depth display available water for freezing, as well as indicating water migration in the soil column at the three study sites. Although the logger setup was identical at all three sites, the different environments showed great moisture variability between them, even though Site 1 and 2 were located in close proximity to one another.

Site 1 was the wettest, followed by Site 2 and lastly Site 3. Soil moisture variability at Site 1 and 2 was similar, while Site 3 showed much less variation in soil moisture content (Figure 5.23, 5.28 and 5.33 in Chapter 5). The variation observed was suggested to be induced by the different climatic settings and surface textures of the two locations (Chapter 3). However, some processes were notably similar. Soil moisture content at both -2.5cm and 5cm was observed to increase after freeze initiation, and subsequently decrease during needle ice growth until the onset of melt at all sites (Table 5.12, 5.13 and 5.14). Increasing soil moisture was evident in data measured 10 and 60 minutes after initiation of growth from all sites, and is presented in Section 5.5. The effect was seen to be more pronounced in the -5cm sensor compared to the sensor closer to the surface, suggesting that during initial freeze, soil water migrated towards the freezing front where it undergoes a phase change to ice (Rempel, 2007). The migration of water towards the freezing front was evident in increasing soil moisture levels just after ice initiation, possibly relating to the strongest soil moisture gradient just after freezing (Section 5.5). With continued needle ice growth, the effect diminished as less water in the soil column was available for upward capillary rise, resulting in a weaker soil moisture gradient.

While the onset of needle ice growth and initiation of decay at Sites 1 and 2, coincided with soil moisture levels decreasing at -2.5 and -5cm, the opposite was observed at -2.5cm depth at Site 3, where soil moisture generally increased slightly during needle ice growth. Differences in moisture dynamics between Site 1 and 2 and Site 3, are suggested to be related to textural and environmental controls. Needle ice development at Site 1 and 2 stopped when soil moisture was limited at the -5cm sensor (Table 5.14 and 5.15) while at Site 3 no limitation of growth was observed, even when no soil moisture was measurable (Figure 5.26). It is suggested that the strong positive soil moisture correlation between wind and soil moisture seen in Section 5.7.3 indicates that a portion of the moisture supply

at Site 3 is a result of atmospheric moisture input. Personal observations and camera images from Marion Island strengthen this assumption, as mist and clouds often occur at the study site (Boelhouwers et al., 2003; Le Roux and McGeoch, 2008).

7.1.3 Soil texture controls on needle ice growth

Section 2.1.3 presents the effect of soil texture on the transport and retainability of moisture within the soil column. Beskow (1935) and Meentemeyer and Zippin (1981) showed that needle ice required fines of ca 15% to supply moisture to the freezing front. Results from Section 5.5 displayed Site 3 to exhibit a markedly lower proportion of fines (particle sizes of less than 0.064mm), when compared to Site 1 and 2. Site 3 had ca 6% of the particle size fraction less than 0.064mm, compared to Site 1 and 2 which have 17% and 22%. It is argued that at Site 3 there is a greater ability of the soil to retain and to transport water to the freezing front than at Site 1 and 2. Section 3.2.2 and 3.1.2 presented that annual moisture input was markedly higher on Marion than at Tiffindell. It is suggested that the coarser material in the top soil at Site 3 (Section 3.3.3) is unable to transport sufficient moisture to the freezing front causing needle ice to emerge from the boundary between the coarser and the underlying finer material (Figure 5.44, 5.46 and 5.47).

The differences in soil moisture content between the study locations is supported by variances in grain size distribution and moisture values recorded at different depths. As discussed above, the -2.5cm sensors at Sites 1 and 2 recorded higher soil moisture values than at 5cm depth when needle ice was observed to grow (Table 5.1, 5.4). Conversely, at Site 3 higher soil moisture values were recorded at -5cm (Table 5.7). Observations of the stratified surface material, with coarser top soil (Section 3.2), suggests a lower ability to retain moisture at -2.5cm compared to -5cm at Site 3. The strong winds and loosely packed material at Site 3 is attributed to aeolian processes removing the finer material as well as upheaval by needle ice action. Figure 3.12 from Section 3.3.2 and Figure 5.44, 5.46, 5.47 from Section 5.4.3 show needle ice heaving soil particles, with little fine material present above the denser soil layer at ca 5-10cm depth. Although Site 3's soil moisture sensor was not positioned at the location shown in Figure 3.12, a similar sub-surface layering, with densely packed fine material overlain by coarser clasts, was present at Site 3. The limited soil moisture holding capacity of the upper-most soil at Site 3 supports observations of differences in soil moisture dynamics between Site 1 and 2 and Site 3, and is suggested to impact needle ice growth location in the soil column as well as sediment heave.

7.1.4 Conditions without needle ice

A connection between soil moisture availability and the growth of needle ice was seen by examining non-growth events in Section 5.8. Measured average soil moisture levels at -2.5cm and -5cm were

4.5% and 13.1% lower for Site 1 and 2.5% and 3.2% for Site 2 for non-growth events compared to average values measured on needle ice growth days. Desiccation was enhanced at the -5cm sensor, which displayed one third of average soil moisture levels during non-growth events from Site 1, and half of the average soil moisture recorded at Site 2.

Soil moisture measurements at Site 3 did not reflect the perennially wet conditions observed at the study site. Site 3 was expected to have a limitless supply of moisture, which was not reflected in the measurements. Both at -2.5cm and -5cm the average soil moisture levels during needle ice events were below the 15% threshold suggested by Branson *et. al.* (1996) and 16% suggested by Meentemeyer and Zippin (1981) for growth. However, needle ice was observed to grow during all periods where the ground temperature dropped below 0°C and when no snow cover was observed. The -2.5 and -5cm sensors are suggested to be located in material with limited moisture transport capacity or that Site 3 is partially supplied by meteoric water.

Results from Section 5.8 indicate that low soil moisture levels are responsible for needle ice not being recorded, despite temperatures being conducive. Table 5.20 and 5.21 display environmental conditions on days where needle ice was observed and days where this was not the case. The importance of available soil moisture for needle ice growth was further established upon analysis in Section 5.4. Notable temperature spikes, or exotherms, were recorded when needle ice growth was observed; these observations are discussed below.

7.2 Latent heat release and zero curtain effects

Analysis of the temperature records from all three study sites showed notable short-term increases in temperature at the onset of most of the identified needle ice events (Figure 5.23, 5.27 and 5.31). The thermal spike most often occurred during the initiation phase of a needle ice event and was followed by a distinct change in the rate of cooling. These observations are explained by building on the previously discussed supercooling of soil water (Section 7.1.1) at both Tiffindell and Marion Island, assuming that sufficient soil moisture exists for the growth of needle ice (Section 7.1.2). The temperature 'spikes' are interpreted as *exotherms* measured in close temporal proximity to the moment of needle ice initiation. Arakawa (1966), Outcalt (1971), Outcalt *et. al.* (1990), Paterson (1994), Rempel (2007) and Kozlowski (2009) explain a release of energy occurring when liquid water undergoes a phase shift into ice. Eighty times as much energy is released when 1g of water at 0°C changes to 1g of ice, when compared to 1g of water at 2°C water decreases its temperature to 1°C (Paterson, 1994). Kozlowski (2009) describes the effects of supercooling and latent heat release (Figure 7.1). The temperature exotherms discussed in Section 5.4 from Chapter 5 occur when supercooled water releases a pulse of latent heat at the initiation of needle ice growth. The initial release consists

of more energy than the cooling from sensible and radiative heat combined, at the surface. Hence, temperatures increase, or spike, in response to the initial phase change. Subsequent to the initial latent heat release, surface energy is balanced by loss of energy from sensible and radiative heat and input of energy from latent heat released during phase transition of water at the base of emerging needle ice. This balance determines the cooling or heating of the soil or a potential thermal equilibrium (Outcalt et al., 1990; Paterson, 1994; Rempel, 2007; Kozlowski, 2009, 2016).

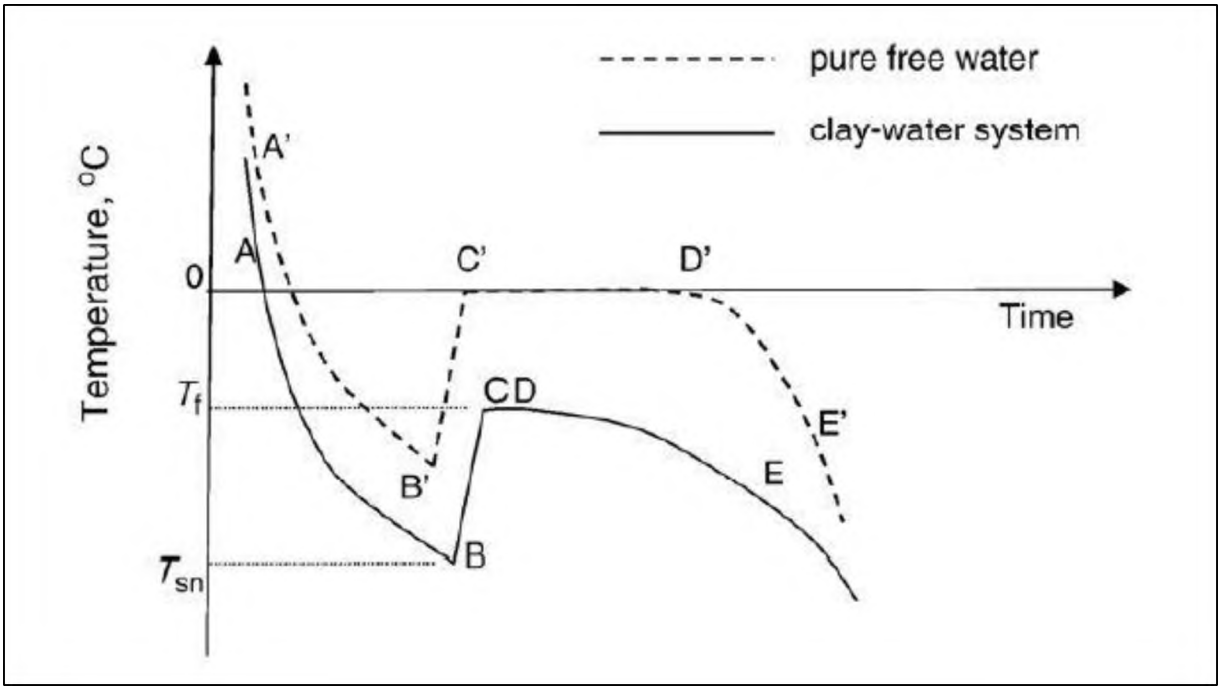

Figure 7.1. Supercooling and latent heat release spike. T_{sn} indicates the temperature of supercooled ice nucleation and T_f the freezing point of the specific water system. The latent heat release spike is the amount of energy released from T_{sn} to T_f. (Kozlowski, 2009). Included with permission from Elsevier License (Feb 7, 2016)

A thermal equilibrium, or what referred to as a "zero-curtain effect" is often presented for discussions of seasonal regimes (Outcalt et al., 1990; Sawagaki, 1995; Hall, 2004; Matsuoka, 2014). The term may not be fitting when describing needle ice on a short time scale of hours, as several periods of thermal equilibrium and thermal non-equilibrium are seen to occur within a single night of needle ice growth (Figure 5.25, 5.29 and 5.35). Results from Section 5.4 and 5.9 show changes in the balance of energy output and energy input to the system controlling cooling, warming or acting in thermal equilibrium.

The single event studied at Site 3 in Section 5.9.3 shows a situation where the surface cooling rate and the latent heat release from the ground were balanced. Measurements displayed in Figure 5.74 show the ground temperatures measured by all four sensors to decrease to 0°C. However, the -2.5cm and -5cm sensors stayed at 0°C for up to 12 hours until their temperature eventually continues to decline (Figure 5.75). It is suggested that this thermal equilibrium is explained by continuous moisture

availability. Ground temperatures at -2.5cm and -5cm only continue to decrease when insufficient soil moisture was available for latent heat release to counteract surface radiative and convective heat loss. The deeper -7.5cm and -10cm temperatures sensors decline to 0°C after the shallower sensors, however, they stay at 0°C for the remainder of the event. This suggests that the deeper sensors at Site 3 were not influenced by moisture starvation and latent heat release continuously counter-balanced surface cooling.

Temperature exotherms resulting from latent heat release are seen in several of the graphed data for needle ice events in Section 5.4 and Section 5.9 (Figure 5.23, 5.27, 5.31, 5.68 and 5.70). Observations of temperature data from the ground sensors during the event displayed in Figure 5.69 shows the exotherm (Figure 5.67) to be visible in the data at all depths. It is, however, difficult to attribute these exotherms to latent heat by phase change at deeper levels, or by energy transport from the surface by heat conductivity as energy migrates within the soil. Exotherms observed in surface temperature measurements at above 0°C can be attributed to latent heat conduction to the surface sensor during phase change at the freezing front, and may not reflect the temperature of ice nucleation (Ozawa and Kinosita, 1989; Kozlowski, 2009).

Latent heat release and soil moisture availability are obviously strongly interconnected. The quantity of soil moisture available may in addition influence the depth of needle ice growth. The depth of needle ice initiation was briefly discussed in Section 7.1.1, but will be further examined below.

7.3 Depth of needle ice growth

Section 5.6 presented a visual analysis of camera imagery for identified needle ice events with different growth depths. Needle ice events were observed to have ice needles growing at the surface as well as beneath the ground. Events with shallow needle ice allowed for visual identification of ice needles, while deeper growth events only displayed the effects of heaving by needle ice or other forms of segregation ice. Although no actual ice needles could be visually identified in the deeper events, Videos 6, 12 and 17 strongly indicate the growth of ice needles.

Upon identification of differing depths of needle ice growth, the role of temperature and soil moisture on the depth of segregation ice development was investigated. Several of the needle ice events presented in Section 5.4 show latent heat release exotherms at needle ice initiation and a subsequent change in cooling rate. The same figures also show needle ice initiation and the exotherm occurring simultaneously (Section 5.4). However, some events show a time-gap between the initial change in cooling rate and visual identification of needle ice growth (Figure 5.25, 5.29 and 5.31). None of these events show needle ice at the surface, suggesting a deeper freezing plane. As an example, the event presented in Figure 5.28 shows that several hours past after the surface temperature falls

below 0°C, before visual identification of needle ice growth followed. It is suggested that during this time, limited supply or connectivity of soil moisture to the surface allowed the freezing front to descend further into the soil column. The limited soil moisture that is available *in situ* does not create ice needles but instead freezes as pore ice, which is visible in the imagery of the event in Figure 5.29 (Figure 7.2)

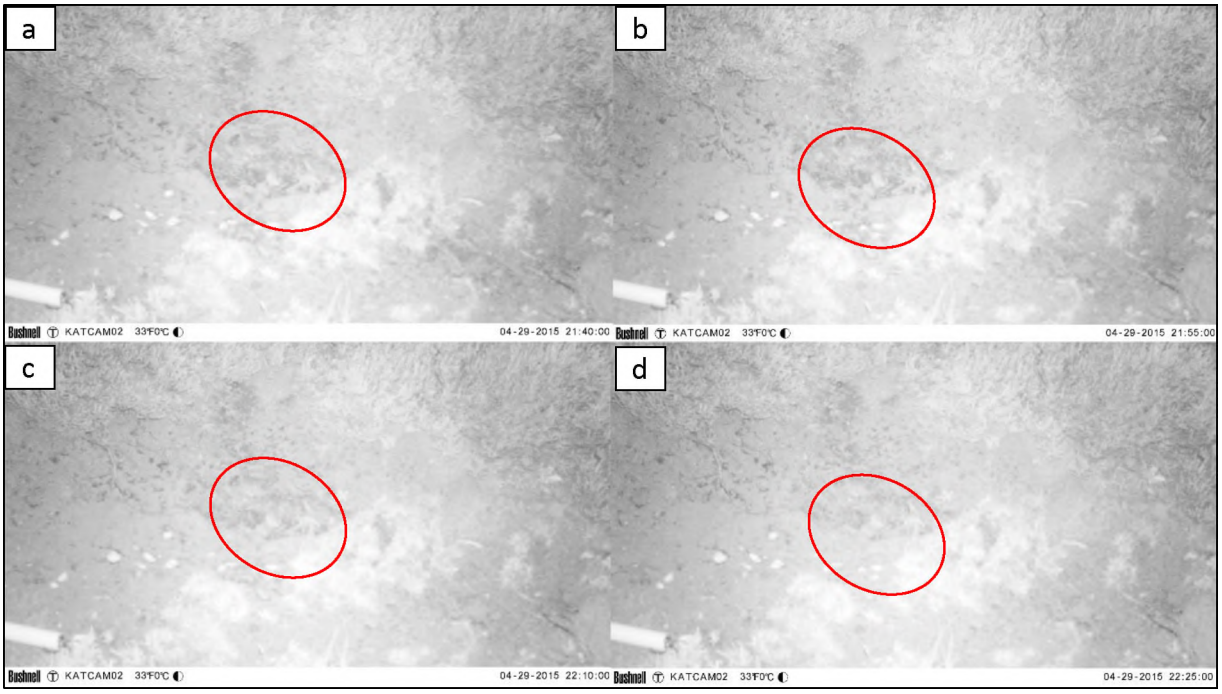

Figure 7.2. Surface freezing of pore ice over 45 minutes from Frame a-d with no observable needle ice growth. The red circles helps indicate the area of freezing, as the infrared image quality is poor.

At Site 3, shallow needle ice growth was observed. It is also clear that the coarse material at the surface of Site 3 is not prone to needle ice growth. Hence, needle ice initiates at the boundary between the coarser top material and the finer material at 5-10cm depth (Figure 5.44, 5.46, 5.47). In summary, the time delay between the start of surface temperatures reaching freezing point and visual heave by segregation ice growth is explained by the time required for the freezing plane to reach the depth where sustained ice nucleation is possible.

7.4 Timing of needle ice growth and decay initiation

Section 5.7 presented results on the timing of needle ice growth initiation, needle ice decay initiation and compares these moments to the moment in time where surface temperatures reach 0°C at the start and end of the freezing event. Even though later analysis shows that the initiation of needle ice occurs when the ground surface ranges between -2.0°C to 2.2°C, (see explanations above) the results from the timing analysis still provided useful outcomes. The premise for the analysis was the discrepancy in time between visual identification of needle ice growth initiation and the moment in

time when surface temperatures reached 0°C. This discrepancy was termed Image Logger Discrepancy (ILD). ILD could be positive, meaning visual identification of needle ice occurred after surface temperatures became 0°C, or *vice versa*.

Figure 5.47-5.62 from Section 5.7 display both growth and melt times for Site 1, 2 and 3. The initiation of needle ice growth and decay occurred both before and after visual observation (Tables 5.16 and 5.17). The frequency distribution of positive versus negative ILDs indicates it is more common for visual identification of needle ice initiation to occur after surface temperatures dropped below 0°C: 35 of 43, 9 of 14 and 13 of 15 events with measurable ILD from Site 1,2 and 3 showing positive ILD respectively (Figure 5.48, 5.53 and 5.58). Table 5.15 to 5.18 present data on the timing of growth and decay initiation, event duration as well as timing of needle ice growth and decay events in relation to sunset and sunrise. However, due to the fractured dataset it is difficult to draw conclusions from the data.

The following discussion will focus on results presented in Chapter 6. Mechanisms of needle ice growth and rates of sediment displacement will be the main focus in addition to non-needle ice related displacement, needle ices impact on vegetation and patterned ground formation.

7.5 Mechanisms of needle ice sediment movement

Using camera imagery to observe needle ice initiation and movement was, at the time of conception, a novel methodology. However, both Matsuoka (2014) and Ueno et al. (2015) recently published on long-term visual monitoring of frost processes from Japan. Ueno et al. (2015) discusses the relationship between deforestation and needle ice activity, using high-frequency visual monitoring, while Matsuoka (2014) focuses on longer-term surface and ground movement by periglacial processes.

The proposed sediment movement mechanisms in the literature (Chapter 2) are heaving and resettling, toppling, rolling, sliding and bouncing. Observations of these mechanisms are often descriptive in nature. Aims for this thesis include to empirically observe needle ice sediment movement mechanisms. Environmental parameters discussed in the previous sections focus on temperature, soil moisture and the related physics and chemistry of needle ice growth, while the following section focuses on the physical aspects of the study site, and how they affect needle ice sediment displacement.

A total of 106 unique needle ice events were captured from the three study sites between 2014-2015 (Table 9.2 in Appendix A). Imagery was used for observations of surface movement at an interval of 15 minutes, identifying displacement mechanisms. Analysis of 82 of these 106 needle ice events

resulted in identification of three needle ice sediment displacement mechanisms. These mechanisms are heaving and resettling, toppling and rolling.

7.5.1 Displacement by heaving and resettling

Displacement by heaving and resettling was the most frequent movement mechanism, observed in all 82 events. Heave was seen initiating at the freezing front, producing freezing by radiative heat loss at the active surface and at varying depths. The location of ice nucleation influences heaving of surface material, which was observed in the camera imagery. Surficial heaving was seen to affect small stones at the surface, while deeper-based heaving moved the whole soil column, including the matrix. Section 6.2 presents the size and type of clast heaved depending on the mechanism of heaving, ultimately affecting material displacement.

7.5.2 Displacement by toppling

Toppling of ice needles was seen to be influenced by heave height and the local slope angle. Local slope angles were variable within the study sites, and toppling was seen to depend on these small-scale changes in slope angle. Video 11 shows slope angles affecting the trajectory of toppling ice needles. At low slope angles toppling was seen to occur in an almost random direction. Observations showed that small scale topographical differences at low slope angles influenced toppling direction of ice needles to a similar degree as the general slope angle of the study site. The opposite was seen in steeper parts of the study sites. Steep (ca 20-25°) micro-slopes showed a tendency for downslope movement by toppling along the maximum local gradient. In addition, such slopes were seen to generate additional sediment displacement. Although few clasts were observed to move distances greater than the height of the ice needle, on the steepest micro gradients, toppling was observed to initiate further movement by rolling in a single case each at Site 2 and Site 3.

7.5.3 Displacement by rolling

Rolling was suggested by Pérez (1988), Mackay and Mathews (1974a), Matsuoka (1998) and Noguchi et. al. (1987) to be a significant movement mechanism in needle ice related sediment displacement. Results from Chapter 5 and 6, do not support this claim for the sites investigated for this study. Rolling was only seen to occur on rounded clasts in two of the 82 needle ice events. However, the added movement measured at Site 2, showed rolling markedly increases displacement distance (displacement of 5.5cm was noted from a single event in Video 10). Based on conditions at Site 2, both clast size and morphology are suggested to impact the rolling capabilities of particles. Sediment movement was often seen to be diminished when a single ice needle was halted by surrounding ice needle clusters during toppling. This effect is also suggested to impact rolling of clasts after toppling.

Size of the clast was suggested to impact the ability to roll, as kinetic energy in larger particles allows for rolling to break through surrounding clasts. Only round to semi-round rocks were seen to roll.

7.5.4 Displacement controls

Slope angle has long been identified as a central control on needle ice sediment displacement (Von Richthofen, 1901), with greater sediment displacement on steeper slope angles (Higashi and Corte, 1971; Mackay and Mathews, 1974; Holness,2001, Matsuoka, 2005). Results from Chapter 6 specifically showed the greatest displacement at Site 2 at steeper slope angles. However, locally steeper slopes (discussed above) produced greater displacement at all three sites. Observations from the 82 needle ice events showed heave and resettling as the dominant sediment displacement mechanism. Displacement by toppling and rolling was more frequent at steeper local-scale (sub-1m) slope angles. Mechanisms of toppling and rolling were also seen to occur during certain environmental conditions and clast physical aspects. Toppling was only seen to occur when ice needles heaved more than ca 1.5cm. Areas of enhanced heaving were most often the locations of toppling, which coincided with high soil moisture contents. Toppling was observed at Site 1, close to the upper margin and at Site 3 in depressions. The mechanism of toppling at Site 2 was seen to be the dominant displacement mechanism during two needle ice events (Video 10 and 11). All mechanisms observed to move sediment displayed a larger movement distance at steeper slope angles. It was seen in Section 6.1 that during very cold conditions, (ca -6°C) the surface sediment layer froze solid. This freezing observably stabilized the surface and in some events hindered ice needles from toppling (Video 5). During such events, only heaving and resettling was seen to be active, producing little surface displacement. The effect of stabilization by freezing was most visible in Site 1 and 3, and less so in Site 2. From visual inspection, it is suggested that the stabilizing effect cannot hinder ice needles from toppling at very steep slope angles (>25°). Toppling produce displacement distances similar to that proposed by Lawler (1993, Figure 14.d, p104).

In addition to heaving and resettling, and toppling, the rolling of clasts was observed at Sites 2 and 3. Although only two clasts were observed to roll, both displayed similar physical parameters. Only spherical to semi-spherical clasts were observed to roll. The mechanism of rolling was seen to occur in clasts that had been destabilized by heaving, and subsequent to melt, rolled. It seems reasonable to suggest that clast shape places an important role in facilitating or restricting rolling movement as a secondary component sediment displacement during needle ice decay. It is proposed that in an area with generally spherical clast shape, such as in fluvial or glacio-fluvial material, the influence the rolling mechanisms on needle ice sediment displacement would be enhanced (e.g. Pérez, 1992).

Slope angle is suggested to impact more than one aspect of needle ice sediment displacement. In addition to enhancing displacement by the heaving and resettling mechanism, additional mechanisms were more frequently observed at steeper slope angles. Results from Section 6.1 show the significance of local environmental parameters during needle ice sediment displacement.

7.5.5 Other mechanisms of needle ice sediment movement

In addition to heaving, toppling, and rolling, sliding, bouncing and tumbling are suggested to be active displacement mechanism in needle ice active environments (Von Richthofen, 1901; Deckert, 1913; Gradwell, 1955; Troll, 1944; Soons and Greenland, 1970; Washburn, 1970; Mackay and Mathews, 1974; Meentemeyer and Zippin, 1980; Pérez, 1987; Lawler, 1989, 1993, Matsuoka, 1998, 2005). During toppling of ice needles in Video 10, 11 and 17, the supported clasts were observed to fall and hit neighbouring ice needles. The effect produced a "cascade" of toppling. In addition, although not visible in the imagery due to the image interval being too long (15min), it is suggested that toppling clasts produce bouncing movement (tumbling), similar to saltation, during melt. However, no evidence of this process was captured. No sliding was observed at any of the three sites.

In summary, the mechanisms of movement by needle ice showed that heaving and resettling produces the primary movement, while toppling and rolling are possible secondary movements depending on heave height, slope angle, freezing intensity and clast morphology. Observations discussed in Section 6.1.3 showed an additional factor influencing needle ice displacement distance, which was clast size. Clast size's influence on displacement mechanisms will subsequently be discussed.

7.5.6 Intra-site growth variability

At all three study sites, a tendency for non-homogenous needle ice growth was observed over the study site surface. Evident in Figures 6.1, 6.2 and 6.3 are portions of each study site that display enhanced needle ice growth. These sub-areas were located at the margins of Site 1 and 2, also in the steeper parts of Site 2 and in the depressions at Site 3 (section 6.1.2).

Taller ice needles at both Site 1 and 2 were visible where steeper slope angles occurred. Site 1 showed enhanced needle ice growth in the marginal areas close to the vegetation border, while Site 2 displayed enhanced areas of needle ice growth in the lower centre of the camera images, where slope angles were steeper (Figure 6.1 and 6.2 in section 6.1.2). At both Site 1 and 2, during events where the majority of the surface showed little to no needle ice growth, the steeper surfaces still produced ice needles (Figure 6.1, 6.2 and 6.7 in section 6.1) (Video 5 and 12). Site 3 showed small scale variability in observed needle ice growth, with areas that produced taller ice needles coinciding with the lower parts of the local topography (Figure 6.3) (Video 17).

The local topography at all three sites had locations displaying preferential needle ice growth that are suggested to be linked to enhanced moisture supply. Enhanced moisture availability at the margins of Site 1 and 2 are produced by a topographical depression. The sink facilitates enhanced moisture supply below the margin of the vegetation boundary at the study site. The increase in soil moisture supply occurs as surface or subsurface water flow reaches the edge of the study area. Water flowing, or seeping down margins, results in greater moisture input just below the soil scarp when compared to the centre of the study area. Similarly, sub-surface topography is suggested to direct the flow of moisture, creating areas of enhanced moisture availability. Areas that showed enhanced heave at Site 2 were located at steep sections of the slope (Figure 6.21 in Chapter 6). Topographical sinks are suggested to increase moisture availability at steeper slope parts, similar to how a waterfall consolidates water on the surface where moisture needs to flow over an edge. Increased sub-surface moisture availability was proposed to be enhanced if a less permeable layer, like bedrock or densely packed soil, is present close below the surface.

At Site 3 taller ice needles were observed in depressions. Two plausible explanations to observations of taller ice needle in depressions are proposed: first, the effect of soil texture and wind speed, and second moisture migration along surface/sub-surface topography. Soil textural properties of Site 3 showed enhanced density of sub-surface fines at approximately 5-10 cm below the surface (Figure 3.12 in Section 3.3.2 and Figure 5.37, 5.38 and 5.39 in Section 5.6.3). Increased fine particle content in the substrate at Site 3 is suggested to relate to frequent frost cycles reported from Marion Island (Hall, 1979; Holness, 2001, 2004; Haussmann et al., 2009). Numerable annual frost cycles heave larger material out of the ground by differential frost heave (Ballantyne, 1996), in addition to deflation by wind creating the stratified soil seen at Site 3 (Section 2.3.1, 3.3 and 4.5). It is suggested that surface moisture moves along this denser, less permeable layer, channelled along the sub-surface topography. Rain water collects in the depressions, resulting in higher soil moisture levels and the subsequent growth of taller ice needles.

A potential mechanism for the growth of relatively taller ice needles in the observed depressions is possibly the result of wind-driven surface sorting. Hedding *et al.* (2015) recently published on wind displacement of sediment at Marion Island. Results showed sorting of particles as a result from wind-blown surface movement. Surface topography at Site 3 has an undulating rippled surface as a result of wind-action. In addition, frequent frost cycles at Site 3, loosen the surface material and makes deflation by wind more prominent (Hall, 1979). Soil samples from site 3 displayed a low portion of fines (Section 5.8) that coincides with particle sorting. Smaller particle sizes are more easily deflated and, hence, are removed from the area surrounding Site 3. Removal of these fines disconnects the surface layer, thereby preventing it from receiving moisture from below, due to the reduced water transport capacity

of the coarser material. Enhanced needle ice growth was possibly due to relatively lower proportions of coarse material in the depression, increasing connectivity so that the freezing front is able to migrate moisture from the sub-surface, thereby facilitating the growth of larger ice needles.

Enhanced moisture supply influences the height of ice needles but, in extension, additionally influences the movement of material. Observations of needle ice related movement mechanisms, showed a relationship between active mechanisms of movement, displacement distance, and needle ice height. In the literature, e.g. Higashi and Corte (1971), Mackay and Mathews (1974a) and Matsuoka (1998, 2005, 2014), sediment movement was proposed to be influenced mainly by heave and resettling. However, they all report on additional movement mechanism that displaced sediment (Section 2.4). Results from camera imagery at all three study sites used in this study displayed needle ice movement by predominantly heaving and resettling, in addition to toppling and rolling, supporting the abovementioned authors' observations.

As discussed above, variability in both temperature and soil moisture produces a small-scale spatially heterogeneous needle ice environment at all three study sites, with temperature changes and changes in soil moisture availability controlling the growth of needle ice.

7.6 Displacement rate of different surface textures

Holness (2001) studied surface displacement by needle ice on different particle sizes. His results showed that finer material moved a greater distance when compared to larger stones. Results discussed in Section 6.1.3 showed similar results. In addition, it is suggested that the reason for this dissimilar movement among surface particle sizes is related to displacement mechanisms.

Section 6.1.3 displayed movement of surface material from 15 needle ice events studied, five from each study site. Surface material was grouped into three classes based on particle size: soil matrix (<2mm), small stones (2-20mm) and large stones (>20mm). Results from measured surface movement of the size classes showed that each class moves at different rates (Section 6.2, 6.3). Measurement of surface material movement also showed that each size class partly moved by different mechanisms. The matrix was predominately deformed by heave and resettling, small stones mostly moved by heave and resettling, but were mainly moved by toppling during heaving in excess of 1.5cm. Larger stones moved individually by heave and resettling, toppling and rolling, (however, toppling and rolling was only seen in a few clasts).

Displacement of surface material by needle ice was measured using the grids presented in Section 4.3.3. For reasons explained in that section, accuracy of surface movement was suggested to be ca

0.5cm. However, accuracy of determining movement was also impacted by the circumstances described below.

Soil matrix displacement could be difficult to measure over longer time periods. The matrix was observed to deform plastically. Hence, points of reference in the fine-grained material were difficult to identify. Measurement difficulties were enhanced over longer time-periods and at time-spans of twelve months soil matrix displacement measurements were considered inaccurate.

Fines (<0.064mm) were observed to move randomly by needle ice. The matrix is observed to consolidate and form a surface crust in response to rainfall events. After rain the consolidated surface matrix broke up by needle ice into aggregates (see difference in Frame a and b in Figure 6.26). These aggregates , similar to the size of small stones, display similar morphology as the aggregates described from the earliest observations of needle ice (Herschel, 1833; LeConte, 1850). These soil aggregates were seen to displace by toppling, in a similar way to small stones. Furthermore, the soil matrix heaved upslope during events displayed in Video 9, 10, 11. Based on analysis of the 81 needle ice events, this effect occurs often and is suggested to relate to decompression of the soil as needles ice uplifts the surface material. Heaving breaks up the soil crust, which is shown to lower the density of the soil matrix. As a result, the matrix could be observed to move upslope when it is only expanding from needle ice heave (Figure 6.6) (top left part of Video 10 and 11). Similar to the soil matrix, *small stone movement* over extended periods were difficult to measure as the particles often displaced in several directions, and identification of individual clasts was difficult. However, after the installation of painted markers at Site 1, in addition to initiation of measurements at Site 2, surface movement values of small clasts were considered accurate, even over longer time periods. Small clasts showed the largest displacement of the three particle size classes. They were affected by heave and resettling, but were observed to attain their largest displacement by frequently toppling during decay of ice needles in events with heave of more than 1.5cm. Toppling of small stones was recorded to move material at all three sites, but was observed to be concentrated at the same areas within each site, which were described to display enhanced heave (Figure 6.1, 6.2 and 6.3 in Chapter 6). The reason for enhanced displacement of small clasts, appears to be connected to them falling freely during decay without obstruction by surrounding material. To clarify, unlike the soil matrix and larger stones, small stones are observed to be fully uplifted, when compared to the matrix and large stones, by few ice needles. During the melting of ice needles supporting small stones, the few supporting ice needles may fall in the same direction. Larger clasts, possibly supported by hundreds of ice needles from many directions, toppling in a single direction appears less likely. Hence, small stones were observed to be transported roughly the height of the ice needle by toppling. This type of displacement where distance moved equals needle ice height was proposed by Mackay and Mathews (1974a) to possibly be the most

influential movement mechanism. In support of this theory, the soil aggregates previously discussed were seen to topple from ice needles, in a similar manner to small clasts, when they were of a similar size.

In summary, fine soil aggregates and small stones in the range of 2-20mm are observed to predominantly be transported by needle ice toppling, from unobstructed decay of ice needles of more than 1.5cm height. *Large stones (>20mm)* were mostly seen to be displaced by the mechanism of heaving and resettling. However, two clasts were seen to be moved by other mechanisms (one rolling and one toppling). Most large clasts were heaved to a similar height as the smaller clasts, especially during tall heaving, although their displacement was measured to be less than the surrounding small stones (Video 8 and 9). It is suggested that the larger surface area of these rocks produced a stabilizing effect during melt. Unlike small stones, a single large clast was observed to be supported by many ice needles, hence, stabilized from toppling. The ice needles supporting the large stone may melt non-uniformly, causing the clast to wobble, before resettling in roughly the same location as before heave (seen in the large clast in the lower left and top-middle portion of Video 8 and 10). A single large clast of ca 5cm diameter was observed to topple on a slope of ca 25° degrees when heaved ca 2 cm, showing that larger clasts can topple, but less frequently. The same clast was seen to heave and resettle in other needle ice events (Video 9, 10, 12 and 13) without toppling (single clast in the top-middle portion of Site 2 in Video 11). The increased weight of large stones, compared to smaller clasts, and if they are heaved to a lesser degree as a result of their weight was not clear from image analysis. However, a very large stone was observed to heave.

Very large stones, such as the one analysed in Section 6.6, displaced in a manner that support the contention that needle ice mainly move large stones by heaving and resettling. For a very large stone, with a surface area of ca 1000cm^2, a volume of ca 8600cm^3 and a weight of possibly 35kg (Section 6.6) to move by toppling, all ice needles supporting it would have to move in the same direction. This was considered unlikely, as the large surface area produces stabilization from possibly hundreds of ice needles.

7.7 Sediment displacement by other processes than needle ice

Section 6.4 presented results on sediment displacement by rain, hail and animal influence. Movement of surface material by these processes was also differentiated by particle size. Trampling by sheep markedly reworked surface material of all sizes at Site 2 on two occasions. Displacement was difficult to quantify due to the random displacement of sediment by the trampling. Hail and rain events were recorded at Sites 1 and 2. Rain did not produce any measurable primary displacement of surface material, however, surficial burying by clay and a change in the surface texture was observed to affect

the creation of surface aggregates, which subsequently displaced as small. However, reworking of surface material by needle ice, and changing the surface texture, is suggested to influence the erosive capacity of rain, although this was not quantifiable (Figure 6.15) (Meentemeyer and Zippin, 1981; Matsuoka, 2014).

Significant sediment displacement by hail was noted at both Site 1 and 2, and was differentiated by particle size. Movement of up to 16cm was recorded by small stones, while no displacement was evident in the 'large stone' class. Matrix displacement could not be quantified, as explained in earlier sections. Measurements indicate that although freeze-thaw action occurs more frequently, displacement by other processes such as hail produced further movement of the small stone class. The repeated heaving of surface material at all three sites was suggested to loosen material, increasing susceptibility to, and hence, the surface displacement by the effects of rain and hail. While visible, no quantification of this effect was possible. Results from Section 6.5 show the influence of processes other than needle ice producing more surface displacement at Site 1 and 2 during the period of March to April 2015. The kinetic energy of hail during three hail events observably displaced small stone sized material further than 19 and 22 needle ice events at Site 1 and 2 respectively during the two-month period.

In addition to stones heaving, heaving of vegetation was also observed at Site 1. The following section will discuss needle ice influence on vegetation stability.

7.8 Vegetation influence and patterned ground formation

Hesselman (1907), Pérez (1992), Goulet (1995), Grab (2002), Haussmann (2009a, 2009b) and Eriksson (2011) showed needle ice to influence vegetation stability. Haussmann (2009a, 2009b) and Eriksson (2011), and personal observations by the author, observed needle ice destroying *Azorella Selago* cushions on Marion Island. No vegetation was present at Site 2 and 3. In addition, no observable or measurable destruction of vegetation could be identified in this study at Site 1, although continuous heaving and resettling of the vegetation patches on the surface of Site 1 was observed. The heaving of the vegetation patch was noticed to occur on days when needle ice was active on the vegetation less surface. It is suggested that needle ice reworking seen at Site 1 did not destroy the already established vegetation, but negated new seedling establishment and growth as a consequence of needle ice action.

Chapter 8 – Conclusions

The research undertaken for this thesis intends to increase knowledge on initiation temperature, sediment movement mechanisms, surface energy balance, biological interactions, patterned ground formation in relation to environmental conditions (temperature, soil moisture, wind speeds), as well as identifying additional areas for further research. A methodology using high-frequency repeat photography has been used to observe geomorphological processes directly influencing surface material. The primary aims of this thesis are, first, to investigate small-scale high resolution variability in environmental parameters, identifying timing, possible threshold limits and criteria relevant to needle ice initiation, growth and melt. Second, the empirical data are coupled with sediment transport, adding new empirically observable evidence of needle ice growth, its destruction and displacement of material. Third, observations develop and apply a new methodology that visually documents needle ice growth/melt using stationary photography at an interval of 15 minutes. Fourth, the results of the research are used to identify and show *in situ* mechanisms involved in slope transport by needle ice. Fifth, identifying needles ice's influence on vegetation destruction and patterned ground formation.

8.1 Growth criteria, latent heat release, growth depth and timing of needle ice

This section presents conclusions relating to Objective 1, 2 and 3 from Section 1.4 in Chapter 1. Several key findings on the criteria of needle ice growth, temperature variability during needle ice initiation, soil moisture and texture controls on needle ice growth, latent heat release, zero-curtain effects, soil depth and timing of needle ice events can be made from the assessment of Chapter 5.

Needle ice initiation occurs at surface temperatures ranging from -2.0°C to 2.2°C. This thesis suggests that ice needles were not necessarily growing at the surface and, thus, that surface temperature measurements did not accurately portray the thermal conditions at the location of needle ice growth. Positive surface temperatures at the time of initial ice nucleation show that the surface sensors were not recording temperatures at the specific location of ice nucleation, i.e. the freezing front. To attain needle ice growth at positive air and ground temperatures it is suggested that the cooling of the ground surface, i.e. the active surface, is not by sensible heat exchange, but rather from radiative heat loss. Such a needle ice growth environment allows for air and ground temperatures to remain above 0°C while the ice nucleation temperature is reached only at the surface of active radiative heat loss, which in this condition coincides with the soil surface.

While most needle ice events occurred at positive surface temperatures, several needle ice events displayed growth to initiate at surface temperatures below 0°C. This study suggests that this is through the effect of supercooling. Freezing point depression occurs in impure water, solutes in the soil water and the pore size distribution of the soil at the study sites further lower the soil water's nucleation

temperature. However, the lower freezing point of impure water can still be further cooled, supercooled, before nucleation occurs. This supercooling of water can account for the negative surface temperatures measured at all three sites during several needle ice events initiation, as well as the latent heat release spikes noticed in conjunction with freezing.

Moisture measurements presented in this thesis are indicative of the availability of soil water for segregation ice formation and show water migration in the soil column. Variations observed in the different environments are suggested to be induced by the different climatic settings and surface textures. Notwithstanding this, some processes act similarly between the study sites. Near-surface soil moisture content was observed to increase after freeze initiation, and subsequently decrease during needle ice growth until the onset of decay. The increase in soil moisture suggest that during initial freeze, soil water migrates towards the freezing front where it undergoes a phase change to ice. This migration was observed to diminish with continued needle ice growth, as less water in the soil column was available for freezing.

This thesis presents the effect of soil texture on the transport and retention of moisture within the soil column. Annual moisture input on Marion Island is markedly higher than that measured at Tiffindell. Yet, this is not reflected in the soil moisture measurements. Results suggest that the markedly lower portion of fines in the top soil of Marion Island limits the ability of the soil to retain and transport water to the freezing front. This causes needle ice to initiate at the boundary between a coarse surface layer and a deeper layer of fine material.

A relationship between soil moisture availability and the growth of needle ice was observed by examining growth events and comparing them to non-growth events. Non-growth events at Tiffindell, when favourable temperature conditions for needle ice growth are seen, are directly related to a lack of subsurface soil moisture where inadequate soil moisture availability limits continued needle ice growth. On Marion Island, the soil moisture sensor measurements did not reflect the perennially wet conditions experienced first-hand. Instead, the perpetual occurrence of needle ice growth whenever temperature conditions are favourable indicate that soil moisture on Marion Island is not a limiting factor. This effect is suggested to relate to the low water retention and low water transport capabilities of the top soil layer at Site 3. Needle ice was observed to grow during all periods experiencing below 0°C without snow cover.

Soil moisture, air, surface and ground temperatures increase from before to after the moment of needle ice initiation. This relates to the effect of latent heat release and moisture migration by the onset of ice production. Needle ice initiation predominantly occur after surface temperatures reached below 0°C, but also before.

This study presents the first evidence of exotherms that coincide with the visual identification of needle ice growth. The exotherms occur during the initiation phase of a needle ice event and are followed by a distinct change in the rate of cooling. Exotherms were measured in close temporal proximity to the moment of needle ice initiation. Latent heat release, as supercooled water freezes, releases a surge of energy indicative of needle ice initiation. The initial release supplies more energy at the freezing front than the combined cooling from sensible and radiative heat loss. Subsequent to the initial heat release, the lowered rate of temperature change reflects the additional component of sustained latent heat release at the freezing front as long as segregation ice growth continues. When temperatures at the freezing front (at or near the soil surface) are balanced between the input of latent heat release and cooling from the surface, the system can reach a thermal equilibrium, which is referred to as a zero-curtain effect. Exotherms observed in surface temperature measurements at above 0°C are considered to be the sensor at the surface measuring latent heat release during phase change, and not the temperature of ice nucleation. Latent heat release is dependent on sustained soil moisture availability.

Needle ice events are observed to have ice needles growing at the observable soil surface as well as at depth. Temperature, soil moisture and adequate capillary suction potential in soil pores are suggested to determine the depth of needle ice initiation. Subsurface needle ice initiation is empirically observable through a time lag between the initial change in cooling rate and visual identification of needle ice growth. It is suggested that during these events, limited supply or connectivity of soil moisture at/to the surface allows the freezing front to descend further into the soil column. A limitation in soil moisture does not produce ice needles at the surface, but instead the moisture that is present freezes as pore ice, followed by a descending freezing front. The descending freezing front results in deeper needle ice (or other segregation ice) growth where sufficient soil moisture is available.

8.2 Mechanisms of sediment transport by needle ice

This study aims to identify needle ice sediment movement mechanisms and provide empirical evidence of theoretical mechanisms controlling surface displacement by needle ice (Objective 4 in Section 1.4). Slope angle controls both the type of movement mechanism as well as the magnitude of displacement. At all three study sites, heave and resettling is the dominant sediment displacement mechanism, while toppling dominates when ice needles heave more than 1.5cm. Rolling occurred when spherical to semi-spherical clasts are destabilized after heave of more than 1.5cm, initiating rolling during needle ice decay. Displacement is limited when very cold (ca -6°C) conditions exists due to freezing of the surface material into a solid crust, which stabilizes the surface soil material. During such events only heaving and resettling is seen to be active.

Locations of enhanced moisture supply result in the increased height of ice needles and increase the movement of material. Observations of needle ice mechanisms show a relationship between mechanisms of movement, displacement distance and needle ice height. The micro-scale spatial variability of needle ice growth height and location is associated with steeper slope angles and enhanced moisture supply. On Marion Island, taller ice needles are systematically favoured in depressions due to the finer soil texture and higher soil moisture levels at these locations.

Previous studies (Holness, 2004) suggest that needle ice displaces finer material further than coarse material. This thesis shows that, in addition to further displacement of finer material, the different material sizes are displaced by different movement mechanisms. Fine material (<0.0064mm) is predominantly displaced by heave and resettling, while toppling and rolling displaces coarser material. Small stones are transported roughly the height of the supporting ice needle when toppling occurs. Movement of surface material was observed to additionally be impacted by non-needle ice related movement. Displacement of material by processes other than needle ice is due to the influence of animals, rain and hail. Movement of surface material by these other processes was also controlled by particle size. Rain did not produce any measurable displacement of surface material, but significant sediment displacement by hail was observed. Needle ice does not destroy vegetation at Site 1 and 2, but possibly influences further vegetation extension. Patterned ground formation is not present at the surface of any of the three roughly 50cm by 50cm study sites.

8.3 Avenues of further needle ice research

Empirical evidence attained in this study corroborates assumptions made on the temperature environment in which needle ice grows and mechanisms responsible for needle ice displacement. Providing a point of departure for additional needle ice research. Using camera imagery for identifying needle ice initiation and mechanisms of sediment transport is considered a success. Visual observation also identified previously undocumented aspects of needle ice growth, including variations in growth depth, surface texture impacting displacement mechanisms, local scale (<1m) topography affecting displacement distance and direction, in addition to the same mechanisms being active in contrasting environments.

Attempts to model needle ice sediment displacement has been undertaken by Higashi and Corte (1971), Mackay and Mathews (1974a) and Matsuoka (1993; 1998; 2005; 2014). These authors have encountered marginal model accuracy when comparing modelled results to empirical evidence. It is the author of this thesis' belief that empirically observed displacement distances and transport mechanisms gained from the use of visual observation can significantly increase the accuracy of future attempts to model sediment transport rates by needle ice displacement. In addition, the

documentation of exotherms in close temporal proximity to visual needle ice initiation provide the currently most accurate indicator of needle ice growth initiation. Such exotherms help to distinguish effective needle ice events from pore ice growth, providing a guideline for future temperature measurement equipment, sensor position and measurement intervals. It has been shown that the release of latent heat increases temperatures in a timespan of ca 30-40minutes, proposing temperature measurement intervals greater than ca 5-10min are unideal for identifying needle ice initiation.

Improvements to the equipment used in this thesis include incorporating higher resolution cameras, more frequent measurements and additional measuring locations. Apart from the limitations discussed in Section 4.6, this study would have benefitted from more frequent and higher resolution observations. Displacement measurements were limited by image resolution, resulting in less accurate and precise displacement distances. In addition, temperature sensors at 1cm intervals in the first 5 centimetres of soil would have aided in locating a descending freezing front and consequently the depth of needle ice initiation. Similarly, soil moisture measurements at -7.5cm and -10cm would have been beneficial. Furthermore, additional environments, such as the Piedras Blancas in Venezuela (Pérez, 1987b) or the UK (Lawler, 1993), where previous needle ice studies have been conducted, would contribute to solidifying mechanisms of sediment displacement by needle ice. Also, measuring at steeper slope angles and on differing aspects may provide insights to needle ice sediment transport modalities.

The introduction to Chapter 2 proposes a need to further knowledge on needle ice as a geomorphic agent. Although, results did not specifically aid in this enterprise. It is the authors belief that applying visual methodologies, using temperature thresholds and movement mechanisms identified from this thesis may be useful in future research. Identifying needle ice influence on both smaller (millimetres to centimetres) and larger (tens of meters to hundreds of meters) scales and in extension connecting observations to weather on a synoptic scale.

References

Alamakee County. 2015. Landowner Conducts Stream Bank Erosion Study. [ONLINE] Available at:http://allamakeeswcd.org/landowner-conducts-stream-bank-erosion-study/ [Accessed 19 January 16]

Anderson, E.W., 1972. Terracettes: A Suggested Classification. Area 4, 17–20.

Arakawa, K., 1966. Theoretical studies of ice segregation in soil. J. Glaciol. 6, 255–260.

Argyll, D., 1880. Ice-Crystals. Nature 274.

Arnalds, O., Aradóttir, A.L., Thorsteinsson, I., 1987. The Nature and Restoration of Denuded Areas in Iceland. Arct. Alp. Res. 19, 518–525.

Ballantyne, C.K., 2013. A 35-Year Record of Solifluction in a Maritime Periglacial Environment. Permafr. Periglac. Process. 24, 56–66.

Ballantyne, C.K., 1996. Formation of miniature sorted patterns by shallow ground freezing: A field experiment. Permafr. Periglac. Process. 7, 409–424.

Beaty, C.B., 1974. Needle Ice and Wind in the White Mountains of California. Geology 2, 565–567.

Beskow, G., 1935a. Tjalbildningen och tjallyf-tningen. Sver. Geol Undersokning Ser. C 375 Arbok 26 3.

Beskow, G., 1935b. Tjalbildningen och tjallyf-tningen. Sver. Geol Undersokning Ser. C 375 Arbok 26 3 242.

Boelhouwers, J.C., 2003. Sensitivity and responses to climate change in the Subantarctic periglacial environment, in: International Permafrost Association: Eighth International Conference on Permafrost. AA Balkema, Rotterdam. pp. 67–71.

Boelhouwers, J.C., 1997. Soil Movement by Frost in the Hex River Mountains, Western Cape, South Africa. South Afr. Geogr. J. 79, 129–135.

Boelhouwers, J.C., 1995. Present-ay soil frost activity at the Hexriver Mountains, Western Cape, South-Africa. Z. Geomorphol. 39, 237–248.

Boelhouwers, J.C., 1994. Periglacial landforms at Giant's Castle, Natal Drakensberg, South Africa. Permafr. Periglac. Process. 5, 129–136.

Boelhouwers, J.C., 1991. Present-day periglacial activity in the Natal Drakensberg, Southern Africa: A Short Review. Permafr. Periglac. Process. 2, 5–12.

Boelhouwers, J.C., Duiker, J.M.C., Van Duffelen, E.A., 1998. Spatial, morphological and sedimentological aspects of recent debris flows in Du Toit's Kloff, Western Cape. South Afr. J. Geol. 101, 73–89.

Boelhouwers, J.C., Holness, S., Sumner, P., 2003. The maritime Subantarctic: a distinct periglacial environment. Geomorphology 52, 39–55.

Boelhouwers, J.C., Meiklejohn, K.I., 2002. Quaternary periglacial and glacial geomorphology of southern Africa: review and synthesis. South Afr. J. Sci. 98, 47–54.

Borg, C.-J., 2012. Mechanisms controlling valley asymmetry development at Abisko, northern Sweden and Sani Pass, southern Africa.

Brady, N.C., Weil, R.R., others, 1996. The nature and properties of soils. Prentice-Hall Inc.

Branson, J., Lawler, D.M., Glen, J.W., 1996. Sediment inclusion events during needle ice growth: A laboratory investigation of the role of soil moisture and temperature fluctuations. Water Resour. Res. 32, 459–466.

Burley, A.J., Kimbell, G.S., Patrick, D.J., 1982. A gravity survey of Lesotho [WWW Document].

Butler, D.R., Malanson, G.P., Resler, L.M., 2004. Turf-banked terrace treads and risers, turf exfoliation and possible relationships with advancing treeline. CATENA 58, 259–274.

Cambardella, C.A., Gajda, A.M., Doran, J.W., Wienhold, B.J., Kettler, T.A., Lal, R., 2001. Estimation of particulate and total organic matter by weight loss-on-ignition. Assess. Methods Soil Carbon 349–359.

Carbutt, C., Edwards, T.J., 2003. The flora of the Drakensberg alpine centre. Edinb. J. Bot. 581–607.

Davison, C., 1889. On the Creeping of the Soilcap through the Action of Frost. Geol. Mag. Decade III 6, 255–261.

Deckert, E., 1913. Nordamerika. Bibliographisches institut.
Elliott, S., 1824. A sketch of the botany of South-Carolina and Georgia. Sketch Bot. South-Carol. Ga. JR Schenck CharlestonFacsimile Ed 1971 Hafner N. Y. N. Y. USA.
Embleton, C., 1992. The frozen earth: Fundamentals of geocryology. Earth-Sci. Rev. 32, 195.
Eriksson, B., 2011. The zoo-geomorphological impact of fossorial rodents in sub-polar alpine environments.
Fisher, O., 1880. Ice-Crystals and Filaments. Nature 396.
French, H., Harbor, J., 2013. 8.1 The Development and History of Glacial and Periglacial Geomorphology, in: Shroder, J.F. (Ed.), Treatise on Geomorphology. Academic Press, San Diego, pp. 1–18.
French, H.M., 2000. Does Lozinski's periglacial realm exist today? A discussion relevant to modern usage of the term "periglacial." Permafr. Periglac. Process. 11, 35–42.
Frenot, Y., Vliet-Lanoë, B.V., Gloaguen, J.-C., 1995. Particle Translocation and Initial Soil Development on a Glacier Foreland, Kerguelen Islands, Subantarctic. Arct. Alp. Res. 27, 107–115.
Fujita, M., others, 1937. Shimobashira no Kenkyu (Investigation of frost needles). Tokyo Jiyugakuen Transl. US Army Cold Reg. Res. Eng. Labs Hanover NH.
Fukuda, H., 1936. Über die Eisfilamente im Boden (Ice columns in soil). Coll. Agric. 135Imperial Univ. Tokyo 453–481.
Goulet, F., 1995. Frost heaving of forest tree seedlings: a review. New For. 9, 67–94.
Grab, S., 2002a. Turf exfoliation in the high Drakensberg, Southern Africa. Geogr. Ann. Ser. Phys. Geogr. 84, 39–50.
Grab, S., 2002b. Characteristics and palaeoenvironmental significance of relict sorted patterned ground, Drakensberg plateau, southern Africa. Quat. Sci. Rev. 21, 1729–1744.
Grab, S., 2001. Needle ice observations from the high Drakensberg, Lesotho. Permafr. Periglac. Process. 12, 227–231.
Grab, S., 1999. Block and Debris Deposits in the High Drakensberg, Lesotho, Southern Africa: Implications for High Altitude Slope Processes. Geogr. Ann. Ser. Phys. Geogr. 81, 1–16.
Grab, S., 1997. Annually re-forming miniature sorted patterned ground in the high Drakensberg, southern Africa. Earth Surf. Process. Landf. 22, 733–745.
Gradwell, M.W., 1957. Patterned ground at a high-country station. N. Z. J. Sci. Technol. 38, 793–806.
Gradwell, M.W., 1955. Soil frost studies at a high country station. II. N. Z. J. Sci. Technol. 37B 267–275.
Hall, K., 2004. Evidence for freeze–thaw events and their implications for rock weathering in northern Canada. Earth Surf. Process. Landf. 29, 43–57. doi:10.1002/esp.1012
Hall, K., 1979a. Sorted stripes orientated by wind action: Some observations from sub-antarctic marion island. Earth Surf. Process. 4, 281–289.
Hall, K., 1979b. Late glacial ice cover and palaeotemperatures on sub-Antarctic Marion Island. Palaeogeogr. Palaeoclimatol. Palaeoecol., Geodynamic and biodynamic effects of the Messinian salinity crisis 29, 243–259.
Hall, K., Boelhouwers, J., Driscoll, K., 1999. Animals as erosion agents in the alpine zone: some data and observations from Canada, Lesotho, and Tibet. Arct. Antarct. Alp. Res. 436–446.
Hallet, B., Prestrud, S., 1986. Dynamics of periglacial sorted circles in western Spitsbergen. Quat. Res. 26, 81–99.
Harlan, R.L., Nixon, J.F., 1978. Ground thermal regime. Geotech. Eng. Cold Reg. 103–163.
Hastenrath, S., 1977. Observations on soil frost phenomena in the Peruvian Andes. Z. Für Geomorphol.
Hastenrath, S., 1976. Variations in low-latitude circulation and extreme climatic events in the tropical Americas. J. Atmospheric Sci. 33, 202–215.
Haussmann, N., Boelhouwers, J.C., McGeoch, M.A., 2009a. Fine Scale Variability in Soil Frost Dynamics Surrounding Cushions of the Dominant Vascular Plant Species (azorella Selago) on Sub-Antarctic Marion Island. Geogr. Ann. Ser. Phys. Geogr. 91, 257–268.
Haussmann, N., McGeoch, M.A., Boelhouwers, J.C., 2009b. Interactions between a cushion plant (Azorella selago) and surface sediment transport on sub-Antarctic Marion Island. Geomorphology 107, 139–148.

Hedding, D.W., Nel, W., Anderson, R.L., 2015. Aeolian processes and landforms in the sub-Antarctic: preliminary observations from Marion Island. Polar Res. 34.

Heilbronn, T.D., Walton, D.W.H., 1984. Plant Colonization of Actively Sorted Stone Stripes in the Subantarctic. Arct. Alp. Res. 16, 161–172.

Herbst, S.N., Roberts, B.R., 1974. alpine vegetation of the Lesotho Drakensberg: a study in quantitative floristics at Oxbow. J. South Afr. Bot.

Herschel, J.F.W., 1833. Notice of a remarkable deposition of ice round the decaying stems of vegetables during frost. Lond. Edinb. Philos. Mag. J. Sci. 2, 110–111.

Hesselman, H., 1907. Studier ofver skogsvaxt a mossar. Skogsvårdsföreningens Tidsskr. 25–47.

Higashi, A., Corte, A.E., 1971. Solifluction: A Model Experiment. Science 171, 480–482.

Higashi, A., Corte, A.E., 1971. Solifluction: A model experiment. Science 171, 480–482.

Hinkel, K.M., Paetzold, F., Nelson, F.E., Bockheim, J.G., 2001. Patterns of soil temperature and moisture in the active layer and upper permafrost at Barrow, Alaska: 1993–1999. Glob. Planet. Change, Inference of Climate Change from Geothermal Data 29, 293–309.

Holness, S., Boelhouwers, J., 1998. Some observations on Holocene changes in periglacial activity at Long Ridge, Marion Island. South Afr. J. Sci. 94, 399.

Holness, S.D., 2004. Sediment movement rates and processes on cinder cones in the maritime Subantarctic (Marion Island). Earth Surf. Process. Landf. 29, 91–103.

Holness, S.D., 2001. The orientation of sorted stripes in the maritime subantarctic, Marion Island. Earth Surf. Process. Landf. 26, 77–89.

Johnston, G.H., 1981. Permafrost engineering design and construction.

Kessler, M.A., Murray, A.B., Werner, B.T., Hallet, B., 2001. A model for sorted circles as self-organized patterns. J. Geophys. Res. Solid Earth 1978–2012 106, 13287–13306.

Kiernan, K., McConnell, A., 2008. Periglacial processes on Heard Island, Southern Indian Ocean. Pap. Proc. R. Soc. Tasman. 142, 1–12.

King, H., 1880. Ice Filaments. Nature 21, 302.

Kozlowski, T., 2016. A simple method of obtaining the soil freezing point depression, the unfrozen water content and the pore size distribution curves from the DSC peak maximum temperature. Cold Reg. Sci. Technol. 122, 18–25. doi:10.1016/j.coldregions.2015.10.009

Kozlowski, T., 2009. Some factors affecting supercooling and the equilibrium freezing point in soil–water systems. Cold Reg. Sci. Technol. 59, 25–33. doi:10.1016/j.coldregions.2009.05.009

Krantz, W.B., 1990. Self-organization manifest as patterned ground in recurrently frozen soils. Earth-Sci. Rev. 29, 117–130.

Krumme, O., 1935. Frost und Schnee in ihrer Wirkung auf den Boden im Hochtaunus. Brönner.

Kück, K.M., Lewis, C.A., 2002. Terracettes and active gelifluction terraces in the Drakensberg of the Province of the Eastern Cape, South Africa: a process study. South Afr. Geogr. J. 84, 214–225.

Lawler, D.M., 1993. Needle ice processes and sediment mobilization on river banks: the River Ilston, West Glamorgan, UK. J. Hydrol. 150, 81–114.

Lawler, D.M., 1989. Some Observations on Needle Ice. Weather 44, 406–409.

Lawler, D.M., 1988. Environmental Limits of Needle Ice: A Global Survey. Arct. Alp. Res. 20, 137–159.

Le Roux, P.C., McGeoch, M.A., Nyakatya, M.J., Chown, S.L., 2005. Effects of a short-term climate change experiment on a sub-Antarctic keystone plant species. Glob. Change Biol. 11, 1628–1639.

LeConte, J., 1850. Observations on a remarkable exudation of ice from the stems of vegetables, and on a singular protrusion of icy columns from certain kinds of earth during frosty weather. Lond. Edinb. Dublin Philos. Mag. J. Sci. 36, 329–342.

Loziński, W., 1912. Die periglaziale Fazies der mechanischen Verwitterung. PA Norstedt & Söner.

Lundqvist, J., 1962. Patterned ground and related frost phenomena in Sweden. Generalstabens Litogr. Anst. Förl.

Mackay, J.R., Mathews, W.H., 1974a. Needle Ice Striped Ground. Arct. Alp. Res. b, 79–84.

Mackay, J.R., Mathews, W.H., 1974b. Movement of sorted stripes, the cinder cone, Garibaldi Park, BC, Canada. Arct. Alp. Res. 347–359.

Matsuoka, N., 2014. Combining Time-Lapse Photography and Multisensor Monitoring to Understand Frost Creep Dynamics in the Japanese Alps. Permafr. Periglac. Process. 25, 94–106.
Matsuoka, N., 2005. Temporal and spatial variations in periglacial soil movements on alpine crest slopes. Earth Surf. Process. Landf. 30, 41–58.
Matsuoka, N., 1998. The relationship between frost heave and downslope soil movement: field measurements in the Japanese Alps. Permafr. Periglac. Process. 9, 121–133.
Matsuoka, N., 1996. Soil moisture variability in relation to diurnal frost heaving on Japanese high mountain slopes. Permafr. Periglac. Process. 7, 139–151.
McDougall, I., Verwoerd, W., Chevallier, L., 2001. K–Ar geochronology of Marion Island, Southern Ocean. Geol. Mag. 138, 1–17. doi:null
Meentemeyer, V., Zippin, J., 1981. Soil moisture and texture controls of selected parameters of needle ice growth. Earth Surf. Process. Landf. 6, 113–125.
Meentemeyer, V., Zippin, J., 1980. Observations of Needle Ice Growth and Potential for Accelerated Erosion on the Georgia Piedmont. Southeast. Geogr. 20, 31–41.
Meiklejohn, K.I., Hedding, D.W., Wunderman, R., Venzke, E., Mayberry, G., 2005. Marion Island. Bull. Glob. Volcanism Netw. 30, 5269–5273.
Meldola, R., 1880. Ice Filaments. Nature 21, 302–302.
Meteotest, 2012. Meteotest: Bern. Meteonorm 7.
Mucina, L., Rutherford, M.C., 2006. The vegetation of South Africa, Lesotho and Swaziland. Strelitzia No19 viii + 807 pp.
Mulder, N., 2009. Contemporary spatio-temporal patterns of snow cover over the Drakensberg : research letter.
Muller, S.W., 1947. Permafrost or permanently frozen ground and related engineering problems.
Naylor, L.A., 2005. The contributions of biogeomorphology to the emerging field of geobiology. Palaeogeogr. Palaeoclimatol. Palaeoecol., Geobiology: Objectives, Concept, PerspectivesGeobiology: Objectives, Concept, Perspectives 219, 35–51. doi:10.1016/j.palaeo.2004.10.013
Nel, W., 2012. A preliminary synoptic assessment of soil frost on Marion Island and the possible consequences of climate change in a maritime sub-Antarctic environment. Polar Res. 31.
Nel, W., Boelhouwers, J., 2014. First observations on needle ice formation in the sub-Antarctic. Antarct. Sci. 26, 327–328.
Nel, W., Sumner, P., 2008. Rainfall and temperature attributes on the Lesotho–Drakensberg escarpment edge, southern Africa. Geogr. Ann. Ser. Phys. Geogr. 90, 97–108.
Noguchi, Y., Tabuchi, H., Hasegawa, H., 1987. Physical factors controlling the formation of patterned ground on Haleakala, Maui. Geogr. Ann. Ser. Phys. Geogr. 329–342.
Oke, T.R., 2002. Boundary Layer Climates. Routledge.
Oke, T.R., Cleugh, H.A., 1987. Urban heat storage derived as energy balance residuals. Bound.-Layer Meteorol. 39, 233–245. doi:10.1007/BF00116120
Ólafsdóttir, R., Guòmundsson, H.J., 2002. Holocene land degradation and climatic change in northeastern Iceland. The Holocene 12, 159–167.
Outcalt, S.I., 1971. An Algorithm for Needle Ice Growth. Water Resour. Res. 7, 394–400.
Outcalt, S.I., 1969. Weather and diurnal frozen soil structure at Charlottesville, Virginia. Water Resour. Res. 5, 1377–1382.
Outcalt, S.I., Nelson, F.E., Hinkel, K.M., 1990. The zero-curtain effect: Heat and mass transfer across an isothermal region in freezing soil. Water Resour. Res. 26, 1509–1516.
Paterson, W.S.B., 1994. The Physics of Glaciers. Butterworth-Heinemann.
Paul, J.., 1885. Peculiar ice-forms (letter sent to B. Woodd Smith). Nature 264.
Pérez, F.L., 1993. Turf destruction by cattle in the high equatorial Andes. Mt. Res. Dev. 13, 107–110.
Pérez, F.L., 1992a. Miniature sorted stripes in the páramo de Piedras Blancas (Venezuelan Andes). J Dixon Abrahams Ed. Periglac. Geomorphol. John Wiley Sons 125–157.
Pérez, F.L., 1992b. Processes of turf exfoliation (Rasenabschälung) in the high Venezuelan Andes. Z. Geomorphol.

Pérez, F.L., 1991. Soil moisture and the distribution of giant Andean rosettes on talus slopes of a desert paramo. Clim. Res. 1, 217–31.
Pérez, F.L., 1988. The movement of debris on a high Andean talus. Z. Für Geomorphol. 77–99.
Pérez, F.L., 1987a. Soil surface roughness and needle ice-induced particle movement in a Venezuelan paramo. Caribb J Sci 23, 3–4.
Pérez, F.L., 1987b. Downslope stone transport by needle ice in a high andean area (venezuela). Rev. Géomorphologie Dyn. 32, 33–50.
Pérez, F.L., 1984. Striated soil in an Andean páramo of Venezuela: its origin and orientation. Arct. Alp. Res. 277–289.
Plug, L.J., Werner, B.T., 2002. Nonlinear dynamics of ice-wedge networks and resulting sensitivity to severe cooling events. Nature 417, 929–933.
Pollock, F., Collier, C.., 1885. Frost formation on Dartmoor. Nature 216–217.
Rae, J., 1880. Peculiar Ice Forms. Nature 81–82.
Rapp, A., 1960. Recent Development of Mountain Slopes in Kärkevagge and Surroundings, Northern Scandinavia. Geogr. Ann. 42, 65–200.
Rempel, A.W., 2010. Frost heave. J. Glaciol. 56, 1122–1128.
Rempel, A.W., 2007. Formation of ice lenses and frost heave. J. Geophys. Res. 112.
Roux, P.C. le, McGeoch, M.A., 2008. Changes in climate extremes, variability and signature on sub-Antarctic Marion Island. Clim. Change 86, 309–329.
Sawagaki, T., 1995. Ground temperature regimes and frost heave activity in the vicinity of Syowa Station, East Antarctica, in: Proceedings of the NIPR Symposium on Antarctic Geosciences. 国立極地研究所, pp. 239–249.
Schubert, C., 1973. Striated ground in the Venezuelan Andes. J. Glaciol. 12, 461–463.
Schulze, B.R., 1971. The climate of Marion Island. Marion Prince Edw. Isl. AA Balkema Cape Town 16–31.
Schulze, R.E., 1979. Hydrology and water resources of the Drakensberg. Report.
Schwalbe, 1884. Untitled report of peculiar ice-formation observation. Nature 472.
Self, S., Keszthelyi, L., Thordarson, T., 1998. The Importance of Pāhoehoe. Annu. Rev. Earth Planet. Sci. 26, 81–110. doi:10.1146/annurev.earth.26.1.81
Selkirk-Bell, J.M., Selkirk, P.M., 2013. Vegetation-Banked Terraces on Subantarctic Macquarie Island: A Reappraisal. Arct. Antarct. Alp. Res. 45, 261–274.
Sharp, J.M., 1976. Ground-water sapping by freeze-and-thaw. Z. Für Geomorphol. 484–487.
Shulgina, T., Bogomolov, V., Genina, E., Gordov, E., Nikitchuk, K., Okladnikov, I., Titov, A., 2009. Studying climate change in Siberia based on climatic indices assessment. Geophys. Res. Abstr. Vienna Austria 2009 11.
Smith, V.R., 2002. Climate Change in the Sub-Antarctic: An Illustration from Marion Island. Clim. Change 52, 345–357.
Smith, V.R., Steenkamp, M., 1992. Soil macrofauna and nitrogen on a sub-Antarctic island. Oecologia 92, 201–206.
Smith, V.R., Steenkamp, M., 1990. Climatic change and its ecological implications at a subantarctic island. Oecologia 85, 14–24.
Smith, V.R., Steenkamp, M., Gremmen, N.J.M., 2001. Terrestrial habitats on sub-Antarctic Marion Island: their vegetation, edaphic attributes, distribution and response to climate change. South Afr. J. Bot. 67, 641–654.
Soons, J.M., 1967. Erosion by Needle Ice in the Southern Alps, New Zealand. Arct. Alp. Environ. 217–227.
Soons, J.M., Greenland, D.E., 1970. Observations on the Growth of Needle Ice. Water Resour. Res. 6, 579–593.
Soons, J.M., Rainer, J.N., 1968. Micro-Climate and Erosion Processes in the Southern Alps, New Zealand. Geogr. Ann. Ser. Phys. Geogr. 50, 1–15.
Sumgin, M.., Kachurin, Tolstikhin, Tumel, 1940. General Pernuifrostology.
Sumner, P., 2004. Relict sorted patterned ground in Lesotho. Permafr. Periglac. Process. 15, 89–93.

Sumner, P., 2003. A contemporary winter ground thermal profile in the Lesotho highlands and implications for active and relict soil frost phenomena. Earth Surf. Process. Landf. 28, 1451–1458. doi:10.1002/esp.1003

Sumner, P. d., Meiklejohn, K.I., Boelhouwers, J.C., Hedding, D.W., 2004. Climate change melts Marion Island's snow and ice. South Afr. J. Sci. 100, 395–398.

Troll, C., 1958. Structure soils, solifluction, and frost climates of the earth [Strukturböden, Solifluktion, und Frostklimate der Erde]. US Army Snow Ice Permafr. Res. Establ. 43, 1–121.

Troll, C., 1944. Strukturböden, solifluktion und Frostklimate der Erde. Geol. Rundsch. 34, 545–694.

Troll, K., 1973. Rasenabschälung Turf Exfoliation als periglaziales Phänomen der subpolaren Zonen und den Hochgebirge.

Troll, K., 1934. Über den Bau und Nervatur der Karpelle von Ranunculus.

Tyson, P.D., Preston-Whyte, R.A., Schulze, R.E., 1976. The climate of the Drakensberg. Town and Regional Planning Commission.

Ueno, K., Kurobe, K., Imaizumi, F., Nishii, R., 2015. Effects of deforestation and weather on diurnal frost heave processes on the steep mountain slopes in south central Japan. Earth Surf. Process. Landf. 40, 2013–2025.

Van Everdingen, R.O., 1998. Multi-Language Glossary of Permafrost and Related Ground-Ice Terms in Chinese, English, French, German, Icelandic, Italian, Norwegian, Polish, Romanian, Russian, Spanish, and Swedish. International Permafrost Association, Terminology Working Group.

Van Vliet-Lanoë, B., 1998. Frost and soils: implications for paleosols, paleoclimates and stratigraphy. Catena 34, 157–183.

Verwoerd, W.J., Russell, S., Berruti, A., 1981. 1980 volcanic eruption reported on Marion Island. Earth Planet. Sci. Lett. 54, 153–156.

Von Richthofen, F.F., 1901. Führer für Forschungsreisende: Anleitung zu Beobachtungen über Gegenstände der physischen Geographie und Geologie. Gebrüder Jänecke.

Vowinckel, E., 1954. Synotische Klimotologie vom gebiet Marion Island. Synop. Climatol. Marion Isl. Area Notos 3, 12–21.

Walker, D.A., Epstein, H.E., Romanovsky, V.E., Ping, C.L., Michaelson, G.J., Daanen, R.P., Shur, Y., Peterson, R.A., Krantz, W.B., Raynolds, M.K., others, 2008. Arctic patterned-ground ecosystems: A synthesis of field studies and models along a North American Arctic Transect. J. Geophys. Res. Biogeosciences 2005–2012 113.

Walton, D.W.H., 1982. The Signy Island terrestrial reference sites: XV. Microclimate monitoring, 1972–74. Br. Antarct. Surv. Bull. 55, 111–126.

Wang, B., French, H.M., 1994. Climate controls and high-altitude permafrost, qinghai-xizang (tibet) Plateau, China. Permafr. Periglac. Process. 5, 87–100.

Washburn, A., 1979. Geocryology. Edw. Arnold Lond.

Washburn, A.L., 1973. Periglacial processes and environments. Lond. Edw. Arnold.

Washburn, A.L., 1970. An approach to a genetic classification of patterned ground. Acta Geogr. Lodz. 24, 437–446.

Wetterhan, D., 1880. Ice-crystals and filaments. Nature 396.

Woodd Smith, B., 1884. Peculiar Ice Forms. Nature 5–6.

Zimbelman, J.R., Williams, S.H., Johnston, A.K., 2012. Cross-sectional profiles of sand ripples, megaripples, and dunes: a method for discriminating between formational mechanisms. Earth Surf. Process. Landf. 37, 1120–1125.

Appendix A

Table 9.1. Sunrise, sunset and duration of sunlight for all needle ice events from Site 1, 2 and 3.

Site 1				Site 2				Site 3			
Needle ice	Timing		h	Needle ice	Timing		h	Needle ice	Timing		h
Date	Sunrise	Sunset	Duration	Date	Sunrise	Sunset	Duration	Date	Sunrise	Sunset	Duration
2014-06-01	06:56	17:19	10:23	2015-04-10	06:25	17:57	11:32	2014-04-27	07:22	17:30	10:08
2014-06-02	06:57	17:19	10:22	2015-04-12	06:26	17:55	11:29	2014-05-13	07:42	17:07	09:25
2014-06-03	06:57	17:19	10:22	2015-04-15	06:28	17:52	11:24	2014-05-15	07:45	17:04	09:19
2014-06-04	06:58	17:19	10:21	2015-04-16	06:29	17:51	11:22	2014-05-16	07:46	17:03	09:17
2014-06-05	07:05	17:23	10:18	2015-04-17	06:29	17:50	11:21	2015-03-01	06:03	19:18	13:15
2014-07-01	07:05	17:23	10:18	2015-04-18	06:30	17:49	11:19	2015-03-11	06:17	18:59	12:42
2014-07-02	07:05	17:24	10:19	2015-04-19	06:31	17:47	11:16	2015-03-12	06:19	18:57	12:38
2014-07-03	07:05	17:24	10:19	2015-04-20	06:31	17:47	11:16	2015-03-14	06:22	18:53	12:31
2014-07-04	06:48	17:43	10:55	2015-04-21	06:32	17:45	11:13	2015-03-20	06:30	18:41	12:11
2014-08-09	06:46	17:45	10:59	2015-04-22	06:32	17:45	11:13	2015-03-27	06:40	18:28	11:48
2014-08-12	06:45	17:45	11:00	2015-04-27	06:35	17:40	11:05	2015-03-30	06:44	18:22	11:38
2014-08-13	06:43	17:46	11:03	2015-04-28	06:36	17:39	11:03	2015-03-31	06:47	18:18	11:31
2014-08-15	06:41	17:48	11:07	2015-04-30	06:37	17:37	11:00	2015-04-02	06:49	18:16	11:27
2014-08-17	06:36	17:50	11:14	2015-05-01	06:38	17:36	10:58	2015-04-03	06:49	18:15	11:26
2014-08-22	06:34	17:51	11:17	2015-05-02	06:39	17:35	10:56	2015-04-11	07:00	17:59	10:59
2014-08-24	05:28	18:23	12:55	2015-05-07	06:41	17:31	10:50				
2014-10-20	05:27	18:23	12:56	2015-05-11	06:44	17:29	10:45				
2014-10-21	05:13	18:34	13:21	2015-05-12	06:45	17:28	10:43				
2014-11-05	05:07	18:43	13:36	2015-05-13	06:45	17:27	10:42				
2014-11-16	05:06	18:44	13:38	2015-05-14	06:46	17:27	10:41				
2014-11-17	05:06	18:44	13:38	2015-05-15	06:46	17:26	10:40				
2014-11-18	05:06	18:45	13:39	2015-05-17	06:48	17:25	10:37				
2014-11-19	05:05	18:46	13:41								
2014-11-20	05:26	19:13	13:47								
2015-01-17	06:24	18:01	11:37								
2015-04-07	06:25	17:58	11:33								
2015-04-09	06:25	17:57	11:32								
2015-04-10	06:26	17:55	11:29								
2014-04-12	06:28	17:52	11:24								
2015-04-15	06:29	17:51	11:22								
2015-04-16	06:29	17:50	11:21								
2015-04-17	06:30	17:49	11:19								
2015-04-18	06:31	17:47	11:16								
2015-04-19	06:31	17:47	11:16								
2015-04-20	06:32	17:45	11:13								
2015-04-21	06:32	17:45	11:13								
2015-04-22	06:35	17:40	11:05								
2015-04-27	06:36	17:39	11:03								
2015-04-28	06:37	17:37	11:00								
2015-04-30	06:38	17:36	10:58								
2015-05-01	06:44	17:29	10:45								
2015-05-11	06:45	17:28	10:43								
2015-05-12	06:45	17:27	10:42								
2015-05-13	06:30	17:30	11:00								
2015-06-04	07:00	17:30	10:30								

Table 9.2. Dates of needle ice events captured by the tri-camera setup. Data and which camera capturing the event are shown along with total and unique needle ice events.

Site 1 2014			Site 1 2015			Site 2 2015			Site 3 2014-2015		
Cam1	*Cam2*	*Cam3*	*Cam1*	*Cam2*	*Cam3*	*Cam1*	*Cam2*	*Cam3*	*Cam1*	*Cam2*	*Cam3*
01-jun	01-jun	01-jun		17-jan		10-apr		10-apr	25-apr		
02-jun	02-jun	02-jun		07-apr	07-apr			11-apr	26-apr		
03-jun	03-jun	03-jun		09-apr	09-apr	12-apr		12-apr			27-apr
04-jun	04-jun	04-jun		10-apr	10-apr	15-apr		15-apr			
05-jun		05-jun		11-apr	11-apr			16-apr	13-maj		13-may
		09-jun		12-apr	12-apr			17-apr	14-maj		14-may
		12-jun		15-apr	15-apr			18-apr	15-maj		
13-jun		13-jun		16-apr	16-apr			19-apr	16-maj		16-may
01-jul		01-jul		17-apr	17-apr			20-apr	28-maj		
02-jul		02-jul		18-apr	18-apr			21-apr	2015	2015	2015
03-jul		03-jul		19-apr	19-apr			22-apr			26-feb
04-jul		04-jul		20-apr	20-apr			27-apr			08-mar
09-aug				21-apr	21-apr			28-apr			11-mar
11-aug				22-apr	22-apr			30-apr			16-mar
12-aug				27-apr	27-apr			01-maj			21-mar
13-aug				28-apr	28-apr			02-maj			24-mar
14-aug				29-apr	29-apr			07-maj			27-mar
15-aug				30-apr	30-apr			12-maj			28-mar
17-aug				01-may	01-may			13-maj			29-mar
22-aug				02-may	02-may			14-maj			31-mar
23-aug					03-may			15-maj			07-apr
24-aug				04-may				16-maj			08-apr
25-aug				07-may	07-may			17-maj			14-apr
26-aug				11-may	11-may			22-maj			16-apr
27-aug				12-may	12-may			03-jun	30-apr		30-apr
20-oct	20-oct	20-oct		13-may	13-may						
21-okt	21-oct	21-oct		14-may	14-may						
	22-oct	22-oct		15-may	15-may						
	23-oct			16-may	16-may						
	05-nov	05-nov		17-may	17-may						
	14-nov	14-nov			22-may						
	16-nov	16-nov		03-jun							
	17-nov	17-nov			04-jun						
	18-nov	18-nov									
	19-nov	19-nov									
	20-nov	20-nov									
	22-nov										
Total number of needle ice events:											**178**
Total number of unique needle ice events:											**106**

Table 9.3. Details concerning initiation of growth (visual and logger), melt and end of melt of needle ice growth events from Site 1. Events in red text use the -2.5cm temperature sensor as a proxy to the +0cm sensor. Additionally, Min Temp and Min Temp Timing show minimum temperatures and timestamps for events which did not show sub-zero temperatures.

Date	Visual Init. of Growth	Freezing	Init. Of Melt	End of Melt	Min Temp	Min Temp Timing
2014-06-01	2016-05-31 19:30	> zero	08:15	10:15	1,14	05:31
2014-06-02	2016-06-01 18:30	> zero	08:15	12:15	0,6	07:14
2014-06-03	2016-06-02 18:00	02:37	08:00	12:30		
2014-06-04	2016-06-03 15:30	22:55	07:45	11:15		
2014-07-01	2016-06-30 21:45	< zero	08:15	11:30	-0,06	21:45
2014-07-02	2016-07-01 18:00	< zero	09:00	11:30	-0,04	18:00
2014-07-03	2016-07-02 18:30	< zero	09:30	11:45	-0,125	18:30
2014-07-04	2016-07-03 19:15	< zero	10:00	10:30	-0,47	19:15
2014-08-09	2016-08-09 00:10	< zero	08:55	11:25	-0,04	00:10
2014-08-12	2016-08-11 20:25	20:05	08:25	10:10		
2014-08-13	2016-08-12 20:10	19:50	09:25	10:40		
2014-08-15	2016-08-14 21:10	21:20	08:10	10:10		
2014-08-17	2016-08-16 20:40	22:50	09:25	10:40		
2014-08-22	2016-08-21 18:25	18:20	09:19	12:55		
2014-08-24	2016-08-23 16:25	15:10	08:10	10:40		
2014-10-20	2016-10-19 23:10	> zero	06:10	08:25	0,8	01:40
2014-10-21	2016-10-21 00:25	> zero	05:55	08:40	0,02	05:20
2014-11-05	2016-11-05 00:25	00:12	05:55	07:25		
2014-11-16	2016-11-15 19:10	19:28	06:25	11:55		
2014-11-17	2016-11-16 19:25	20:30	06:40	11:25		
2014-11-18	2016-11-17 19:40	03:24	06:10	08:55		
2014-11-19	2016-11-19 02:25	> zero	05:40	07:40	0,29	04:10
2014-11-20	2016-11-20 02:55	> zero	05:55	06:55	0,75	03:50
2015-01-17	2016-01-17 03:55	04:15	06:25	08:10		
2015-04-07	2016-04-07 02:25	> zero	07:25	08:40	1,03	03:35
2015-04-09	2016-04-09 02:55	> zero	07:25	09:40	0,9	05:47
2015-04-10	2016-04-09 22:10	> zero	06:55	09:55	1,1	00:44
2014-04-12	2016-04-11 23:55	> zero	06:55	09:10	1,2	05:45
2015-04-15	2016-04-15 03:10	> zero	07:10	10:40	0,6	07:30
2015-04-16	2016-04-15 18:40	> zero	09:10	12:25	0,35	07:50
2015-04-17	2016-04-16 18:40	23:02	07:25	12:25		
2015-04-18	2016-04-17 18:25	22:15	07:25	12:25		
2015-04-19	2016-04-18 18:40	21:15	07:40	10:55		
2015-04-20	2016-04-19 16:55	20:13	08:40	12:40		
2015-04-21	2016-04-20 18:25	22:12	07:10	12:10		
2015-04-22	2016-04-21 18:10	> zero	07:10	10:40	0,07	06:23
2015-04-27	2016-04-26 21:25	> zero	07:25	10:10	0,35	06:30
2015-04-28	2016-04-27 18:25	04:08	07:40	10:40		
2015-04-30	2016-04-29 23:25	05:19	07:40	10:25		
2015-05-01	2016-04-30 20:10	23:20	07:25	11:10		
2015-05-11	2016-05-10 21:10	> zero	07:55	10:25	0,5	06:30
2015-05-12	2016-05-11 23:40	> zero	07:40	10:55	0,18	06:35
2015-05-13	2016-05-12 22:55	02:42	07:40	11:10		

Table 9.4. Details concerning initiation of growth (visual and logger), melt and end of melt of needle ice growth events from Site 2. Additionally, Min Temp and Min Temp Timing show minimum temperatures and timestamps for events which did not show sub-zero temper

Date	Visual Init. of Growth	Freezing	Init. Of Melt	End of Melt	Min Temp	Min Temp Timing
2015-04-10	2016-04-09 23:10	02:55	06:40	11:55		
2015-04-12	2016-04-11 23:40	>zero	06:40	10:40	0,2	23:47
2015-04-15	2016-04-15 04:25	03:55	09:55	12:55		
2015-04-16	2016-04-15 19:25	23:50	09:55	16:10	0,1	19:16
2015-04-17	2016-04-16 18:25	20:00	09:55	16:40	0,2	17:46
2015-04-18	2016-04-17 17:55	17:55	09:55	16:55		
2015-04-19	2016-04-18 17:25	17:40	06:55	13:25		
2015-04-20	2016-04-19 18:10	17:25	10:10	16:40		
2015-04-21	2016-04-20 18:25	17:40	09:55	16:10		
2015-04-22	2016-04-21 19:10	19:35	10:25	11:55		
2015-04-27	2016-04-27 00:25	>zero	10:25	11:40	0,4	05:50
2015-04-28	2016-04-27 22:10	>zero	10:25	12:55	0	22:16
2015-04-30	2016-04-30 01:10	02:25	10:40	13:25		
2015-05-01	2016-04-30 19:10	20:15	10:25	14:40		
2015-05-02	2016-05-02 01:55	>zero	08:40	11:25	0	06:20
2015-05-07	2016-05-06 22:10	21:45	10:40	14:10		
2015-05-11	2016-05-10 20:40	>zero	10:10	10:55	0	06:10
2015-05-12	2016-05-11 21:10	00:30	09:55	12:10	0	20:35
2015-05-13	2016-05-12 23:10	23:00	10:55	14:55		
2015-05-14	2016-05-14 02:10	>zero	10:40	12:40	0,2	01:00
2015-05-15	2016-05-14 20:10	>zero	08:25	09:40	1,1	01:20
2015-05-17	2016-05-16 23:40	>zero	07:55	10:25	2,1	04:45

Table 9.5. Details concerning initiation of growth (visual and logger), melt and end of melt of needle ice growth events from Site 3.

Date	Visual initiation of growth	Freezing	Init. Of Melt	End of Melt
2014-04-27	01-00 17:11	16:01		
2014-05-13	01-00 14:11	12:21		
2014-05-15	01-00 17:21	15:01	09:21	14:11
2014-05-16	01-00 17:11	15:01		
2015-03-01	01-00 19:11	18:51	08:51	13:11
2015-03-11	01-00 22:31	02:51	07:51	08:41
2015-03-12	01-00 20:01	16:41	06:01	09:11
2015-03-14	01-00 21:31	18:51	06:41	11:01
2015-03-20	01-00 16:21	16:21	06:21	13:41
2015-03-27	01-00 22:21	21:01	08:21	12:01
2015-03-30	01-00 23:11	22:41	09:11	15:21
2015-04-01	01-00 18:21	15:41	07:51	23:41
2015-04-02	01-00 18:31	17:01	07:31	23:31
2015-04-03	01-00 01:11	22:41	08:51	11:51
2015-04-11	01-00 18:01	20:11	08:51	13:21
2015-04-30	01-00 22:41		04:31	09:31

Appendix B

Single needle ice event analysis

Video 1 - November 16-17 2014

https://www.dropbox.com/s/kudks3yfv8basrg/Video%201%20-%20Site%201%20November%2016-17%202014.mp4?dl=0

Video 2 - April 17-18 2015

https://www.dropbox.com/s/kudks3yfv8basrg/Video%201%20-%20Site%201%20November%2016-17%202014.mp4?dl=0

Video 3 - May 14-15 2014

https://www.dropbox.com/s/91jve2wf5idvb0n/Video%203%20-%20Site%203%20May%2014-15%202014.mp4?dl=0

Site 1

Video 4 - July 2 2014

https://www.dropbox.com/s/8golu4zz2tep6xe/Video%204%20-%20Site%201%20Event%201%20July%202%202014.mp4?dl=0

Video 5 - August 22 2014

https://www.dropbox.com/s/w0kmuel4so4lke0/Video%205%20-%20Site%201%20Event%202%20Aug%2022%202014.mp4?dl=0

Video 6 - November 16 2014

https://www.dropbox.com/s/5t4flezw7bjugbu/Video%206%20-%20Site%201%20Event%203%20Nov%2016%202014.mp4?dl=0

Video 7 - November 18 2014

https://www.dropbox.com/s/uhb4tu0lppb7ujh/Video%207%20-%20Site%201%20Event%204%20Nov%2018%202014.mp4?dl=0

Video 8 - Apr 17 2015

https://www.dropbox.com/s/z3nsu76c3ac858c/Video%208%20-%20Site%201%20Event%205%20Apr%2017%202015.mp4?dl=0

Site 2

Video 9 - April 10 2015

https://www.dropbox.com/s/7gzxspmnsq780et/Video%209%20-%20Site%202%20Event%201%20Apr%2010%202015.mp4?dl=0

Video 10 - April 12 2015

https://www.dropbox.com/s/wj9l0ass92b84qr/Video%2010%20-%20Site%202%20Event%202%20Apr%2012%202015.mp4?dl=0

Video 11 - April 16 2015

https://www.dropbox.com/s/63ckztit043yrj9/Video%2011%20-%20Site%202%20Event%203%20Apr%2016%202015.mp4?dl=0

Video 12 - April 22 2015

https://www.dropbox.com/s/u5mtuj2gyxtjy4h/Video%2012%20%20-%20Site%202%20Event%204%20Apr%2022%202015.mp4?dl=0

Video 13 - May 07 2015

https://www.dropbox.com/s/q1qd1p31sqzbgu4/Video%2013%20-%20Site%202%20Event%205%20May%2007%202015.mp4?dl=0

Site 3

Video 14 - April 27 2014

https://www.dropbox.com/s/qi94po0l7kjysv0/Video%2014%20-%20Site%203%20Event%201%20Apr%2027%202014.mp4?dl=0

Video 15 - May 15 2014

https://www.dropbox.com/s/mfzql3fb2r4j3tk/Video%2015%20-%20Site%203%20Event%202%20May%2015%202014.mp4?dl=0

Video 16 - March 14 2015

https://www.dropbox.com/s/r4nna3bbyddcj98/Video%2016%20-%20Site%203%20Event%203%20Mar%2014%202015.mp4?dl=0

Video 17 - March 30 2015

https://www.dropbox.com/s/j8svoihthil79x5/Video%2017%20-%20Site%203%20Event%204%20Mar%2030%202015.mp4?dl=0

Video 18 - April 11 2015

https://www.dropbox.com/s/1p2e6dsltjvff9f/Video%2018%20-%20Site%203%20Event%205%20Apr%2011%202015.mp4?dl=0